THE
PHYSICAL
SOCIETY

MEMOIRS

OF THE

COLLEGE OF SCIENCE

UNIVERSITY OF KYOTO

SERIES A

VOL. XXVII, No. 2

July 1954

KYOTO

Digitized by the Internet Archive
in 2024

https://archive.org/details/memoirs-faculty-science-kyoto-phys-astro-geophys-chem_1954-07_27_2

MEMOIRS OF THE COLLEGE OF SCIENCE, University of Kyoto, Series A,
Vol. XXVII, No. 2, Article 1, 1954

THE VERTICAL DISTRIBUTIONS OF THE TEMPERATURE AND DENSITY IN THE LOWER IONOSPHERE*

BY

Yuji INOUE

Institute of Geophysics, University of Kyoto

(*Received April 13, 1954*)

ABSTRACT

The vertical distributions of the temperature and density in the lower ionosphere, D, E and F_1 regions, are derived simultaneously by supposing the dissociative, thermal and mechanical equilibria. It is assumed that the atmosphere is well mixed and the chemical composition of the ionosphere is the same as that of the atmosphere at the ground. At the height of the ionosphere, the nitrogen molecule remains undissociated, while oxygen is dissociated by the solar ultraviolet radiation, which is supposedly of the Planckian radiation with the temperature 5713°K. The investigation on the photo-dissociation of molecular oxygen, based on the absorption coefficients inquired by R. Penndorf, enables us to secure some important result, namely the relation between the rate of the dissociative absorption and the optical depth of the dissociating radiation. The gas-kinetic energy in the lower ionosphere is mainly supplied by the excess energy made in the case of the photodissociation and is lost effectively by the inelastic collision with the molecule resulting in the vibrational excitation of the latter and the subsequent emission by the quadrupole transition. The formation of molecular oxygen is due to radiative association. Unfortunately, little is known about the rate of this process. Thus it was deduced in this paper from the ionospheric data. We have chosen as a reference level of height the level in the E region, where the total particle concentration can be roughly detected by the radio echos. However, with respect to the temperature and temperature gradient, their absolute values can be derived by the equilibrium considerations. The equilibrium equations were solved by the numerical method.

Some important results obtained by the present calculation are as follows:
(i) There occur a steep temperature gradient and the almost abrupt decrease of the particle concentration of molecular oxygen in the E region.
(ii) The theoretical possibility for the existence of the particle concentrations enough to account for the generation of the F_1 and F_2 layers has been shown.

It must be remarked that our theoretical pressure distribution is not in agreement with that of the ambient pressure measured during the rocket flights. However, the matter does not seem to be decisive yet if we reflect upon the uncertainties inherent in the theory on the one hand and the observation on the other.

The problems of the F_2 region related with the present problem are discussed briefly. Also, the effect of thermal conduction is examined.

*Contribution to Geophysical Papers dedicated to Prof. M. Hasegawa on his sixtieth birthday.

1. Introduction

Up to the present time, many investigations (**1**–**5**) have been made to determine the vertical distribution of the particle concentration in the ionosphere, by assuming the temperature distribution. However, the derivation of the vertical distribution of the particle concentration by assuming the latter seems to be unsatisfactory unless the latter has been firmly established. The particle concentration and the temperature at a level of the ionosphere are closely connected with each other. Hence, in order to get the accurate information of these distributions, it is much more desirable to find a method capable of deducing simultaneously the temperature and particle concentrations at every altitude. It seems relevant and desirable from the theoretical point of view to establish the distributions in the lower ionosphere satisfying the dissociative, thermal and mechanical equilibria simultaneously. Such an idea has first been proposed by H. E. Moses and Ta-You Wu. (**6**) The present calculations are at variance with them about the principal process of the loss of gas-kinetic energy in the lower ionosphere. D. R. Bates (**7**) has investigated precisely every atomic processes responsible for the heat gain and heat loss. He has presumed that oxygen in the ionosphere is completely in the dissociative condition, and in consequence he ascribed less importance, contrary to the present work, to the dissociative absorption of molecular oxygen on the gain of gas-kinetic energy. With respect to the loss of gas-kinetic energy, his inspection about the emissions of the vibrational energy of various ionospheric molecules was made by assuming the thermodynamical equilibrium. However, it seems much more plausible to suppose that the distribution of the vibrational levels under the ionospheric condition does not obey the Boltzmann distribution.

2. The mechanical equilibrium in the lower ionosphere

The principal constituents of the ionosphere are oxygen and nitrogen, as generally accepted from the evidence of the spectra of the night sky and the polar aurorae. As pointed out by various authors (**1**–**6**, **8**), the absorption of the solar radiation in the continuum of the Schumann-Runge bands causes a heavy dissociation of oxygen in the ionosphere, and the oxygen is present mainly as molecules at the lower level, while as atoms at greater heights. The detailed calculations of Wulf and Deming (**1**), and, recently, of Penndorf (**4**) have shown that the transition takes place in a region near but slightly above 100 km level. While, the degree of dissociation of nitrogen in the ionosphere is at present a controversial question; G. Herzberg and L. Herzberg (**9**) have suggested that the nitrogen is dissociated to a much small extent by absorption in the forbidden bands $a^1\Pi_g \rightarrow X^1\sum_g^+$ below 1250Å and subsequent predissociation. It may not be expected from this process that nitrogen is considerably dissociated in the conditions of the ionosphere, so that it probably

remains in the molecular state up to a very great height in the ordinary conditions. As pointed out by Chapman, this may be implied by the appearance of the band spectra attributed to molecular nitrogen in sunlit aurorae up to about over 1000 km level (**10**).

The rocket measurements have been made of the helium content in the air at a height more than 70 km, and they have shown that it is not appreciably different from that at the ground (**11**). It seems to be relevant to suppose that the atmosphere is considerably stirred up to this level. There is at present no knowledge about the mixing of the atmosphere above this level. While, it is generally accepted by radio measurements that in the region of the ionosphere there are motions of the air whose wind-velocities are as great as 100 m sec^{-1} or more (**12**). As to the existence of such motions of the air, it may be supposed that by them the atmosphere is considerably stirred up to the top of the ionosphere.

The conceivable constituents other than oxygen and nitrogen seem to be so scarce that they probably have no direct influence upon the phenomena discussed in this paper.

Hence for the conclusion, it may hold good to presume that the gases in the lower ionosphere consist of nitrogen and oxygen in the same proportion as at the ground, provided that nitrogen is undissociated, while oxygen is heavily dissociated by the solar ultraviolet.

In view of this, assigning generally a parameter η, which is also independent of height, to express the relative proportion of oxygen and nitrogen, the particle concentrations of oxygen and nitrogen at any height may be expressed by the relation:

$$\eta\left[n(O_2, z)+\frac{1}{2}n(O, z)\right]=n(N_2, z), \qquad (1)$$

$n(O, z)$, $n(O_2, z)$, and $n(N_2, z)$ being the particle concentrations per cm^3 at a height z of atomic oxygen, molecular oxygen, and molecular nitrogen respectively. Let $N(z)$ be the total particle concentration per cm^3 at a height z, it follows that

$$N(z)=n(O, z)+n(O_2, z)+n(N_2, z). \qquad (2)$$

Substitution of (1) into (2) yields

$$N(z)=n(O, z)\left[1+\frac{\eta}{2}+(1+\eta)\,\chi(z)\right], \qquad (3)$$

where

$$\chi(z)=\frac{n(O_2, z)}{n(O, z)}.$$

Let $M(z)$ be the mean molecular mass and let M_0 be the mass of atomic oxygen. The variation of the mean molecular mass with height is described by

$$M(z) = \frac{\left(1+\frac{7}{8}\eta\right)(1+2\chi)}{1+\frac{\eta}{2}+(1+\eta)\,\chi} M_0 . \qquad (4)$$

It may be supposed that velocities of air motions in the lower ionosphere are not so great as the mechanical equilibrium of the atmosphere is very far remote from that for a rest atmosphere, so that the hydrostatic equilibrium of the atmorphere may be approximately available for the lower ionosphere. Neglecting the variation of the gravitational acceleration g with height, we have

$$\frac{d}{dz} \log_e P(z) = -\frac{M(z)\, g}{KT(z)} , \qquad (5)$$

where $P(z)$ and $T(z)$ are the pressure and the temperature at the height z respectively, and K Boltzmann's constant.

Table 1

λ Å	$\log_{10} K_\nu$, cm^2	$h\nu - h\nu_0$, eV	$\log_{10} K_\nu I_\nu(\infty)$ sec^{-1}
1300	$\bar{1}9.5403$	2.44	$\bar{7}.0633$
1350	$\bar{1}8.8195$	2.09	$\bar{6}.6196$
1400	$\bar{1}7.1367$	1.76	$\bar{5}.1931$
1450	$\bar{1}7.2672$	1.46	$\bar{5}.5611$
1500	$\bar{1}7.1673$	1.17	$\bar{5}.6835$
1550	$\bar{1}7.0253$	0.91	$\bar{5}.7466$
1600	$\bar{1}8.8420$	0.66	$\bar{5}.7551$
1650	$\bar{1}8.6010$	0.43	$\bar{5}.6937$
1700	$\bar{1}8.3010$	0.21	$\bar{5}.5635$
1750	$\bar{1}9.5403$	0.00	$\bar{6}.9605$
1800	$\bar{2}0.6375$	1.77	$\bar{6}.2068$
1850	$\bar{2}1.2810$	1.59	$\bar{8}.9886$
1900	$\bar{2}2.4440$	1.41	$\bar{8}.2833$
1950	$\bar{2}3.6375$	1.24	$\bar{9}.6021$
2000	$\bar{2}4.9395$	1.09	$\bar{9}.0212$
2050	$\bar{2}4.6902$	0.94	$\bar{1}0.8848$
2100	$\bar{2}4.3424$	0.79	$\bar{1}0.6420$
2150	$\bar{2}4.1461$	0.66	$\bar{1}0.5465$
2200	$\bar{2}5.9395$	0.52	$\bar{1}0.4330$
2250	$\bar{2}5.5911$	0.40	$\bar{1}0.1775$
2300	$\bar{2}5.2553$	0.28	$\bar{1}1.9269$
2350	$\bar{2}6.9395$	0.17	$\bar{1}1.6924$
2400	$\bar{2}6.7404$	0.06	$\bar{1}1.5717$
2450	$\bar{2}4.0531$	0.00	——
2500	$\bar{2}5.7832$	0.00	——

3. The photodissociation of molecular oxygen and the gain of gas-kinetic energy in the lower ionosphere

The photodissociation of molecular oxygen takes place by the absorption of the solar radiation in the continuum of the Schumann-Runge and of the Herzberg bands. The latter has no appreciable effect in the ionospheric region. The photodissociative absorption coefficient K_ν of molecular oxygen in the range of wavelength concerned has been investigated by Penndorf (4). His result as reproduced in Table 1 will be used in the present work.

When the photodissociation takes place, the absorption of radiation with energy

$h\nu$ exceeding the threshold energy necessary for dissociating molecular oxygen, contributes to the increase of the gas-kinetic energy in the lower ionosphere. Thus, $h\nu - h\nu_0$ is the appropriate part of the original quantum $h\nu$ transformed to the kinetic energy, in which $h\nu_0$ means the threshold energy, that is, 7.047 eV for the Schumann-Runge transition, and 5.080 eV for the Herzberg transition (**13**). Values of $h\nu - h\nu_0$ are given in Table 1. But all of these energies are, in general, not available for local heating: due to the dissociative recombination a certain fraction of it would be spent in converting into radiation or in exciting the molecular oxygen generated. This, however, is not necessary to be taken into account by the reasoning that the rate of recombination is very slow, as is generally accepted, and that the temperature in the lower ionosphere is supposed to be as low as about 300°K.

The solar ultraviolet radiation in the range of wavelengths capable of dissociating molecular oxygen is supposed to be of a diluted black-body radiation with the temperature 5713°K.

Let $I_\nu(\infty)\, d\nu$ be the incident flux of the dissociating radiation in quanta per cm^2 per sec from the sun in frequencies within the range from ν to $\nu + d\nu$ received at the top of the earth's atmosphere. The numerical values of $K_\nu I_\nu(\infty)$ are given in Table 1. Let $I_\nu(z)\, d\nu$ be the flux of quanta per cm^2 and per second of the dissociating radiation in the frequency range between ν and $\nu + d\nu$ at the height z in the ionosphere. For shortness of the representation of solutions it is convenient to introduce $\sigma_m(z)$, $\tau_m(z)$, $D(z)$, and $\varepsilon D(z)$ defined as:

$$\sigma_m(z) = \int_z^\infty n(O_2, z')\, dz', \tag{6}$$

$$\tau_m(z) = \int_z^\infty K_{1450\text{Å}} n(O_2, z')\, dz', \tag{7}$$

$$D(z) = \int_\nu K_\nu I_\nu(z)\, d\nu, \tag{8}$$

and

$$\varepsilon D(z) = \int_\nu K_\nu (h\nu - h\nu_0)\, I_\nu(z)\, d\nu, \tag{9}$$

where

$$I_\nu(z) = I_\nu(\infty) \exp[-K_\nu \sigma_m(z)] \tag{10}$$

is the ordinary exponential solution of the equation for the pure absorption:

$$\frac{dI_\nu(z)}{dz} = K_\nu n(O_2, z)\, I_\nu(z), \tag{11}$$

and the integrations in (8) and (6) cover the frequency range concerned. $D(z)\, n(O_2, z)$

is the rate of the photodissociative absorption per cm^3 and per second at the height z, $\varepsilon D(z)\, n(O_2, z)$ is the rate of the gain of gas-kinetic energy in erg $cm^{-3}\, sec^{-1}$ due to the photodissociation of the height z, $K_{1450Å}$ is the maximum absorption coefficient in the frequency range concerned, $\sigma_m(z)$ is the number of molecular oxygen in a column with a base of unit aera of the atmosphere above the height z, and $\tau_m(z)$ is the optical depth of the dissociating radiation as to the maximum absorption coefficient $K_{1540Å}$, the suffix m distinguishing the molecular from the atomic oxygen. The integrations of $D(z)$ and $\varepsilon D(z)$ have been carried out numerically step by

Table 2

$\log_e \tau_m(z)$	$\log_{10} \varepsilon D(z)$ erg sec^{-1}	$\log_{10} D(z)$ sec^{-1}	λ_{max} Å	$\lambda - \lambda_{abs.}$ Å
−2.50	$\bar{16}.3683$	$\bar{4}.2103$	1600	1300–1850
−2.00	$\bar{16}.3541$	$\bar{4}.2041$	1600	1300–1850
−1.50	$\bar{16}.3243$	$\bar{4}.1761$	1600	1300–1850
−1.00	$\bar{16}.2742$	$\bar{4}.1303$	1600	1300–1850
−0.50	$\bar{16}.1986$	$\bar{4}.0719$	1600–1650	1300–1850
0.00	$\bar{16}.0969$	$\bar{5}.9993$	1650	1300–1850
0.50	$\bar{17}.9385$	$\bar{5}.8819$	1650	1300–1850
1.00	$\bar{17}.7058$	$\bar{5}.7177$	1650–1700	1300–1850
1.50	$\bar{17}.3983$	$\bar{5}.5109$	1700	1300–1850
2.00	$\bar{17}.0449$	$\bar{5}.2624$	1700	1450–1850
2.50	$\bar{18}.7068$	$\bar{6}.9974$	1700	1550–1850
3.00	$\bar{18}.4548$	$\bar{6}.7539$	1750	1600–1900
3.50	$\bar{18}.3201$	$\bar{6}.4969$	1750	1650–1950
4.00	$\bar{18}.2393$	$\bar{6}.1938$	1750	1700–1950
4.50	$\bar{18}.1987$	$\bar{7}.9523$	1750	1700–1950
5.00	$\bar{18}.1408$	$\bar{7}.7839$	1800	1750–1950
5.50	$\bar{18}.0473$	$\bar{7}.6201$	1800	1750–1950
6.00	$\bar{19}.9009$	$\bar{7}.4579$	1800	1750–1950

step in each interval of 50Å, and the computed results are shown in Table 2 and Fig. 1. Since, at present, there is little knowledge concerning the distribution of molecular oxygen with height, $\log_e \tau_m(z)$ will be taken as a measure of height. The wavelength appropriate for the maximum photodissociative absorption, λ_{max}, and the range of wavelength of the appreciable absorption, $\lambda - \lambda_{abs}$, for each $\log_e \tau_m(z)$ are given in Table 2. Inspection of Fig. 1 reveals that both $\log_e D(z)$ and $\log_e \varepsilon D(z)$ show locally linearity against $\log_e \tau_m(z)$. This is not unexpected, but has a simple physical interpretation: taking (6), (7), (8) and (10) into account, equation (11) can be written as:

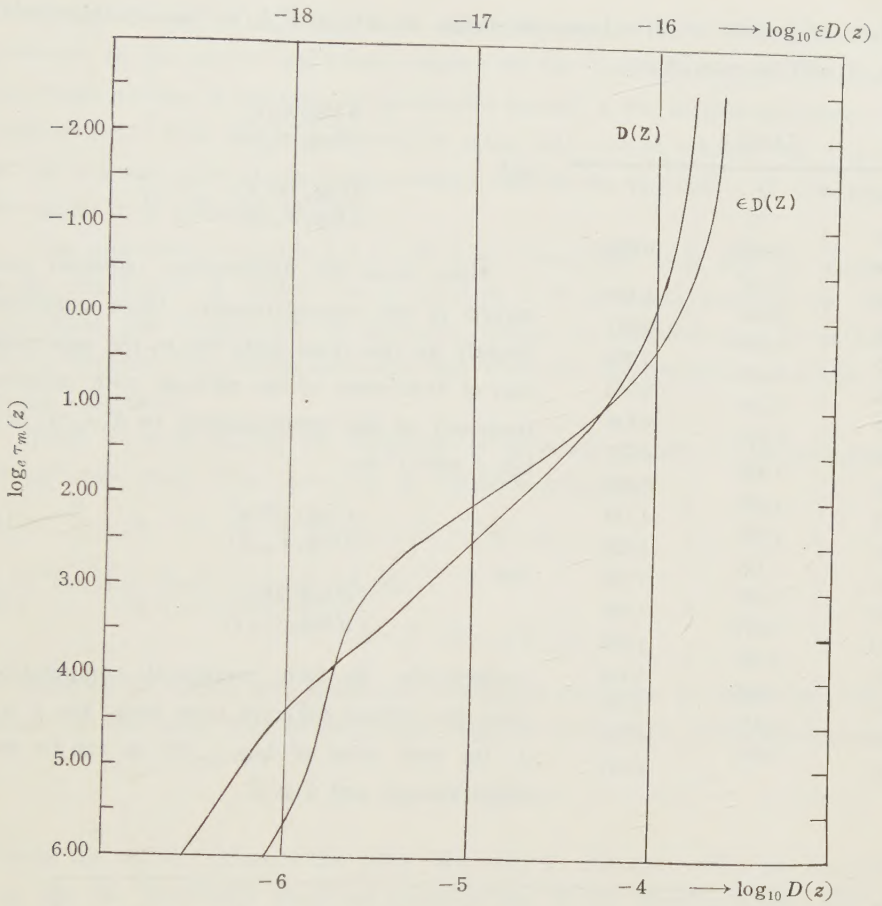

Fig. 1. Distributions of $D(z)$ and $\varepsilon D(z)$ in relation to $\log_e \tau_m(z)$.

$$\frac{d \log_e D(z)}{d \log_e \tau_m(z)} = \frac{\int_\nu K_\nu I_\nu(z)(-K_\nu \sigma_m(z))\, d\nu}{\int_\nu K_\nu I_\nu(z)\, d\nu}. \tag{12}$$

Similarly, referring to (9) equation (11) can be written as:

$$\frac{d \log_e \varepsilon D(z)}{d \log_e \tau_m(z)} = \frac{\int_\nu K_\nu I_\nu(z)(h\nu - h\nu_0)(-K_\nu \sigma_m(z))\, d\nu}{\int_\nu K_\nu I_\nu(z)(h\nu - h\nu_0)\, d\nu}. \tag{13}$$

$h\nu$–quanta are absorbed effectively in a region where the optical depth for the radiation is nearly equal to unity. It may be supposed that the dissociating radiation mainly absorbed at the level z, corresponding to a value of $\sigma_m(z)$, is specified by the condition that $K_\nu \sigma_m(z)$ is nearly equal to unity. Putting $K_\nu \sigma_m(z) \simeq 1$ in (12) and

(13), and integrating over a frequency-range in which $K_\nu I_\nu(z)$ has an appreciable amount, it will be seen that

$$\frac{d \log_e D(z)}{d \log_e \tau_m(z)} = -1 ,$$

and

$$\frac{d \log_e \varepsilon D(z)}{d \log_e \tau_m(z)} = -1 .$$

Now, since the dissociating radiation concerned is not monochromatic, these quantities slightly deviate from unity due to the superposition of absorption of the photons with adjacent frequency to that corresponding to $K_\nu \sigma_m(z) \simeq 1$. Let f and f' be

$$\frac{d \log_e \varepsilon D(z)}{d \log_e \tau_m(z)} = -f , \qquad (14)$$

and

$$\frac{d \log_e D(z)}{d \log_e \tau_m(z)} = -f' \qquad (15)$$

respectively. In fact, numerical computations give the values different from unity for f and f' for each level of $\log_e \tau_m(z)$, as can be seen from Table 3 and Fig. 2.

Table 3

$\log_e \tau_m(z)$	f	f'
−2.50	0.0654	0.0285
−2.00	0.137	0.129
−1.50	0.231	0.211
−1.00	0.348	0.269
−0.50	0.468	0.334
0.00	0.729	0.541
0.50	1.071	0.757
1.00	1.416	0.952
1.50	1.627	1.144
2.00	1.557	1.221
2.50	1.160	1.121
3.00	0.620	1.184
3.50	0.372	1.396
4.00	0.187	1.112
4.50	0.266	0.775
5.00	0.431	0.754
5.50	0.674	0.747
6.00		

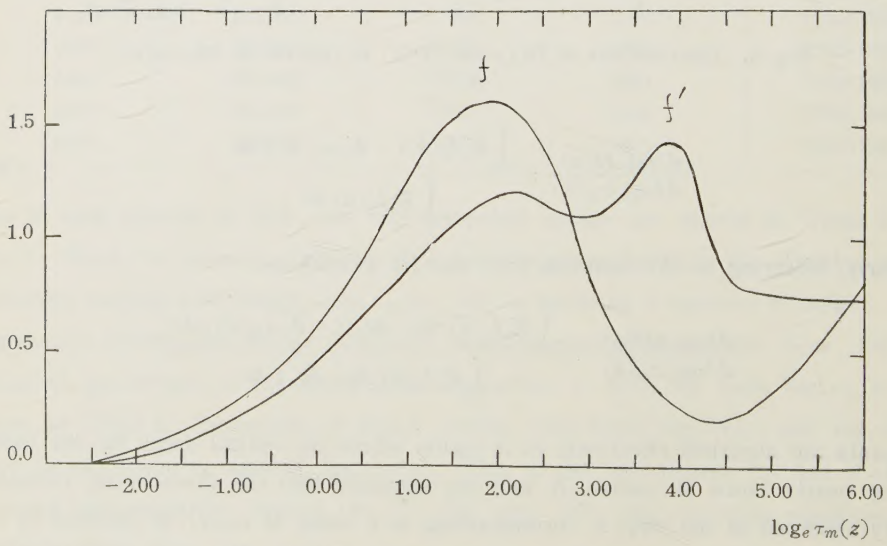

Fig. 2. f and f' plotted against $\log_e \tau_m(z)$.

In conclusion, it is found, as a result of examination of the other conceivable processes of the gain of gas-kinetic energy in the lower ionosphere, that the most important process of the gain of gas-kinetic energy is the photodissociation of molecular oxygen. This rate is expressed by $\varepsilon D(z)\, n(O_2, z)$ in erg cm^{-3} sec^{-1}. $\varepsilon(z)$, that is, the average gain of gas-kinetic energy due to the absorption of one photon at the height z, is given in Fig. 3.

The dissociative equilibrium in the lower ionosphere must now be investigated. In the atmosphere of such a low temperature as is generally supposed for the lower ionosphere, the dissociation of molecular oxygen by collisions may be unimportant. While, the photodissociation mentioned above decides the formation of atomic oxygen in the ionosphere.

Next, we must discuss the formation of molecular oxygen in the ionosphere. In general, free atoms form molecules by radiative association

$$X+Y \rightarrow XY+h\nu\,, \tag{16}$$

or by the three-body collision (**14**, **15**)

$$X+Y+Z \rightarrow XY+Z\,. \tag{17}$$

The rates of the former for various cases have been examined by Bates (**14**) ; the cross section of the latter may be expressed, with a considerably good approximation, by

$$Q_c \simeq \pi r^2 \cdot \frac{r}{l} \cdot n_z\,, \tag{18}$$

r being the atomic radius, l the mean free path for effective collisions between the atom and the third body when the concentration of the latter is unity, and n_z the particle concentration of the third body. If it is possible that the third body is a molecule, and that the internal energy to be transferred is absorbed completely, by a resonance process, as a potential energy of the third body, l may take values down to 10^{14}cm. Then taking r to be 10^{-8}cm, Q_c becomes as large as $10^{-24}cm^2$ at the bottom of the ionosphere, where the particle concentration of the third body, capable of being of resonant absorption, may be supposed to be as great as $10^{14}cm^{-3}$. If resonance transfer is not possible, the excess energy must be partially taken up as kinetic energy of the relative motion of the atomic systems. Then l may be of the order of 10^{18}cm or more, hence Q_c reduces to the values of the order of $10^{-28}cm^2$ (**16**). At the lower gas density below the certain critical value, radiative association must be of the dominant process.

Atomic oxygen in the state ^1D is yielded with a considerably high rate by the photodissociation of the Schumann-Runge transition, but it falls rapidly to the ground state ^3P with emission of the forbidden radiation ; under the ionospheric condition it

may be unimportant on the reaction of association. This may be concluded from the intensity of the night sky radiation 6300Å, corresponding to the transition $^1D \rightarrow {}^3P$. Hence, it is sufficient to consider the association between oxygen atoms in the ground state, ^3P. Inspection of the configuration of the potential curves of molecular oxygen (17) shows that the radiative associations for molecular oxygen appear primarily to make the transitions from the $^3\sum_u^+$ state to the second or third excited vibrational levels in the electronic states of $^1\sum_g^+$, $^1\Delta_g$, and $^3\sum_g^-$, viz.

$$\mathrm{O}(^3P)+\mathrm{O}(^3P) \rightarrow \mathrm{O}_2 \text{ (second or third vibrational levels of } {}^1\textstyle\sum_g^+,\ {}^1\Delta_g, \text{ and } {}^3\textstyle\sum_g^-) + h\nu . \tag{19}$$

About the rates of the processes mentioned above, we have at present no experimental as well as theoretical knowledge. The probability of radiative association is very sensitive to the configuration of the potential curves of a molecule; in the most favourable case the effective cross section would become as great as $10^{-21}\mathrm{cm}^2$ (15), in the order of magnitude. Making a reciprocal deduction of the effective cross section from experimental values of the absorption coefficient, as to such slow encounters as in the ionosphere, the deduced values associated with both the Schumann-Runge transition of oxygen and the $^3\Pi_{0u}^+ \rightarrow {}^1\sum_g^+$ transition of Cl_2–molecule (18) would be obtained to be of the order as small as $10^{-26}\mathrm{cm}^2$. The actual value of the cross section associated with the reaction (19) would lie between the two extremities quoted above. The computations by Bates (14), though for other molecules, show the rate coefficients for a few specific reactions to be of the order of 10^{-17} or $10^{-18}\mathrm{cm}^3\,\mathrm{sec}^{-1}$, which lies between the maximum acceptable value of the order of $10^{-16}\mathrm{cm}^3\,\mathrm{sec}^{-1}$ and the values of the order of $10^{-21}\mathrm{cm}^3\,\mathrm{sec}^{-1}$ deduced from the experimental results of absorption coefficient. If this order of magnitude were applied to our case (19), the radiative association would sufficiently surpass the association by the three-body collision even at the bottom of the ionosphere. After the discussion described above, though it leaves some uncertainties in the quantitative examination for this probability, it does not seem to be unreasonable to suppose that the radiative association (19) is the dominant process down to the bottom of the ionosphere. Though we shall use in the following this cross section as the standard value, it may be wise at our present stage to try another way to determine it from the structure of the lower ionosphere, as will be shown in § 5.

Let Qv be the rate coefficient of the radiative association concerned, which may be supposed to be independent of temperature. The dissociative equilibrium of molecular oxygen is described by

$$Qvn(\mathrm{O}, z)\, n(\mathrm{O}, z) = \frac{1}{3} D(z)\, n(\mathrm{O}_2, z) , \tag{20}$$

the factor 1/3 having been introduced to express roughly the effect of no diurnal variation of the degree of dissociation; the reason for this lies in the fact that Qv is very small.

4. The processes of loss of gas-kinetic energy and the thermal equilibrium in the lower ionosphere

In the lower ionosphere molecules play an important part in the loss of gas-kinetic energy. Band emissions are sensitive to a possible deviation from the thermodynamical equilibrium. As is well known, the temperatures of the upper atmosphere derived by different method of measurement are often of different values: from the intensity distribution of the rotational spectra of polar aurorae, Vegard (**19**) has proposed, for the negative nitrogen band 4278Å, that the auroral temperature comes out to be of the order 343°K; from the intensity-distribution of the vibrational spectra in the ultraviolet negative and positive nitrogen bands, Rosseland and Steenshould **20**) have derived the corresponding temperature to be very high, something between 2000 and 3000°K. These facts indicate that the condition under which the bands are emitted may differ appreciably from those of the thermodynamical equilibrium. Making allowance for the fact that the density in the ionosphere is extremely tenuous, there would be such spectral evidences as to the band emissions even in the ordinary ionosphere. It should be borne in mind that such deviation from the thermodynamical equilibrium can possibly exist in the ordinary ionosphere.

The rotational level of molecular oxygen and nitrogen can be easily excited by impacts of gas-particles; however, the reciprocal process of this, i. e. the exchange of energy by collisions from rotational to translational levels, also easily takes place, and the rate of the spontaneous emission of rotational energy is very small; such rotational excitations cannot play any important role in the process of the loss of gas-kinetic energy. The detailed discussion on this point has been made by Spitzer: it may be shown after a reasonably good approximation that the total energy radiated from the rotational excited states as a loss of gas-kinetic energy is always less than those emitted from molecules in which Boltzmann's distribution among the excited rotational states is established by collisions.

But emission from vibrationa llevels merits some detailed treatments. Molecular oxygen has first vibrational level lying at 0.1950 eV above the zeroth, and in the case of nitrogen the first vibrational level lies at 0.292 eV above the zeroth (**22**). Let these values be denoted by $\varepsilon_V(O_2)$, and $\varepsilon_V(N_2)$ respectively. The values of the Einstein coefficients of the quadrupole emissions for oxygen $\delta(O_2)$ and for nitrogen $\delta(N_2)$ are unknown, but they are certainly very low, as quadrupole transitions are involved. If it were assumed that the moment-lengths of the quadrupole appropriate to molecular

oxygen and nitrogen were 1.204Å and 1.094Å, respectively, it would seem likely that the rates of the emission $\delta(O_2) \simeq 7.04\times10^{-4}\,\mathrm{sec}^{-1}$ for $h\nu$ of 0.195 eV, and $\delta(N_2) \simeq 3.65\times10^{-3}\,\mathrm{sec}^{-1}$ for $h\nu$ of 0.292 eV. These values may be adopted without risk of serious error (23).

The probability of transformation from translational to vibrational energy by collisions among gas-particles has been calculated by Jackson and Mott(24). To treat the ionospheric problems conveniently, the rate of such excitation in the $0 \rightarrow 1$ transition, which alone needs to be taken into account, will be modified, making allowance for that the gas-particles have Maxwellian velocity distribution appropriate to some temperature T, to the following forms for each type of collision;

$$W_1(O_2|O) \simeq 4.31\times10^{-6} T^{1/6} \exp\left(-2.201\times10^2/T^{1/3}\right), \tag{21}$$

and

$$W_1(N_2|O) \simeq 1.21\times10^{-5} T^{1/6} \exp\left(-2.835\times10^2/T^{1/3}\right), \tag{22}$$

where the suffix 1 refers to the excitation of the first vibrational level of the molecules considered, and the designations $(O_2|O)$, and $(N_2|O)$ are used to refer to the type of encounter: the formers within the round brackets represent the excited molecules, while the latters represent the colliding particles.

In the remainder of this paper it will be assumed that the velocities of the particles in the atmosphere are distributed according to Maxwell's law, and the parameter T in that law will be referred to as the kinetic temperature of the atmosphere.

The transfer of the relative kinetic energy between two molecules on impact to their vibrational energies is impossible unless the relative kinetic energy is so large that it can excite the vibrational states of both molecules together; this transfer is not necessary to be considered in the lower ionosphere.

The excitations to higher vibrational levels need not be taken into account in the process of the loss of gas-kinetic energy in the lower ionosphere. The excited vibrational energy can also reciprocally convert into translational energy by collisions. The rate of such de-excitation is of the same order as that of the excitation, because an encounter with a sufficient high speed is generally necessary to transform between vibrational and translational energy. Under the ionospheric conditions, the rates of the spontaneous quadrupole emissions for the vibrational energy are greater than those of exchange from vibrational to translational energy by collisions, viz.

$$\delta(O_2) \gg W_1'(O_2|O)\, n(O, z), \tag{23}$$

and

$$\delta(N_2) \gg W_1'(N_2|O)\, n(O, z), \tag{24}$$

where the prime refers to the de-excitations.

Hence, when the vibrational levels of a molecule are excited by the impacts of

gas-particle, a greater part of the excited vibrational energies are emitted in the form of radiation, because the atmosphere is transparent so that the radiation can freely escape out of the atmosphere. If the excitations to higher states can be neglected, the loss of gas-kinetic energy in this case is described by the following form:

$$\varepsilon W n_m n_0 \frac{\delta n_m'}{\delta n_m' + W' n_m' n_0}, \tag{25}$$

where ε is the excitation energy, W the rate of excitation by impacts, W' the rate of de-excitation, δ the rate of spontaneous emission for the excited state, n_m the particle concentration of molecule in the ground levels, n_m' that of the excited state, and n_0 that of the colliding gas-particles. According to (23) and (24), it may be said that the vibrational energies excited by the impacts of gas-particles are released in the forms of radiation. Thus, to a good approximation, the loss of gas-kinetic energy can be expressed as

$$\varepsilon W n_m n_0 . \tag{26}$$

In the case of the radiative association of oxygen, the relative kinetic energy between the two oxygen atoms turns out to be the radiation, and hence the atmosphere is cooled down, as was proposed by Moses and Wu. However, if this were a significant effect, by the condition of the thermal equilibrium between the heat gain due to the photodissociation of molecular oxygen:

$$\frac{1}{3} D(z)\, n(\mathrm{O}_2, z) = Qvn(\mathrm{O}, z)\, n(\mathrm{O}, z),$$

and the heat loss:

$$\frac{1}{3} \varepsilon D(z)\, n(\mathrm{O}_2, z) = \varepsilon_0 Qvn(\mathrm{O}, z)\, n(\mathrm{O}, z),$$

in which ε_0 means the average energy to be lost in one reaction, we are led to the result that

$$\varepsilon(z) = \varepsilon_0 .$$

Considering that $\varepsilon_0 \simeq \frac{3}{2} KT$, and that the minimum value of $\varepsilon(z)$ is about 0.5×10^{-2} erg, as can be seen from Fig. 3, the gas-kinetic temperature of the lower ionosphere would have been much higher than 2500°K, contrary to the observations. As is generally the case, when thermal equilibrium is established by the photodissociation with its reciprocal process, even if it is not completely reciprocal, the gas-kinetic temperature of the atmosphere settles to a great value near the temperature of the incident radiation.

From the discussion mentioned above, we take the following procedure as the most effective process responsible for the loss of gas-kinetic energy in the lower ionosphere: a molecule is excited vibrationally by impact with an atomic oxygen

with sufficiently large knietic energy enough for the excitation. The excited vibrational energy is lost in the form of radiation, since the atmosphere is almost transparent for such infrared radiation.

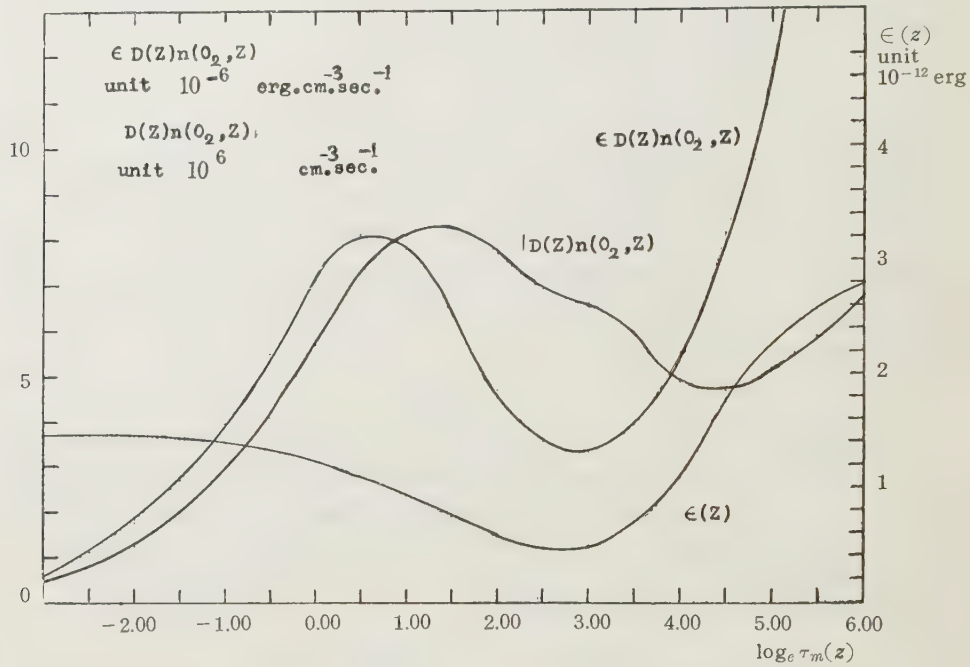

Fig. 3. $\varepsilon(z)$, $D(z)\,n(O_2, z)$ and $\varepsilon D(z)\,n(O_2, z)$ plotted against $\log_e \tau_m(z)$.

It follows that using (21), (22) and (26), the rate of the loss of gas-kinetic energy in the lower ionosphere $L_V(z)$ is expressed by

$$L_V(z) = \varepsilon_V(O_2)\,W_1(O_2|O)\,n(O_2, z)\,n(O, z) + \varepsilon_V(N_2)\,W_1(N_2|O)\,n(N_2, z)\,n(O, z), \tag{27}$$

where the designation L_V expresses the loss by the vibrational excitations; and (z) specifies explicitly that it is the function of the height. L_V does not contain δ; only some accurate information on W_1 is required in order to get the loss of gas-kinetic energy.

We shall next turn to the comparative study of the two terms on the right-hand side of (27). The excitation energy for nitrogen is about 1.5 times that for oxygen. Below the dissociative transition layer of oxygen, near above 100 km, it may be supposed that the relative proportions of molecular oxygen to molecular nitrogen is equal to 1/4, and that the temperature is as low as 300°K. Under these conditions, it can be concluded from the difference between the excitation energies that oxygen

molecules are decidedly effective. In regard to the colliding particles, it can be said that the atomic oxygen is effective, because molecules are excluded from consideration. Above the dissociative transition layer, the particle concentration of molecular oxygen decreases rapidly owing to the strong photodissociation and the very slow association of oxygen; molecular nitrogen is obliged to play the role of excited molecule. Thus, the second term of (27) is more effective than the first above the level where

$$\frac{n(O_2, z)}{n(N_2, z)} \simeq 4.22 \exp(-6.34\times 10/T^{1/3}), \tag{28}$$

as can be seen from (21) and (22). Table 4 gives the values of $4.22\exp(-6.34\times 10/T^{1/3})$ in relation to temperature T. It is difficult, as yet, to determine where this critical level is to be placed because of the uncertainty of the temperature and the degree of the dissociation. However, as is implied, since the temperature is about 700°K in this critical level, it will be seen from Table 4 that $n(N_2, z)$ there should become about 300 times as great as $n(O_2, z)$. It may be seen from the inspection of Fig. 1 that the absorption of the dissociating radiation begins sharply at certain level, and hence both $\varepsilon D(z)$ and $D(z)$ may be regarded to be nearly constant above this level; the lower ionosphere may be separated into the two regions in this respect: one is the weak absorption region, and the other is the strongly absorbing region. On the other hand, the region in which the first term of (27) is greater than the second will be designated as the region A. The region B will be designated as the region where the second term is effective. Since molecular oxygen is considerably abundant in the region A, the region A, of course, may also correspond to the strong absorption region; in the region B, molecular oxygen is less populated, hence the region B may correspond to the region of weak absorption.

Table 4

T	$4.22\times\exp(-6.34\times 10/T^{1/3})$
200	7.63×10^{-5}
250	1.70×10^{-4}
300	3.04×10^{-4}
350	4.89×10^{-4}
400	7.33×10^{-4}
450	1.00×10^{-3}
500	1.36×10^{-3}
550	1.76×10^{-3}
600	2.19×10^{-3}
650	2.68×10^{-3}
700	3.22×10^{-3}
750	3.79×10^{-3}
800	4.27×10^{-3}
860	5.00×10^{-3}

Thus, the thermal equilibrium in the lower ionosphere can be expressed by

$$\frac{1}{3}\varepsilon D(z)\, n(O_2, z) = L_V(z), \tag{29}$$

where the factor 1/3 refers to taking into account that the diurnal temperature-variation in the lower ionosphere is of a negligible amount, because $L_V(z)$ is very small compared with the energy stored up in the atmosphere.

5. Derivation of the particle concentrations and of the temperature in the lower ionosphere

It is relevant to suppose that in the lower ionosphere the vertical distributions of the particle concentrations of various constituents, and of the temperature should be determined simultaneously so as to satisfy the dissociative equilibrium of oxygen, the thermal equilibrium, as well as the mechanical equilibrium of the atmosphere. These equilibria have been reviewed in the previous sections.

Let us begin with the problem of the region A, which practically corresponds to the E and D regions of the ionosphere, as is easily seen from the discussion of the previous section. In this region the equation for the thermal equilibrium can be represented by

$$\frac{1}{3}\varepsilon D(z)\ n(\mathrm{O}_2, z) = \varepsilon_V(\mathrm{O}_2)\ W_1(\mathrm{O}_2|\mathrm{O})\, n(\mathrm{O}_2, z)\, n(\mathrm{O}, z)\,. \tag{30}$$

The equation for the dissociative equilibrium has been given by (20). As $D(z)$ and $\varepsilon D(z)$ cannot be expressed in terms of simple analytical functions, computation was performed by the numerical method.

Equations (30) and (20) lead to

$$n(\mathrm{O}, z) = \frac{1}{3}\varepsilon D(z)/\varepsilon_V(\mathrm{O}_2) W_1(\mathrm{O}_2|\mathrm{O})\,, \tag{31}$$

$$n(\mathrm{O}_2, z) = \frac{1}{3} Qv\cdot\varepsilon D(z)^2/D(z)\cdot\varepsilon_V(\mathrm{O}_2)^2\cdot W_1(\mathrm{O}_2|\mathrm{O})^2\,, \tag{32}$$

and

$$\chi(z) = Qv\varepsilon D(z)/D(z)\cdot\varepsilon_V(\mathrm{O}_2) W_1(\mathrm{O}_2|\mathrm{O})\,. \tag{33}$$

Substituting (3), (4), (31), and (33) into the equation for the mechanical equilibrium of the atmosphere (5), and neglecting the unimportant term $\frac{d}{dz}\log_e T(z)$*, equation (5) becomes

$$\frac{d}{dz}\log_e \varepsilon D(z) - \frac{d}{dz}\log_e W_1(\mathrm{O}_2|\mathrm{O}) - \frac{(1+\eta)\,\chi(z)}{1+\frac{\eta}{2}+2(1+\eta)\,\chi(z)}\,\frac{d}{dz}\log_e D(z)$$
$$= -\frac{1}{\mathfrak{H}_a}\,\frac{\left(1+\frac{7}{8}\eta\right)(1+2\chi(z))}{1+\frac{\eta}{2}+2(1+\eta)\,\chi(z)}\,, \tag{34}$$

where $\mathfrak{H}_a = \dfrac{KT}{M_0 g}$, namely, the scale height associated with atomic oxygen in a uniform atmosphere with temperature T.

The variation of the particle concentration of molecular oxygen with height may

* A rigorous treatment retaining this term is possible. The calculation runs parallel to the followings in spite of its greater complexity.

be described, taking equations (32) and (34) into account, by

$$\frac{d}{dz}\log_e n(O_2, z) = -\frac{1}{\mathfrak{H}_m}\frac{\left(1+\frac{7}{8}\eta\right)(1+2\chi(z))}{1+\frac{\eta}{2}+2(1+\eta)\chi(z)} - \frac{1+\frac{\eta}{2}}{1+\frac{\eta}{2}+2(1+\eta)\chi(z)}\frac{d}{dz}\log_e D(z), \tag{35}$$

where $\mathfrak{H}_m = \frac{KT}{2M_0 g}$, namely, the scale height associated with molecular oxygen in a uniform atmosphere with temperature T. The vertical distribution of the particle concentration of molecular oxygen represented by (35) differs, of course, from that expressed by

$$\frac{d}{dz}\log_e n(O_2, z) = -\frac{1}{\mathfrak{H}_m}. \tag{36}$$

For convenience, we shall abbreviate the right-hand side of (35) as follows:

$$\frac{d}{dz}\log_e n(O_2, z) = -\frac{1}{H_m(z)}. \tag{37}$$

If we put

$$a(z) = \frac{\mathfrak{H}_m}{H_m},$$

it measures the deviation of the vertical distribution of molecular oxygen from that of a uniform atmosphere without dissociation. H_m is the local scale height expressing the vertical distribution of molecular oxygen. As can be seen from equation (35), the photodissociation exerts a strong influence upon the vertical distribution of molecular oxygen; it gives rise to such a deviation as is mentioned above.

Using the local scale height H_m, it approximately yields from the definitions (6) and (7) that

$$\frac{d}{dz}\log_e \tau_m(z) = -\frac{1}{H_m}, \tag{38}$$

and

$$\frac{d}{dz}\log_e \sigma_m(z) = -\frac{1}{H_m}, \tag{39}$$

respectively. Therefore the relations (14) and (15) can be written as:

$$\frac{d}{dz}\log_e D(z) = \frac{f'}{H_m}, \tag{40}$$

and

$$\frac{d}{dz}\log_e \varepsilon D(z) = \frac{f}{H_m} \tag{41}$$

respectively. Making substitution of (40), (41) and (37) into equation (35), $a(z)$ can be transformed to

$$a(z) = \frac{\left(1+\frac{7}{8}\eta\right)(1+2\chi(z))}{(1-f')\left(1+\frac{\eta}{2}\right)+2(1+\eta)\,\chi(z)}. \tag{42}$$

The vertical distribution of atomic oxygen is deduced by the similar process to that described above, viz.

$$\frac{d}{dz}\log_e n(\mathrm{O}, z) = -\frac{1-f'}{2H_m}. \tag{43}$$

Let us turn to the discussion about $a(z)$. If we consider the case when the gases in the lower ionosphere consist of nitrogen and oxygen in the same proportions as the atmosphere at the ground, η is constant and equal to 4, and substituting this into (42), we are led to

$$a(z) = \frac{c(1+2\chi)}{A+\chi}, \tag{44}$$

where $c = \frac{9}{20}$ and $A = \frac{3}{10}(1-f')$. If we consider the case of pure oxygen ionosphere, η vanishes, and (42) becomes

$$a(z) = \frac{c'(1+2\chi)}{A'+\chi'}, \tag{45}$$

where $c' = \frac{1}{2}$ and $A' = \frac{1}{2}(1-f')$. The difference of $a(z)$ between these two cases is small, so that it can be seen that $a(z)$ depends little upon η, but the dissociative absorption strongly affects $a(z)$, especially in the region where χ is small, that is, the particle concentration of atomic oxygen is greater than that of molecular oxygen. Hereafter, we will consider only the case $\eta = 4$.

On substitution of (40), (41) and (42) into equation (34), we obtain the equation for the vertical distribution of temperature, viz.

$$\frac{d}{dz}\log_e W_1(\mathrm{O_2}|\mathrm{O}) = \frac{a(z)}{\mathfrak{H}_a}(1-f'+2f), \tag{46}$$

which, on making use of (21), and regarding the slowly varying term $T^{1/6}$ as a constant, can be written as:

$$\frac{B(\mathrm{O_2})}{3}\,\frac{1}{T^{1/3}}\,\frac{dT}{dz} = \frac{M_0 g}{K}a(z)(1-f'+2f), \tag{47}$$

where $B(\mathrm{O_2})$ is 2.201×10^2. Since $a(z)$ is a slowly varying quantity, the integration of (47) can be performed approximately as

$$\frac{B(\mathrm{O_2})\,K}{2M_0 g b(z)}(T^{2/3}-T_i^{2/3}) = z-z_i, \tag{48}$$

where

$$b(z) = a(z)(1-f'+2f), \tag{49}$$

and T_i is the temperature at an initial level z_i.

Provided we know the particle concentrations of molecular and atomic oxygen at a reference level, then by aid of the relations (37) and (43), we can determine those at any height measured in unit of H_m from the reference level; our knowledge is still in the unit of scale height and not in kilometers.

Now, we can derive the variation of $\chi(z)$ with respect to $\sigma_m(z)$: $\sigma_m(z)$ may be regarded as $n(O_2, z)H_m(z)$ approximately, viz.

$$\sigma_m(z) = H_m(z)\, n(O_2, z), \tag{50}$$

which, taking account of $H_m(z) = \frac{\mathfrak{H}_m(z)}{a(z)}$ and (44), can be written as:

$$\sigma_m(z)a(z) = n(O_2, z)\, \mathfrak{H}_m(z). \tag{51}$$

Then the equation for $\mathfrak{H}(z)$ can be obtained, viz.

$$\chi^2 + (A - 2c\lambda_m)\chi - c\lambda_m = 0, \tag{52}$$

where

$$\lambda_m = \frac{\sigma_m(z)}{\mathfrak{H}_m n(O, z)}. \tag{53}$$

The solution of (52) can be obtained as follows:

$$\chi = c\lambda_m - \frac{A}{2} + \left[\left(c\lambda_m - \frac{A}{2}\right)^2 + c\lambda_m\right]^{\frac{1}{2}}. \tag{54}$$

It can be easily shown that to adopt $\log_e \sigma_m(z)$ or $\log_e \tau_m(z)$ as a measure of height, as have been made in § 3, has the same meaning as to measure the height in the unit of H_m. Hence, it will readily be made to express any value of $\sigma_m(z)$ or $\tau_m(z)$ in terms of height measured in the unit of H_m from the reference level.

To push our calculation further we must determine where the reference level is to be taken, and must fix $\log_e \tau_m(z)$. For this purpose, let us discuss a few reliable observational facts.

(i) Attempts for the determination of the electron collision frequency in the E layer were made by Baily and Martyn (**25**), and their calculations on the interaction of radio waves led to the value 2×10^5 per sec. The cross section of elastic collision of slow electron with atomic oxygen was evaluated by Yamanouchi (**26**) as $2.41\times10^{-15}\text{cm}^2$. Assuming the same order of magnitude for both the molecular oxygen and nitrogen, $NT^{1/2}$ in this level becomes $1.33\times10^{14}\text{cm}^{-3}\ \text{deg}^{\frac{1}{2}}$, corresponding to $\nu = 2.0\times10^5$ per sec.

(ii) The sporadic E ionization appears frequently about 10 km below the maximum level of the E layer; it is well known that they are in a non-uniform

state, and have the semi-transparent property for radio waves. G. J. Phillips (12) deduced from the fading observations by using the method of S. N. Mitra (27) that at a height of about 100 km the E layer had an irregular structure in which the smallest size of irregularity is about 200 m. The maximum level of the E layer is supposed to be at a height of 110 km or slightly above. Hence, the irregularity deduced by Phillips may be considered to correspond to that of the sporadic E ionization; the minimum dimension of irregularity of the sporadic E ionization may be supposed to be 200 m. From this fact it can be said that turbulent motions of the air are occurring in the region of the sporadic E. The velocity of the eddy system with the minimum dimension is nearly equal to the mean velocity of the gas-kinetic motion in the surrounding gases. If the state of turbulence persists to a dimension of 200 m., the Reynolds number of the eddies associated with this dimension must be as great as about 1000. On the other hand, the Reynolds number may be described by

$$R = 2.88\frac{VL}{V_0}\pi\sigma^2 N(z) ,$$

where V and L are the velocity and the dimension of the eddy system under consideration respectively, $\pi\sigma^2$ the mean cross section for the elastic collision of gas particles and V_0 the mean velocity of gas particles in the surrounding. If, for example, R were taken to be 1000, which might well be the case, and the value of σ^2 were assumed to be $3.0\times10^{-16}\mathrm{cm}^2$, in the case in which the minimum dimension L equals to $2.0\times10^4\mathrm{cm}$, regarding V as V_0, the total particle concentration $N(z)$ at the level where the sporadic E ionization is occurring would be deduced to be $1.84\times10^{13}\mathrm{cm}^{-3}$. It would be concluded, therefore, that the level of this total particle concentration should be situated about 10 km below the maximum level of the E layer.

(iii) It can be shown that the formation of the D layer is attributed to the ionization of atomic oxygen by the scattered radiation produced in the ionosphere with the aid of the solar visible radiation, whose energy of the quantum is 9.48 eV or in wavelength 1302Å. As is well known, the absorption coefficient appropriate to nitrogen near this wavelength is so small that the field of this scattered radiation is scarcely affected by absorption of nitrogen. But the scattering will be cut down by absorption of molecular oxygen in the lower boundary of the ionosphere. Thus, the field of this scattered radiation has a fairly sharp boundary. Because the absorption coefficient of molecular oxygen for this radiation is supposed to be about $3.47\times10^{-19}\mathrm{cm}^2$, it corresponds to the level defined by

$$\tau_{1302\text{Å}} = 3.47\times10^{-19}\,\sigma_m(z) \simeq 1 , \quad \text{i. e. } \sigma_m(z) \simeq 2.88\times10^{18}\mathrm{cm}^{-2},$$

or $\log_e \tau_m(z) \simeq 4.00$. It may be supposed that the maximum level of the D layer is

situated at this level. Therefore, $\log_e \tau_m(z) \simeq 4.00$ must be about 15 or 20 km below the maximum level of the E layer.

No serious inconsistencies exist among these three facts. Therefore, we shall take the level of $NT^{1/2} \simeq 1.33\times10^{14}\mathrm{cm}^{-3}\,\mathrm{deg}^{\frac{1}{2}}$ as the reference level, whose height will be denoted by z_0.

Now, we shall evaluate $\log_e \tau_m(z)$ at the reference level, and we shall determine the physical state at that level. For our purpose, we make use of equation (54). If we rewrite $c\lambda_m(z)$ of (53) contained in (54), by using (31), it follows that

$$c\lambda_m(z) = \left(\frac{3c\varepsilon_V(\mathrm{O}_2)\,M_0 g}{K}\right)\frac{\sigma_m(z)}{\varepsilon D(z)}\,\frac{W_1(\mathrm{O}_2|\mathrm{O})}{T}\,, \tag{55}$$

where $\dfrac{\sigma_m(z)}{\varepsilon D(z)}$ is a known function for any value of $\log_e \tau_m(z)$, $\dfrac{W_1(\mathrm{O}_2|\mathrm{O})}{T}$ is a function of temperature only, and the remaining quantities are constants. Thus, $c\lambda_m(z)$ depends on T with respect to the parameter of $\log_e \tau_m(z)$. $\dfrac{A}{2}$ in (54) is, as is defined by (44),

$$\frac{A}{2} = \frac{1+\frac{\eta}{2}}{4(1+\eta)}(1-f')\,, \tag{56}$$

where f' is known for any value of $\log_e \tau_m(z)$. Thus the right-hand side of equation (54) depends on T by taking $\log_e \tau_m(z)$ as a parameter. On the other hand, the left-hand side of equation (54), $\chi(z)$, becomes, when (31) and (3) are taken into account,

$$\chi(z) = \frac{3\varepsilon_V(\mathrm{O}_2)\,NT^{1/2}}{1+\eta}\,\frac{1}{\varepsilon D(z)}\,\frac{W_1(\mathrm{O}_2|\mathrm{O})}{T^{1/2}} - \frac{1+\frac{\eta}{2}}{1+\eta}\,. \tag{57}$$

This is, also, a function of temperature for each value of $\log_e \tau_m(z)$.

And $NT^{1/2} = 1.33\times10^{14}$. In general, assuming $NT^{1/2}$ to be an appropriate constant, except for the non-conceivable value in the concerning region of the atmosphere, T and χ for any $\log_e \tau_m(z)$ can be found from the rewritten equation of (54) : inserting (55), (56) and (57) into (54) it can be reduced to

$$\begin{aligned}\frac{3\varepsilon_V(\mathrm{O}_2)\,NT^{1/2}}{1+\eta}\,\frac{1}{\varepsilon D(z)}\,\frac{W_1(\mathrm{O}_2|\mathrm{O})}{T^{1/2}} - \frac{1+\frac{\eta}{2}}{1+\eta} &= \frac{3c\varepsilon_V(\mathrm{O}_2)\,M_0 g}{K}\,\frac{\sigma_m(z)}{\varepsilon D(z)}\,\frac{W_1(\mathrm{O}_2|\mathrm{O})}{T} \\ &- \frac{1+\frac{\eta}{2}}{4(1+\eta)} + \left[\left(\frac{3c\varepsilon_V(\mathrm{O}_2)\,M_0 g}{K}\,\frac{\sigma_m(z)}{\varepsilon D(z)}\,\frac{W_1(\mathrm{O}_2|\mathrm{O})}{T} - \frac{1+\frac{\eta}{2}}{4(1+\eta)}\right)^2\right. \\ &\left. + \frac{3c\varepsilon_V(\mathrm{O}_2)\,M_0 g}{K}\,\frac{\sigma_m(z)}{\varepsilon D(z)}\,\frac{W_1(\mathrm{O}_2|\mathrm{O})}{T}\right]^{1/2}. \end{aligned} \tag{58}$$

From (58), T corresponding to any $\log_e \tau_m(z)$ can be found. χ for any obtained

value of T can be determined by using (57). Thus, under the condition that $NT^{1/2} \simeq 1.33\times10^{14}$, T-diagram with $\log_e \tau_m(z)$ as a parameter is given in Fig. 4. A similar treatment is, of course, possible for the case when N is a constant.

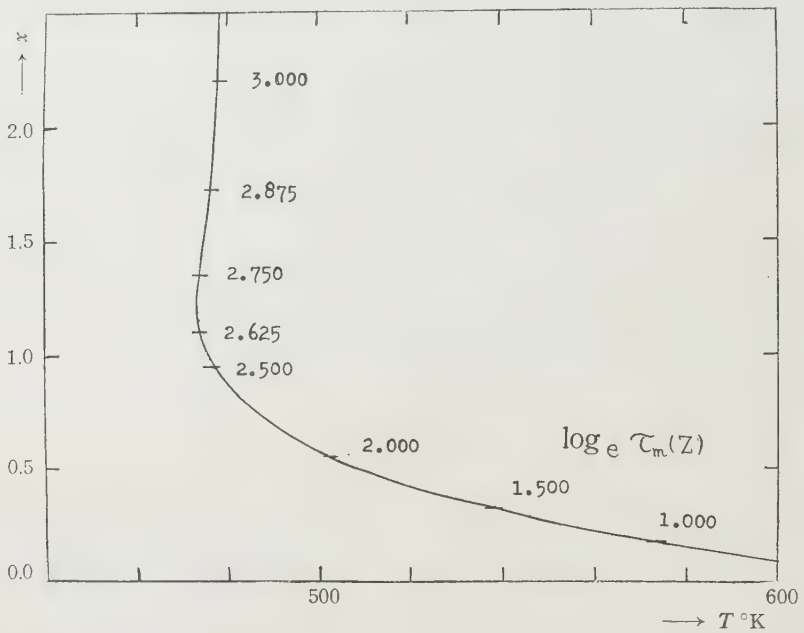

Fig. 4. The solution of (58) with $\log_e \tau_m(z)$ as a parameter.

Now, we must determine to what place in the $T-\chi$ diagram the reference level is to be located. To do this, selection is made so that the results of our computation are self-consistent: if we take a $(T-\chi)$ pair corresponding to one of $\log_e \tau_m(z)$, $n(\mathrm{O}, z)$ and $n(\mathrm{O}_2, z)$ appropriate for it can easily be obtained from (3) and (31). For the other $\log_e \tau_m(z)$ than the selected $\log_e \tau_m(z)$, $n(\mathrm{O}, z)$ and $n(\mathrm{O}_2, z)$ are found by the relations (37) and (43). Making allowance for (42), we examine whether the condition is satisfied for every value of $\log_e \tau_m(z)$. Such successive approximations can readily approach to a self-consistent selection of $\log_e \tau_m(z)$. The result is that $\log_e \tau_m(z) \simeq 2.625$. It may be significant in view of energy consideration that the point $\log \tau_m(z) \simeq 2.625$ in Fig. 4 expresses the minimum of temperature.

Table 5

$\log_e \tau_m(z_0) = 2.625,$	$A = -0.0363,$
$\log_{10} D(z_0) = \bar{6}.9365,$	$n(\mathrm{O}, z_0) = 7.28\times10^{11},$
$\log_{10} \varepsilon D(z_0) = \bar{18}.6438,$	$n(\mathrm{O}_2, z_0) = 7.88\times10^{11},$
$\log_{10} \sigma_m(z_0) = 17.8728,$	$N(z_0) = 6.13\times10^{12},$
$T(z_0) = 474\ K,$	$a(z_0) = 1.37,$
$\chi(z_0) = 1.10,$	$\mathfrak{H}_m(z_0) = 12.56$ km.,
$f' = 1.12,$	$H_m(z_0) = 9.16$ km.,

The physical state at the reference level may be expressed by the following quantities. Be the difference of $\log_e \tau_m(z)$ between arbitrary adjacent levels, and let Δz be the difference of height between these levels. Numerical computation is made with the step $\Delta \log_e \tau_m(z) = 0.5$. Equation (38) can be approximated as

$$\frac{\Delta \log_e \tau_m(z)}{\Delta z} = -\frac{1}{\bar{H}_m}.$$

When $\Delta \log_e n(z)$ is taken sufficiently small, $\bar{H}_m$ may be considerably accurately replaced by the mean value of H_m between two levels concerned. With this approximation, (37) becomes

$$\frac{\Delta \log_e n(O_2, z)}{\Delta \log_e \tau_m(z)} = 1.$$

It follows then that

$$n(O_2, z+\Delta z) = n(O_2, z)\, e^{\Delta \log_e \tau_m(z)},$$

and it can, in general, be said that

$$n(O_2, z) = n(O_2, z_0) \exp\left[\log_e \tau_m(z) - \log_e \tau_m(z_0)\right].$$

Similarly, it yields from (43) that

$$\frac{\Delta \log_e n(O, z)}{\Delta \log_e \tau_m(z)} = \frac{1-\bar{f}'}{2},$$

and

$$n(O, z) = n(O, z_0)\, e^{\sum \frac{1-\bar{f}'}{2} \Delta \log_e \tau_m(z)}, \tag{60}$$

where $\bar{f}'$ stands for the mean value of f' in each interval, and $\sum$ replaces the integration for each interval.

Making use of (58) and (59) $n(O, z)$ and $n(O_2, z)$ at each value of $\log_e \tau_m(z)$ can be derived. As is seen from (59), $n(O, z)$ exhibits a maximum or minimum at the place where $1-f' = 0$. Inspection of Fig. 2 shows that at the point where $\log_e \tau_m(z) \simeq 1.50$, $1-f'$ steps into the negative side from the positive side, and at the point where $\log_e \tau_m(z) \simeq 4.50$, $1-f'$ changes sign. The former corresponds to a maximum, and the latter corresponds to a minimum.

$\chi(z)$ at each level can be obtained. Further calculation of $a(z)$ by (44) and $b(z)$ by (49) can be made.

From the known value of $n(O, z)$ and the relation (34), each value of $W_1(O_2|O)$ is found. $T(z)$ at each level can readily be seen. If (46) be transformed into

$$\frac{K\bar{T}(z)}{M_0 g \bar{b}(z)} \Delta \log_e W_1(O_2|O) = \Delta z, \tag{61}$$

where $\bar{T}(z)$ and $\bar{b}(z)$ are the mean values of $T(z)$ and $b(z)$ between the two levels

considered, the difference of height between any adjacent levels can be found. The local scale height $H = \dfrac{KT}{Mg}$ as a gradient of the total particle concentration is known at each level. The computations described above are given in Table 6 according to sequence of reduction:

Qv can be obtained from the dissociative equilibrium (20), with the result:

$$Qv = 4.28 \times 10^{-18} \mathrm{cm^3\ sec^{-1}}, \tag{62}$$

which is in general in agreement with Bates (**14**), who considered several cases other than oxygen.

Now, as is seen in Fig. 2, f and f' become very small when $\log_e \tau_m(z) < -1.50$: the gradients of $\varepsilon D(z)$ and $D(z)$ with height become then very small. This means that the dissociative absorption of molecular oxygen does not appreciably affect the dissociating radiation field in the region where $\log_e \tau_m(z) < -1.50$. On the other hand, the particle concentration of molecular oxygen decreases and the temperature rises to about 800°K. Then molecular nitrogen becomes to have a considerable effect upon the loss of gas-kinetic energy. This region corresponds to the region B designated in §4.

We shall now consider this region. $\varepsilon D(z)$ and $D(z)$ together can be approximated to the constant values of $\varepsilon D(\infty)$ and $D(\infty)$ respectively. We must take into account the loss of gas-kinetic energy by molecular nitrogen as well as by molecular oxygen. The equation for thermal equilibrium becomes then

$$\begin{aligned}\frac{1}{3}\varepsilon D(\infty)\, n(\mathrm{O_2},\, z) = {} & \varepsilon_V(\mathrm{O_2})\, W_1(\mathrm{O_2}|\mathrm{O})\, n(\mathrm{O_2},\, z)\, n(\mathrm{O},\, z) \\ & + \varepsilon_V(\mathrm{N_2})\, W_1(\mathrm{N_2}|\mathrm{O})\, n(\mathrm{N_2},\, z)\, n(\mathrm{O},\, z)\,,\end{aligned} \tag{63}$$

and the equation for the dissociative equilibrium (20) is

$$\frac{1}{3} D(\infty)\, n(\mathrm{O_2},\, z) = Qvn(\mathrm{O},\, z)\, n(\mathrm{O},\, z)\,. \tag{64}$$

Inserting (1) and (64) into (63) it yields that

$$\begin{aligned}&\frac{1}{3}\varepsilon D(\infty) - \frac{2}{3}\varepsilon_V(\mathrm{N_2})\, W_1(\mathrm{N_2}|\mathrm{O})\, \frac{D(\infty)}{Qv} \\ &= \left[\varepsilon_V(\mathrm{O_2})\, W_1(\mathrm{O_2}|\mathrm{O}) + 4\varepsilon_V(\mathrm{N_2})\, W_1(\mathrm{N_2}|\mathrm{O})\right] n(\mathrm{O},\, z)\,.\end{aligned} \tag{65}$$

Comparison between (21) and (22) leads to the conclusion that for any conceivable temperature of the ionosphere,

$$\varepsilon_V(\mathrm{O_2})\, W_1(\mathrm{O_2}|\mathrm{O}) \ll 4\varepsilon_V(\mathrm{N_2})\, W_1(\mathrm{N_2}|\mathrm{O})\,,$$

so that the right-hand side of (65) becomes $\varepsilon_V(\mathrm{O_2})\, W_1(\mathrm{O_2}|\mathrm{O})\, n(\mathrm{O},\, z)$, and we have

Table 6

$\log_e \tau_m(z)$	$D(z)$ sec^{-1}	$\varepsilon D(z)$ erg sec^{-1}	$\bar{f}$	$\bar{f}'$	$\log_{10} \frac{n'(O,z)}{n(O,z_0)}$	$\log_{10} \frac{n'(O_2,z)}{n(O_2,z_0)}$	$n(O_2,z)$	$n'(O,z)$	$N(z)$	$x(z)$
−2.50	1.62×10^{-4}	2.34×10^{-16}	0.0654	0.0285	−0.4768	−2.2257	4.69×10^{9}	2.43×10^{11}	7.52×10^{11}	0.0193
−2.00	1.60×10^{-4}	2.26×10^{-16}	0.137	0.129	−0.3716	−2.0086	7.73×10^{9}	3.10×10^{11}	9.68×10^{11}	0.0249
−1.50	1.50×10^{-4}	2.11×10^{-16}	0.231	0.211	−0.2770	−1.7914	1.27×10^{10}	3.85×10^{11}	1.22×10^{12}	0.0331
−1.00	1.35×10^{-4}	1.88×10^{-16}	0.348	0.269	−0.1913	−1.5743	2.10×10^{10}	4.69×10^{11}	1.51×10^{12}	0.0448
−0.50	1.18×10^{-4}	1.58×10^{-16}	0.468	0.334	−0.1120	−1.3571	3.46×10^{10}	5.63×10^{11}	1.86×10^{12}	0.0615
0.00	9.99×10^{-5}	1.25×10^{-16}	0.729	0.541	−0.0397	−1.1400	5.71×10^{10}	6.65×10^{11}	2.28×10^{12}	0.0859
0.50	7.62×10^{-5}	8.68×10^{-17}	1.071	0.757	0.0113	−0.9229	9.42×10^{10}	7.48×10^{11}	2.71×10^{12}	0.126
1.00	5.22×10^{-5}	5.08×10^{-17}	1.416	0.952	0.03768	−0.7057	1.55×10^{11}	7.95×10^{11}	3.16×10^{12}	0.195
1.50	3.24×10^{-5}	2.50×10^{-17}	1.627	1.144	0.04292	−0.4885	2.56×10^{11}	8.04×10^{11}	3.69×10^{12}	0.318
2.00	1.83×10^{-5}	1.11×10^{-17}	1.557	1.221	0.02725	−0.2714	4.22×10^{11}	7.76×10^{11}	4.44×10^{12}	0.544
2.50	9.94×10^{-6}	5.09×10^{-18}	1.160	1.121	0.00328	−0.05428	6.96×10^{11}	7.34×10^{11}	5.68×10^{12}	0.948
2.625	8.70×10^{-6}	4.40×10^{-18}	1.160	1.121	0.00000	0.00000	7.88×10^{11}	7.29×10^{11}	6.13×10^{12}	1.082
3.00	5.68×10^{-6}	2.85×10^{-18}	0.620	1.184	−0.00981	0.1629	1.15×10^{12}	7.12×10^{11}	7.87×10^{12}	1.611
3.50	3.14×10^{-6}	2.09×10^{-18}	0.372	1.396	−0.02975	0.3800	1.89×10^{12}	6.80×10^{11}	1.15×10^{13}	2.780
4.00	1.56×10^{-6}	1.74×10^{-18}	0.187	1.112	−0.07273	0.5971	3.12×10^{12}	6.16×10^{11}	1.74×10^{13}	5.060
4.50	8.96×10^{-7}	1.58×10^{-18}	0.266	0.775	−0.08490	0.8143	5.14×10^{12}	5.99×10^{11}	2.75×10^{13}	8.580
5.00	6.08×10^{-7}	1.38×10^{-18}	0.431	0.754	−0.06051	1.0314	8.48×10^{12}	6.33×10^{11}	4.43×10^{13}	13.374
5.50	4.17×10^{-7}	1.12×10^{-18}	0.674	0.747	−0.03384	1.2486	1.40×10^{13}	6.74×10^{11}	7.19×10^{13}	20.736
6.00	2.87×10^{-7}	7.96×10^{-19}			−0.00636	1.4657	2.30×10^{13}	7.18×10^{11}	1.17×10^{14}	32.092

$a(z)$	$T(z)$ °K	$D(z)\,n(O_2,z)$ $cm^{-3}sec^{-1}$	$\varepsilon D(z)\,n(O_2,z)$ erg $cm^{-3}sec^{-1}$	$\bar{a}(z)$	$\bar{b}(z)$	$\Delta\log_e W_1(O_2\|O)$	Δz km	$\Delta z - z_0$ km	H_m km	H km
1.47	845	7.63×10^{5}	1.10×10^{-6}	1.52	1.67	0.2751	7.24	48.57	14.48	28.8
1.57	817.5	1.24×10^{6}	1.74×10^{-6}	1.64	1.87	0.2864	6.52	41.33	13.04	28.2
1.70	789	1.91×10^{6}	2.69×10^{-6}	1.75	2.19	0.3127	5.87	34.81	11.74	27.3
1.79	759	2.84×10^{6}	3.95×10^{-6}	1.83	2.61	0.3564	5.38	28.94	10.76	25.9
1.87	727.5	4.09×10^{6}	5.47×10^{-6}	1.96	3.15	0.4009	4.78	23.56	9.56	23.7
2.06	693	5.69×10^{6}	7.13×10^{-6}	2.24	4.32	0.4819	3.99	18.78	7.98	22.9
2.42	655	7.17×10^{6}	8.17×10^{-6}	2.52	6.01	0.5966	3.35	14.79	6.70	22.0
2.62	611.5	8.10×10^{6}	7.89×10^{-6}	2.52	7.26	0.7202	3.09	11.44	6.18	19.8
2.42	563	8.30×10^{6}	6.40×10^{-6}	2.17	6.75	0.7776	3.30	8.35	6.60	18.0
1.92	518	7.72×10^{6}	4.67×10^{-6}	1.69	4.88	0.7234	3.93	5.05	7.86	15.9
1.45	480	6.92×10^{6}	3.55×10^{-6}	1.41	3.09	0.1375	1.12	1.12	9.43	14.9
1.36	473.5	6.87×10^{6}	3.47×10^{-6}	1.29	2.83	0.4126	3.59	0.00	10.15	14.4
1.21	453	6.52×10^{6}	3.27×10^{-6}	1.16	1.23	0.2643	5.08	−3.59	10.15	13.4
1.11	441	5.94×10^{6}	3.95×10^{-6}	1.06	0.369	0.0872	5.50	−8.67	11.00	13.2
1.00	438	4.87×10^{6}	5.42×10^{-6}	0.976	0.256	0.0655	5.91	−14.17	11.82	12.9
0.950	433.5	4.62×10^{6}	8.13×10^{-6}	0.939	0.711	0.1893	6.08	−20.08	12.15	12.8
0.928	427	5.16×10^{6}	1.17×10^{-5}	0.923	1.02	0.2768	6.05	−26.15	12.10	12.5
0.918	415	5.83×10^{6}	1.56×10^{-5}	0.915	1.47	0.4002	5.88	−32.20	11.76	12.00
0.912	398.5	6.60×10^{6}	1.83×10^{-5}					−38.08		

$$\frac{1}{3}\varepsilon D(\infty)-\frac{2}{3}\varepsilon_V(\mathrm{N_2})\ W_1(\mathrm{N_2}|\mathrm{O})\frac{D(\infty)}{Qv}=\varepsilon_V(\mathrm{O_2})\ W_1(\mathrm{O_2}|\mathrm{O})\ n(\mathrm{O},z)\,. \tag{66}$$

The left-hand side of (66) depends on the temperature only through $W_1(\mathrm{N_2}|\mathrm{O})$. Defining $F(T)$ as follows:

$$F(T)=\frac{\varepsilon D(\infty)\ Qv}{2D(\infty)\ \varepsilon_V(\mathrm{N_2})\ W_1(\mathrm{N_2}|\mathrm{O})}, \tag{67}$$

which is a function of temperature only, we find, from (66),

$$n(\mathrm{O},z)=\frac{1}{3}\frac{\varepsilon D(\infty)}{\varepsilon_V(\mathrm{O_2})\ W_1(\mathrm{O_2}|\mathrm{O})}\frac{F(T)-1}{F(T)}\,. \tag{68}$$

From (68), $n(\mathrm{O},z)$ can be expressed in terms of a function of temperature only.

Since $n(\mathrm{O_2},z)$ is negligible compared with $n(\mathrm{O},z)$, (3) and (4) can be replaced by the approximate relations

$$N(z)=\left(1+\frac{\eta}{2}\right)n(\mathrm{O},z)\,, \tag{69}$$

and

$$M(z)=\frac{1+\frac{7}{8}\eta}{1+\frac{\eta}{2}}M_0\,. \tag{70}$$

Making transformation of the equation for the hydrostatic equilibrium (5) by the similar treatment to that described in the case of the region A, we obtain

$$G(T)\frac{dT}{dz}=\frac{1+\frac{7}{8}\eta}{1+\frac{1}{2}\eta}\frac{M_0 g}{K}, \tag{71}$$

where

$$G(T)=\frac{B(\mathrm{N_2})}{3(F-1)\ T^{1/3}}+\frac{B(\mathrm{O_2})}{3T^{1/3}}-1\,, \tag{72}$$

$$B(\mathrm{N_2})\simeq 2.835\times 10^2\,,$$

and

$$B(\mathrm{O_2})\sim 2.201\times 10^2\,.$$

It is possible from (71) to find step of height Δz corresponding to the step of temperature ΔT at any height, viz.

$$\frac{K}{M_0 g}\frac{1+\frac{1}{2}\eta}{1+\frac{7}{8}\eta}\overline{G(T)}\ \Delta T=\Delta z\,, \tag{73}$$

where $G(T)$ is some mean value of $G(T)$ in each step. Provided that ΔT is

taken sufficiently small, we get Δz at each height with good approximation. We have divided into the 5°K step where the temperature gradient is steep, and the 1°K step where the temperature gradient is very small. We determine successively upward from the level $\log_e \tau_m(z) = -1.50$ so far as the solution is obtainable. Thus, computation was possible up to about 165 km above the reference level. But above 100 km from the reference level we must take into account the gain of gas-kinetic energy by the ionization of the F_1 and F_2 layers. On this account, we must simultaneously make allowance for the problem of the distribution of electron concentration. We shall leave over the problem above 100 km from the reference level without further consideration. The main quantities of the computed results are tabulated in Table 7 according to the sequence of reduction.

Table 7

T °K	$F(T)$	$G(T)$	$W_1(O_2, O)$	$n(O, z)$	$n(O_2, z)$	$N(z)$	$(z-z_0)$ km	$\varepsilon D(z)\, n(O_2, z)$ erg cm^{-3}sec^{-1}	$D(z)\, n(O_2, z)$ cm^{-3}sec^{-1}
780	4.329	10.054	5.396×10^{-16}	3.58×10^{11}	1.01×10^{10}	1.12×10^{12}	34.81	2.36×10^{-6}	1.64×10^{6}
800	3.342	11.249	6.628×10^{-16}	2.65×10^{11}	5.55×10^{9}	8.23×10^{11}	42.35	1.29×10^{-6}	9.01×10^{5}
820	2.601	13.144	8.128×10^{-16}	1.90×10^{11}	2.86×10^{9}	5.84×10^{11}	50.98	6.67×10^{-7}	4.63×10^{5}
840	2.041	16.396	9.782×10^{-16}	1.31×10^{11}	1.35×10^{9}	3.98×10^{11}	61.38	3.15×10^{-7}	2.19×10^{5}
860	1.614	22.899	1.185×10^{-15}	8.06×10^{10}	5.14×10^{8}	2.44×10^{11}	75.17	1.20×10^{-7}	8.34×10^{4}
880	1.286	41.148	1.407×10^{-15}	3.97×10^{10}	1.25×10^{8}	1.20×10^{11}	96.69	2.91×10^{-8}	2.02×10^{4}
900	1.038	323.87	1.676×10^{-15}	5.55×10^{9}	2.44×10^{6}	1.67×10^{10}	165.78	5.69×10^{-10}	3.95×10^{2}

We shall evaluate the vertical distribution of the optical depth with respect to the ionizing radiation of atomic oxygen, which is of importance in the consideration of the ionization of the E region. Let $K_a \simeq 4.5\times10^{-18}\text{cm}^2$ be the absorption coefficient of the ionizing radiation for atomic oxygen. Let $\sigma_a(z)$ be the number of atomic oxygen in a column of unit base above a height z, viz.

$$\int_z^\infty n(O, z')\, dz' = \sigma_a(z)\,, \tag{74}$$

and further let $\tau_a(z)$ be this optical depth. Then, according to definition, it follows that

$$K_a\sigma_a(z) = \tau_a(z)\,. \tag{75}$$

$\tau_a(z)$ and $n(O, z)$ are reproduced in Fig. 7. $T(z)$ is expressed in Fig. 5. $n(O_2, z)$ and $N(z)$ are indicated in Fig. 6. $\varepsilon D(z)\, n(O_2, z)$ and $D(z)\, n(O_2, z)$ in Fig. 3 are plotted by using the results of computation. They show together to exhibit a flat maximum and a gradual change in the E region.

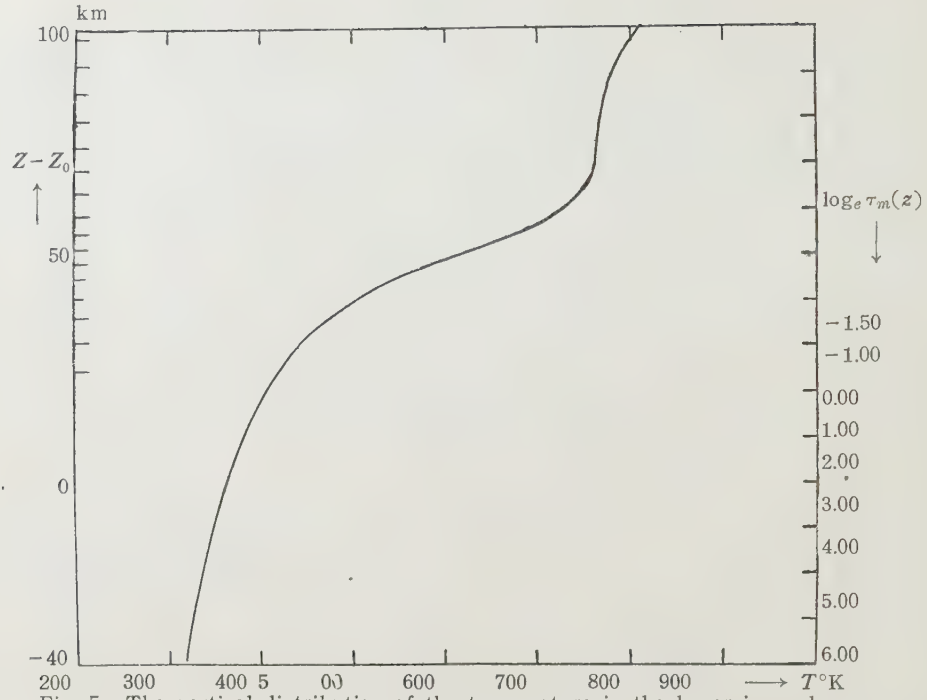

Fig. 5. The vertical distribution of the temperature in the lower ionosphere.

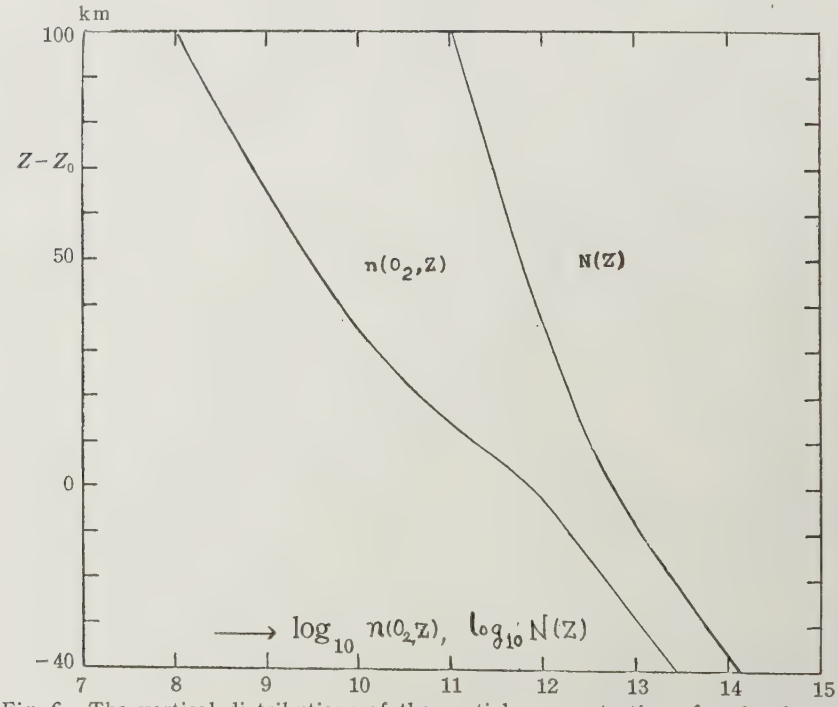

Fig. 6. The vertical distributions of the particle concentration of molecular oxygen and of the total particle concentration in the lower ionosphere.

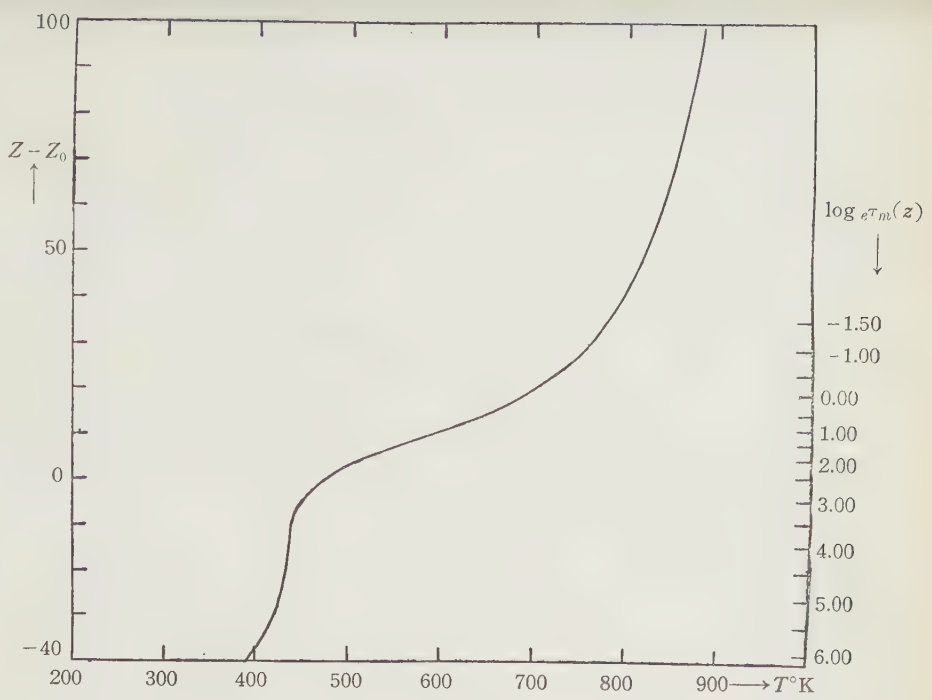

Fig. 5 The vertical distribution of the temperature in the lower ionosphere.

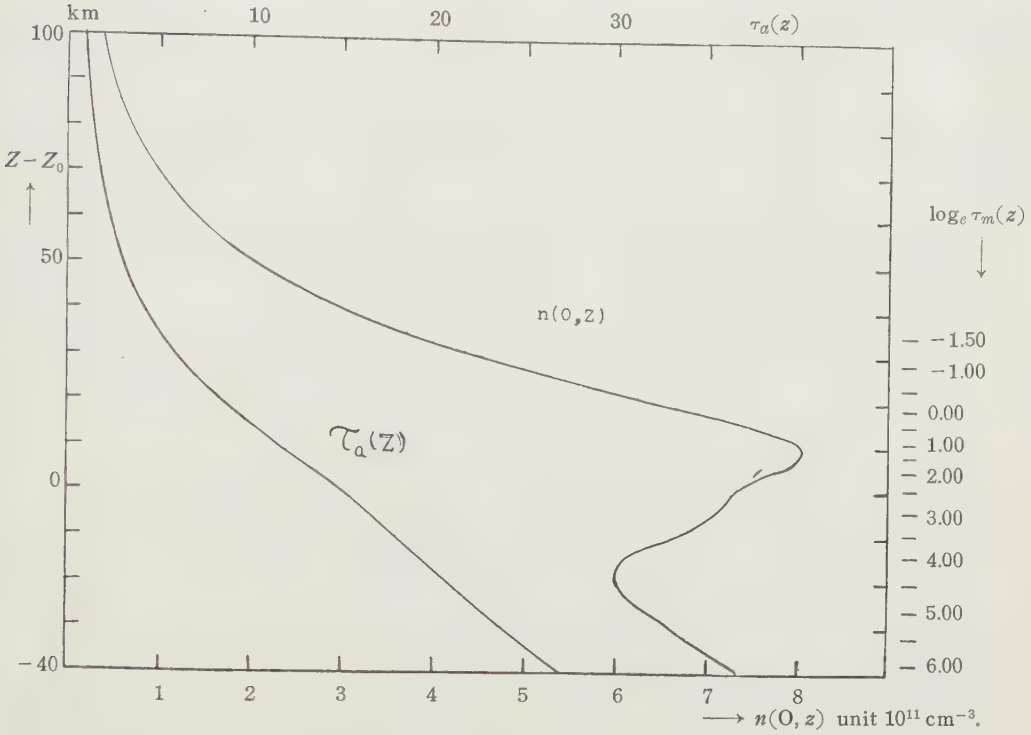

Fig. 7. The vertical distribution of the particle concentration of atomic oxygen and the optical depth $\tau_a(z)$ of the ionizing radiation in the lower ionosphere.

6. Discussion, conclusion and further problem

There is a considerable difference between the distribution of pressure from rocket measurements (28) and the theoretical results derived here. This might be partially attributed to the deduction of pressure from rocket measurements. On the other hand, our result depends on the distribution of the dissociative absorption coefficient with wavelength. There would be some uncertainties on the coefficient over some range from the Schumann-Runge limit toward Herzberg region. The accuracy of information on the coefficient in this range of wavelength is of importance in determining the temperature and the particle concentrations in the region below 100 km, which is in close connection with the free oscillation of the atmosphere as has been suggested by Pekeris (29). Thus, it will be desirable to re-examine closely the dissociative absorption coefficient in this range. As the absorption in the Schumann-Runge region, where the values of its coefficient are to be correct, takes a significant part for our results above the reference level, the results in this region may be reliable. To determine the actual height of the reference level, we must make

allowance for the ionization of the E region. It would, however, nót be unnatural to locate the reference level at the height 120 km from the ground level.

There seems to be a resemblance between the temperature curve in Fig. 5 and the $\varepsilon D(z)$-curve described in logarithmic scale in Fig. 1. This resemblance may be interpreted as follows: As is seen from Fig. 7, $n(O, z)$ in the E region varies slowly. Hence it may be written approximately as:

$$\varepsilon D(z) \propto W_1(O_2|O),$$

and assuming only the principally variable part of the right-hand side, it follows that

$$\log_e \varepsilon D(z) \propto -\frac{B(O_2)}{T^{1/3}},$$

from which the resemblance mentioned above may be accounted for.

A study is made of the effect of the ionization in the F regions on the gain of gas-kinetic energy. As far as its effect is negligible, the temperature in the F_1 region remains constant. Inspection of $\varepsilon D(z)\, n(O_2, z)$ in Table 7 gives a knowledge on the variation of the dissociative gain of gas-kinetic energy with height. On the other hand, to determine the gain by ionization, we must know the mechanism for the ionization in the F regions. It may be supposed that the line emissions from the solar corona are attributed to the ionization associated with the formation of both the F_2 and F_1 layers together. Any possibility of unobservable ionization that has been suggested by Bates(**7**) might not be considered. Hence, we tentatively assume that the average gain to the gas-kinetic energy seems likely to be about 13 eV photon. It does not seem unerasonable to assume that the electron recombination coefficient is 3×10^{-10} cm^3 sec^{-1} for the F_2 layer and 7×10^{-9} cm^3 sec^{-1} for the F_1 layer. The maximum electron concentration is 1.8×10^6 cm^{-3} for the F_2 layer and 3.3×10^5 cm^{-3} for the F_1 layer. Thus, the gain of gas-kinetic energy will be about 2.0×10^{-8} erg cm^{-3} sec^{-1} for the F_2 layer and about 1.6×10^{-8} erg cm^{-3} sec^{-1} for the F_1 layer. On comparing with $\varepsilon D(z)\, n(O_2\, z)$ in Table 7, it may be said that the gain of gas-kinetic energy made by ionization predominates over the dissociative gain in the F_2 region, but the latter increases rapidly with decreasing height and in the F_1 region the former becomes smaller than the latter. Making allowance for the fact that the scattered ionizing radiation contributes to the formation of the F_1 layer, and that because the F_1 layer lies in great optical depth, the flow of the direct incident radiation to the F_1 level is remarkably dependent upon the solar zenith angle, the true gain due to ionization in the F_1 region will be further reduced from 1.6×10^{-8} erg cm^{-3} sec^{-1}. Summarizing, it may be supposed that in the F_1 region the gain made by ionization has no appreciable effect. Since we cannot avoid the con-

clusion that the diurnal variation of temperature in the F_2 region cannot be great, we shall average the gain by ionization through the day and assume the above value multiplied by 0.3 for the average value. Adding the dissociative gain to it, we get 6.60×10^{-9} erg cm^{-3} sec^{-1} for the total gain of gas-kinetic energy, for which a temperature of 1250°K is appropriate.

We must now investigate the effect of thermal conduction in the ionosphere, which was suggested by Bates as one of the most effective losses of gas-kinetic energy. There is in the E region an abrupt temperature gradient of about 10 K°/km. The temperature in the F_1 region remains constant unless a great amount of heat is transported by thermal conduction to the F_1 level from the upper region. The gain or loss of heat by thermal conduction Q is expressed by

$$Q=\frac{d}{dz}\left(\lambda\frac{dT}{dz}\right), \tag{76}$$

where (**30**)

$$\lambda=\frac{75}{64\sigma^2}\left(\frac{K^3T}{\pi M_0}\right)^{\frac{1}{2}}\simeq 5.16\times10^2\,T^{1/2}. \tag{77}$$

First, we shall begin with the evaluation of the thermal conduction in the E region. We shall inquire about a place that the temperature changes most abruptly, at the height 10 km above the reference level, where $\log_e\tau_m(z)$ ranges from 1.00 to 1.50. Inserting (47) and (77) into (76), it yields that

$$\begin{aligned}\frac{d}{dz}\left(\lambda\frac{dT}{dz}\right)&=\frac{d}{dz}\left[\frac{3M_0g\lambda}{KB(O_2)}\,T^{1/3}b(z)\right],\\&\simeq 1.33\times10^{-3}\,\frac{d}{dz}\left[T^{5/6}b(z)\right].\end{aligned} \tag{78}$$

Substituting the values appropriate for that level, we obtain

$$\frac{d}{dz}\left(\lambda\frac{dT}{dz}\right)\simeq 8.84\times10^{-8}\ \text{erg cm}^{-3}\,\text{sec}^{-1}. \tag{79}$$

In comparing with $\varepsilon D(z)\,n(O_2,z)$ given in Table 6, taking account of the factor 1/3 for no detectable diurnal variation of temperature, the effect of thermal conduction becomes only about 1/27 of the dissociative gain at the level concerned. The thermal equilibrium in the E region is little affected by the thermal conduction.

We shall discuss briefly the effect of thermal conduction for the F_1 region. The temperature of the F_2 level, at about 300 km height, would be about 1250°K, as has been considered before. Assuming that the temperature between the F_1 and F_2 levels rises linearly, its gradient would become 3.5°K/km. Taking into consideration that the isothermal region of 900°K is found below the F_1 level, the flow of heat by thermal conduction from the upper region will be stopped there. In consequence, the

temperature rises in some degree making a temperature gradient and then heat flows to lower region. It seems relevant to suppose that above the F_2 level the temperature gradient is extremely small, so that the heat generation to affect the F_1 region must take place at the region between F_1 and F_2. The maximum gain of gas-kinetic energy in this region will be about 6.60×10^{-9} erg cm^{-3} sec^{-1}, as has been studied just before. If it were supposed, as an upper limit, that all the gain in this region flows into the F_1 level by the thermal conduction, and that the heat flow is spent on raising the temperature in a range of altitude as great as one scale height there, the gain by the thermal conduction in the F_1 level would be about 1.65×10^{-8} erg cm^{-3} sec^{-1}. As is seen from $\varepsilon D(z)\, n(O_2, z)$ given in Table 7, this is comparable with the dissociative gain at 100 km above the reference level. Since the quantities quoted in the above discussion would be regarded as an extremely over-estimated, the thermal conduction from the upper region would not have an appreciable effect on the thermal equilibrium in the region below the F_1 level, but it might have some effect in the region above the F_1 level.

It is interesting that the particle concentrations $n(O, z)$ and $n(N_2, z)$ deduced from the present research are favourable for the formation of the F_1 and F_2 layers.

We have shown that the temperature of F_2 region will be about 1250°K. It must be said that this temperature is intimately connected with the degree of the stirring of the atmosphere: If the stirring of the atmosphere halts at a certain height, the atmosphere above it will be distributed by a diffusive equilibrium and the relative populations of molecular nitrogen to atomic oxygen there will reduce to a much small value. As regards the loss of gas-kinetic energy, the most effective process would not be the vibrational excitation by impacts of atomic oxygen, which have been quoted in the present work, but it would become the excitation to the metastable states ^1D and ^1S of atomic oxygen by electron impacts (31). Inspection of the ionospheric observational data suggests that the stirring of the atmosphere ceases, if possible, between the F_1 and F_2 layers. Would it be the case, the temperature at great height would rise up over 2000°K. However, the existence of N_2^+–spectra at great height seems to show that this is not the case. In the F_2 region, the temperature is about 1250°K. It is not meaningless to add here that the observed intensity of the oxygen line 5577Å in the night sky light cannot be accounted for by the excitation by the electron impact.

In conclusion, it may be emphasized that the quantitative results of the present work depend much on the accuracy of information about the dissociative absorption coefficients of molecular oxygen. By the future establishment of these molecular data, the properties of the upper atmosphere could be researched theoretically with sufficient accuracy.

The author wishes to express his sincere thanks to Prof. M. Hasegawa for the facilities he has given in this institution, and to Prof. S. Miyamoto for the valuable advices and discussions.

REFERENCES

1. O. R. WULF and L. S. DEMING, *Terr. Mag.*, **41** (1936), 299; **43** (1938), 283.
2. R. C. MAJUNDAR, *Indian J. Phys.*, **12** (1938), 75.
3. H. RAKSHIT, *Indian J. Phys.*, **21** (1947), 57.
4. R. PENNDORF, *J. Geo. Res.*, **54** (1949); *Phys. Rev.*, **77** (1950), 561.
5. S. CHAPMAN, *Phil. Mag.*, **10** (1930), 367.
6. H. E. MOSES and TA-YOU WU, *Phys. Rev.*, **83** (1951), 109.
7. D. R. BATES, *Proc. Phys. Soc.* **64** (1951), 805.
8. S. CHAPMAN, *Proc. Roy. Soc.* A. **132** (1931), 353.
9. G. HERZBERG and L. HERZBERG, *Nature*, **161** (1948), 283.
10. G. CHAPMAN, *Proc. Phys. Soc.* **64** (1951), 833.
11. K. F. CHACKETT, F. A. PANETH and E. J. WILSON, *Nature*, **164** (1949), 128.
12. J. A. RATCLIFFE, *Nature*, **167** (1951), 626.
13. G. HERZBERG, *Molecular Spectra and Molecular Structure, Diatomic Molecules*, (2nd ed., 1950, Van Nostrand) Chap. VII, p. 447.
14. D. R. BATES, *Mon. Not.*, **111** (1951), 363.
15. G. HERZBERG, *ibid.* Chap. VII, pp. 400–402.
16. H. S. W. MASSEY, *Nagative Ion*, (2nd ed., 1950, Cambridge Univ. Press) Chap. III, sect. 3.2.
17. G. HERZBERG, *ibid.* Chap. VII, p. 446.
18. G. E. GIBSON and N. S. BAYLISS, *Phys. Rev.*, **44** (1933), 188.
G. E. GIBSON, O. K. RICE and N. S. BAYLISS, *Phys. Rev.*, **44** (1933), 193.
19. L. VEGARD, *Geofys. Pub. Oslo*, **9** (1932), No. 11.
20. S. ROSSELAND, *Theoretical Astrophysics*, (1936, Clarendon Press, Oxford) Chap. XVII, p. 244.
21. L. SPITZER, *Ap. J.* **109** (1949), 337.
22. G. HERZBERG, *ibid*, Table 39, p. 552, 560.
23. G. HERZBERG, *ibid*, Chap. V, p. 278–279.
24. J. M. JACKSON and N. F. MOTT, *Proc. Roy. Soc.* A, **137** (1932), 703.
25. V. A. BAILY and D. F. MARTYN, *Wireless Engr.* **12** (1935), 122.
26. T. YAMANOUCHI, *Nippon Sugaku-Buturigaku-Kaisi*, **17** (1943), 5.
27. S. N. MITRA, *Proc. I.E.E.*, **96**, Part III (1949), 441.
28. N. BEST, R. HAVENS and H. LAGOW, *Phys. Rev.*, **71** (1947), 915.
29. C. L. PEKERIS, *Proc. Roy. Soc.* A, **158**, (1937) 650.
30. S. CHAPMAN and T. G. COWLING, *The Mathematical Theory of Non-uniform Gases*, (1939, Cambridge Univ. Press) Chap. 10, p. 169.
31. T. YAMANOUCHI, *Saikin Buturigaku no Syomondai*, (1948, Iwanami Syoten, Tokyo) p. 135 (in Japanese).

MEMOIRS OF THE COLLEGE OF SCIENCE, University of Kyoto, Series A,
Vol. XXVII, No. 2, Article 2, 1954

ON THE MAGNETIC ANOMALIES AND THEIR SECULAR VARIATIONS AROUND MAEYAMA ON SIMABARA PENINSULA*†

BY

Wasiro YODA

Geophysical Institute, Kyoto University

(*Received April 13, 1954*)

ABSTRACT

A magnetic survey was carried out by the writer in 1923 at 87 points around volcanic mountain Maeyama near the Volcano Unzen, and the magnetic anomalies due to the mountain were examined. Since then, 29 years had passed without any remarkable volcanic or seismic activity on Simabara Peninsula, until in 1952 when the writer carried out a second survey in the same district. A careful comparison of the results of these two surveys shows that the magnetic anomalies have remained almost unchanged, but that the magnetization of the mountain block appears to have slightly progressed.

1. Introduction

As magnetic anomalies due to volcanic mountains have had definite influence on the results of general magnetic surveys in several cases in our country, it is practically necessary to examine the nature of the magnetization of volcanic mountains. Further, some relations between great earthquakes and geomagnetic anomalies have been suspected by geophysicists since early times in Japan. If some tectonic as well as volcanic earthquakes were caused by changes in the states of magma underground, then these changes would definitely be accompanied by a variation in temperature, which would give rise to the time variation of the local magnetic anomaly. In this respect, time variation observations of the magnetic field have been taken to be a necessary factor in the study of seismology, especially for the purpose of possible earthquake prediction. In this connexion, there arise two fundamental problems: 1) What is the nature of the magnetization of volcanic mountains? and 2) How does the magnetic anomaly vary with time, not only when the earthquake or the volcano is active, but also when it is calm?

---

* Contribution to Geophysical Papers dedicated to Prof. M. Hasegawa on his sixtieth birthday.

† A more detailed description on the survey will be published in Japanese in "Tikyu Buturi" Vol. 9 in the near future.

As early as 1904, A. Tanakadate suggested in his report (1) "A Magnetic Survey of Japan" that magnetic anomalies observed at a few points around Mt. Fuji could be well explained by assuming that the mountain was magnetized almost in the direction of magnetic meridian. In 1923, the present writer performed exact measurments of 3 magnetic components at 87 points around a volcanic hill, Maeyama, located on Simabara Peninsula and concluded that the hill was magnetized by induction almost in the same direction as that of the magnetic field. (The report (2) was published in Japanese.) It has now been established by many workers (3) in this field that the volcanic mountain is induced almost in the same direction as that of the present magnetic field.

We now have many reports on the existence of anomalous magnetic variations in cases of volcanic eruptions and of large earthquakes. Among them two reports (the one by T. Nagata (4) about anomalous magnetic variation immediately before and after the formation of a volcano, Usu in Hokkaido and the other by T. Rikitake (5) about the magnetic observations around Mt. Mihara, an active volcano) are of special importance inasmuch as they elucidate the relation between volcanic eruption and time variation of the magnetic field.

A somewhat remarkable earthquake occurred near Simabara Peninsula in December, 1922. But since the magnetic survey around Maeyama Hill, there had been neither earthquakes nor volcanic eruptions to consider. As it seemed interesting to the writer to examine how the anomaly of the magnetic field suffered from change during this period, he undertook a survey again in 1952 in the same region as before. From the results (6) of magnetic observations by the Hydrographic Office in Japan in 1922, 1933, 1942 and 1950 at the writer's station No. 3, it can be seen that there were no remarkable fluctuations in the magnetic secular variation in this region throughout the period.

The writer's second survey was carried out from August 2 to September 8 in 1952 in cooperation with Mr. T. Ogawa and Mr. M. Yasuhara. A magnetometer of the Hydrographic Office type was used and the three elements were measured at as nearly the same points as those selected in the former case. Among the 58 stations, 39 were within a few meters, 17 were within ten meters and only 2 were about fifty meters from the former stations. The name numbers of these stations which succeeded the former ones are expressed in Fig. 5.

2. The corrections

a) *Instrumental corrections.* Instrumental corrections were obtained through a comparison carried out on Oct. 7–8, 1952 at the Kakioka Geomagnetic Observatory, and were 6′.90 for the declination, −1′.20 for the dip, and none for the horizontal intensity.

b) *Correction of daily variation.* For this purpose, the records of daily changes at the Aso Observatory ($\lambda = 131°00'$ E, $\varphi = 32°54'$ N) were utilized, as the Aso Observatory is situated on nearly the same latitude as that of Maeyama. The deficiencies of those records were supplied by hourly values observed at the Kakioka Observatory ($\lambda = 140°10'$ E, $\varphi = 36°15'$ N).

c) *Correction of day-to-day variation.* As the day-to-day variations at Kakioka and Aso were very similar, it can be assumed that the value at Maeyama may also be similar to them. To apply these corrections the writer takes values at 0 o'clock on August 16 as standard, when it was most quiet. By this correction, the secular variation and the magnetic disturbances such as magnetic storms can be eliminated.

d) *Reduction to the central point* ($\lambda = 130°20'.50$ E, $\varphi = 32°46'.00$ N). In order to know the exact anomalies, it is necessary to reduce the values from each point to those at a standard point. The writer selected it at the nearly central point of Maeyama. According to the Geographical Survey Institute, the distributions of each magnetic element in the whole Japan at 1950.0 are as follows (**7**):

$$\left.\begin{aligned} D &= 6°\,51'.8 + 23'.58\,\Delta\varphi - 6'.48\,\Delta\lambda - 0'.420\,(\Delta\varphi)^2 + 0'.162\,\Delta\varphi\Delta\lambda - 0'.672\,(\Delta\lambda)^2\,, \\ H &= 29898^{\gamma} - 400^{\gamma}.3\,\Delta\varphi - 72^{\gamma}.2\,\Delta\lambda - 9^{\gamma}.75\,(\Delta\varphi)^2 + 12^{\gamma}.88\,\Delta\varphi\Delta\lambda - 3^{\gamma}.48\,(\Delta\lambda)^2\,, \\ I &= 50°\,43'.9 + 72'.48\,\Delta\varphi - 9'.36\,\Delta\lambda - 0'.744\,(\Delta\varphi)^2 - 0'.138\,\Delta\varphi\Delta\lambda + 0'.066\,(\Delta\lambda)^2\,, \end{aligned}\right\} \quad (1)$$

where $\Delta\varphi = \varphi - 37°$ $\Delta\lambda = \lambda - 138°$ (in degree), and west in D, north in H, and down in I, are taken as positive respectively.

From these, we can take the following rates at the central point:

$$\frac{\partial D}{\partial \varphi} = 0'.431\,, \qquad \frac{\partial D}{\partial \lambda} = 0'.052\,,$$

$$\frac{\partial H}{\partial \varphi} = -6^{\gamma}.94\,, \qquad \frac{\partial H}{\partial \lambda} = -1^{\gamma}.22\,,$$

$$\frac{\partial I}{\partial \varphi} = 1'.33\,, \qquad \frac{\partial I}{\partial \lambda} = -0'.163 \qquad \text{(per minute)}.$$

These can be reduced to the values at the central point.

e) *Altitude correction.* Of the altitude correction, the writer applies Dr. Tanakadate's formula (**8**). From the above expressions (1), we obtain the three elements and the three components at that point as follows:

$$D = 5°\,20'.1\,, \qquad H = 32182^{\gamma}\,, \qquad I = 46°\,35'.0\,,$$

$$N = 32043^{\gamma}\,, \qquad W = 2992^{\gamma}\,, \qquad V = -34012^{\gamma}\,,$$

where we take north, west and upward as positive for the components respectively. The obtained rates of the three elements are as follows:

Table I. Corrected observed values.

No.	D	H	I	F	N	W	V
1	5° 35.5	32318	46° 39.9	47092	32164	3149	34253
3	26.0	32287	21.5	46783	32142	3057	33856
4	32.6	32393	26.0	47001	32241	3129	34056
5	20.5	32388	17.0	46864	32247	3015	33872
6	34.4	32200	32.4	46813	32048	3127	33980
8	17.6	32234	23.4	46733	32096	2974	33837
9	26.2	32325	30.7	46970	32180	3063	34078
10	21.8	31920	47° 11.7	46975	31780	2984	34464
11	23.8	32239	46° 33.9	46891	32096	3032	34050
13	11.7	32376	20.3	46894	32243	2932	33925
14	37.4	32614	45° 57.7	46917	32456	3196	33727
15	45.0	32571	46° 12.2	47061	32407	3263	33969
16	52.6	32532	06.7	46927	32361	3331	33820
17	57.2	32457	06.5	46816	32282	3366	33738
18	53.7	32247	12.4	46596	32077	3312	33635
19	6° 07.6	32196	45° 55.5	46285	32012	3436	33253
20	5° 46.3	32345	46° 02.8	46603	32181	3253	33549
21	17.6	32456	45° 57.9	46693	32318	3994	33568
22	33.0	32358	46° 08.0	46694	32206	3130	33664
23	20.4	32496	45° 50.4	46646	32355	3024	33463
31	33.9	32369	46° 07.9	46708	32217	3139	33674
32	52.5	32365	23.3	46922	32195	3313	33973
33	42.0	32564	04.1	46936	32403	3234	33802
34	41.8	32463	07.4	46837	32303	3222	33761
35	44.8	32586	12.9	47092	32422	3263	33998
36	53.4	32383	05.0	46686	32212	3323	33629
37	6° 16.0	32410	38.0	47200	32217	3538	34312
38	5° 55.8	32505	08.6	46915	32331	3358	33829
39	44.3	32362	19.8	46867	32200	3236	33901
40	15.5	32328	25.1	46894	23192	2963	33970
41	28.3	32444	14.0	46903	32296	3094	33871
42	22.5	32495	17.9	47033	32353	3044	34002
43	21.9	32445	09.3	46838	32303	3034	33780
44	09.0	32522	45° 43.0	46580	32391	2919	33346
45	11.1	32178	46° 41.7	46915	32046	2908	34141
46	29.7	32312	26.3	46888	32163	3094	33976
47	21.0	32263	32.0	46898	32122	3008	34038
48	26.0	32343	29.7	46982	32197	3063	34076
49	26.5	32298	26.4	46869	32153	3063	33964
55	44.1	32296	08.2	46607	32134	3227	33604
57	55.9	32364	20.1	46874	32191	3345	33909
58	53.9	32338	17.9	46805	32166	3323	33838
59	53.1	32323	20.9	46826	32153	3314	33881
60	6° 01.3	32421	11.8	46839	32243	3401	33805
61	5° 50.5	32439	16.1	46926	32271	3302	33908
62	45.7	32545	15.1	47064	32380	3267	33999
63	33.3	32575	13.2	47080	32422	3153	33992
64	6° 05.1	32455	18.7	46986	32272	3440	33976
65	5° 42.9	32625	09.2	47097	32463	3249	33966
66	13.7	32792	45° 49.5	47058	32656	2988	33750
67	00.0	32867	48.9	47156	32742	2865	33816
68	05.4	32781	47.5	47013	32651	2908	33699
69	31.0	32689	58.0	47029	32537	3143	33811
70	11.3	32436	46° 22.6	47014	32303	2933	34034
71	44.6	32435	31.3	47138	32272	3246	34205
72	51.9	32476	25.6	47115	32306	3319	34135
74	48.4	32353	25.4	46934	32187	3273	34002
77	48.6	32384	18.4	46879	32217	3278	33896
mean	5° 38.0	32430.3	46° 13.95	46885.9	32275.3	3183.4	33858.8

$$\frac{\partial D}{\partial z} = -0'.205\,, \quad \frac{\partial H}{\partial z} = -15^{\gamma}.5\,, \quad \frac{\partial I}{\partial z} = -0'.085 \qquad \text{(per km.)}.$$

Therefore the magnitude of each element will increase as the points will descend.

3. The distribution of the corrected observed values

The corrected elements and their components are shown in Table I, where the vertical component is reckoned positive downward.

The differences of each value from some standard one are set forth in Figs. 1 to 3. At a glance we can see that they are very similar to the corresponding figures obtained at 1923.50 (**9**).

In the first place, the distribution of the declination, as expressed in Fig. 1, may be divided into four quadrants by two lines drawn in the N–S and E–W directions. In the NE and SW quadrants they are in general smaller than the mean value, while in the SE and NW quadrants they are greater.

In the distribution of the horizontal intensity as shown in Fig. 2, in the northern and the southern parts they are greater than the mean and in the western and eastern parts they are smaller. In the distribution of the inclination or dip as shown in Fig. 3, at the northern and southern feet of the mountain they are smaller than the mean and in the distant and the eastern parts they are greater. In the case of

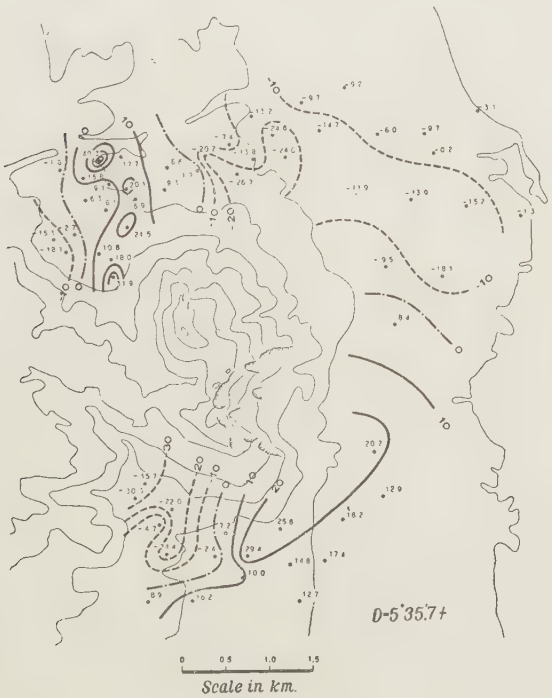

Fig. 1. Distribution of the declination at 1952.63.

Fig. 2. Distribution of the horizontal intensity at 1952. 63.

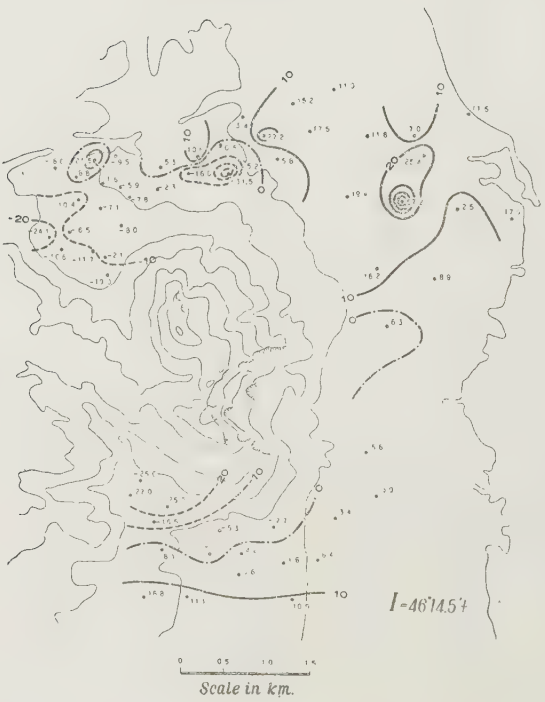

Fig. 3. Distribution of the inclination at 1952. 63.

inclination, the result seems to be apparently contradictory to the general feature described by the buried magnetic body underneath the mountain, but it must be supposed that the positive anomalic region of dip must be enclosed within the inner boundary of the observed region.

From these three figures we can suppose that the mountain block of Maeyama is magnetized almost parallel to the earths' magnetic field.

4. The magnetic anomalies of the first and second order

Two observations about the general magnetic distribution in the whole Japanese region at 1950.0 have been made, namely, one by the Geographic Survey Institute (G. S. I.) and the other by the Hydrographic Office (H. G. O.) (**10**). The differences between the writer's observed values and the results derived from the above general expressions, may be seen as the anomalies of the earth magnetism. They can be called the magnetic anomalies of the first order and they include both the regional anomalies in the western Kyushu and local ones around Maeyama. The values of each element at the central point deduced from two general expressions are as follows:

	D	*H*	*I*	*F*	*N*	*W*	*V*
G. S. I.	5° 24′. 2	32228$^{\gamma}$	46° 38′. 1	46935$^{\gamma}$	32085$^{\gamma}$	3035$^{\gamma}$	34122$^{\gamma}$
H.G.O.	5° 24. 4	32327	46° 20. 9	46832	32183	3046	33885

From this table it will be seen that the values of D are nearly equal, but the values of H and I are different, and the three components also are different from each other. Therefore two different anomalies of the first order will be obtained, but the differences are common to every point. We cannot distinguish how much of it will belong to regional and how much to local, so that we cannot judge which will be better. While the survey of the H. G. O. included the writer's point No. 3, that of G. S. I. did not have a point in Simabara Peninsula. Consequently the values in the expression of H. G. O. include values in Simabara Peninsula, but those of G. I. S. do not. Therefore the expressions of G. I. S. are more convenient in ascertaining regional and local anomalies. The differences between the observed values and those of G. S. I. are called magnetic anomalies of the first order.

In these anomalies we can see that the western components are in general superior to the eastern ones, so we can understand that the anomalies of the first order contain both local anomalies due to Maeyama and regional anomalies which include general western components. The regional anomalies are perhaps due to the great mountain block called Unzen, situated to the westward of Maeyama. If this is true, for obtaining the local anomalies due to Maeyama it is nescessary to get rid of the regional anomalies which are also perhaps predominant in the south and upward components.

Table II. Anomaly of the second order.

No.	D''	H''	I''	N''	W''	V''
1	−0.2	90	1.8	79	−10	131
3	−9.7	59	−16.6	57	−102	−266
4	−3.1	165	−12.1	156	−30	−66
5	−15.2	160	−21.1	162	−144	−250
6	−1.3	−28	−5.7	−37	−32	−142
8	−18.1	6	−14.7	11	−185	−285
9	−9.5	97	−7.4	95	−96	−44
10	−13.9	−308	33.6	−305	−175	342
11	−11.9	11	−4.2	11	−127	−72
13	−24.0	148	−17.8	158	−227	−197
14	1.7	386	−40.4	371	37	−395
15	9.3	343	−25.9	322	104	−153
16	16.9	304	−31.4	276	172	−302
17	21.5	229	−31.6	197	207	−384
18	18.0	19	−25.7	−8	153	−487
19	31.9	−32	−42.6	−73	277	−869
20	10.6	117	−35.3	96	94	−573
21	−18.1	228	−40 2	233	−165	−554
22	−2.7	130	−30.1	121	−29	−458
23	−15.3	268	−47.7	270	−135	−659
31	−1.8	141	−30.2	132	−20	−458
32	16.8	137	−14.8	110	154	−149
33	6.3	336	−34.0	318	65	−320
34	6.1	235	−30.7	218	63	−361
35	9.1	358	−25.2	337	104	−124
36	17.7	155	−33.1	127	164	−493
37	40.3	182	−0.1	132	379	190
38	20.1	277	−29.5	246	199	−293
39	8.6	134	−18.3	115	77	−221
40	−20.2	100	−13.0	107	−196	−152
41	−7.4	216	−24.1	211	−65	−251
42	−13.2	267	−20.2	268	−115	−120
43	−13.8	217	−28.8	218	−125	−342
44	−26.7	294	−55.1	306	−240	−776
45	−24.6	−50	3.6	−39	−251	19
46	−6.0	84	−11.8	78	−65	−146
47	−14.7	35	−6.1	37	−151	−84
48	−9.7	115	−8.4	112	−96	−46
49	−9.2	70	−11.7	68	−96	−158
55	8.4	68	−29.9	49	68	−518
57	20.2	136	−18.0	106	186	−213
58	18.2	110	−20.2	81	164	−284
59	17.4	95	−17.2	68	155	−241
60	25.6	193	−26.3	158	242	−317
61	14.8	211	−22.0	186	143	−214
62	10.0	317	−23.0	295	108	−123
63	−2.4	347	−24.9	337	−6	−130
64	29.4	227	−19.4	187	281	−146
65	7.2	397	−28.9	378	90	−156
66	−22.0	564	−48.6	571	−171	−372
67	−35.7	639	−49.2	657	−294	−306
68	−30.3	553	−50.6	566	−251	−423
69	−4.7	461	−40.1	452	−16	−311
70	−24.4	208	−15.5	218	−226	−88
71	8.9	207	−6.8	187	87	83
72	16.2	248	−12.5	221	160	13
74	12.7	125	−12.7	102	114	−120
77	12.9	156	−19.7	132	119	−226

Fig. 4. Horizontal anomaly
1952.63
(The second order)
Full line: Observed.
Broken line: Calculated.

Fig. 5. Vertical anomaly
1952.63
(The second order)
Full line: Observed.
Broken line: Calculated.

But since these components are unknown numerically and moreover their values are supposed to be nearly equal at all points, they will be overlooked for a while. But the declination and westward components of the anomalies due to Maeyama must be symmetrical with respect to the magnetic axis which nearly runs from south to north. Therefore the regional anomlies due to Unzen block can be avoided by obtaining differences between the observed values and their means. Now, it is not unreasonable to consider that the differences from their means in D and W, and differences from G. I. S. in H, I, N, and V are the anomalies due to Maeyama in general, and they are called anomalies of the second order and tabulated in Table II. Figs. 4 and 5 represent their horizontal and vertical vectors respectively in full lines. The horizontal vectors denote elegantly the magnetic lines of Maeyama which is magnetized approximately in the same direction as the earth's magnetic field. The vertical anomalies are almost all directed upward as if they agreed with the direction of the magnetic field due to Maeyama, supposed to be magnetized by the induction of the earth field as explained hereafter.

5. The local anomalies due to Maeyama

As stated above, it is very natural that the magnetic anomalies of the second order should be due to Maeyama, but it is impossible to calculate the magnetic field numerically unless the geometrical form of Maeyama is known. In the previous case, the writer explained the distributions of anomalies through the assumption of a simple magnet underneath Maeyama. But in this case he considered that it is more reasonable to assume that the form of Maeyama is an oblate spheroid whose minor axis is vertical. Königsberger (11) obtained the formulae to express the magnetic anomalies due to an oblate spheroid, by the induction of the field. Taking the x axis to magnetic north, y axis to east and z axis to downward, as positive, the formulae are as follows:

$$\frac{\Delta H}{H} = \frac{K}{1-KL} 3V_0 \tan I \frac{xz}{\sqrt{X}\sqrt{a^2+\nu}(b^2+\nu)} + \frac{K}{1-KM} 3V_0 \left[\frac{\sqrt{a^2+\nu}\, x^2}{\sqrt{X}(b^2+\nu)^2} - \frac{1}{2e^3}\left(\tan^{-1} l - \frac{l}{1+l^2}\right)\right],$$

$$\Delta D = \frac{K}{1-KL} 3V_0 \tan I \frac{yz}{\sqrt{X}\sqrt{a^2+\nu}(b^2+\nu)} + \frac{K}{1-KM} 4V_0 \frac{\sqrt{a^2+\nu}}{\sqrt{X}(b^2+\nu)^2} xy,$$

$$\frac{\Delta V}{V} = \frac{K}{1-KL} 3V_0 \left[\frac{z^2}{\sqrt{X}(a^2+\nu)^{\frac{3}{2}}} - \frac{l-\tan^{-1} l}{e^3} \right] + \frac{K}{1-KM} \frac{3V_0}{\tan I} \frac{xz}{\sqrt{X}\sqrt{a^2+\nu}(b^2+\nu)},$$

where $2a$ is the length of the minor axis, $2b$ the length of the major axis and K magnetic susceptibility, and

$$e = \sqrt{b^2 - a^2},\quad u = \frac{e}{a},\quad l = \frac{e}{\sqrt{a^2+\nu}},\quad V_0 = \frac{4}{3}\pi ab^2,$$

$$X = (x^2+y^2+z^2)^2 + (b^2-a^2)\left[(b^2-a^2) - 2\{z^2-(x^2+y^2)\}\right],$$

$$\nu = \frac{1}{2}\left(x^2+y^2+z^2-a^2-b^2+\sqrt{X}\right),$$

$$L = -4\pi\frac{1+u^2}{u^3}\left(u-\tan^{-1}u\right),$$

$$M = -4\pi\frac{1+u^2}{u^2}\tan^{-1}\frac{u^3}{1+u^2}.$$

It is reasonable to obtain the magnitudes and azimuths of a and b, and the position of the centre of the spheroid by the method of least squares, as there are many observed values. Since, however, the procedure is too complicated, the writer has used the following method.

In the first place, the writer assumed that the centre of the spheroid coincided with the geographic centre of Maeyama which had been taken as the central point in § 2. In the second place the writer selected ten of the observed stations which seemed to be normal, and compared the magnetic susceptibilities K deduced respectively from ΔH, ΔD and ΔV through varying the major axis b or the minor axis a and the depth of the centre of the spheroid. That is, (1) asuming that a is 0.7 km and the centre of the spheroid is on the sea level, the writer finds that the probable value of b is 1.4 km in the case when the three values of K obtained from ΔH, ΔD and ΔV are nearly equal, (2) assuming that b is 1.4 km and the upper surface of the spheroid almost coincides with the mountain surface whose top is supposed to be at 700 meters high above the sea level, it seems that the probable value of a is 0.7 km. One representative of these considerations is given in Fig. 6. It was concluded that the major axis $2b$ is equal to 2.8 km, minor axis $2a$ to 1.4 km and the centre of the spheroid is at the sea level.

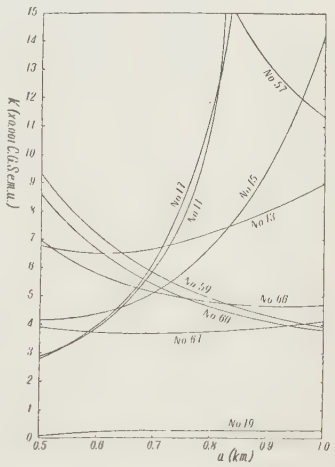

Fig. 6. Relation between the magnetic susceptibility (K) by H and the minor axis (a) of the oblate spheroid, at 10 stations.

With these values, the anomalies of each point are calculated, but in this case the x-axis is taken to the magnetic north which is westward by about 5°30′ to the geographical north.

Comparing the observed and calculated values, magnetic susceptibilities are obtained, the extreme values having been rejected, and the means for each element are as follows:

from	ΔD	$K_D = 0.0051$	C. G. S. E. M. U.	(33)
	ΔH	$K_H = 0.0062$	„	(30)
	ΔV	$K_V = 0.0058$	„	(26)

The numbers in the bracket denote the numbers of stations which were utilized. The mean value of K is 0.0057 C. G. S. E. M. U. and it is supposed to be the probable value. The calculated anomalies of each point with this value of K, are represented in Figs. 4 and 5 with dotted lines. But ΔN and ΔW in the figures refer to the geographical north and west. We can observe a fairly good agreement in both arrows. That is to say, it seems that the writer's assumptions are not incorrect.

6. The secular variations of the magnetic anomalies due to Maeyama

The writer's principal purpose of the second survey was to study the secular variations of the magnetic anomalies during the past twenty-nine years.

The variations of each observed element between 1923. 50 and 1952. 63 are tabulated in Table III, and expressed in Figs. 7, 8, 9 and 10. Their means are obtained from them excluding six points which have extreme values.

What part of them may be attributed to regional and what part of them may be attributed to local anomalies must be ascertained. The writer applied the following method.

The magnetic anomalies in both epochs must be due to the mountain block of Maeyama and other local substances, and any appreciable essential differences of their features have not been recognised. Therefore there must be a simple relation between the deviations of the same element at each point from some standard values which may be different at each epoch. From this reason the writer takes the second order anomalies expressed in Table II as abscissa, and the corresponding values at 1923. 50 as ordinate in Figs. 11, 12 and 13. For convenience, the differences between the observed values and their mean, expressed in the Table IV (**12**) in the previous paper, were used as the latter values. The following equations were obtained for each element, but 8 points for D or H, 13 points for V which have extreme values have been excluded.

$$\text{For } D \quad y = 0.94\,x + 0.'23 \pm 2.'48\,,$$
$$H \quad y = 0.94\,x - 169^{\gamma} \pm 27.^{\gamma}5\,,$$
$$V \quad y = 0.90\,x + 246^{\gamma} \pm 44.^{\gamma}5\,,$$

in minute for D and in γ for H and V. The constant terms in these equations can be considered as the corrections of the mean values which are taken as ordinates. Then the corrected mean values or the standard values at 1923.50 are as follows:

Table III$_1$. Secular variation of the declination (1923.50–1952.63).

No.	D_2 (1952.63)	D_1 (1923.50)	d (D_2–D_1)	$d-d_m$
1	5° 35.5	4° 55.6	39.9	1.7
3	26.0	45.3	40.7	2.5
4	32.6	58.4	34.2	−4.0
5	20.5	41.6	38.9	0.7
6	34.4	5° 00.0	34.4	−3.8
8	17.6	4° 45.8	31.8	−6.4
9	26.2	38.8	47.4	9.2
10	21.8	44.6	37.2	−1.0
11	23.8	44.5	39 3	1.1
13	11.7	39.2	32.5	−5.7
14	37.4	5° 01.8	35.6	−2.6
15	45.0	03.6	41.4	3.2
16	52.6	11.3	41.3	3.1
17	57.2	18.8	38.4	0.2
18	53.7	17.5	36.2	−2.0
19	6° 07.6	29.8	37.8	−0.4
20	5° 46.3	06.9	39.4	1.2
21	17.6	27.5	50.1	11.9
22	33.0	4° 53.7	39.3	1.1
23	20.4	40.7	39.7	1.5
31	33.9	5° 05.8	28.1	−10.1
32	52.5	09.5	43.0	4.8
33	42.0	04.9	37.1	−1.1
34	41.8	08.1	33.7	−4.5
35	44.8	10.6	34.2	−4.0
36	53.4	16.4	37.0	−1.2
37	6° 16.0	02.2	73.8	35.6
38	5° 55.8	07.6	48.2	10.0
39	44.3	4° 58.5	45.8	7.6
40	15.5	58.1	17.4	−20.8
41	28.3	49.6	38.7	0.5
42	22.5	50.4	32.1	−6.1
43	21.9	16.5	65.4	27.2
44	09.0	35.6	33.4	−4.8
45	11.1	24.3	46.8	8.6
46	29.7	50.5	39.2	1.0
47	21.0	45.2	35.8	−2.4
48	26.0	47.9	38.1	−0.1
49	26.5	42.8	43.7	5.5
55	44.1	5° 08.8	35.3	−2.9
57	55.9	08.5	47.4	9.2
58	53.9	12.9	41.0	2.8
59	53.1	08.9	44.2	6.0
60	6° 01.3	17.6	43.7	5.5
61	5° 50.5	14.1	36.4	−1.8
62	45.7	10.9	34.8	−3.4
63	33.3	4° 55.9	37.4	−0.8
64	6° 05.1	31.8	33.3	−4.9
65	5° 42.9	5° 00.9	42.0	3.8
66	13.7	4° 37.1	36.6	−1.6
67	00.0	23.0	37.0	−1.2
68	05.4	31.3	34.1	−4.1
69	31.0	56.2	34.8	−3.4
70	11.3	57.6	13.7	−24.5
71	44.6	5° 08.6	36.0	−2.2
72	51.9	17.3	34.6	−3.6
74	48.4	09.0	39.4	1.2
77	48.6	11.2	37.4	−0.8
			d_m=38.16	

Table III$_2$. Secular variation of the horizontal intensity.

No.	H_2 (1952.63)	H_1 (1923.50)	h (H_2-H_1)	h-h_m
1	32318	31919	399	−34
3	32287	31738	549	116
4	32393	31833	560	127
5	32388	31814	574	141
6	32200	31864	336	−97
8	32234	31849	385	−48
9	32325	31866	459	26
10	31920	31390	530	97
11	32239	31740	499	66
13	32376	31904	472	39
14	32614	32141	473	40
15	32571	32108	463	30
16	32532	32074	458	25
17	32457	32014	443	10
18	32247	31910	337	−96
19	32196	31730	466	33
20	32345	31859	486	53
21	32456	32024	432	−1
22	32358	31918	440	7
23	32496	32084	412	−21
31	32369	32056	313	−120
32	32365	31950	415	−18
33	32564	32165	399	−34
34	32463	32028	435	2
35	32586	32152	434	1
36	32383	31905	478	45
37	32410	31968	442	9
38	32505	32104	401	−32
39	32362	31953	409	−24
40	32328	31782	546	113
41	32444	31988	456	23
42	32495	31985	510	77
43	32445	32015	430	−3
44	32522	32110	412	−21
45	32178	31754	424	−9
46	32312	31966	346	−87
47	32263	31901	362	−71
48	32343	32064	279	−154
49	32298	31945	353	−80
55	32296	31924	372	−61
57	32364	32025	339	−94
58	32338	31874	464	31
59	32323	31913	410	−23
60	32421	32034	387	−46
61	32439	32014	425	−8
62	32545	32155	390	−43
63	32575	32150	425	−8
64	32455	32077	378	−55
65	32625	32221	404	−29
66	32792	32384	408	−25
67	32867	32398	469	36
68	32781	32387	394	−39
69	32689	32062	627	194
70	32436	32018	418	−15
71	32435	31997	438	5
72	32476	32064	412	−21
74	32353	31938	415	−18
77	32384	31925	459	26
			h_m=432.5	

Table III$_3$. Secular variation of the inclination (1923.50–1952.63).

No.	I_2 (1952.63)	I_1 (1923.50)	i (I_2–I_1)	$i-i_m$
1	46° 39.9	46° 52.6	−12.7	0.1
3	21.5	35.8	−14.3	−1.5
4	26.0	39.4	−13.4	−0.6
5	17.0	31.0	−14.0	−1.2
6	32.4	42.9	−10.5	2.3
8	23.4	39.0	−15.6	−2.8
9	30.7	40.0	−9.3	3.5
10	47° 11.7	47° 23.6	−12.9	−0.1
11	46° 33.9	46° 48.7	−14.8	−2.0
13	20.3	35.6	−15.3	−2.8
14	45° 57.7	10.9	−13.2	−0.4
15	46° 12.2	28.5	−16.3	−3.8
16	06.7	16.4	−9.7	3.1
17	06.5	21.2	−14.7	−1.9
18	12.4	05.7	6.7	19.5
19	45° 55.5	16.8	−21.3	−8.5
20	46° 02.8	15.5	−12.7	0.1
21	45° 57.9	06.2	−8.3	4.5
22	46° 08.0	21.7	−13.7	−0.9
23	45° 50.4	03.2	−12.8	0.0
31	46° 07.9	27.2	−19.3	−6.5
32	23.3	34.2	−10.9	1.9
33	04.1	13.7	−9.6	3.2
34	07.4	23.1	−15.7	−2.9
35	12.9	22.9	−10.0	2.8
36	05.0	26.4	−21.4	−8.6
37	38.0	18.3	19.7	32.5
38	08.6	21.4	−12.8	0.0
39	19.8	31.1	−11.3	1.5
40	25.1	35.9	−10.8	2.0
41	14.0	23.3	−9.3	3.5
42	17.9	38.5	−20.6	−7.8
43	09.3	24.7	−15.4	−2.6
44	45° 43.0	07.4	−24.4	−11.6
45	46° 41.7	44.9	−3.2	9.6
46	26.3	33.4	−7.1	5.7
47	32.0	41.5	−9.5	3.3
48	29.7	40.4	−10.7	2.1
49	26.4	29.9	−3.5	9.3
55	08.2	24.7	−16.5	−3.7
57	20.1	22.9	−2.8	10.0
58	17.9	32.4	−14.5	−1.7
59	20.9	35.2	−14.3	−1.5
60	11.8	27.1	−15.3	−2.5
61	16.1	37.3	−21.2	−8.4
62	15.1	29.6	−14.5	−1.7
63	13.2	20.7	−7.5	5.3
64	18.7	27.8	−9.1	3.7
65	09.2	23.2	−14.0	−1.2
66	45° 49.5	06.6	−17.1	−4.3
67	48.9	11.0	−22.1	−9.3
68	47.5	00.9	−13.4	−0.6
69	58.0	09.3	−11.3	1.5
70	46° 22.6	29.0	−6.4	6.4
71	31.3	47.7	−16.4	−3.6
72	25.6	36.0	−10.4	2.4
74	25.4	40.7	−15.3	−2.5
77	18.4	32.6	−14.2	−1.4
			$i_m=-12.83$	

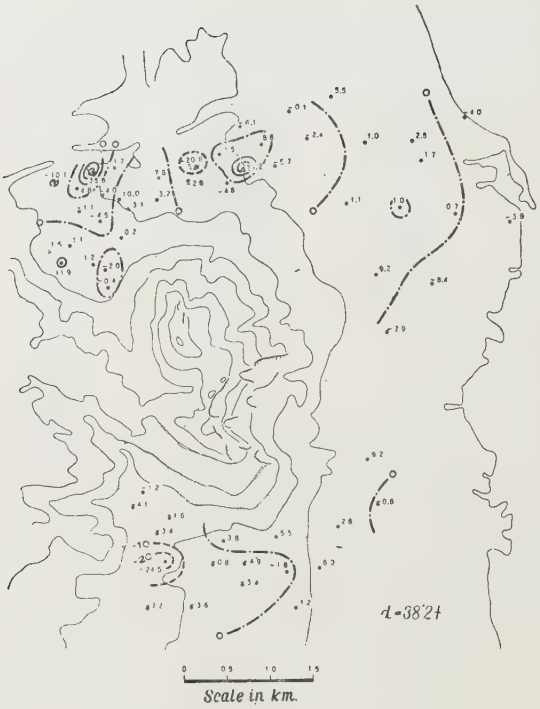

Fig. 7. Secular variation of the declination. (1923.50–1952.63)

Fig. 8. Secular variation of the horizontal intensity. (1923.50–1952.63)

Fig. 9. Secular variation of the inclination.
(1923.50–1952.63)

Fig. 10. Secular variation of the horizontal and the vertical components.
(1923.50–1952.63)

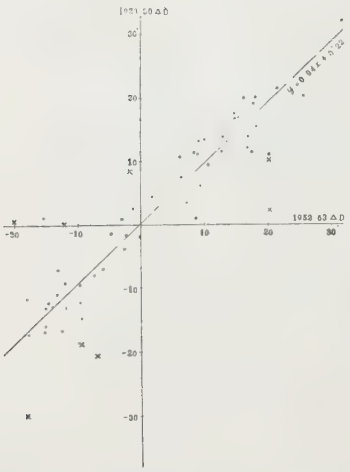

Fig. 11. Relation between the anomalies of the declination at 1952.63 and those at 1923.50.

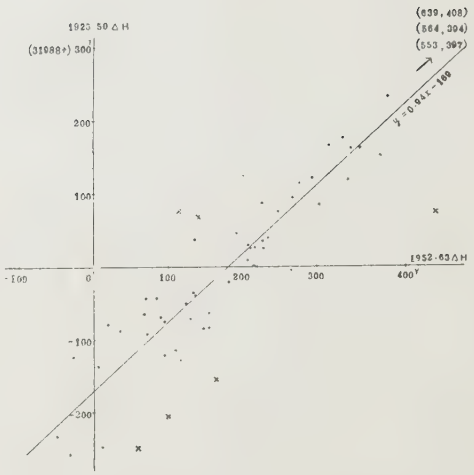

Fig. 12. Relation between the anomalies of the horizontal intensity at 1952.63 and those at 1923.50.

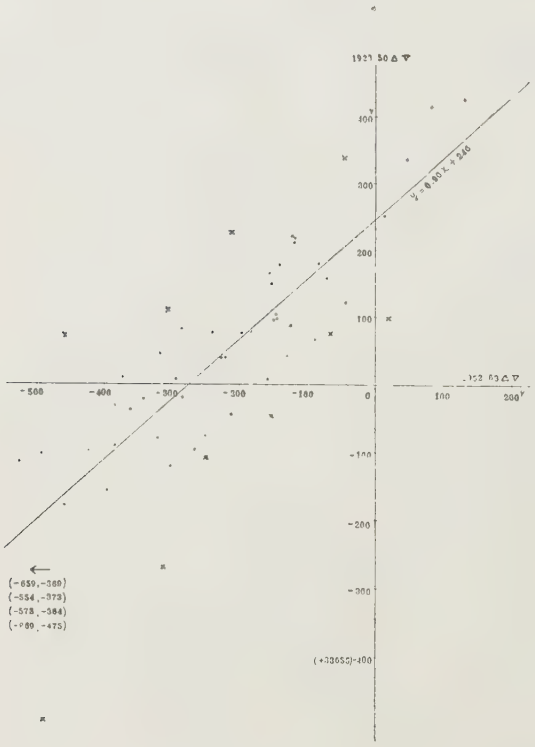

Fig. 13. Relation between the anomalies of the vertical component at 1952.63 and those at 1923.50.

Table IV_1. The variations of the anomalies (D).

No.	1952.63	1933.50	diff.	No.	1952.63	1923.50	diff.
1	−0.2	−2.1	1.9	41	−7.4	−8.1	0.7
3	−9.7	−12.4	2.7	42	−13.2	−7.3	−5.9
4	−3.1	0.7	−3.8	43	−13.8	−41.2	27.4
5	−15.2	−16.1	0.9	44	−26.7	−22.1	−4.6
6	−1.3	2.3	−3.6	45	−24.6	−33.4	8.8
8	−18.1	−11.9	−6.2	46	−6.0	−7.2	1.2
9	−9.5	−18.9	9.4	47	−14.7	−12.5	−2.2
10	−13.9	−13.1	−0.8	48	−9.7	−9.8	0.1
11	−11.9	−13.2	1.3	49	−9.2	−14.9	5.7
13	−24.0	−18.5	−5.5	55	8.4	11.1	−2.7
14	1.7	4.1	−2.4	57	20.2	10.8	9.4
15	9.3	5.9	3.4	58	18.2	15.2	3.0
16	16.9	13.6	3.3	59	17.4	11.2	6.2
17	21.5	21.1	0.4	60	25.6	19.9	5.7
18	18.0	19.8	−1.8	61	14.8	16.4	−1.6
19	31.9	32.1	−0.2	62	10.0	13.2	−3.2
20	10.6	9.2	1.4	63	−2.4	−1.8	−0.6
21	−18.1	−30.2	12.1	64	29.4	34.1	−4.7
22	−2.7	−4.0	1.3	65	7.2	3.2	4.0
23	−15.3	−17.0	1.7	66	−22.0	−20.6	−1.4
31	−1.8	8.1	−9.9	67	−35.7	−34.7	−1.0
32	16.8	11.8	5.0	68	−30.3	−26.4	−3.9
33	6.3	7.2	−0.9	69	−4.7	−1.5	−3.2
34	6.1	10.4	−4.3	70	−24.4	−0.1	−24.3
35	9.1	12.9	−3.8	71	8.9	10.9	−2.0
36	17.7	18.7	−1.0	72	16.2	19.6	−3.4
37	40.3	4.5	35.8	74	12.7	11.3	1.4
38	20.1	9.9	10.2	77	12.9	13.5	−0.6
39	8.6	0.8	7.8				
40	−20.2	0.4	−20.6				

Table IV_2. The variations of the anomalies (H).

No.	1952.63	1923.50	diff.	No.	1952.63	1923.50	diff.
1	90	100	−10	19	−32	−89	57
3	59	−81	140	20	117	40	77
4	165	14	151	21	228	205	23
5	160	−5	165	22	130	99	31
6	−28	45	−73	23	268	265	3
8	6	30	−24	31	141	237	−96
9	97	47	50	32	137	131	6
10	−308	−429	121	33	336	346	−10
11	11	−79	90	34	235	209	26
13	148	85	63	35	358	333	25
14	386	322	64	36	155	86	69
15	343	289	54	37	182	149	33
16	304	255	49	38	277	285	−8
17	229	195	34	39	134	134	0
18	19	91	−72	40	100	−37	137

Continued

No.	1952.63	1923.50	diff.	No.	1952.63	1923.50	diff.
41	216	169	47	62	317	336	−19
42	267	166	101	63	347	331	16
43	217	196	21	64	227	256	−31
44	294	291	3	65	397	402	−5
45	−50	−65	15	66	564	565	−1
46	84	147	−63	67	639	579	60
47	35	82	−47	68	553	568	−15
48	115	245	−130	69	461	243	218
49	70	126	−56	70	208	199	9
55	68	105	−37	71	207	178	29
57	136	206	−70	72	248	245	3
58	110	55	55	74	125	119	6
59	95	94	1	77	156	106	50
60	193	215	−22				
61	211	195	16				

Table IV$_3$. The variations of the anomalies (V).

No.	1952.63	1923.50	diff.	No.	1952.63	1923.50	diff.
1	131	180	−49	41	−251	−324	73
3	−266	−344	78	42	−120	−29	−91
4	−66	−172	106	43	−342	−269	−73
5	−250	−357	107	44	−776	−507	−269
6	−142	−70	−72	45	19	−148	167
8	−285	−163	−122	46	−146	−150	4
9	−44	−125	81	47	−84	−67	−17
10	342	227	115	48	−46	93	−139
11	−72	−88	16	49	−158	−241	83
13	−197	−172	−25	55	−518	−364	−154
14	−395	−406	11	57	−213	−293	80
15	−153	−97	−56	58	−284	−267	−17
16	−302	−369	67	59	−241	−170	−71
17	−384	−338	−46	60	−317	−201	−116
18	−487	−748	261	61	−214	−21	−193
19	−869	−721	−148	62	−123	−26	−97
20	−573	−610	37	63	−130	−205	75
21	−554	−619	65	64	−146	−143	−3
22	−458	−430	−28	65	−156	−82	−74
23	−659	−615	−44	66	−372	−238	−134
31	−448	−176	−272	67	−306	−137	−169
32	−149	−151	2	68	−423	−346	−77
33	−320	−327	7	69	−311	−520	209
34	−361	−286	−75	70	−88	−181	93
35	−124	−160	36	71	83	167	−84
36	−493	−351	−142	72	13	6	7
37	190	−443	633	74	−120	−36	−84
38	−293	−241	−52	77	−226	−208	−18
39	−221	−208	−13				
40	−152	−295	143				

$$D_m = 4^\circ\ 57.'5 + 0.'2 = 4^\circ\ 57.'7$$
$$H_m = 31988^\gamma - 169^\gamma = 31819^\gamma$$
$$V_m = 33655^\gamma + 246^\gamma = 33901^\gamma$$

Making use of these standards, the preceding equations may be written as follows:

$$\text{For } D \quad y_2 = 0.94\, x_2\,,$$
$$H \quad y_2 = 0.94\, x_2\,,$$
$$V \quad y_2 = 0.90\, x_2\,.$$

y_2 must be the second order anomaly at 1923.50, since x_2 is the second order anomaly at 1952.63.

The coefficients of the above equations have an interesting meaning, that is, they represent the ratios of the second order anomalies at 1923.50 to those at 1952.63. The fact that their values are very near to unity means that these two groups of anomalies are nearly equal. But their values are a little smaller than unity, and this means that the anomalies at 1923.50 are smaller than those at 1952.63, indicating that the anomalies have somewhat increased in the past twenty-nine years. The mean value of the three coefficients is 0.927 and it means that the increment is about one-thirteenth of the previous value. But, since the probable errors are rather large, as shown in the above, the increments are not so accurate as the numerical values express.

The anomalies at both epochs and their differences are expressed in Table IV. The coefficients of the equations which express the relations of those differences and the anomalies at 1952.63, are 0.06, 0.06 and 0.10 respectively. The distributions of the differences are very similar to Figs. 1, 2 and 5 respectively This means that these anomalies have been added in the past twenty-nine years by about one-thirteenth of the previous ones.

Finally, it is noticeable that these relations are perfectly independent of the distribution of the magnetic bodies beneath Maeyama which the writer assumed as an oblate spheroid in expressing the magnetic anomalies themselves, and also independent of the standard values with which the writer obtained the anomalies.

7. Conclusion

1. There were almost similar magnetic anomalies around Maeyama at 1952,63 as at 1923.50.
2. To explain these anomalies, the writer assumes an oblate spheroid whose centre is situated at the sea level and at nearly the geographycal centre of Maeyama, the minor axis of which is vertical and equal to 1.4 km, and the major axis of which is horizontal and equal to 2.8 km. The magnetic field around Maeyama seems

to be due to magnetic induction by the earth's magnetic field. The magnetic susceptibility of Maeyama is about 0.0057 C. G. S. E. M. U..

3. To deduce the magnetic susceptibility, the position and the dimensions of the spheroid are modified in several cases, and the above position and dimensions are presented as most probable. Therefore these geometical forms will suggest the form of Maeyama as that of a volcano.
4. In a general view, the magnetic anomalies due to Maeyama have almost not changed for the past 29 years.
5. But the tendency of the variation of the magnetic anomalies is positive, and the increment of the magnetic susceptibility is about one-thirteenth for that internal.
6. As Simabara Peninsula has been calm in seismic and in volcanic aspects for the past 29 years, so it has also been calm in its magnetic nature. It rather proceeds somewhat in magnetization and, to speak without reserve, the temperature of the rock beneath the mountain seems to descend and the stability of it also seems to proceed, in some degree.

In conclusion, the writer wishes to express his sincere thanks to the late Prof. T. Sida and Prof. M. Hasegawa for their guidance. His cordial thanks are also due to Dr. M. Ota for his well-intended aid in the comparison of the instruments and in other cases. The writer also wishes to express his hearty thanks to the members of the Kakioka Geomagnetic Observatory and the Aso Volcanic Observatory for placing their observed records at his disposal.

REFERENCES

1. A. TANAKADATE, *The Journal of the College of Science, Imperial University of Tokyo, Japan*, **14** (1904), 179.
2. W. YODA, On the magnetic anomalies around Maeyama at Simabara Peninsula, *Tikyu Buturi* (Geophysics), **3** (1939), 26 (in Japanese).
3. Among them the following paper deals rather fully not only with the point distribution but also with the magnetic elements.
   T. MINAKAMI, Magnetic surveys of Volcano Asama, (Part 2), *Bull. Earthq. Res. Inst.* **18** (1940), 178.
4. T. MINAKAMI, T. ISIKAWA and K. YAGI, The 1944 eruption of Volcano Usu in Hokkaido, Japan. *Bull. Volcanologique Organe de l'Association de Volcanologie, de l'Union Géodésique et Géophysique Internationale*, Série II, **11** (1951), 120.
5. T. RIKITAKE, The distribution of magnetic dip in Ôsima Island and its change that accompanied the eruption of Volcanic Mihara, 1950. *Bull. Earthq. Res. Inst.* **24** (1951), 161.
   T. RIKITAKE, Changes in magnetic dip that accompanied the activities of Volcano Mihara (The second report). *Bull. Earthq. Res. Inst.* **29** (1951), 499.
6. S. IMAI, Recent three magnetic elements in Japan, *Suiro-Yōhō*. **25** (1951), 254 (in Japanese).
7. I. TUBOKAWA, Reduction of the results obtained by the magnetic survey of Japan

(1948–51) to the epoch 1950.0 and deduction of the empirical formulae expressing the magnetic elements. *Bull. Geograph. Surv. Institute*, **3** (1952), 1.

8. See ref. (1)
9. See ref. (2)
10. S. IMAI, On the recent distribution of the terrestrial-magnetic elements in Japan. *Hydrographic Bulletin* No. **36** (1953), 108 (in Japanese).
11. J. KÖNIGSBERGER, Zur Deutung der Karten magnetischer Isanomalen und Profile. *Beiträge zur Geophysik*, **19** (1928), 241.
12. See ref. (2)

MEMOIRS OF THE COLLEGE OF SCIENCE, University of Kyoto, Series A,
Vol. XXVII, No. 2, Article 3, 1954

SEISMOMETRIC INVESTIGATION OF THE EARTH'S INTERIOR
PART I. ON THE STRUCTURE OF THE EARTH'S UPPER LAYER

BY
Yoshimichi KISHIMOTO

(*Received December 3, 1953*)

ABSTRACT

The thickness and seismic velocity of the sedimentary and the upper layer of the earth were determined by the seismometric investigation of local and near earthquakes observed at the Kamigamo Geophysical Observatory in Kyoto. From the analysis of the direct and the refracted seismic waves the structure of the sedimentary layer and the upper layer near Kyoto were deduced as 3.8 km/sec (P_s), 2.2 km/sec (S_s), and 5.4 km/sec (P_{g1}), 3.1 km/sec (S_{g1}), for the velocities of P- and S-waves, and 1.5 km and 6 km for the thickness of layer respectively. It was also inferred that there exists a layer of 5.8 km/sec (P_{g2}), 3.3 km/sec (S_{g2})-velocity underlying the upper layer.

1. Introduction

The internal structure of the earth has been an attractive subject of research and investigated by many researchers from various standpoints. In ancient times the interior of the earth was simply imagined to be in a hot and molten state covered by a thin and cooled surface layer, inferred from the knowledge of volcano-eruption and lava-effusion. But since the middle of nineteenth century it was physically ascertained that the earth as a whole should be considerably rigid as deduced from the theoretical and observational investigation of precessional and nutational motion, tidal deformation, and latitude variation of the earth. On the other hand, the density distribution of the earth's interior has been early investigated since Newton from the theoretical consideration of the figure of the rotating earth, surface gravity distribution, and the mean and surface density of the earth.

But beyond the above-mentioned investigation of elasticity and density distribution, the observation of seismic waves and the analysis of seismograms give us far stronger clues in the exploration of the interior of the earth. Since the brilliant start of seismometric investigation of the earth's interior by E. Wiechert in 1907 many important and unexpected facts concerning the earth's structure have been revealed

in succession by many researchers. Among them the existence of the central core is the most attractive and essential problem which may characterize the internal structure of the earth and reveal the formation of the earth and the origin of the solar system. The Mohorovičić discontinuity, the 20°–discontinuity and otherminor ones are also interesting and suggestive properties peculiar to the earth, and the inner core recently discussed may greatly serve for the development of study on the nature of the core.

In spite of a great progress of research of the earth's interior during the last fifty years there remain a great majority of unsolved problems which are very interesting and important for solving the secret of the earth itself. Among these, the fluidal and heavy property of the core, the positive proof of the existence of the inner core, the temperature distribution in the core and mantle, the motion of the core as an origin of geomagnetism, the sudden transition from the mantle to the core at the core boundary, the density relation between two media at the discontinuities of Mohorovičić and of 20° and the core–boundary, the fine structure of the crust in every part of the world, the visco-elastic property and the plastic flow of the crust and the mantle, and various other problems should be investigated and solved in the near future from the theoretical and the observational standpoints.

In our seismometric investigation of the earth's interior the following research projects are scheduled: As the First Part, the structures of the sedimentary layer and the upper layer of the crust are investigated by the analysis of seismograms of local and near earthquakes obtained at Kamigamo Geophysical Observatory. In the Second Part, the fine structure of the crust as a whole in the neighbourhood of Kyoto will be discussed. In the Third Part, some discontinuities in the mantle will be investigated by comparing the reflected and refracted waves at the respective interface of discontinuity from the seismograms observed at many seismological observatories in Japan; especially the density ratio between two media at the respective interface of the 13°–and 20°–and other discontinuities will be studied in detail. In the Fourth Part, the investigation of the nature of the core and the problem of the inner core in relation to various methods of seismometry will be discussed.

2. Kamigamo Geophysical Observatory

In this article (Part I) and the next Part II, seismometric investigation was made mainly of the seismograms obtained at the Kamigamo Geophysical Observatory during the past forty years or more. Hence it is considered to be necessary at this time to give a description of the Observatory. The Observatory is situated 135° 46′ E and 35° 04′ N in the northern part of Kyoto City, and stands on a hill of 190 m height above sea level and 100 m in relative height, the rock formation being chert mixed with shale and sandstone of Chichibu Paleozoic system. A part of the buildings

of the Observatory was constructed early in 1900 as the observation room for geomagnetic elements under the Earthquake Investigation Committee in Japan. In 1909 all the buildings and their equipment were transferred from the Committee to the Kyoto University, and thenceforth the Observatory has been under the Geophysical Institute in the Faculty of Science of the Kyoto University as an observation station named the Kamigamo Geophysical Observatory. The Observatory has been directed first by the late Professor T. Shida during the period of 1909 to 1936, and next by Professor K. Sassa during the period of 1937 to 1951, and at present by Professor E. Nishimura.

The Observatory has been serving for the study and observation of geodesic, seismological and geomagnetic phenomena, and has really been instrumental in making some valuable contributions to the progress of geodesy and seismology. Among these, the work by Shida on the elasticity of the earth and the earth's crust in 1912 was made from the tiltmetric observation data at the underground room of the Observatory, and he discussed for the first time the secondary effect of oceanic tides on earth tidal variation and obtained the good values of the diminishing factor and elasticity of the earth's mantle. Shida announced his study on the mechanism of earthquake-occurrence in 1917 deduced from the quadrantal distribution of the direction and amplitudes of first motion of seismic P-and S-waves observed at the Observatory and others. This is the famous Shida-theory of the "push-pull" zone and the first investigation on the nature and behaviour of earthquake at the instance of its occurrence as derived from the observation of seismic waves. In 1926 Shida and Sassa showed for the first time the existence of some earthquakes of extremely deep focus from the analysis of seismograms obtained at the Observatory which was beyond the common knowledge of those days on the depth of focus and opened a gate to a way for a new and attractive research field of seismology. Recently Sassa and Nishimura have published many papers on the study of phenomena foretelling the occurrence of destructive earthquakes as derived from the analysis of data obtained at the Observatory and its allied stations, and observed with the tiltmeter, the extensometer, the magnetometer, the seismograph and other instruments.

At the present time the Observatory is equipped with the following instruments:

a) The large Wiechert seismograph (W_H and W_V)

The horizontal component (Inverted pendulum-type): Inertia mass (1000 kg), Period of pendulum (12 sec), Static magnification (200), Damping ratio (1/4)

The vertical component: Inertia mass (1300 kg), Period of free oscillation of mass (5 sec), Static magnification (180), Damping ratio (1/4)

They are set up at the underground room of the stone building and their seismograms of mechanical registration on sooted paper are exchanged

every day, the length of one minute-mark on the seismograms being nearly 30 mm.

b) The Omori horizontal seismograph (O_H)

(Horizontal pendulum-type): Inertia mass (50 kg), Period of pendulum (8 sec), Static magnification (50), Damping ratio (1/4)

The two horizontal components are set at the first floor of the stone building and their seismograms of mechanical registration on the sooted paper are exchanged every day, the length of one minute-mark on the seismograms being nearly 30 mm.

c) The seismograph of Galitzin-type (G_b)

Two horizontal and one vertical components:

Periods of pendulum and galvanometer are 4 sec and 0.5 sec respectively, maximum magnification: 2,000/mm/m, length of one minute-mark on the photographed seismograms is 55 mm. Set up the underground room of the stone building.

d) The short period seismograph of variable reluctance-type (R_1)

Two horizontal and one vertical components:

Periods of pendulum and galvanometer are 0.35 sec and 0.35 sec respectively, maximum magnification: 70,000/mm/m, length of one minute-mark: 300 mm. Set up at the underground room of the stone building.

e) The tiltmeter of horizontal pendulum-type (T_H)

Two components of fused silica tiltmeter:

Sensibility: 0.″003/mm/3m. Set up at the bottom of the concrete dry well in the underground room of the stone building, the depth of the well being 9 m below the ground surface. The photographed tiltgrams are exchanged once a week, the length of the one day-mark being 70 mm.

f) The mercury tiltmeter (T_M)

Two components: sensibility: 0.″44/mm by telescopic reading from the distance of 4 m. Set up on the concrete floor of the underground room of the stone building. Reading is made once a week.

g) The gravimeter of double bifilar type (G_I)

Sensibility: 10^{-8}g/mm/4 m. Set up at the end of the adit of 20 m-length and 10 m-depth. The record is exchanged once two weeks and the length of one day-mark is 25 mm.

h) The geomagnetic variometer (M_D and H_Z)

The variometer for declination and the variometer for vertical intensity: sensibility: 0.′4/mm/4 m, and 2γ/mm/4 m, respectively. Set up at the

next room of the gravimeter. The record is exchanged once two weeks and the length of one day-mark is 25 mm.

i) The usual meteorological instruments

And the Seismological Bulletin of the Observatory has been published semiannually since the beginning of 1952 as one station of the International Seismological Observations listed.

3. Structure of the upper layer

Since the first and definite discussion of the discontinuous layer of the earth's crust by A. Mohorovičić in 1910 on the Kulpa Valley Earthquake of October 8, 1909, and the detailed report on the Oppau Explosion of September 21, 1921 by O. Hecker in 1922, the structure of the earth's crust has been seismologically investigated by many researchers from the analysis of seismic waves of near natural earthquakes and artificial explosions. Recently, in succession of the great artificial explosion on April 18, 1948 at Heligoland, the earth's surface, granitic and basaltic layers have been discussed in detail from huge amount of data in many artificial explosions of large and small scales obtained at various places in the world.

Seismometric investigation during the past more than forty years of the structure of the earth's crust at various places in the world tell us that the crust itself shows a great deal of local character in its fine structure. Namely the number of layers of discontinuity, their thickness and their respective seismic velocity of the earth's crust are all diverse from one place to another with regard to each continent and ocean, or more regionally to mountainous areas and level ground. In our country the crustal structure was investigated in detail by T. Matuzawa [1928, 1929, 1932] from the analysis of seismograms of near natural earthquakes obtained at some stations in Japan, giving the structure of the sedimentary layer of 3.8 km-thickness, the granitic layer of 16 km-thickness with the velocity of 5.0 km/sec ($\bar{P}$) and 3.15 km/sec ($\bar{S}$), the intermediate layer of 30 km-thickness with the velocity of 6.2 km/sec (P^*) and 3.7 km/sec (S^*), and the basement layer with the velocity of 7.5 km/sec (P_n) and 4.5 km/sec (S_n), respectively. And the crustal structure of north part of Honshû has been investigated by recent five artificial explosions at Isibuti in 1950 and 1951 [1950, 1951, 1952] and Kamaisi in 1952 and 1953 giving the thin layer of 1.3 km-thickness with the velocity of 5.26 km/sec (P_1) and underlying layer with the velocity of 6.13 km/sec (P_2) and 3.37 km/sec (S_2) in the case of the first Isibuti Explosion.

In our investigation the seismometric data of the local and near earthquakes around Kyoto are mainly obtaind at the Kamigamo Geophysical Observatory during the past forty years, hence giving the regional structure of the crust around Kyoto. The earthquakes used in the present analysis are listed in the following Table I and their position of epicenters are shown in Fig. 1.

Table I. List of the earthquakes used in the present investigation; where latitude and longitude of epicenter and focal depth are given by the Central Meteorological Observatory of Japan.

No.	Date	Epicentral region	Latitude and longitude of epicenter	Focal depth	P~S	Duration time of forerunner		Maximum total amplitude	Amplitude of initial motion			Emergent angle	Observatory	Seismograph
	d h m		N E	km	sec.	P sec.	S sec.	μ	N μ	E μ	Z μ	degr.		
1	1953 Jan. 31 18 43	Kyoto Pref.	—	—	2.3	—	—	Scale out	+2.5	+2.5	−8.3	69	K	W
2	" " 19 11 08	—	—	—	2.5	—	—	100	−0.9	−4.4	−5.1	51	"	"
3	1936 Oct. 26 12 50	near Kyoto City	—	—	2.7	—	—	110	+3.0	−2.0	+16.1	79	"	"
4	1935 June 1 08 39	Osaka Pref.	—	—	3.2	—	—	Scale out	+4.5	+6.0	+9.1	52	"	"
5	1952 July 31 15 40	near Kyoto City	—	—	3.5	—	—	17	−0.8	+0.6	+1.9	65	"	"
6	" Aug. 14 04 00	Lake Biwa	35.2, 136.0	shallow	4.1	—	—	107	+2.3	+3.0	−6.6	63	"	"
7	" July 10 17 37	Kyoto Pref.	34.9, 135.6	shallow	4.3	—	—	42	+3.1	+3.1	+5.2	53	"	"
8	1953 Feb. 9 13 56	Kyoto Pref.	35.1, 135.4	—	4.7	—	—	78	−1.0	−8.7	−7.2	42	"	"
9	" May 5 18 56	—	—	—	5.3	—	—	21	+1.1	+1.1	+1.0	32	"	"
10	1952 Apr. 7 19 17	Wakayama Pref.	34.6, 135.5	shallow	8.2	—	—	44	+1.8	+1.4	−3.8	62	"	"
11	" Feb. 3 21 27	near Akashi City	34.6, 135.0	—	10.0	—	—	115	−6.8	−13.5	−12.0	41	"	"
12	1937 Feb. 5 09 57	near Toyooka City	—	—	10.2	0.8	—	13	+2.1	−4.1	−3.9	43	"	"
13	1941 Dec. 20 20 27	near Tsu City	—	—	10.3	—	—	10	+1.2	−4.5	+8.3	63	"	"
14	1952 Aug. 9 21 42	Nara Pref.	34.3, 135.8	65	10.5	—	—	Scale out	+6.3	−2.5	+13.6	66	"	"
15	1941 March 16 18 52	Osaka Bay	—	—	10.8	—	—	10	−2.3	−2.8	−3.9	50	"	"
16	1952 June 27 06 00	Gifu Pref.	35.5, 136.7	30	11.3	—	—	Scale out	−3.8	−14.4	+21.8	60	"	"
17	1953 Feb. 6 23 08	Chita Peninsula	34.7, 136.9	—	12.0	1.3	—	10	−0.5	+2.0	+1.4	36	"	"
18	1944 Sept. 15 07 16	—	—	—	12.5	1.1	—	82	+0.4	+0.9	—	—	"	"
19	1949 Jan. 6 23 48	Wakayama Pref.	33.8, 135.5	30	12.5	—	—	32	+4.0	−1.3	+9.0	67	"	"
20	1952 Nov. 25 13 22	Wakayama Pref.	—		13.1	1.0	—	—	—	—	—	—	A	G
21	1922 March 10 18 25	—	—	—	14.5	1.2	—	Scale out	+6.0	+1.5	+6.1	47	K	W
22	1951 Aug. 28 09 54	Wakayama Pref.	34.1, 135.2	very shallow	14.5	1.2	—	35	−2.0	−2.0	−2.2	40	"	"
23	1945 Jan. 12 00 —	—	—	—	16.0	1.3	2.0	Scale out	−3.0	−3.3	+3.6	41	"	"

24	1948	May 25	05	29	Kii Channel	—	—	16.1	1.3		120	—	—	—	-	A	"
25	1935	Dec. 8	01	57	near Wakayama City	—	—	16.3	1.2	2.8	25	+7.2	+1.5	+8.0	50	K	"
26	1943	Apr. 23	23	34	Kii Channel	—	30	16.3	1.5		48	+1.3	+0.9	+1.3	42	"	"
27	1920	May 19	01	13	—	—	—	16.9	1.5	—	70	+7.5	+3.5	+8.9	50	"	"
28	1937	Feb. 4	08	28	Wakayama Pref.	—	—	16.9	1.5	—	20	+3.3	+1.5	+3.9	50	"	"
29	1949	Jan. 27	22	01	Atsumi Bay	34.7, 137.2	very shallow	17.1	1.5	2.9	65	+4.5	−10.2	+13.6	54	A	"
30	1953	Jan. 27	00	09	Tottori Pref.	—	20	17.5	1.3	—	10	−2.1	−3.5	−2.6	34	"	"
31	1949	Feb. 3	10	16	Atsumi Bay	34.7, 137.2	very shallow	17.6	1.5	2.7	18	—	−4.5	−5.4	-	"	"
32	1926	March 15	16	57	Aichi Pref.	—	—	17.7	1.5	—	Scale out	−2.9	+11.5	−12.8	50	K	"
33	1949	May 18	04	41	near Fukui City	36.1, 136.1	very shallow	17.9	1.8 2.3	—	28	−4.1	−2.8	+4.2	43	"	"
34	1948	June 28	18	21	After shock of Fukui Earthq.	36.2, 136.2	20	18.8	-	—	180	−10.0	−6.8	+14.8	54	"	"
35	"	Aug. 13	21	34	Lake Hamana	34.8, 137.5	very shallow	19.6	2.1	—	85	−0.9	+3.8	−4.1	50	"	"
36	1953	March 13	12	50	Shima Peninsula	34.1, 137.1	20	19.6	-	—	50	−1.2	+0.8	−1.4	47	"	"
37	"	May 31	13	09	near Daishôji	36.7, 136.0	10	20.1	2.0	—	140	—	-	-	-	"	"
38	1948	July 2	22	30	After shock of Fukui Earthq.	—	-	20.3	2.2	—	24	−3.5	−6.0	+5.6	41	"	"
39	1950	March 9	17	59	Off Shionomisaki	33.2, 136.3	40	21.9	-	—	70	+9.2	−3.5	+13.1	57	A	"
40	1945	June 24	—	—	—	-	—	23.2	2.1 2.8	—	48	—	—	—	-	K	"
41	"	Jan. 3	21	13	—	—	—	24.4	2.0	—	240	−0.8	+11.8	−4.7	14	"	"
42	1952	Aug. 8	22	28	Tokushima Pref.	-	very shallow	24.5	2.2	-	—	—	—	—	-	"	G
43	1949	June 17	23	17	Lake Hamana	34.7, 137.6	10	25.5	1.8 3.7	—	46	—	—	—	—	A	W
44	1936	Oct. 20	23	15	Shizuoka Pref.	35.0, 138.2	shallow	25.8	1.4? 3.1	—	Scale out	+0.6	−4.5	+4.0	44	K	"
45	1944	Aug. 3	10	42	-	—	—	30.7	2.9 5.8	3.1	38	+1.2	−3.8	−3.6	45	"	"
46	1938	Apr. 15	09	08	Yamanashi Pref.	35.3, 138.4	—	30.9	2.1 3.5	3.2	65	+5.5	−4.3	+5.3	40	"	"

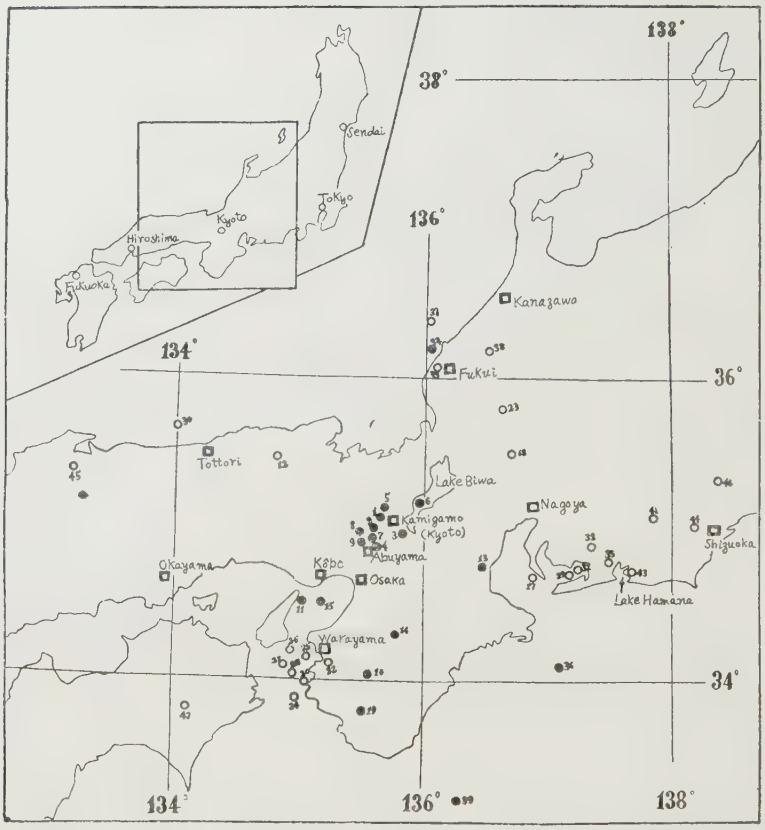

Fig. 1. Position of epicenter of the earthquake listed in Table I. Earthquakes accompanied by the forerunner are denoted by the open circles, and those not accompanied by the dots.

a) *The sedimentary layer*

The sedimentary layer around Kyoto is a mixed layer of chert, shale and sandstone of Chichibu Paleozoic formation. Its thickness and seismic velocity were roughly determined from both the laboratory experiments and the analysis of the minute and local earthquakes close by Kyoto. Thus the seismic velocity and thickness of the sedimentary layer around Kyoto are tentatively estimated to be 3.8 km/sec for P-wave and 2.2 km/sec for S-wave, and 1.5 km-thickness respectively. For the detailed study of the sedimentary layer at various places the reader may preferably refer to the article published by A. Kamitsuki and T. Mikumo [1953] and its succeeding papers.

b) *The upper granitic layer*

Concerning the so-called granitic layer underlying the surface sedimentary layer its seismic velocity may be determined from the time-distance curve of direct P-and S-waves for some near earthquakes observed at several nearby seismological stations.

In the present case five earthquakes (List-number 6, 7, 11, 20 in Table I and the earthquake of Apr. 9, 1953 at Wakayama) are selected for determination of the seismic velocity of the granitic layer around Kyoto, their travel-time for the *P*-and *S*-wave observed at several seismological stations being altogether plotted as seen in Fig. 2. As the travel-times, in Fig. 2, for both waves within some epicentral distance, say, from 10 km to 80 km as deduced from the following investigation, are considered to be those of waves directly transmitted through the granitic layer, the gradient of a straight line most plausibly connecting every point by the method of least squares may give the propagation velocity of both waves in the medium of the granitic layer. The values thus determined are as follows:

The seismic velocity in the granitic layer:

P-wave: 5.4 ± 0.08 km/sec

S-wave: 3.1 ± 0.12 km/sec

The Poisson's ratio of the granitic layer:

0.25_4

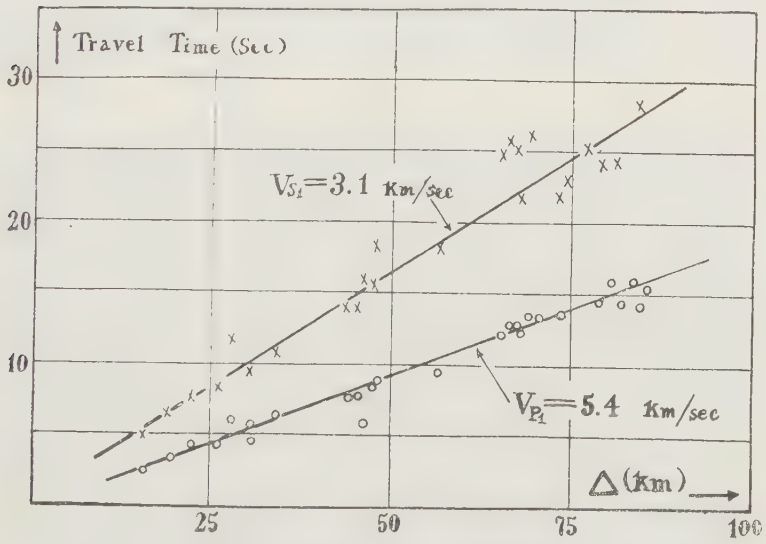

Fig. 2. Travel time-distance curves for P_{g1} and S_{g1}.

As for the thickness of the granitic layer the refracted waves are generally in use and the so-called critical distance is usually examined in the time-distance curve of near earthquakes, observed at possibly large number of seismological stations. But this method of the critical distance is practically inaccurate for the determination of the fine structure of the granitic layer in some cases for the reason that the very feeble refracted waves (forerunners) forerunning the direct wave are often missed or

misread in the observation with the usual seismograph of low magnification, and on the other hand the earthquakes of sufficient large magnitude never occur at the focal depth within several kilometers. In the present investigation the forerunners of many local and near earthquakes observed at one station (Kamigamo Geophysical Observatory) were examined in detail instead of one earthquake observed at many stations. Some examples of this sort of forerunners observed at Kamigamo and Abuyama with the Wiechert Large Seismographs and the Galitzin Seismographs are shown in Fig. 3, and their duration time (arrival time difference between the refracted and direct waves) are also tabulated in Table I.

In Fig. 4 the duration time of forerunners with regard to the local and near earthquakes listed in Table I are plotted referring to their $P\sim S$ times as the abscissa. In the figure the earthquakes unaccompanied by the forerunners are also plotted on the line of 0 sec-duration time, and the open circle (○) and the dot (●) denote the earthquakes whose angle of emergency at Kamigamo or Abuyama are less than 54 and greater than 54° respectively, and those denoted by the black triangle (▲) has too longer duration time compared with those belonging to the open-circle group and are considered to be suitably classified into another group whose detailed consideration will be seen in Part II of our investigation. In this figure it is clearly understood that both the too near earthquakes within the epicentral distance from Kamigamo or Abuyama of some 10 sec-$P\sim S$ time (nearly 80 km) and those of too large emergent angle greater than 54° at Kamigamo or Abuyama are lacking in forerunners. And it means as a matter of course that the direct wave arrived earlier before the refracted wave in the former case and, in the latter, the foci of earthquakes were situated under the granitic layer concerned. In the present case, the group of earthquakes denoted by the open circle in the figure whose foci are certainly situated in the granitic layer concerned may be treated in the main.

Before getting to analyse the forerunner concerned it is convenient to transform the $P\sim S$ time into epicentral distance (exactly speaking, the hypocentral distance) in the present treatment. For its purpose the selected 23 earthquakes were used and thence the Ômori-factor k (hypocentral distance in km $= k\times(P\sim S)$sec) was determined as 8.0 for the regions concerned by the method of least squares. It is a question that a constant value of k is adopted for the so large of epicentral distance (80km~300km), but in the present case a constant k will tentatively be used. Then applying this factor k to the earthquakes accompanied by the forerunner and adopting the values already determined for the velocities of P- and S-waves as 5.4km/sec and 3.1km/sec respectively, the data in Fig. 4 were transformedly represented as the usual travel time-distance curve as shown in Fig. 5. It is to be mentioned that the values concerned in the figure

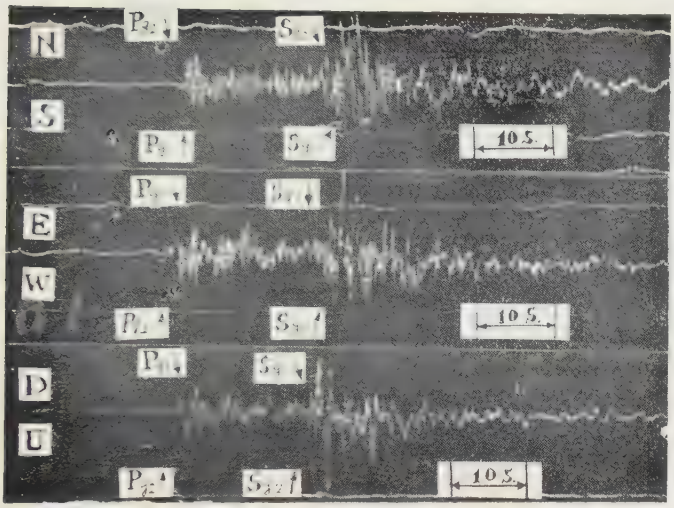

(a)

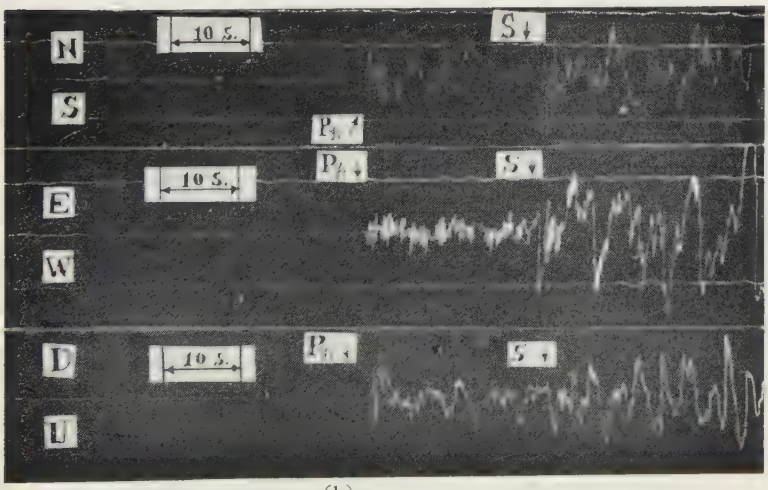

(b)

Fig. 3 (1). Examples of seismograms accompanied and unaccompanied by the forerunner, affected by the different depth of their respective foci (the large Wiechert Seismograph); (a) Accompanied by the forerunner: No.29, 1949 Jan. 27 th 22 h 01m, Atsumi Bay, $P\sim S = 17.1$ sec, $P_{g2}\sim P_{g1} = 1.5$ sec, very shallow. (b) Unaccompanied : No. 39, 1950 March 9 th 17 h 59 m, off Shionomisaki, $P\sim S = 21.9$ sec, focal depth=40 km.

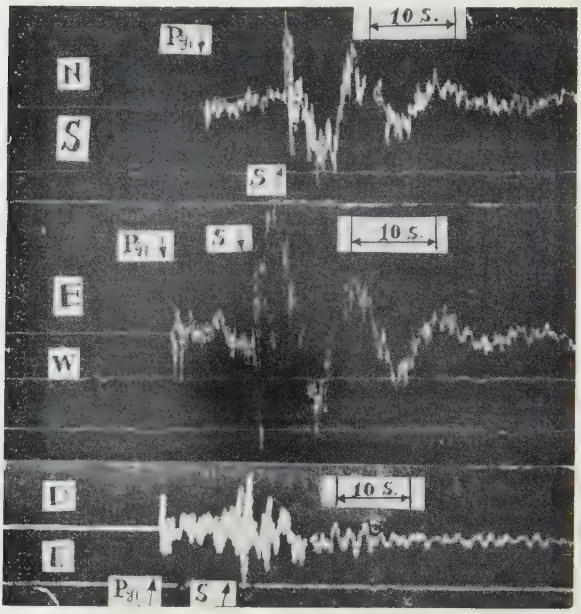

(a)

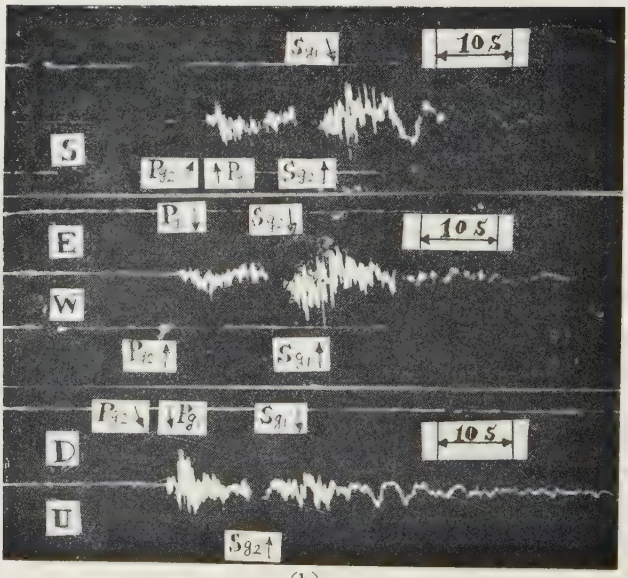

(b)

Fig. 3 (2). Appearance of the forerunner and the increasing of its duration time with epicentral distance (the large Wiechert Seismograph);

(a) Unaccmpanied by the forerunner due to too short epicentral distance: No. 11, 1952 Feb. 3rd 21h 27m, near Akashi City, $P \sim S = 10.0$ sec.

(b) No. 25, 1935 Dec. 8th 01 h 57 m, near Wakayama Ctiy, $P \sim S = 16.3$ sec, $P_{g2} \sim P_{g1} = 1.2$ sec.

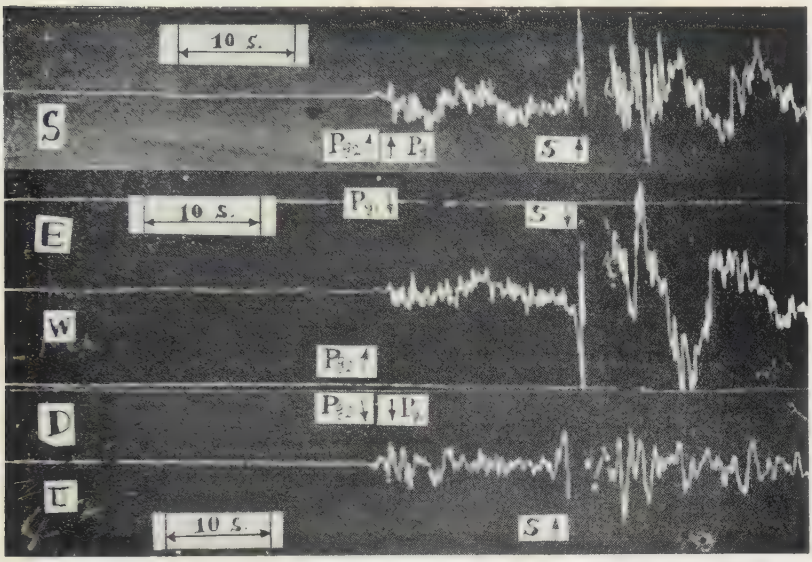

(c)

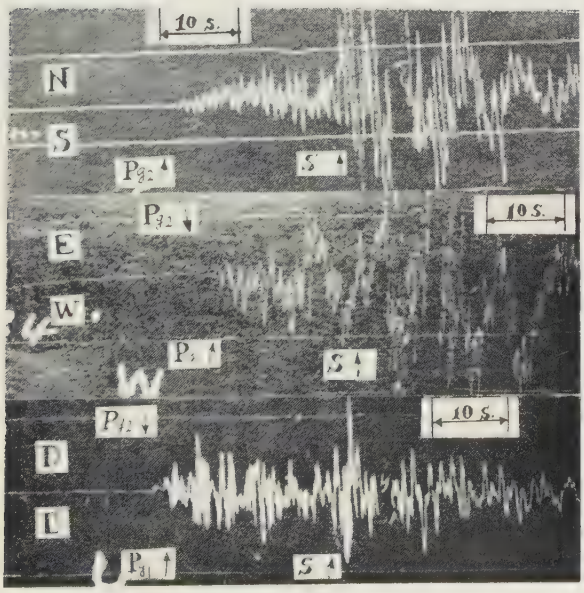

(d)

(c) No. 26, 1943 Apr. 23 rd 23 h 34 m, Kii Channel, $P \sim S = 16.9$ sec, $P_{g2} \sim P_{g1} = 1.5$ sec.
(d) No. 35, 1948 Aug. 13 th 21h 34 m, Lake Hamana, $P \sim S = 19.6$sec, $P_{g2} \sim P_{g1} = 2.1$ sec.

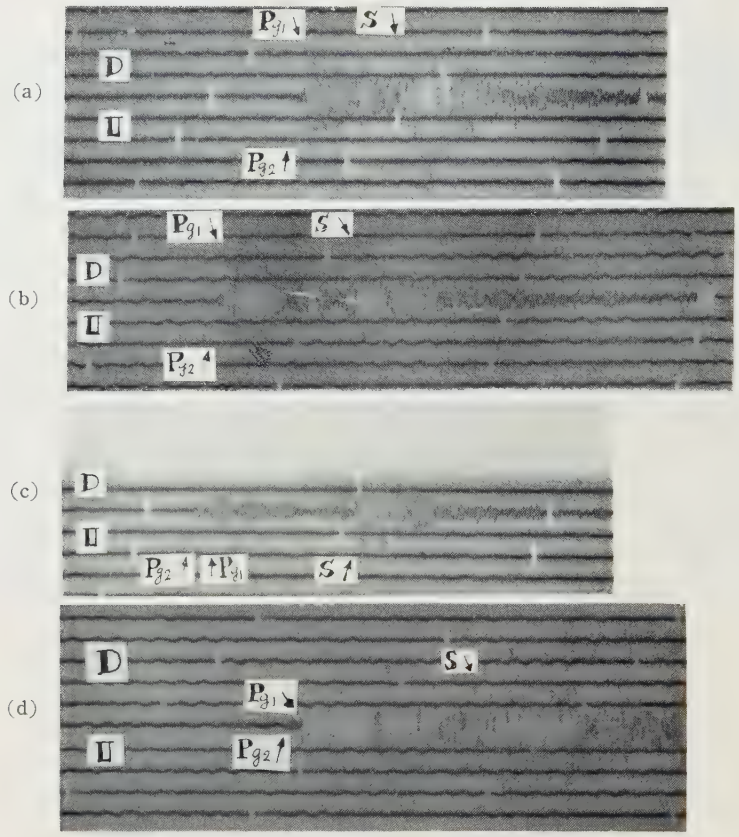

Fig. 3 (3). Examples of the seismograms of the Galitzin Seismograph (vertical component) accompanied by the forerunner; (a) 1953 July 1st 01 h 56 m, $P\sim S = 14.0$ sec, $P_{g2}\sim P_{g1} = 1.6$ sec. (b) 1953 July 8th 10 h 59 m, $P\sim S = 20.0$ sec, $P_{g2}\sim P_{g1} = 1.4$ sec. (c) 1953 July 3rd 02 h 31 m, $P\sim S = 21.9$ sec, $P_{g2}\sim P_{g1} = 2.5$ sec. (d) No. 42, 1952 Aug. 8th 22 h 28 m, Tokushima Pref., $P\sim S = 24.5$ sec, $P_{g2}\sim P_{g1} = 2.2$ sec.

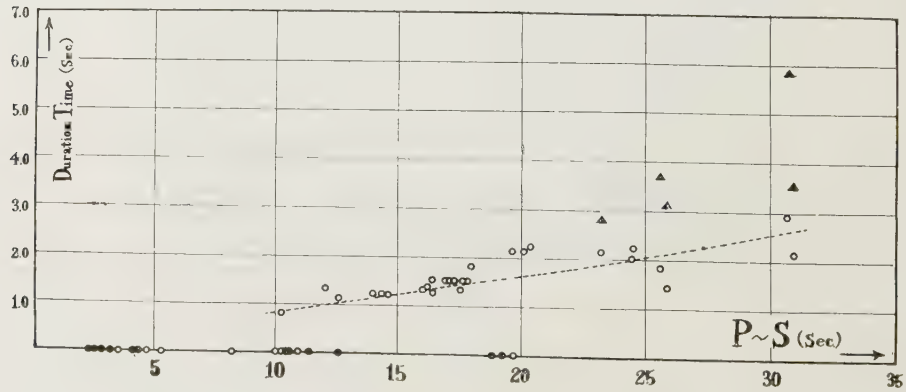

Fig. 4. Relation between the duration time of forerunners and the $P\sim S$ time of their respective earthquakes.

are all referring to the stripped earth of the sedimentary layer. Moreover the curves of the direct wave are two-fold calculated for 2 km- and 6 km-focal depth respectively. From this figure the velocity of refracted wave was calculated as 5.8 km/sec(P_{g2}) and 3.3 km/sec (S_{g2}) respectively, thus giving the Poisson's ratio of 0.26$_1$. But in this case the so-called critical distance as the intersection of the travel-time curve of the refracted wave with the direct one as seen in Fig. 5, is not simply available for determination of the layer thickness, as in case of the artificial explosion, because of the finite focal depth of their respective earthquakes. If we provisionally assume the horizontally parallel structure of the earth's crust in some area around Kyoto, the thickness of the upper granitic layer may plausibly be calculated as 6 km from the above obtained numerical data of the duration time of forerunner and the propagation velocity in the medium.

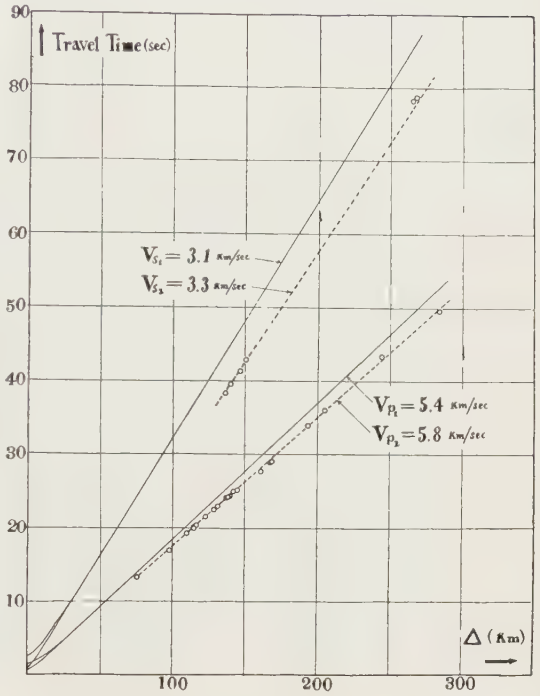

Fig. 5. Travel time-distance curves for P_{g1}, S_{g1} (full line) and P_{g2}, S_{g2} (broken line)

c) *The lower granodioritic layer*

The thickness of 6 km determined above for the upper granitic layer having the velocity of 5.4 km/sec (P_{g1}) and 3.1 km/sec(S_{g1}) is considered to be too small compared with those of 16 km for the granitic layer obtained by T. Matuzawa [1929]. But this value of 6 km-thickness may be highly trustworthy for Kyoto area because of the clear existence of forerunner and its accurate value of duration time. And moreover the forerunner concerned is rightly interpreted as the refracted waves from the above stated reasons, that is, non-appearance of the forerunner in question in the case of earthquakes with the focal depth greater than 20 km, the amplitude ratio of the forerunner to the direct wave in their respective horizontal and vertical components, the value of propagation velocity of the direct wave presumed and other reasons. Therefore as a way of reconcilement for inconsistency and a plausible interpretation it may favourably be supposed that the so-called granitic layer of the earth's crust is composed of two slightly different media—the upper and the lower granitic layers,

at least in some areas around Kyoto. The lower granitic layer is considered to be a mingled layer of granitic and basaltic medium (perhaps of granodioritic or its allied medium), as deduced from its velocity of 5.8 km/sec(P_{g2}) and 3.3 km/sec(S_{g2}). Its thickness and relation to the basaltic layer may be fully discussed in Part II of our investigation.

4. Some considerations

Of the present treatment some considerations may be taken on this occasion. They may be useful for making clear the degree of accuracy of argument on the crustal structure and serve for the future development of our investigation.

i) *Focal depth and the emergent angle*

From the reason that the earthquakes treated in the present investigation are generally local or near ones of minute scale their focal depth are for the most part not exactly determined. But, as seen in Fig. 4 and Table I, the earthquakes with the greater emergent angle than 54° all not forerun by the refracted waves in the epicentral distance of from 80 km to less than 200 km. Namely only the earthquakes whose foci are situated in the upper granitic layer show the forerunner in question in the moderate epicentral distance. And really as shown concurrently in Fig. 6 the practically observed values of the emergent angle of the direct P-wave at Kamigamo or Abuyama as listed in Table I and calculated curves of emergent angle in cases of the focal depth of 1.0 km below the surface in the sedimentary layer(a), 2 km and 6 km below the upper interface in the upper granitic layer ((b) and (c) respectively), and 2 km below the lower interface in the lower granodioritic layer (d) respectively, the relation between the focal depth and the emergent angle are clearly understood with reference to the determined crustal structure and the epicentral distance. That is, it may be concluded that the earthquakes with the focus in the upper granitic layer alone show the forerunner concerned in the epicentral distance of from 80 km to 200 km. And moreover these conditions may also give an indirect proof of propriety of the crustal structure determined. As examples of seismograms which do and

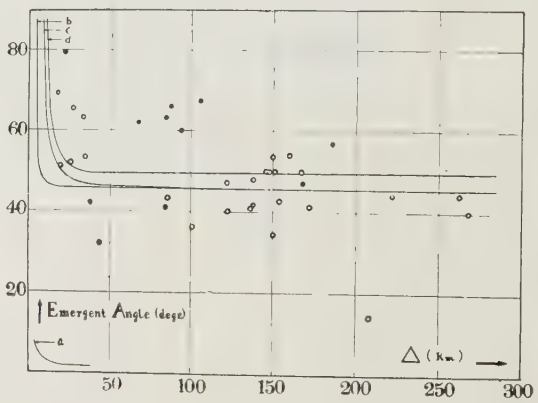

Fig. 6. Relation between the emergent angles of the direct P-waves and the hypocentral distances of their respective earthquakes

do not show the forerunner in question, two aftershocks of the great Fukui Earthquake of June 28, 1948 are shown in Fig. 7, their focal depth being estimated to be about 7 km and 20 km respectively.

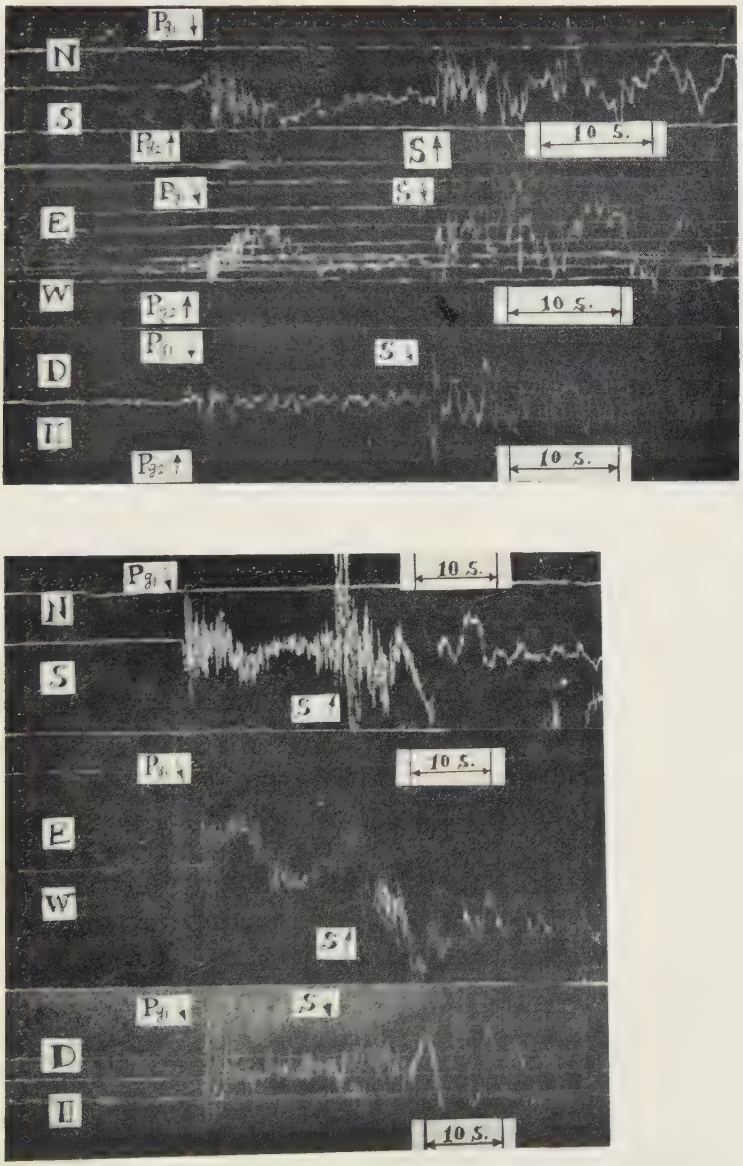

Fig. 7. Two aftershocks of the great Fukui Earthquake of June 28, 1948; (a) Accompanied by the forerunner: No. 38, 1948 July 2nd 12h 30m, $P \sim S = 20.3$ sec, focal depth $\fallingdotseq 7$km, $P_{g_2} \sim P_{g_1} = 2.2$sec. (b) Unaccompanied: No. 34, 1948 June 28th 18h 21m, $P \sim S = 18.8$ sec, focal depth $= 20$km.

ii) *Forerunner with the longer duration time*

For some earthquakes observed at more than 200 km epicentral distance the forerunner with far longer duration time compared with those in question are occasionally observed as shown in Fig. 4 denoted by the black triangle (▲). These are considered to be the refracted waves through the deeper layer under the lower granodioritic layer and its problem will be fully treated in Part II of our investigation. But it is appropriate to be previously announced on this occasion that the forerunner of longer duration has some characteristic appearances clearly distinguished from those of short duration in question in this article, and may propose an attractive problem for study of the crustal structure and the mode of wave propagation.

iii) *Reflected waves*

In the present treatment the refracted waves alone were analysed for investigation of the crustal structure, but the concurrent study with the refracted and reflected waves are most desirable in this sort of study. On the reflection at the boundaries of the respective layer in the earth's crust at many districts may in some detail be investigated by A. Kamitsuki and T. Mikumo, but the some treatments on reflected waves at the crustal boundary around Kyoto will be made in Part II of our investigation.

iv) *Low-velocity layer*

On the low-velocity layer proposed by B. Gutenberg the detailed discussion will be given in Part II of our investigation. But the forerunner in question of the present treatment is not interpreted as the waves with its focus in the low-velocity layer propagated downward and again risen to the surface, from the reason that the amplitude ratio observed of the forerunner to the direct wave is exceedingly small and moreover the rate of increase with depth of the propagation velocity is considered to be insufficient to raise the downward propagated wave to the earth's surface in such a shallow layer as discussed in the present article.

Acknowledgment

The writer wishes to express his heartfelt thanks to Prof. E. Nishimura for his kind guidance throughout the present study and also to Prof. K. Sassa for his generous permission for analysing seismograms obtained at the Kamigamo Geophysical Observatory and the Abuyama Seismological Observatory during the past so many years. The cost for the study was partly covered by the grant-in-aid for Scientific Research of the Ministry of Education.

REFERENCES

KAMITSUKI, A. and T. MIKUMO, Investigation of the structure of the earth's crust in relation to local earthquakes (Preliminary), *Bull. Disaster Prevention Research Inst.*, No. 6 (1953), 39–47.

MATUZAWA, T., K. HASEGAWA and S. HAENO, On the forerunners of earthquake-motions of certain earthquakes, *Bull. Farthq. Res. Inst.*, **4** (1928), 85–106.

MATUZAWA, T., Observation of some of recent earthquakes and their time-distance curves (Part I), *Bull. Farthq. Res. Inst.*, **5** (1928), 1–28.

———— , ———— (Part II), *Bull. Earthq. Res. Inst.*, **6** (1929), 177–204.

———— , ———— (Part III), *Bull. Earthq. Res. Inst.*, **6** (1929), 205–212.

———— , ———— (Part IV), *Bull. Earthq. Res. Inst.*, **6** (1929), 213–229.

MATUZAWA, T., K. YAMADA and T. SUZUKI, On the forerunners of earthquake-motions (The second paper), *Bull. Earthq. Res Inst.*, **7** (1929), 241–260.

MATUZAWA, T. and T. FUKUTOMI, Zwei merkwürdige Wellengruppen bei einigen Erdbeben in Kwanto und die dritte Mitteilung über den vorlaufenden Teil der Erdbebenbewegungen, *Bull. Earthq. Res. Inst.*, **10** (1932), 499–516.

The Research Group for Explosion Seismology, Explosion seismic observations in North-Eastern Japan, *Bull. Earthq. Res. Inst.*, **29** (1951), 97–106.

———— , The second explosion seismic observations in North-Eastern Japan, *Bull. Earthq. Res. Inst.*, **30** (1952), 272–279.

MEMOIRS OF THE COLLEGE OF SCIENCE, University of Kyoto, Series A,
Vol. XXVII, No. 2, Article 4, 1954

AN EXPANSION FORMULA FOR THE LIFT ON A CIRCULAR-ARC AEROFOIL IN A STREAM BOUNDED BY A PLANE WALL

BY

S. TOMOTIKA and H. FUJIKAWA

(*Received June 4, 1953*)

SUMMARY

Starting with Green's general exact formula for the lift acting on a circular-arc aerofoil placed in any position in a stream bounded by an infinite plane wall, an expansion formula for the lift is obtained correct to the order of $(l/H)^2$, where l is the chord-length of the arc-aerofoil and H is the distance of the mid-point of the chord from the bounding wall. The result is found to be in complete agreement, up to the order of $(l/H)^2$, with an expansion formula for the lift on a circular-arc aerofoil near a plane wall, which has been obtained recently by the junior writer by extending Green's new method useful for calculating approximate expansion formulae for the lift and moment of an arbitrary two-dimensional aerofoil placed near an infinite plane wall.

1. Introduction

The lift acting on a circular-arc aerofoil placed in any position in a stream bounded by an infinite plane wall has been evaluated by Green (**1**) in an exact manner, by using suitable conformal transformations. Later on, the senior writer has reinvestigated (**2**), in conjunction with Tamada and Umemoto, the problem *ab initio* by employing suitable conformal transformations, which are somewhat different from those used by Green. It has been found that except for the difference in notation, our general exact formula for the lift acting on the aerofoil is in perfect agreement with the corresponding formula of Green.

By carrying out detailed numerical calculations for three circular-arc aerofoils, the cambers of which are respectively 0.022, 0.053 and 0.097 approximately, the value of the angle of incidence being taken to be 5° in all cases, we have investigated the manner in which the ground effect upon the lift of an aerofoil is modified by its camber.

Since, however, not only the general exact formula for the lift but also the equations for determining various parameters are all very complicated, it is extremely difficult and almost hopeless to repeat detailed numerical calculations for arc-aerofoils of different cambers and for various values of the angle of incidence. Therefore, it is desirable to derive an approximate expansion formula for the lift useful for numerical computations.

In a recent paper (3) Green has devised an ingenious general method for calculating series expansion formulae for the lift and moment acting on a two-dimensional aerofoil with arbitrary shape in the presence of an infinite plane wall, and applying the method Green himself has obtained the first three terms in the series expansion for the lift acting on a circular-arc aerofoil of arbitrary camber.

Quite recently, the junior writer (4) has extended Green's analysis and obtained an expansion formula correct to the order of $(l/H)^4$ for the lift Y acting on a circular-arc aerofoil in the presence of a plane wall, where l is the chord-length of the aerofoil and H is the distance of the mid-point of the chord from the bounding wall. Thus, omitting, for the sake of simplicity, the third and higher powers of l/H, the result is

$$\frac{Y}{Y_0} = 1-\frac{1}{2}\left(\sin\theta+\tan\alpha\,\cos\theta\right)\frac{l}{H} + \frac{1}{64}\left\{(8-6\cos 2\theta)+12\tan\alpha\sin 2\theta + \tan^2\alpha(13+8\cos 2\theta)+\frac{2\sin\theta}{\sin\theta+\tan\alpha\cos\theta}\right\}\left(\frac{l}{H}\right)^2, \tag{1.1}$$

where θ is the angle of incidence and 4α is the angle which the arc subtends at its centre. Y_0 denotes the lift acting on the same aerofoil when placed in an unlimited uniform stream of velocity U and is given by the well-known formula:

$$Y_0 = \pi\rho l U^2(\sin\theta+\tan\alpha\cos\theta)\,, \tag{1.2}$$

where ρ is the density of the fluid concerned.

It should naturally be expected that such an expansion formula for the lift would have been derived from the general exact formula, by assuming H to be very large and developing various functions in series. The object of the present paper is to derive the expansion formula by starting with Green's general formula for the lift.

2. The conformal transformations

For the sake of reference we shall first reproduce the principal results of Green's analysis which are necessary for our present purpose. For details of the analysis reference should be made to Green's original work (1).

Taking the plane of two-dimensional fluid motion as the z-plane, we consider a steady irrotational continuous flow of an incompressible inviscid fluid past a circular-arc aerofoil AA′ which is placed in any position near an infinite plane wall HH′. We take the x-axis along the wall HH′ and assume that the fluid at infinity flows with a constant velocity U in the positive direction of the x-axis.

Two different cases now arise; in the first case, the circle on which the arc lies intersects the bounding wall at two real points X and Y (Fig. 1), while in the second case the circle on which the arc lies does not intersect the wall at real points (Fig. 2). However, as shown by Green, the results for the second case can be derived from those for the first case so that it suffices to consider only the first case.

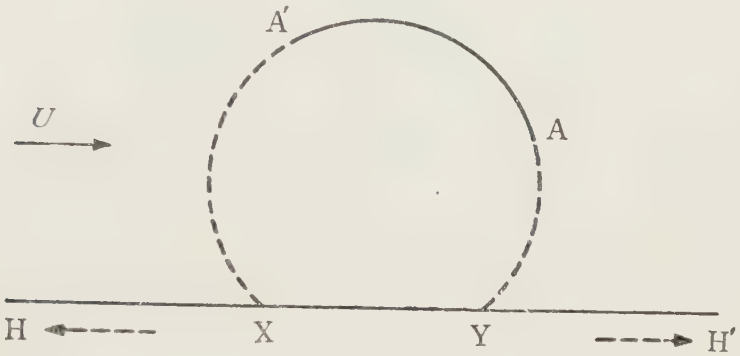

Fig. 1. z-plane.

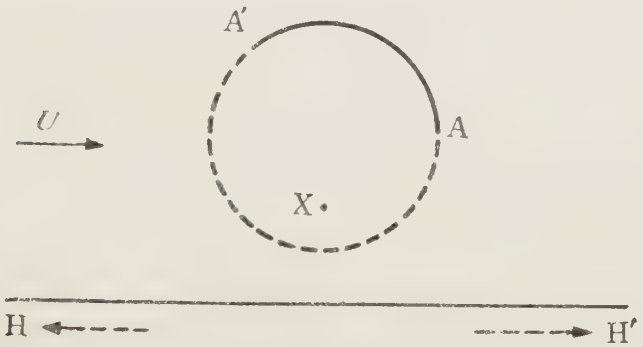

Fig. 2. z-plane.

We take the origin O of the z-plane at the mid-point of the segment XY whose length will be denoted by 2λ. Then, after several transformations, the z-plane is transformed conformally into an annular region in a Z-plane bounded by two concentric circles of radii 1 and $q(<1)$ (Fig. 3), the circular-arc AA′ corresponding to the inner circle and the bounding wall HH′ to the outer circle. The various points are transformed as:

$$\left.\begin{aligned} &\mathrm{A} = qe^{i\theta_1},\ \mathrm{A}' = qe^{i\theta_2},\ \mathrm{X} = e^{i\theta_3},\ \mathrm{Y} = e^{i\theta_4}, \\ &\mathrm{H} = \mathrm{H}' = -1, \end{aligned}\right\} \tag{2.1}$$

where the arguments $\theta_1, \theta_2, \theta_3, \theta_4$ satisfy the following four relations:

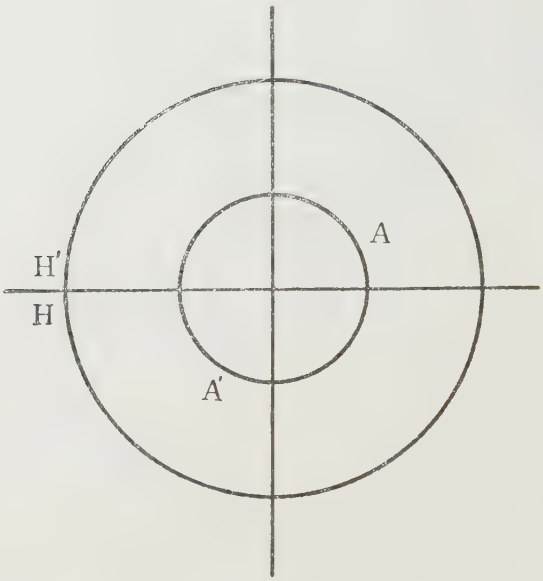

Fig. 3. Z-plane.

$$\frac{\vartheta_1'\{(\theta_1-\theta_3)/2\pi\}}{\vartheta_1\{(\theta_1-\theta_3)/2\pi\}}+\frac{\vartheta_4'\{(\theta_2-\theta_3)/2\pi\}}{\vartheta_4\{(\theta_2-\theta_3)/2\pi\}}=0\,, \tag{2.2}$$

$$\theta_1+\theta_2=\theta_3+\theta_4-2\pi\,, \tag{2.3}$$

$$\theta_4-\theta_3=2(\delta'-\pi)=-2\delta \text{ (say)}, \tag{2.4}$$

$$\pi > \theta_1 > \theta_2 > -\pi\,. \tag{2.5}$$

Here, $2\delta'$ denotes the angle which the segment XY subtends at the centre O′ of the arc AA′ (Fig. 4).

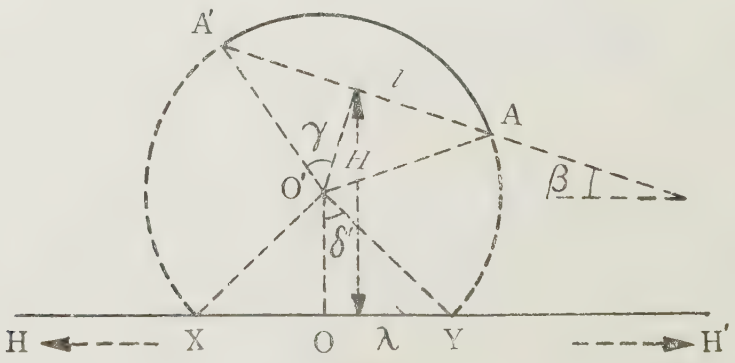

Fig. 4.

If we put

$$\left.\begin{aligned}\theta_1-\theta_2&=2\alpha\,,\\ \theta_3-\delta=\theta_4+\delta&=\phi\,,\end{aligned}\right\} \tag{2.6}$$

we have, from (2.3) and (2.4),

$$\left.\begin{aligned}\theta_1 &= \phi+\alpha-\pi,\\ \theta_2 &= \phi-\alpha-\pi,\end{aligned}\right\} \tag{2.7}$$

and the relation (2.2) can be rewritten in the form:

$$\frac{\vartheta_3'\{(\delta+\alpha)/2\pi\}}{\vartheta_3\{(\delta+\alpha)/2\pi\}}+\frac{\vartheta_3'\{(\delta-\alpha)/2\pi\}}{\vartheta_3\{(\delta-\alpha)/2\pi\}}=0. \tag{2.8}$$

The same relations as (2.7) and (2.8) hold as well for the second case when the circle on which the arc lies does not intersect the wall at real points, provided that we generalise the definitions of λ and δ. In the first case, λ and δ are both real numbers and satisfy the conditions:

$$\lambda \gtrless 0, \quad \pi \gtrless \delta \gtrless -\pi, \tag{2.9}$$

while, in the second case, $i\lambda$ and $i(\pi-\delta)$ are real numbers subject to the conditions:

$$i\lambda \gtrless 0, \quad i(\pi-\delta) \gtrless 0. \tag{2.10}$$

With this extension of our definitions, the expressions for the forces acting on the aerofoil as evaluated in the first case can be used, as they stand, in the second case.

3. Geometrical parameters defining the circular-arc aerofoil

We shall now consider the geometrical parameters defining the circular-arc aerofoil AA′. Let l be the length of the chord AA′, a the radius of the arc AA′, 2γ the angle which the arc AA′ subtends at its centre O′ and H the distance of the mid-point of the chord AA′ from the bounding wall HH′. Further, let β be the acute angle which the chord AA′ makes with the wall. This β is nothing but the angle of incidence of the arc-aerofoil.

Then, we have from Fig. 4, the following relations:

$$\frac{l}{a}=2\sin\gamma, \quad \frac{\lambda}{a}=\sin\delta, \quad \frac{H}{a}=\cos\beta\cos\gamma-\cos\delta, \tag{3.1}$$

from which we get

$$\frac{H}{l}=\frac{\cos\beta\cos\gamma-\cos\delta}{2\sin\gamma}. \tag{3.2}$$

On the other hand, we have, from the transformation equations which are omitted here, the following expressions for $\tan\beta$ and H/l, namely:

$$\tan\beta=\frac{d(1-b^2)\sin\delta}{d(1+b^2)\cos\delta-b(1+d^2)}, \tag{3.3}$$

$$\frac{H}{l}=\frac{\sin\beta}{2(1-b^2)(1-d^2)}(1+b^2+d^2+b^2d^2-4bd\cos\delta)\,, \tag{3.4}$$

where

$$b=\frac{\vartheta_2\{(\phi+\delta)/2\pi\}}{\vartheta_2\{(\phi-\delta)/2\pi\}}\,,\quad d=\frac{\vartheta_3\{(\delta+\alpha)/2\pi\}}{\vartheta_3\{(\delta-\alpha)/2\pi\}}\,. \tag{3.5}$$

Solving equations (3.2), (3.3) and (3.4) for d and b, we get

$$\left.\begin{aligned} d&=\left\{\frac{\cos(\delta-\gamma)-\cos\beta}{\cos(\delta+\gamma)-\cos\beta}\right\}^{\frac{1}{2}}\,,\\ b&=-\left\{\frac{\cos(\delta-\beta)-\cos\gamma}{\cos(\delta+\beta)-\cos\gamma}\right\}^{\frac{1}{2}}\,,\end{aligned}\right\} \tag{3.6}$$

and combining these with (3.5) we have ultimately

$$\left\{\frac{\cos(\delta-\gamma)-\cos\beta}{\cos(\delta+\gamma)-\cos\beta}\right\}^{\frac{1}{2}}=\frac{\vartheta_3\{(\delta+\alpha)/2\pi\}}{\vartheta_3\{(\delta-\alpha)/2\pi\}}\,, \tag{3.7}$$

$$-\left\{\frac{\cos(\delta-\beta)-\cos\gamma}{\cos(\delta+\beta)-\cos\gamma}\right\}^{\frac{1}{2}}=\frac{\vartheta_2\{(\phi+\delta)/2\pi\}}{\vartheta_2\{(\phi-\delta)/2\pi\}}\,. \tag{3.8}$$

Thus, if the values of β, γ and l/H are prescribed, these two equations, together with equations (2.8) and (3.2), determine the values of α, δ, ϕ and q.

4. The general expression for the lift acting on the arc-aerofoil

The resultant force acting on the circular-arc aerofoil can be calculated by the use of Blasius's first formula. Referring the detailed calculations to Green's paper, only the final results will be given here. Thus, denoting the x- and y-components of the resultant force by X and Y respectively, we have

$$X=0,\quad YD/l\rho U^2=Y_1+Y_2+Y_3+Y_4+Y_5\,, \tag{4.1}$$

where

$$\begin{aligned} Y_1=&-\left\{\frac{\vartheta_1'^2(0)\vartheta_4^2(\theta_1/2\pi)}{\vartheta_2^2(0)\vartheta_3^2(\theta_1/2\pi)}+\frac{\vartheta_2''(0)}{\vartheta_2(0)}\right\}\\ &\times\left[4E\left\{\frac{\vartheta_1'^2(0)\vartheta_4^2(\theta_1/2\pi)}{\vartheta_2^2(0)\vartheta_3^2(\theta_1/2\pi)}+\frac{\vartheta_2''(0)}{\vartheta_2(0)}-\frac{\vartheta_1'''(0)}{3\vartheta_1'(0)}\right\}\right.\\ &\left.-\vartheta_1'^3(0)\left\{\frac{\vartheta_1(\theta_1/\pi)}{\vartheta_3^4(\theta_1/2\pi)}-\frac{\vartheta_1(\theta_2/\pi)}{\vartheta_3^4(\theta_2/2\pi)}\right\}\right]\,, \end{aligned} \tag{4.2}$$

$$Y_2=-\frac{2E\vartheta_1'^3(0)\vartheta_1(\theta_1/\pi)}{3\vartheta_3^4(\theta_1/2\pi)}\left\{\frac{\vartheta_1'(\theta_1/\pi)}{\vartheta_1(\theta_1/\pi)}-\frac{2\vartheta_3'(\theta_1/2\pi)}{\vartheta_3(\theta_1/2\pi)}\right\}\,, \tag{4.3}$$

$$Y_3=\frac{\vartheta_1'^4(0)\vartheta_1^2(\alpha/\pi)\vartheta_1^2\{(\theta_1+\theta_2)/2\pi\}}{\vartheta_3^4(\theta_1/2\pi)\vartheta_3^4(\theta_2/2\pi)}\left\{\frac{\vartheta_1'\{(\theta_1+\theta_2)/2\pi\}}{\vartheta_1\{(\theta_1+\theta_2)/2\pi\}}-\frac{\vartheta_1'(\alpha/\pi)}{\vartheta_1(\alpha/\pi)}\right\}\,, \tag{4.4}$$

$$Y_4=\frac{\vartheta_1'^4(0)\vartheta_1^2(\alpha/\pi)\vartheta_1^2\{(\theta_1+\theta_2)/2\pi\}}{\vartheta_3^4(\theta_1/2\pi)\vartheta_3^4(\theta_2/2\pi)}\,\frac{2\pi\sin(\beta-\gamma)}{\cos\delta-\cos(\beta-\gamma)}\,, \tag{4.5}$$

$$Y_0 = \frac{\pi \cot\delta\vartheta_1'(0)\vartheta_1(\delta/\pi)\vartheta_1(\alpha/\pi)}{\vartheta_3^2\{(\delta+\alpha)/2\pi\}\vartheta_3^2\{(\delta-\alpha)/2\pi\}} \times\left[\frac{\vartheta_1'^2(0)}{\vartheta_2^2(0)}\left\{F+\frac{\vartheta_4^2(\theta_2/2\pi)}{\vartheta_3^2(\theta_2/2\pi)}-\frac{3\vartheta_4^2(\theta_1/2\pi)}{\vartheta_3^2(\theta_1/2\pi)}\right\}\right.$$
$$\left.+\frac{2}{3}E\left\{E-\frac{\vartheta_1'(\alpha/\pi)}{\vartheta_1(\alpha/\pi)}+\frac{\vartheta_3'(\theta_1/2\pi)}{\vartheta_3(\theta_1/2\pi)}-\frac{\vartheta_3'(\theta_2/2\pi)}{\vartheta_3(\theta_2/2\pi)}\right\}\right], \tag{4.6}$$

$$\frac{D\sin\delta}{2\sin\gamma} = -E\left[\frac{\vartheta_2'\{(\phi+\delta)/2\pi\}}{\vartheta_2\{(\phi+\delta)/2\pi\}}-\frac{\vartheta_2'\{(\phi-\delta)/2\pi\}}{\vartheta_2\{(\phi-\delta)/2\pi\}}\right]^3, \tag{4.7}$$

$$E=\frac{\vartheta_3'\{(\delta+\alpha)/2\pi\}}{\vartheta_3\{(\delta+\alpha)/2\pi\}}-\frac{\vartheta_3'\{(\delta-\alpha)/2\pi\}}{\vartheta_3\{(\delta-\alpha)/2\pi\}}+\frac{\vartheta_3'(\theta_2/2\pi)}{\vartheta_3(\theta_2/2\pi)}-\frac{\vartheta_3'(\theta_1/2\pi)}{\vartheta_3(\theta_1/2\pi)}, \tag{4.8}$$

and

$$F=\frac{\vartheta_4^2\{(\delta+\alpha)/2\pi\}}{\vartheta_3^2\{(\delta+\alpha)/2\pi\}}+\frac{\vartheta_4^2\{(\delta-\alpha)/2\pi\}}{\vartheta_3^2\{(\delta-\alpha)/2\pi\}}. \tag{4.9}$$

5. Calculation of α, δ, ϕ and q

Starting from the above general expression for Y, we shall derive an expansion formula for the lift on the arc-aerofoil. To this end, we have to obtain the expansions of α, δ and ϕ in series of ascending q and then to obtain the expansion of q in powers of l/H.

Now, equation (2.8) can be put in the form:

$$\vartheta_3'\{(\delta-\alpha)/2\pi\}\vartheta_3\{(\delta+\alpha)/2\pi\}+\vartheta_3'\{(\delta-\alpha)/2\pi\}\vartheta_3\{(\delta+\alpha)/2\pi\}=0, \tag{5.1}$$

which, when the well-known q-expansion formula for the function $\vartheta_3(v)$ is used, becomes (5):

$$\sin\delta\cos\alpha+q\sin 2\delta+2q^3\sin 2\delta\cos 2\alpha$$
$$+q^4(3\sin 3\delta\cos\alpha+\sin\delta\cos 3\alpha)+2q^7\sin 4\delta+\cdots=0. \tag{5.2}$$

From this equation we can obtain the expansion of $\cos\alpha$ in powers of q. The result is

$$\cos\alpha=-2q\cos\delta+4q^3\cos\delta-4q^5\cos\delta(3+2\cos^2\delta)$$
$$+32q^7\cos\delta(1+3\cos^2\delta)+\cdots. \tag{5.3}$$

The relation between α and δ having thus been known, we shall next proceed to express δ in powers of q by means of equation (3.7). As mentioned already, the object of the present paper lies in the derivation of an expansion formula for Y/Y_0 in powers of l/H, which can be adequately used only when l/H is fairly small, i.e. when H is fairly large. Therefore, it suffices to deal with the second case where the circle on which the arc-aerofoil lies does not intersect the bounding wall at real points. In this case, the value of q is sufficiently small, but, owing to the extension of δ as in (2.10), the value of $\cos\delta$ becomes very large.

Thus, for convenience, we shall put $q\cos\delta=\sigma$. Then, equation (5.3) can be written as:

$$\cos\alpha=-2\sigma+4q^2(\sigma-2\sigma^3)+O(q^4)\,, \tag{5.4}$$

from which we have

$$\sin\alpha=(1-4\sigma^2)^{\frac{1}{2}}\left\{1+8q^2\frac{\sigma^2-2\sigma^4}{1-4\sigma^2}+O(q^4)\right\}. \tag{5.5}$$

Next, we have, from the first equation in (3.6),

$$\sigma\cos\gamma-q\cos\beta=\frac{d^2+1}{d^2-1}q\sin\delta\sin\gamma\,, \tag{5.6}$$

while, after several calculations, we get, from the second equation in (3.5),

$$\frac{d^2+1}{d^2-1}=-\frac{(1-12\sigma^2+32\sigma^4)+4q^2(1-2\sigma^2-64\sigma^6)+O(q^4)}{4q\sin\delta(1-4\sigma^2)^{\frac{1}{2}}\{(1-4\sigma^2)+4q^2(\sigma^2+8\sigma^4)+O(q^4)\}}\,. \tag{5.7}$$

Eliminating $(d^2+1)/(d^2-1)$ from (5.6) and (5.7), we have an equation for determining σ in terms of q. Thus,

$$\begin{aligned}&4(1-4\sigma^2)^{\frac{1}{2}}(\sigma\cos\gamma-q\cos\beta)\{(1-4\sigma^2)+4q^2(\sigma^2+8\sigma^4)+O(q^4)\}\\&=-\sin\gamma\{(1-12\sigma^2+32\sigma^4)+4q^2(1-2\sigma^2-64\sigma^6)+O(q^4)\}\,.\end{aligned} \tag{5.8}$$

In order to solve this equation, we assume that σ can be developed into a series of ascending q as:

$$\sigma=\sigma_0+\sigma_1q+\sigma_2q^2+\sigma_3q^3+\cdots\,, \tag{5.9}$$

where σ_0, σ_1, σ_2, σ_3, ... are certain functions of β and γ. Substituting this series in (5.8) and equating the coefficients of the same powers of q on both sides, we get

$$4(1-4\sigma_0^2)^{\frac{1}{2}}(\sigma_0-4\sigma_0^3)\cos\gamma=-\sin\gamma(1-12\sigma_0^2+32\sigma_0^4)\,, \tag{5.10}$$

$$(1-4\sigma_0^2)^{\frac{1}{2}}\{(1-16\sigma_0^2)\sigma_1\cos\gamma-(1-4\sigma_0^2)\cos\beta\}=2\sigma_0\sigma_1(3-16\sigma_0^2)\sin\gamma\,, \tag{5.11}$$

$$\begin{aligned}&(1-4\sigma_0^2)^{\frac{1}{2}}\left[12\sigma_0\sigma_1\cos\beta-\cos\gamma\left\{6\sigma_0\sigma_1^2\frac{3-16\sigma_0^2}{1-4\sigma_0^2}-4\sigma_0^3(1+8\sigma_0^2)-\sigma_2(1-16\sigma_0^2)\right\}\right]\\&\quad=-\sin\gamma\{(1-2\sigma_0^2-64\sigma_0^6)-3\sigma_1^2(1-16\sigma_0^2)-2\sigma_0\sigma_2(3-16\sigma_0^2)\}\,,\end{aligned} \tag{5.12}$$

$$\begin{aligned}&(1-4\sigma_0^2)^{\frac{1}{2}}\left[2\cos\beta\left\{3\sigma_1^2\frac{1-8\sigma_0^2}{1-4\sigma_0^2}-2\sigma_0^2(1+8\sigma_0^2)+6\sigma_0\sigma_2\right\}\right.\\&\qquad+\cos\gamma\left\{\sigma_3(1-16\sigma_0^2)-12\sigma_0\sigma_1\sigma_2\frac{3-16\sigma_0^2}{1-4\sigma_0^2}\right.\\&\qquad\left.\left.+16\sigma_0^4\sigma_1\frac{7-40\sigma_0^2}{1-4\sigma_0^2}-6\sigma_1^3\frac{1-8\sigma_0^2}{1-4\sigma_0^2}+8\sigma_0^2\sigma_1^3\frac{3-8\sigma_0^2}{(1-4\sigma_0^2)^2}+4\sigma_0^2\sigma_1(3+8\sigma_0^2)\right\}\right]\\&=2\sin\gamma\{-16\sigma_0\sigma_1^3+2\sigma_0\sigma_1(1+96\sigma_0^4)+3\sigma_1\sigma_2(1-16\sigma_0^2)+\sigma_0\sigma_3(3-16\sigma_0^2)\}\,.\end{aligned} \tag{5.13}$$

From these equations we can determine the coefficients σ_i's successively as functions of β and γ. The values of the first four coefficients will be given below.

$$\left.\begin{aligned}
&\sigma_0 = -\frac{1}{2}\sin\frac{\gamma}{2}, \qquad \sigma_1 = \cos^2\frac{\gamma}{2}\cos\beta,\\
&\sigma_2 = -\frac{1}{2}\sin\frac{\gamma}{2}\left\{\left(1+3\cos^2\frac{\gamma}{2}\right)-6\cos^2\frac{\gamma}{2}\cos^2\beta\right\},\\
&\sigma_3 = 2\sin^2\frac{\gamma}{2}\cos^2\frac{\gamma}{2}(4\cos^3\beta-3\cos\beta).
\end{aligned}\right\} \tag{5.14}$$

Using (5.9) together with these values of the σ_i's, we have, from (5.4) and (5.5),

$$\begin{aligned}
\cos\alpha = {}&\sin\frac{\gamma}{2}-2q\cos^2\frac{\gamma}{2}\cos\beta+2q^2\sin\frac{\gamma}{2}\cos^2\frac{\gamma}{2}\left(1-3\cos^2\beta\right)\\
&+2q^3\cos^2\frac{\gamma}{2}\left\{\left(2+3\sin^2\frac{\gamma}{2}\right)\cos\beta-8\sin^2\frac{\gamma}{2}\cos^3\beta\right\}+O(q^4),
\end{aligned} \tag{5.15}$$

$$\begin{aligned}
\sin\alpha = {}&\cos\frac{\gamma}{2}\left[1+2q\sin\frac{\gamma}{2}\cos\beta-2q^2\left\{\sin^2\frac{\gamma}{2}+\left(1-3\sin^2\frac{\gamma}{2}\right)\cos^2\beta\right\}\right.\\
&\left.-2q^3\sin\frac{\gamma}{2}\left\{3\sin^2\frac{\gamma}{2}\cos\beta+4\left(1-2\sin^2\frac{\gamma}{2}\right)\cos^3\beta\right\}\right]+O(q^4).
\end{aligned} \tag{5.16}$$

In a similar manner, we get from (3.8) the expansion for $\cos\phi$ in powers of q in the form:

$$\cos\phi = \mu_0+\mu_1 q+\mu_2 q^2+\mu_3 q^3+\cdots, \tag{5.17}$$

where

$$\left.\begin{aligned}
&\mu_0 = -\cos\beta, \qquad \mu_1 = 2\sin\frac{\gamma}{2}\sin^2\beta,\\
&\mu_2 = 4\sin^2\frac{\gamma}{2}\sin^2\beta\cos\beta,\\
&\mu_3 = 2\sin\frac{\gamma}{2}\sin^2\beta\left\{\left(1-2\sin^2\frac{\gamma}{2}\right)+2\left(1+\sin^2\frac{\gamma}{2}\right)\cos^2\beta\right\}.
\end{aligned}\right\} \tag{5.18}$$

Also, we have the expansion for $\sin\phi$ in the form:

$$\begin{aligned}
\sin\phi = {}&\sin\beta\left[1+2q\sin\frac{\gamma}{2}\cos\beta+2q^2\sin^2\frac{\gamma}{2}\left(2\cos^2\beta-1\right)\right.\\
&\left.+2q^3\sin\frac{\gamma}{2}\left\{\left(1-4\sin^2\frac{\gamma}{2}\right)\cos\beta+2\left(1+\sin^2\frac{\gamma}{2}\right)\cos^3\beta\right\}\right]+O(q^4).
\end{aligned} \tag{5.19}$$

Lastly, we get from (3.2) the expansion for l/H in ascending powers of q in the form:

$$\frac{l}{H} = 8q\cos\frac{\gamma}{2}\left\{1+2q\sin\frac{\gamma}{2}\cos\beta+O(q^2)\right\}, \tag{5.20}$$

and solving this equation for q, we have

$$q\cos\frac{\gamma}{2} = \frac{1}{8}\frac{l}{H}-\frac{1}{32}\tan\frac{\gamma}{2}\cos\beta\left(\frac{l}{H}\right)^2+O\left[\left(\frac{l}{H}\right)^3\right]. \tag{5.21}$$

6. An expansion formula for the lift

Making use of the preceding various expansions we have obtained, after lengthy calculations, expansions in powers of q for various quantities such as Y_1, Y_2, Y_3, Y_4, Y_5 and D as defined in (4.2)–(4.9). The results are

$$\begin{aligned}
Y_1+Y_2 = &-256\pi^5 q^2 \cos^2\frac{\gamma}{2} \\
&\times\left\{\sin\beta\cos\beta+\tan\frac{\gamma}{2}(3-\cos^2\beta)+4\tan^2\frac{\gamma}{2}\sin\beta\cos\beta+\tan^3\frac{\gamma}{2}(1+2\cos^2\beta)\right\} \\
&+512\pi^5 q^3\cos^3\frac{\gamma}{2}\left\{\sin^2\beta\cos\beta+\tan\frac{\gamma}{2}\sin\beta(1+4\cos^2\beta)\right. \\
&\qquad+\tan^2\frac{\gamma}{2}(12\cos\beta-7\cos^3\beta)+16\tan^3\frac{\gamma}{2}\sin\beta\cos^2\beta \\
&\qquad\left.+\tan^4\frac{\gamma}{2}\left(\cos\beta+6\cos^3\beta\right)\right\}+O(q^4), \qquad (6.1)
\end{aligned}$$

$$\begin{aligned}
Y_3 = &-256\pi^5 q^2\cos^2\frac{\gamma}{2}\left(\sin\beta\cos\beta+\tan\frac{\gamma}{2}\sin^2\beta\right) \\
&+512\pi^5 q^3\cos^3\frac{\gamma}{2}\left\{\sin^2\beta\cos\beta+\tan\frac{\gamma}{2}\sin\beta(1+4\cos^2\beta)\right. \\
&\qquad\left.+5\tan^2\frac{\gamma}{2}\sin^2\beta\cos\beta\right\}+O(q^4), \qquad (6.2)
\end{aligned}$$

$$Y_4 = 512\pi^5 q^3\cos^3\frac{\gamma}{2}\left(4\sin^2\beta\cos\beta+2\tan\frac{\gamma}{2}\sin^3\beta-2\cot\frac{\gamma}{2}\sin^3\beta\right)+O(q^4), \qquad (6.3)$$

$$\begin{aligned}
Y_5 = &\,256\pi^5 q\cos\frac{\gamma}{2}\left(\tan\frac{\gamma}{2}\sin\beta+\tan^2\frac{\gamma}{2}\cos\beta\right) \\
&-256\pi^5 q^2\cos^2\frac{\gamma}{2}\left\{2\sin\beta\cos\beta+2\tan\frac{\gamma}{2}\cos^2\beta\right. \\
&\qquad\left.+6\tan^2\frac{\gamma}{2}\sin\beta\cos\beta-\tan^3\frac{\gamma}{2}\left(1-4\cos^2\beta\right)\right\} \\
&+512\pi^5 q^3\cos^3\frac{\gamma}{2}\left\{\tan\frac{\gamma}{2}\sin\beta(6+5\cos^2\beta)+\tan^2\frac{\gamma}{2}\cos\beta(4+3\cos^2\beta)\right. \\
&\qquad+4\tan^3\frac{\gamma}{2}\sin\beta(1+\cos^2\beta) \\
&\qquad\left.+\tan^4\frac{\gamma}{2}\cos\beta(3+2\cos^2\beta)\right\}+O(q^4), \qquad (6.4)
\end{aligned}$$

and

$$\begin{aligned}
D = 256\pi^4\cot\frac{\gamma}{2}&\left\{q\cos\frac{\gamma}{2}\tan^2\frac{\gamma}{2}-2q^2\cos^2\frac{\gamma}{2}\tan\frac{\gamma}{2}\left(2+\tan^2\frac{\gamma}{2}\right)\cos\beta\right. \\
&\left.-q^3\cos^3\frac{\gamma}{2}\left(2+\tan^2\frac{\gamma}{2}\right)\left(2\sin^2\beta-3\tan^2\frac{\gamma}{2}\right)+O(q^4)\right\}. \qquad (6.5)
\end{aligned}$$

Thus, by (4.1) we have an expansion in powers of q for the total lift Y acting on the arc-aerofoil in the form:

$$
\begin{aligned}
YD/256\pi^5 l\rho U^2 = {} & q\cos\frac{\gamma}{2}\left(\tan\frac{\gamma}{2}\sin\beta+\tan^2\frac{\gamma}{2}\cos\beta\right)\\
& -q^2\cos^2\frac{\gamma}{2}\left(4\sin\beta\cos\beta+4\tan\frac{\gamma}{2}+10\tan^2\frac{\gamma}{2}\sin\beta\cos\beta\right.\\
& \qquad \left.+6\tan^3\frac{\gamma}{2}\cos^2\beta\right)\\
& +2q^3\cos^3\frac{\gamma}{2}\left\{6\sin^2\beta\cos\beta+\tan\frac{\gamma}{2}\sin\beta(10+11\cos^2\beta)\right.\\
& \qquad +\tan^2\frac{\gamma}{2}\cos\beta(21-9\cos^2\beta)+\tan^3\frac{\gamma}{2}\sin\beta(4+20\cos^2\beta)\\
& \qquad \left.+\tan^4\frac{\gamma}{2}\cos\beta(4+8\cos^2\beta)-2\cot\frac{\gamma}{2}\sin^3\beta\right\}+O(q^4)\,, \qquad (6.6)
\end{aligned}
$$

or, dividing the both sides by D as given by (6.5),

$$
\begin{aligned}
Y/\pi l\rho U^2 = {} & \left(\sin\beta+\tan\frac{\gamma}{2}\cos\beta\right)-4q\cos\frac{\gamma}{2}\left(\sin\beta+\tan\frac{\gamma}{2}\cos\beta\right)^2\\
& +q^2\cos^2\frac{\gamma}{2}\left\{\sin\beta(16-12\cos^2\beta)+\tan\frac{\gamma}{2}\cos\beta(30-28\cos^2\beta)\right.\\
& \qquad +\tan^2\frac{\gamma}{2}\sin\beta(5+24\cos^2\beta)\\
& \qquad \left.+\tan^3\frac{\gamma}{2}\cos\beta(5+8\cos^2\beta)\right\}+O(q^3)\,. \qquad (6.7)
\end{aligned}
$$

Now, it is naturally expected that in the limit when the distance H of the mid-point of the chord from the wall becomes infinitely large, the above expression (6.7) would degenerate into the well-known formula for the lift Y_0 acting on a circular-arc aerofoil placed in an unbounded stream, the length as well as the angle of incidence of the aerofoil being considered to be of the same values in both cases. In effect, we easily find that

$$
Y_0 = \lim_{q\to 0} Y = \pi l\rho U^2\left(\sin\beta+\tan\frac{\gamma}{2}\cos\beta\right), \qquad (6.8)
$$

which is nothing else than the well-known formula for the lift acting on an arc-aerofoil placed in an unlimited stream.

Combining (6.7) with (6.8) we have

$$
\begin{aligned}
\frac{Y}{Y_0} = {} & 1-4q\cos\frac{\gamma}{2}\left(\sin\beta+\tan\frac{\gamma}{2}\cos\beta\right)\\
& +q^2\cos^2\frac{\gamma}{2}\left\{(14-12\cos^2\beta)+16\tan\frac{\gamma}{2}\sin\beta\cos\beta\right.\\
& \qquad \left.+\tan^2\frac{\gamma}{2}(5+8\cos^2\beta)+\frac{2\sin\beta}{\sin\beta+\tan\frac{\gamma}{2}\cos\beta}\right\}+O(q^3)\,, \qquad (6.9)
\end{aligned}
$$

and if use is made of (5.21), we obtain ultimately an expansion formula for Y/Y_0 in powers of l/H in the form:

$$\frac{Y}{Y_0}=1-\frac{1}{2}\left(\sin\beta+\tan\frac{\gamma}{2}\cos\beta\right)\frac{l}{H}$$
$$+\frac{1}{64}\left\{\left(8-6\cos 2\beta\right)+12\tan\frac{\gamma}{2}\sin 2\beta\right.$$
$$\left.+\tan^2\frac{\gamma}{2}(13+8\cos 2\beta)+\frac{2\sin\beta}{\sin\beta+\tan\frac{\gamma}{2}\cos\beta}\right\}\left(\frac{l}{H}\right)^2, \qquad (6.10)$$

where the third and higher powers of l/H have been neglected. Except for the difference in notation this expansion formula is in perfect agreement with the formula (1.1), which, as mentioned in the introduction, has been obtained by the junior writer by extending Green's new method (**3**).

In conclusion the writers wish to express their cordial thanks to Dr. K. Tamada for valuable discussions.

REFERENCES

1. A. E. GREEN, 'The forces acting on a circular-arc aerofoil in a stream bounded by a plane wall.' *Proc. London Math. Soc.*, **46** (1940), 19–54.
2. S. TOMOTIKA, K. TAMADA, and H. UMEMOTO, 'The lift and moment acting on a circular-arc aerofoil in a stream bounded by a plane wall.' *Quart. J. Mech. and Applied Math.*, **4** (1951), 1–22.
3. A. E. GREEN, 'The two-dimensional aerofoil in a bounded stream.' *Quart. J. Math.* (Oxford), **18** (1947), 167–177.
4. H. FUJIKAWA, 'Note on the lift acting on a circular-arc aerofoil in a stream bounded by a plane wall.' *Journ. Phys. Soc. Japan*, **9** (1954), 240–243.
5. S. TOMOTIKA, T. NAGAMIYA, and Y. TAKENOUTI, 'The lift on a flat plate placed near a plane wall, with special reference to the effect of the ground upon the lift of a monoplane aerofoil.' *Report Aeron. Res. Inst., Tokyo Imp. Univ.*, No. 97 (1933).

MEMOIRS OF THE COLLEGE OF SCIENCE, University of Kyoto, Series A,
Vol. XXVII, No. 2, Article 5, 1954

VECTORIAL STABILITY CRITERIA OF THE FEED-BACK PHYSICAL SYSTEM
PART I

BY

Kentaro TASHIRO

(*Received September 10, 1952*)

1. Introduction

In this paper the author presents new considerations about the stability of the feed-back physical systems. The "stability" is one of the most important factors in the study of the feed-back physical systems or the closed-loop control systems, and among many papers which treat the stability of the closed-loop control systems, those of A. Hurwitz, H. Nyquist and K. Küpfmüller may be fundamental.

As Küpfmüller's method contains the treatment of integral equations, many scientists and control engineers seem to prefer Hurwitz's method or Nyquist's method or the latter's improved forms.

Hurwitz's conditions for stability have beautiful mathematical expressions, but by his method, it is indeed possible to know whether a system is stable or not but very difficult to know how the system can be stabilized. It is also difficult to know the relation between the degree of the characteristic equation of the system and the stability.

Nyquist's method has a merit of its being practical, and it has been improved to convenient forms, but in this method one must seek necessarily for the frequency response over $0 \sim \infty$ frequency range. Furthermore, this method is not intuitive and by this method it is not easy to know the degree of stabillity, how to stabilize the system, and the relation between the degree of the system and the stability.

The author reports about his new stability criterion which makes clear the relation between the degree and the stability and lets know how to stabilize the system.

2. Matrix representation of the feed-back physical system or the closed-loop control system

When we assume the given system is linear and composed of independent elements, and denote the input and the output quantities of the ν-th element and its transient impedance with u_ν, x_ν and $Z_{\nu\nu}$ respectively, the physical system is represented by

the following matrix equation, and the impedance matrix of this system has all vanishing non-diagonal elements.

$$\begin{pmatrix} u_1 \\ u_2 \\ u_3 \\ \vdots \\ u_n \end{pmatrix} = \begin{pmatrix} Z_{11} & 0 & 0 & 0 & \cdots & 0 \\ 0 & Z_{22} & 0 & 0 & \cdots & 0 \\ 0 & 0 & Z_{33} & 0 & \cdots & 0 \\ 0 & 0 & 0 & \ddots & & \vdots \\ \vdots & \vdots & \vdots & & \ddots & 0 \\ 0 & 0 & 0 & \cdots & 0 & Z_{nn} \end{pmatrix} \cdot \begin{pmatrix} x_1 \\ x_2 \\ x_3 \\ \vdots \\ x_n \end{pmatrix}, \tag{1}$$

or

$$[u_\nu] = [Z_{\nu\nu}] \cdot [x_\nu], \tag{1'}$$

where u_ν, x_ν and $Z_{\nu\nu}$ can also be matrices. In the following, we shall omit 0 expressing zero-element in the impedance matrix.

As it suffices to deal with the differential deviations of quantities when the automatic control system is considered, the equation of the system can be linear, no matter whether the system is linear or not, as:

$$[\Delta u_\nu] = [Z_{\nu\nu}] \cdot [\Delta x_\nu] \qquad (\nu = 1, 2, \cdots, n). \tag{2}$$

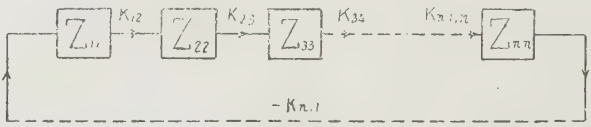

Fig. 1.

If n elements of the system are connected as in Fig. 1, we obtain the closed-loop control system and the connections are expressed with connection coefficients by the following equations:

$$\left.\begin{aligned} K_{\nu,\nu-1}\Delta x_\nu &= \Delta u_{\nu-1}, \quad (\nu = 1, 2, \cdots, n-1) \\ -K_{n,1} \cdot \Delta x_n &= \Delta u_1, \end{aligned}\right\} \tag{3}$$

or

$$\begin{pmatrix} \Delta u_1 \\ \Delta u_2 \\ \Delta u_3 \\ \vdots \\ \Delta u_n \end{pmatrix} = \begin{pmatrix} & & & & -K_{n,1} \\ K_{1,2} & & & & \\ & K_{2,3} & & & \\ & & K_{3,4} & & \\ & & & \ddots & \\ & & & K_{n-1,n} & \end{pmatrix} \cdot \begin{pmatrix} \Delta x_1 \\ \Delta x_2 \\ \Delta x_3 \\ \vdots \\ \Delta x_n \end{pmatrix}. \tag{4}$$

In (4), the connection coefficient $-K_{n,1}$ needs not be negative for the system to be an oscillator, but for the system to be an automatic control it must necessarily be negative.

Combining (2) and (3), we obtain the control equation

$$\begin{pmatrix} Z_{11} & & & K_{n,1} \\ -K_{1,2} & Z_{22} & & \\ & -K_{2,3} & Z_{33} & \\ & \ddots & \ddots & \\ & & \ddots & \ddots \\ & & -K_{n-1,n} & Z_{nn} \end{pmatrix} \cdot \begin{pmatrix} \Delta x_1 \\ \Delta x_2 \\ \Delta x_3 \\ \vdots \\ \Delta x_n \end{pmatrix} = \begin{pmatrix} 0 \\ 0 \\ 0 \\ \vdots \\ 0 \end{pmatrix}, \tag{5}$$

or

$$[\boldsymbol{Z}]\cdot[\Delta \boldsymbol{x}] = [0], \tag{5'}$$

where $[\boldsymbol{Z}]$ is the transient impedance matrix which represents the characteristics of the control system, and may also be called the control characteristic matrix. It must be noticed that the direction of signal transmission with respect to the elements of this matrix is of counter-clockwise.

The impedance matrix of a complicated system composed of many elements connected can be obtained by the tensor transformation of impedance, with invariant power, from the primitive networks before connection to the connected networks. Namely, if the transformation matrix of the connections is $[C]$, then the impedance $[Z']$ after connection is given by the following relation from the impedance $[Z]$ before connection :

$$[Z'] = [C]_t\cdot[Z]\cdot[C],$$

where $[C]_t$ is the transposed matrix of $[C]$.

For example, the detector of the automatic voltage regulator of generator (Fig. 2) is resolved into primary elements like Fig. 3. The transformation matrix in this case and the impedance of the primitive system are given by

$$[C] = \begin{array}{c} \\ x_1 \\ x_2 \\ x_3 \\ y_1 \\ y_2 \end{array} \begin{array}{c} \begin{array}{cc} x & y \end{array} \\ \begin{pmatrix} 1 & \\ 1 & \\ 1 & \\ & 1 \\ & 1 \end{pmatrix} \end{array} \quad \text{and} \quad [Z] = \begin{array}{c} \\ x_1 \\ x_2 \\ x_3 \\ y_1 \\ y_2 \end{array} \begin{array}{c} \begin{array}{ccccc} x_1 & x_2 & x_3 & y_1 & y_2 \end{array} \\ \begin{pmatrix} Mp^2 & & & & \\ & C_f & & -C_f & \\ & & C_k p & & \\ & -C_f & & C_f & \\ & & & & C_{kf}p \end{pmatrix} \end{array},$$

where p, M, C_f and C_k and C_{kf} mean $\frac{d}{dt}$, mass, a coefficient of restoring force and frictional coefficients respectively. Thus, the impedance after connection becomes

$$[Z'] = [C_t]\cdot[Z]\cdot[C] = \begin{pmatrix} Mp^2+C_k p+C_f & -C_f \\ -C_f & C_{kf}p+C_f \end{pmatrix}.$$

As shown in Fig. 4, the amplifier has the impedance $(L_2 p+r_2)$, and the input and

the output are related as

$$-K_2\Delta x = \Delta v_2 = (L_2 p + r_2)\Delta i_2 .$$

The impedance of the manipulator is $(L_3 p + r_3)$, and the relation between the input and the output is obtained from Fig. 5.

$$K_3\Delta i_2 = \Delta v_3 = (L_3 p + r_3)\Delta i_3 ,$$

and

$$\Delta v = K_0\Delta i_3 .$$

Then, the characteristic matrix of the generator control system (Fig. 2) is given as follows:

$$[Z] = \begin{array}{c} \\ \Delta v \\ \Delta x \\ \Delta y \\ \Delta i_2 \\ \Delta i_3 \end{array} \begin{array}{c} \begin{array}{ccccc} \Delta v & \Delta x & \Delta y & \Delta i_2 & \Delta i_3 \end{array} \\ \begin{pmatrix} 1 & & & & K_0 \\ -K_1 & (Mp^2 + C_k p + C_f) & -C_f & & \\ & -C_f & (C_k p + C_f) & & \\ & K_2 & & (L_2 p_2 + r_2) & \\ & & & -K_3 & (L_3 p + r_3) \end{pmatrix} \end{array} .$$

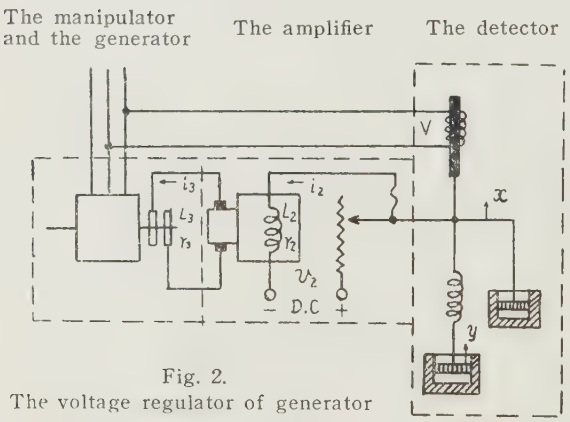

Fig. 2.
The voltage regulator of generator

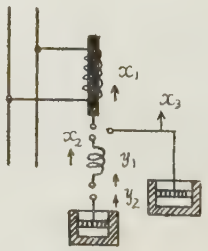

Fig. 3.
The primary elements of the detector

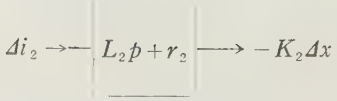

Fig. 4. Amplifier

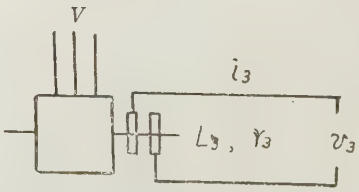

Fig. 5. Manipulator circuit

3. Vector representation of characteristics of the feed-back physical system

As stated above, the control equation of a closed-loop system is

$$[Z]\cdot[\Delta x]=[0],$$

where

$$[Z]=\begin{bmatrix} Z_{11} & & & & K_{n,1} \\ -K_{1,2} & Z_{22} & & & \\ & -K_{2,3} & Z_{33} & \ddots & \\ & & \ddots & \ddots & \\ & & & -K_{n-1,n} & Z_{nn} \end{bmatrix}.$$

Therefore the condition that the solution $[\Delta x]\neq[0]$ exists, i.e. the characteristic equation of the system is

$$|[Z]|=0. \tag{6}$$

The left side of this equation is an n-th degree polynominal of p. Thus we write:

$$|[Z]|=a_0p^n+a_1p^{n-1}+a_2p^{n-2}+\cdots\cdots+a_{n-1}p+a_n, \tag{7}$$

where a_ν's $(\nu=1,2,\cdots,n)$ are all real numbers because each element of the physical system has real constants.

The behaviour of the system is characterized by the roots of characteristic equation (6), and there exist n relations between the roots λ_i $(i=1,2,\cdots n)$ and the coefficients a_ν/a_0 $(\nu=1,2,\cdots,n)$. So, if a set of values of λ_i $(i=1,2,\cdots,n)$ are given, the coefficients a_ν/a_0, $(\nu=1,2,\cdots,n)$ are uniquely determined, and, conversely if a_ν/a_0 $(\nu=1,2,\cdots,n)$ are given, the values of λ_i $(i=1,2,\cdots,n)$ are uniquely obtained.

Thus, a set of roots λ_i $(i=1,2,\cdots,n)$ and a set of coefficients a_ν/a_0 $(\nu=1,2,\cdots,n)$, make one to one correspondence. In other words, a set of roots λ_i $(i=1,2,\cdots,n)$ uniquely corresponds to a vector whose components are $\xi_\nu=a_\nu/a_0$ $(\nu=1,2,\cdots,n)$, and this vector is called the characteristic vector, as it represents the behaviour of the physical system.

$\lambda_1,\lambda_2,\cdots,\lambda_n$ being roots of the characteristic equation, the general solution of the control equation is given by

$$\Delta x=A_1e^{\lambda_1t}+A_2e^{\lambda_2t}+\cdots\cdots+A_ne^{\lambda_nt},$$

where $A_1,A_2,\cdots,A_n$ are arbitrary constants.

The condition for the control system being stable is that the real parts α_i's of characteristic roots $\lambda_i=\alpha_i+j\omega_i$ are all negative, and if one or more of α_i's are zero or positive, the system is no longer stable. Accordingly, the condition for the physical

system to be in the critical state of stability is that at least one of α_i's is zero, and this condition is called the condition of critical stability. And as coefficients a_ν $(\nu = 1, 2, \cdots, n)$ of the characteristic equation:

$$a_0 p^n + a_1 p^{n-1} + a_2 p^{n-2} + \cdots\cdots + a_{n-1} p + a_n = 0$$

are continuous functions of characteristic roots λ_i $(i = 1, 2, \cdots, n)$, there must exist the stability region of the physical system which is continuous in the characteristic vector space.

4. Representation of characteristic roots in real coordinate system

As the characteristic equation has all real coefficients, each complex root is accompanied by its conjugate root λ_i^*, and these two roots $\lambda_i = \alpha_i + j\omega_i$, $\lambda_i^* = \alpha_i - j\omega_i$ are transformed into a pair of real numbers

$$\left.\begin{aligned} \beta_i &= -(\lambda_i + \lambda_i^*) = -2\alpha_i \,, \\ \gamma_i &= \lambda_i \lambda_i^* = \alpha_i^2 + \omega_i^2 \,. \end{aligned}\right\} \quad (8)$$

and

Conversely, if β_i and γ_i are given, λ_i and λ_i^* are readily obtained as roots of the equation:

$$p^2 + \beta_i p + \gamma_i = 0 \,, \quad (9)$$

where $\beta_i^2 - 4\gamma_i < 0$.

Any two real roots λ_i, λ_i' which correspond to imaginary $\omega = j\sigma$, (σ : real) can also be transformed into a pair of real numbers by

$$\left.\begin{aligned} \beta_i &= -(\lambda_i + \lambda_i') = -2\alpha_i \,, \\ \gamma_i &= \lambda_i \lambda_i' = \alpha_i^2 + \omega_i^2 = \alpha_i^2 - \sigma_i^2 \,, \end{aligned}\right\} \quad (8')$$

and

where

$$\beta_i^2 - 4\gamma_i \geqq 0 \,,$$

and the inverse transformation is performed by (9) also.

So, in case of an even-degree characteristic equation $(n = 2m)$, we can represent all the characteristic roots λ_i's in the system of pairs of coordinates (β_i, γ_i), $(i = 1, 2, \cdots, m)$. In case of an odd-degree characteristic equation $(n = 2m+1)$, one more real axis δ must be added to these pairs of coordinates.

Thus, the characteristic roots can be transformed into an n-dimensional vector $(\beta_1, \gamma_1, \beta_2, \gamma_2, \cdots)$, and the characteristic equation can be expressed in the form of the product of quadratic factors as follows.

When n is even $(2m)$

$$a_0 p^n + a_1 p^{n-1} + a_2 p^{n-2} + \cdots\cdots + a_{n-1} p + a_n$$
$$= a_0 (p^2+\beta_1 p+\gamma_1)(p^2+\beta_2 p+\gamma_2) \cdots\cdots (p^2+\beta_m p+\gamma_m) = 0\,, \tag{10}$$

and when n is odd $(2m+1)$

$$a_0 p^n + a_1 p^{n-1} + a_2 p^{n-2} + \cdots\cdots + a_{n-1} p + a_n$$
$$= a_0 (p^2+\beta_1 p+\gamma_1)(p^2+\beta_2 p+\gamma_2) \cdots\cdots (p^2+\beta_m p+\gamma_m)(p+\delta) = 0\,. \tag{10'}$$

The consideration about the stability is formulated as follows : in case when $\beta^2-4\gamma < 0$, i.e. oscillatory root, the stability region is given by $[\beta = -2\alpha > 0, \gamma = \alpha^2+\omega^2 > 0]$ and the critical stability is given by $[\beta = 0, \gamma = \omega^2 > 0]$, and in case when $\beta^2-4\gamma \geqq 0$, i.e. non-oscillaroty root, the two roots become $\alpha-\sigma$ and $\alpha+\sigma$, and the stability region is given by $[\beta = -2\alpha > 0\,,\ \gamma = \alpha^2+\omega^2 = (\alpha-\sigma)(\alpha+\sigma) > 0]$ and the critical stability is given by $[\beta = 0$, or $\gamma = 0]$.

Thus in other words, the stability region in (β, γ)-space is the first quadrant, and the critical stability is given by the boundaries of this quadrant i.e. $\beta = 0$ and $\gamma = 0$.

The hypersurface of critical stability is generated by fixing one of the coordinate axes, for instance β_m or γ_m at zero.

The stability region and the hypersurface of critical stability in ξ-vector space are obtained by the mapping from (β, γ)-space to ξ-vector space.

i) $\gamma_m = 0$

When $n = 2m$, the characteristic equation is

$$p^n + \xi_1 p^{n-1} + \xi_2 p^{n-2} + \cdots + \xi_{n-1} p + \xi_n$$
$$= (p^2+\beta_1 p+\gamma_1)(p^2+\beta_2 p+\gamma_2) \cdots (p^2+\beta_{m-1} p+\gamma_{m-1})(p+\beta_m)\, p = 0\,,$$

or

$$(p^2+\beta_1 p+\gamma_1)(p^2+\beta_2 p+\gamma_2) \cdots (p^2+\beta_{m-1} p+\gamma_{m-1})(p+\beta_m)$$
$$= p^{n-1} + \xi_1' p^{n-2} + \xi_2' p^{n-3} + \cdots + \xi_{n-2}' p + \xi_{n-1}' = 0\,, \tag{11}$$

where ξ_ν's $(\nu = 1, 2, \cdots, n-1)$ are the components of the $(n-1)$-dimensional stable-vector. Thus, the hypersurface of critical stability corresponding to $\gamma_m = 0$ in the n-dimensional ξ-vector space is a stable region in the $(n-1)$-dimensional characteristic vector space.

When $n = 2m+1$, the characteristic equation is

$$p^n + \xi_1 p^{n-1} + \xi_2 p^{n-2} + \cdots + \xi_{n-1} p + \xi_n$$
$$= (p^2+\beta_1 p+\gamma_1)(p^2+\beta_2 p+\gamma_2) \cdots (p^2+\beta_{m-1} p+\gamma_{m-1})(p+\beta_m)\, p(p+\delta) = 0\,,$$

or

$$(p^2+\beta_1 p+\gamma_1)(p^2+\beta_2 p+\gamma_2)\cdots(p^2+\beta_{m-1}p+\gamma_{m-1})(p+\delta)(p+\beta_m)$$
$$=p^{n-1}+\xi_1' p^{n-2}+\xi_2' p^{n-3}+\cdots+\xi_3' p+\xi_{n-1}'=0\,. \tag{11'}$$

Thus, the hypersurface of critical stability corresponding to $\gamma_m=0$ in the n-dimensional ξ-vector space is also a stable region in the $(n-1)$-dimensional characteristic vector space.

ii) $\beta_m=0$

When $n=2m$, the characteristic equation is

$$p^n+\xi_1 p^{n-1}+\xi_2 p^{n-2}+\cdots+\xi_{n-1}p+\xi_n$$
$$=(p^2+\beta_1 p+\gamma_1)(p^2+\beta_2 p+\gamma_2)\cdots(p^2+\beta_{m-1}p+\gamma_{m-1})(p^2+\gamma_m)$$
$$=(p^{n-2}+\zeta_1 p^{n-3}+\zeta_2 p^{n-4}+\cdots+\zeta_{n-3}p+\zeta_{n-2})(p^2+\gamma_m)=0\,, \tag{12}$$

where $[\zeta_\nu]$ $(\nu=1,2,\cdots n-2)$ is an $(n-2)$-dimensional stable vector.

So, the hypersurface of critical stability in the n-dimensional vector space is the $(n-2)$-dimensional stable vector operated by $(p^2+\gamma_m)$.

When $n=2m+1$, the characteristic equation is

$$p^n+\xi_1 p^{n-2}+\xi_2 p^{n+2}+\cdots+\xi_{n-1}p+\xi_n$$
$$=(p^2+\beta_1 p+\gamma_1)(p^2+\beta_2 p+\gamma_2)\cdots(p^2+\beta_{m-1}p+\gamma_{m-1})(p^2+\gamma_m)(p+\delta)$$
$$=(p^{n-2}+\zeta_1 p^{n-3}+\zeta_2 p^{n-4}+\cdots+\zeta_{n-3}p+\zeta_{n-2})(p^2+\gamma_m)=0\,. \tag{12'}$$

Thus, the hypersurface of critical stability corresponding to $\beta_m=0$ in the n-dimensional characteristic vector space is an $(n-2)$-dimensional stable vector operated by $(p^2+\gamma_m)$.

From the above it follows that the region of critical stability in the n-dimensional characteristic vector space consists of two kinds of hypersurfaces, of which one is a stable region of the $(n-1)$-dimensional vector space and the other is generated from an $(n-2)$-dimensional stable vector operated by $(p^2+\gamma_m)$.

5. Successive transformations of ξ-vector

We shall denote the n-dimensional characteristic vector with $[\xi_\nu^n]$ $(\nu=1,2,\cdots,n)$ in the following.

Then, we have

$$p^n+\xi_1^n p^{n-1}+\xi_2^n p^{n-2}+\cdots+\xi_{n-1}^n p+\xi_n^n$$
$$=(p^2+\beta_1 p+\gamma_1)(p^2+\beta_2 p+\gamma_2)\cdots(p^2+\beta_m p+\gamma_m)\,,\qquad \text{for}\quad n=2m \tag{13}$$

or

$$=(p+\delta)(p^2+\beta_1 p+\gamma_1)(p^2+\beta_2 p+\gamma_2)\cdots(p^2+\beta_m p+\gamma_m)\,,\quad \text{for}\quad n=2m-1. \tag{13'}$$

And we can easily deduce the following equation

$$p^n+\xi_1^n p^{n-1}+\xi_2^n p^{n-2}+\cdots+\xi_{n-1}^n p+\xi_n^n$$
$$=(p^2+\beta_m p+\gamma_m)(p^{n-2}+\xi_1^{n-2}p^{n-2}+\xi_2^{n-2}p^{n-4}+\cdots+\xi_{n-2}^{n-2})\ .$$

Thus, a stable region of the n-dimensional characteristic vector is obtained by operating the factor $(p^2+\beta p+\gamma)$ to the $(n-2)$-dimensional stable vector. This relation is expressed by

$$[\xi_\nu^n]=[C_{n-2}^n]\cdot[\xi_\mu^{n-2}], \tag{14}$$

where $\nu=1,2,\cdots,n$: $\mu=1,2,\cdots,n-2$.

Or, if we define $\xi_0^n=\xi_0^{n-2}=1$, (14) is transformed to

$$\begin{pmatrix}\xi_0^n\\ \xi_1^n\\ \xi_2^n\\ \vdots\\ \xi_{n-2}^n\\ \xi_{n-1}^n\\ \xi_n^n\end{pmatrix}=\begin{pmatrix}1 & & & & & \\ \beta & 1 & & & & \\ \gamma & \beta & 1 & & & \\ & \gamma & \beta & \ddots & & \\ & & \gamma & \ddots & \ddots & \\ & & & \ddots & \ddots & 1\\ & & & & \beta & \\ & & & & \gamma & \end{pmatrix}\cdot\begin{pmatrix}\xi_0^{n-2}\\ \xi_1^{n-2}\\ \xi_2^{n-2}\\ \vdots\\ \xi_{n-2}^{n-2}\end{pmatrix}. \tag{14'}$$

$[C_{n-2}^n]$ is indeed a rectangular matrix of $(n+1)$ rows and $(n-1)$ columns, but it is possible to replace it with a square matrix $[C^n]$ by adding two zero components ξ_{n-1}^{n-2}, ξ_n^{n-2} to the vector $[\xi_\nu^{n-2}]$, $(\nu=1,2,\cdots,n-2)$. Thus we have

$$\begin{pmatrix}\xi_0^n\\ \xi_1^n\\ \xi_2^n\\ \vdots\\ \xi_{n-2}^n\\ \xi_{n-1}^n\\ \xi_n^n\end{pmatrix}=\begin{pmatrix}1 & & & & & \\ \beta & 1 & & & & \\ \gamma & \beta & 1 & & & \\ & \gamma & \beta & \ddots & & \\ & & \gamma & \ddots & \ddots & \\ & & & \ddots & \ddots & 1\\ & & & & \beta & 1\\ & & & & \gamma & \beta & 1\end{pmatrix}\cdot\begin{pmatrix}\xi_0^{n-2}\\ \xi_1^{n-2}\\ \xi_2^{n-2}\\ \vdots\\ \xi_{n-2}^{n-2}\\ 0\\ 0\end{pmatrix}, \tag{14''}$$

or

$$[\xi^n]=[C^n]\cdot[\xi^{n-2}].$$

Since (14) is a reduction formula, we can write, in case when $n=2m+1$,

$$[\xi^n]=[C_{n-2}^n]\cdot[C_{n-4}^{n-2}]\cdot[C_{n-6}^{n-4}]\cdots[C_1^3]\cdot[\xi^1], \tag{15}$$

and in case when $n=2m$,

$$[\xi^n]=[C_{n-2}^n]\cdot[C_{n-4}^{n-2}]\cdot[C_{n-6}^{n-4}]\cdots[C_0^2]\cdot[\xi^0], \tag{15'}$$

where $[\xi^n]$ denotes $[\xi_\nu^n]$, $(\nu=0,1,2,\cdots,n)$, $\xi_0^n=1$ including, of course $[\xi^0]=\xi_0^0=1$ and

$$[\xi^1] = \begin{bmatrix} 1 \\ \delta \end{bmatrix}, \qquad \delta > 0 .$$

Thus we find that (15′) is deduced from (15) by putting $\xi_1^1 = \delta = 0$.

With an n-dimensional stable vector $\xi_\nu^n \equiv \xi_\nu$, $(\nu = 0, 1, 2, \cdots, n)$, and an $(n-2)$-dimensional stable vector $\xi_\mu^{n-2} \equiv \xi_\mu$, $(\mu = 0, 1, 2, \cdots, n-2)$, (14′) is expanded as:

$$\begin{aligned}
\xi_0 &= \zeta_0 , \\
\xi_1 &= \zeta_1 + \beta\zeta_0 , \\
\xi_2 &= \zeta_2 + \beta\zeta_1 + \gamma\zeta_0 , \\
\xi_3 &= \zeta_3 + \beta\zeta_2 + \gamma\zeta_1 , \\
&\cdots\cdots\cdots\cdots \\
&\cdots\cdots\cdots\cdots \\
\xi_{n-3} &= \zeta_{n-3} + \beta\zeta_{n-4} + \gamma\zeta_{n-5} , \\
\xi_{n-2} &= \zeta_{n-2} + \beta\zeta_{n-3} + \gamma\zeta_{n-4} , \\
\xi_{n-1} &= \beta\zeta_{n-2} + \gamma\zeta_{n-3} , \\
\xi_n &= \gamma\zeta_{n-2} ,
\end{aligned} \tag{16}$$

where β and γ are positive real parameters.

If we put $\zeta_{n-2} = 0$ in equation (16), ξ-vector is reduced to an $(n-1)$-dimensional stable vector, since the vector:

$$[\xi_{n-2}, \xi_{n-1}, \xi_n] = \zeta_{n-2}[1, \beta, \gamma], \tag{17}$$

which is enclosed by dotted lines in (16), vanishes.

By repeating this procedure we can at last get to the 2-dimensional stable vector:

$$[\xi_0, \xi_1, \xi_2] = \zeta_0[1, \beta, \gamma].$$

Conversely, by adding a vector of type (17) which is called the successive transformation vector, one by one, the stable ξ-vectors of higher dimensions are obtained successively.

6. Hypersurface of critical stability

The characteristic vectors which satisfy the condition of critical stability i.e. the characteristic vectors of critical stability are obtained by putting $\gamma = 0$ or $\beta = 0$ in equation (14″).

i) $\gamma = 0$:

$\xi_n = 0$ follows, and the stability region of the $(n-1)$-dimensional characteristic vector forms a part of the critical-stability-hypersurface of the n-dimensional vector space.

ii) $\beta = 0$:

We obtain a hypersurface in the n-dimensional ξ-vector space, which is subject

to one of β_i's being equal to zero, and this hypersurface is a boundary of the stability region of the n-dimensional ξ-vector space.

Namely, putting $\beta = 0$ in equation (14″), we get

$$\begin{pmatrix} \xi_0 \\ \xi_1 \\ \xi_2 \\ \vdots \\ \xi_{n-2} \\ \xi_{n-1} \\ \xi_n \end{pmatrix} = \begin{pmatrix} 1 & & & & & \\ 0 & 1 & & & & \\ \gamma & 0 & \ddots & & & \\ & \gamma & \ddots & \ddots & & \\ & & \ddots & \ddots & 1 & \\ & & & \ddots & 0 & 1 \\ & & & & \gamma & 0 & 1 \end{pmatrix} \cdot \begin{pmatrix} \zeta_0 \\ \zeta_1 \\ \zeta_2 \\ \vdots \\ \zeta_{n-2} \\ 0 \\ 0 \end{pmatrix} \tag{18}$$

The vector of critical stability, which is defined by (18) and we call the critical vector, is resolved into two vectors:

$$\begin{aligned} [\xi_{2\nu}] &= [C_{(\gamma)}] \cdot [\zeta_{2\nu}] \quad (\nu = 0, 1, 2, \cdots m), \\ [\xi_{2\nu+1}] &= [C_{(\gamma)}] \cdot [\zeta_{2\nu+1}] \quad (\nu = 0, 1, 2, \cdots m'), \end{aligned} \tag{19}$$

where

$$m' = \begin{cases} m-1 & \text{for } n = 2m, \\ m & \text{for } n = 2m+1, \end{cases}$$

and

$$[C_{(\gamma)}] = \begin{pmatrix} 1 & & & & \\ \gamma & 1 & & & \\ & \gamma & 1 & & \\ & & \gamma & \ddots & \\ & & & \ddots & 1 \\ & & & & \gamma \quad 1 \end{pmatrix}.$$

From (19), we obtain

$$\begin{aligned} [\zeta_{2\nu}] &= [C_{(\gamma)}]^{-1} \cdot [\xi_{2\nu}], \\ [\zeta_{2\nu+1}] &= [C_{(\gamma)}]^{-1} \cdot [\xi_{2\nu+1}], \end{aligned} \tag{20}$$

where

$$[C_{(\gamma)}]^{-1} = \begin{pmatrix} 1 & & & & & \\ -\gamma & 1 & & & & \\ \gamma^2 & -\gamma & 1 & & & \\ -\gamma^3 & \gamma^2 & -\gamma & 1 & & \\ \cdots & \cdots & \cdots & \cdots & \ddots & \\ \cdots & \cdots & \cdots & \cdots & \ddots & \\ \cdots & \cdots & \cdots & \cdots & \ddots & \\ \cdots & \cdots & \cdots & \cdots & \ddots & \\ \cdots & \cdots & \cdots & \gamma^2 & -\gamma & 1 \end{pmatrix}.$$

The last two components of $[\zeta]$ expressed by (20) give:

$$\left.\begin{aligned}\xi_{n-1} &= \gamma\xi_{n-3}-\gamma^2\xi_{n-5}+\gamma^3\xi_{n-7}\cdots\cdots\cdots\cdots\cdots,\\ \xi_n &= \gamma\xi_{n-2}-\gamma^2\xi_{n-4}+\gamma^3\xi_{n-6}\cdots\cdots\cdots\cdots\cdots,\end{aligned}\right\} \tag{21}$$

and these equations correspond to those which can be obtained by eliminating ζ_ν from (18), i.e. the equation of the critical vector.

Equations (21) represent a hyperline for a given γ which is an intersection of two hypersurfaces defined by these two equations. When γ is taken as a parameter, the hyperline represented by (21) moves as γ varies, and generates a hypersurface in the n-dimensional space and this space is called the hypersurface of critical stability.

It should be noted that one of the equations (21) is related only to the axes of odd numbers and the other only to those of even numbers, and if n is odd, the degrees of the two equations referring to γ are both $(n-1)/2$, and if n is even, the degrees of the two equations are $(n-2)/2$ and $n/2$ respectively.

Equations (21) for successive numbers of dimension are arranged as follows:

$$\left.\begin{aligned}
&\text{1-dimension}\quad \xi_0,\\
&\text{2-dimensions}\quad \xi_1,\\
&\text{3-dimensions}\quad \xi_2=\gamma\xi_0,\\
&\text{4-dimensions}\quad \xi_3=\gamma\xi_1,\\
&\text{5-dimensions}\quad \xi_4=\gamma\xi_2-\gamma^2\xi_0,\\
&\text{6-dimensions}\quad \xi_5=\gamma\xi_3-\gamma^2\xi_1,\\
&\text{7-dimensions}\quad \xi_6=\gamma\xi_4-\gamma^2\xi_2+\gamma^3\xi_0,\\
&\qquad\qquad \xi_7=\gamma\xi_5-\gamma^2\xi_3+\gamma^3\xi_1,\\
&\qquad\qquad \cdots\cdots\cdots\cdots\cdots\cdots\cdots\cdots\cdots\cdots\cdots\cdots\\
&\qquad\qquad \cdots\cdots\cdots\cdots\cdots\cdots\cdots\cdots\cdots\cdots\cdots\cdots\\
&n\text{-dimensions}\quad \xi_{n-1}=\gamma\xi_{n-3}-\gamma^2\xi_{n-5}+\gamma^3\xi_{n-7}-\cdots\cdots\cdots,\\
&\qquad\qquad \xi_n=\gamma\xi_{n-2}-\gamma^2\xi_{n-4}+\gamma^3\xi_{n-6}-\cdots\cdots\cdots.
\end{aligned}\right\} \tag{22}$$

Any two consecutive equations, in the above system of equations (22), express a hypersurface of critical stability, and with the ascending number of dimension, the pair of equations slides from one to the next. This is the successive character of the hypersurface of critical stability.

7. Stability criterion

The surface of critical stability evidently serves as stability criterion. Practically it is convenient to use plane diagrams which are produced by sections of the critical stability-hypersurface by planes.

Any n-dimensional stable vector is formed by adding successively vectors of

type (17) on the 3-dimensional vector $[\xi_{n-2}, \xi_{n-1}, \xi_n]$ of (16).

So, we put in (16)

$$\xi_0 = \text{const.}, \quad \xi_1 = \text{const.}, \cdots, \xi_{n-3} = \text{const.},$$

$$\xi_{n-2} = x, \quad \xi_{n-1} = y, \quad \xi_n = z.$$

Then, the vector $\boldsymbol{A}(x, y, z)$ is determined as a function of β, γ, and ζ_{n-2}, i.e.

$$\boldsymbol{A} = \boldsymbol{R} + \boldsymbol{S}, \tag{23}$$

where

$$\boldsymbol{R} = \zeta_{n-2}(\boldsymbol{i}_{n-2} + \beta \boldsymbol{i}_{n-1} + \gamma \boldsymbol{i}_n),$$

$$\boldsymbol{S} = (\beta\zeta_{n-3} + \gamma\zeta_{n-4})\,\boldsymbol{i}_{n-2} + \gamma\zeta_{n-3}\boldsymbol{i}_{n-1}.$$

$\boldsymbol{R}$ has the direction which is determined by β and γ. ζ_{n-2} can vary within the $(n-2)$-dimensional stability region. $\boldsymbol{S}$ is a 2-dimensional stable vector of the $(n-1)$-dimensional stability region.

Thus, if $\boldsymbol{R}$ is supperposed upon the section of the $(n-1)$-dimensional stable vector by the (ξ_{n-2}, ξ_{n-1})-plane, we can obtain the section of the n-dimensional stable vector by a 3-dimensional space.

$\boldsymbol{R}$ is a successive transformation vector, as mentioned before. With this vector added one can obtain an n-dimensional stable vector from an $(n-1)$-dimensional vector.

If β tends to zero, then $\zeta_0, \zeta_1, \cdots \zeta_{n-3}$ become functions of γ only and

$$\boldsymbol{R} = \zeta_{n-2}(\boldsymbol{i}_{n-2} + \gamma \boldsymbol{i}_n),$$

$$\boldsymbol{S} = \gamma(\zeta_{n-4}\boldsymbol{i}_{n-2} + \zeta_{n-3}\boldsymbol{i}_{n-1}),$$

and

$$\boldsymbol{A} = \boldsymbol{R} + \boldsymbol{S}.$$

That is, a section $\boldsymbol{A}$ of the n-dimensional critical stability-hypersurface by the three-dimensional space $(\xi_{n-2}, \xi_{n-1}, \xi_n)$ is composed of a section $\boldsymbol{S}$ of the $(n-1)$-dimensional critical stability-hypersurface by the two-dimensional space (ξ_{n-2}, ξ_{n-1}) and a transformation vector $\boldsymbol{R} = \zeta_{n-2}(\boldsymbol{i}_{n-2} + \gamma \boldsymbol{i}_n)$.

It is clear that the stability region exists on that side of the section of the critical stability-hypersurface by the three-dimensional space $(\xi_{n-2}, \xi_{n-1}, \xi_n)$, on which exists the stability region of the $(n-1)$-dimensional vector which is the base of the n-dimensional vector.

Generally it is shown as follows that when $\boldsymbol{R} = \zeta_{n-2}(\boldsymbol{i}_{n-2} + \gamma \boldsymbol{i}_n)$ moves in the direction of γ increasing, holding its starting point on the locus of the end point of $\boldsymbol{S}$, the stability region is included only on the right side of $\boldsymbol{R}$, but not on its left side.

We differentiate partially each equation of the n-dimensional stable vector (16) with respect to β and γ respectively, fixing $\xi_0, \xi_1, \cdots, \xi_{n-3}$ at constant values, and

put $\beta = 0$ in these results. Then the relations on the critical stability hypersurface of $\beta = 0$ are obtained.

They are

$$\left.\begin{aligned}
&\frac{\partial \zeta_0}{\partial \beta} = 0\,,\\
&\frac{\partial \zeta_1}{\partial \beta} = -\zeta_0\,,\\
&\frac{\partial \zeta_2}{\partial \beta} = -\zeta_1\,,\\
&\frac{\partial \zeta_3}{\partial \beta} = -\zeta_2+\gamma\zeta_0\,,\\
&\frac{\partial \zeta_4}{\partial \beta} = -\zeta_3+\gamma\zeta_1\,,\\
&\frac{\partial \zeta_5}{\partial \beta} = -\zeta_4+\gamma\zeta_2-\gamma^2\zeta_0\,,\\
&\qquad\cdots\cdots\cdots\cdots\cdots\cdots\cdots\cdots\cdots\cdots\\
&\qquad\cdots\cdots\cdots\cdots\cdots\cdots\cdots\cdots\cdots\cdots\\
&\frac{\partial \zeta_{n-3}}{\partial \beta} = -\zeta_{n-4}+\gamma\zeta_{n-6}-\gamma^2\zeta_{n-8}+\cdots\,,\\
&\frac{\partial \xi_{n-2}}{\partial \beta} = \zeta_{n-3}-\gamma\zeta_{n-5}+\gamma^2\zeta_{n-7}-\gamma^3\zeta_{n-9}+\cdots\,,\\
&\frac{\partial \xi_{n-1}}{\partial \beta} = \zeta_{n-2}-\gamma\zeta_{n-4}+\gamma^2\zeta_{n-6}-\gamma^3\zeta_{n-8}+\cdots\,,\\
&\frac{\partial \xi_n}{\partial \beta} = 0\,,
\end{aligned}\right\} \tag{24}$$

where we have $\dfrac{\partial \zeta_{n-2}}{\partial \beta} = 0$ owing to $\dfrac{\partial \xi}{\partial \beta} = \left(\dfrac{\partial \xi}{\partial \beta}\right)_{\substack{\gamma=\text{const.}\\ \zeta_{n-2}=\text{const.}}}$, because in the section of the vector by the 3-dimensional space $(\xi_{n-2}, \xi_{n-1}, \xi_n)$ the degrees of freedom are 3 and so for the independent variables, β, γ and ζ_{n-2} can be adopted.

Also, we have

$$\begin{aligned}
&\frac{\partial \zeta_0}{\partial \gamma} = 0\,,\\
&\frac{\partial \zeta_1}{\partial \gamma} = 0\,,\\
&\frac{\partial \zeta_2}{\partial \gamma} = -\zeta_0\,,\\
&\frac{\partial \zeta_3}{\partial \gamma} = -\zeta_1\,,\\
&\frac{\partial \zeta_4}{\partial \gamma} = -\zeta_2+\gamma\zeta_0\,,
\end{aligned}$$

$$
\begin{aligned}
&\frac{\partial \zeta_5}{\partial \gamma} = -\zeta_3 + \gamma\zeta_1 , \\
&\qquad \cdots\cdots\cdots\cdots\cdots\cdots\cdots\cdots \\
&\qquad \cdots\cdots\cdots\cdots\cdots\cdots\cdots\cdots \\
&\frac{\partial \zeta_{n-3}}{\partial \gamma} = -\zeta_{n-5} + \gamma\zeta_{n-7} - \gamma^2\zeta_{n-9} + \cdots , \\
&\frac{\partial \xi_{n-2}}{\partial \gamma} = \zeta_{n-4} - \gamma\zeta_{n-6} + \gamma^2\zeta_{n-8} - \gamma^3\zeta_{n-10} + \cdots , \\
&\frac{\partial \xi_{n-1}}{\partial \gamma} = \zeta_{n-3} - \gamma\zeta_{n-5} + \gamma^2\zeta_{n-7} - \gamma^3\zeta_{n-9} + \cdots , \\
&\frac{\partial \xi_n}{\partial \gamma} = \zeta_{n-2} .
\end{aligned}
\tag{25}
$$

On the other hand, from (20) we have

$$
\begin{aligned}
\zeta_0 &= \xi_0 , \\
\zeta_1 &= \xi_1 , \\
\zeta_2 &= \xi_2 - \gamma\xi_0 , \\
\zeta_3 &= \xi_3 - \gamma\xi_1 , \\
\zeta_4 &= \xi_4 - \gamma\xi_2 + \gamma^2\xi_0 , \\
\zeta_5 &= \xi_5 - \gamma\xi_3 + \gamma^2\xi_1 , \\
&\qquad \cdots\cdots\cdots\cdots\cdots\cdots\cdots\cdots \\
&\qquad \cdots\cdots\cdots\cdots\cdots\cdots\cdots\cdots \\
\zeta_{n-3} &= \xi_{n-3} - \gamma\xi_{n-5} + \gamma^2\xi_{n-7} - \gamma^3\xi_{n-9} + \cdots , \\
\zeta_{n-2} &= \xi_{n-2} - \gamma\xi_{n-4} + \gamma^2\xi_{n-6} - \gamma^3\xi_{n-8} + \cdots .
\end{aligned}
\tag{26}
$$

Substituting (26) into (24) and (25), we get

$$
\begin{aligned}
&\frac{\partial \xi_{n-2}}{\partial \beta} = \xi_{n-3} - 2\gamma\xi_{n-5} + 3\gamma^2\xi_{n-7} - \cdots\cdots , \\
&\frac{\partial \xi_{n-1}}{\partial \beta} = \xi_{n-2} - 2\gamma\xi_{n-4} + 3\gamma^2\xi_{n-6} - \cdots\cdots , \\
&\frac{\partial \xi_n}{\partial \beta} = 0 , \\
&\frac{\partial \xi_{n-2}}{\partial \gamma} = \xi_{n-4} - 2\gamma\xi_{n-6} + 3\gamma^2\xi_{n-8} - \cdots\cdots , \\
&\frac{\partial \xi_{n-1}}{\partial \gamma} = \xi_{n-3} - 2\gamma\xi_{n-5} + 3\beta^2\xi_{n-7} - \cdots\cdots , \\
&\frac{\partial \xi_n}{\partial \gamma} = \zeta_{n-2} = x ,
\end{aligned}
$$

from which we obtain

$$\frac{\partial \xi_n}{\partial \beta^{-2}} = \frac{\partial \xi_{n-1}}{\partial \gamma},$$
$$\frac{\partial \xi_{n-1}}{\partial \beta} = \frac{\partial \xi_n}{\partial \gamma} - \gamma \frac{\partial \xi_{n-2}}{\partial \gamma},$$
$$\frac{\partial \xi_n}{\partial \beta} = 0.$$

And on the other hand we have

$$\frac{\partial \xi_{n-2}}{\partial \zeta_{n-2}} = \frac{\partial \xi_{n-2}}{\partial x} = 1,$$
$$\frac{\partial \xi_{n-1}}{\partial \zeta_{n-2}} = \frac{\partial \xi_{n-1}}{\partial x} = \beta,$$
$$\frac{\partial \xi_n}{\partial \zeta_{n-2}} = \frac{\partial \xi_n}{\partial x} = \gamma.$$

Now, we consider any characteristic vector $\boldsymbol{A}_0$ which ends on the surface of critical stability ($\beta = 0$), and take the following differential vectors.

$$\left.\begin{aligned} d_x \boldsymbol{A} &= \left(\frac{\partial \boldsymbol{A}}{\partial x}\right)_0 dx, \\ d_\beta \boldsymbol{A} &= \left(\frac{\partial \boldsymbol{A}}{\partial \beta}\right)_0 d\gamma, \\ d_\gamma \boldsymbol{A} &= \left(\frac{\partial \boldsymbol{A}}{\partial \gamma}\right)_0 d\gamma, \end{aligned}\right\} \tag{27}$$

where $\left(\frac{\partial \boldsymbol{A}}{\partial x}\right)_0$ denotes a partial differential coefficient with respect to x at $\beta = 0$, $\gamma = \text{const}$, and so forth. From $\boldsymbol{A} = \xi_{n-2}\boldsymbol{i}_{n-2} + \xi_{n-1}\boldsymbol{i}_{n-1} + \xi_n \boldsymbol{i}_n$, it follows that

$$\left.\begin{aligned} \frac{\partial \boldsymbol{A}}{\partial \beta} &= \frac{\partial \xi_{n-1}}{\partial \gamma}\boldsymbol{i}_{n-2} + \left(x - \gamma \frac{\partial \xi_{n-2}}{\partial \gamma}\right)\boldsymbol{i}_{n-1}, \\ \frac{\partial \boldsymbol{A}}{\partial \gamma} &= \frac{\partial \xi_{n-2}}{\partial \gamma}\boldsymbol{i}_{n-2} + \frac{\partial \xi_{n-1}}{\partial \gamma}\boldsymbol{i}_{n-1} + x\boldsymbol{i}_n, \\ \frac{\partial \boldsymbol{A}}{\partial x} &= \boldsymbol{i}_{n-1} + \gamma \boldsymbol{i}_n. \end{aligned}\right\} \tag{28}$$

Since $d\boldsymbol{A}$ and $d_x\boldsymbol{A}$ lie on the surface of critical stability, the vector product $[d_\gamma \boldsymbol{A} \cdot d_x \boldsymbol{A}]$ is perpendicular to the surface of critical stability, and when $dx > 0$ and $d\gamma > 0$, it has its sense pointing to the right side of the vector $\boldsymbol{R}$, with reference to the moving direction of the generating line $\boldsymbol{R}_{\beta=0}$ with increasing γ. This sense which is indicated by the vector product $[d\boldsymbol{A} \cdot d_x \boldsymbol{A}]$, ($dx > 0$, $d\gamma > 0$) is called the right side or positive side of the critical stability-surface (Fig. 6).

The stability region (the region for $\beta > 0$) should lie on that side of the critical stability-surface, to which the sense of the vector

$$(d_x \boldsymbol{A})_{\beta=0} = \left(\frac{\partial \boldsymbol{A}}{\partial \beta}\right)_{\beta=0} \cdot d\beta$$

for $d\beta > 0$ points.

Therefore, on which side of the critical stability-surface the stability region exists can be determined by the sign of the ratio:

$$d_\beta \boldsymbol{A} \cdot [d_\gamma \boldsymbol{A} \cdot d_x \boldsymbol{A}] / d\beta d\gamma dx .$$

If this is positive, the stability region lies on the right side of the critical surface, and if negative, on the left side.

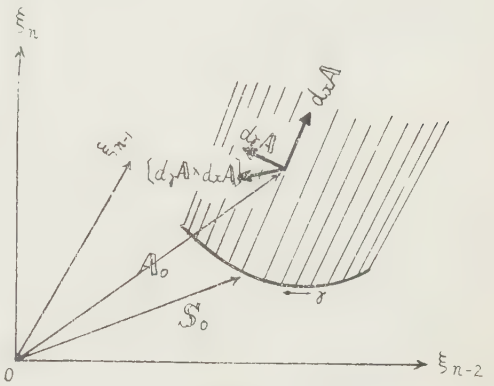

Fig. 6.

From (27) and (28) we obtain

$$d_\beta \boldsymbol{A} \cdot [d_\gamma \boldsymbol{A} \cdot d_x \boldsymbol{A}] / d\beta d\gamma dx = \left(\frac{\partial \boldsymbol{A}}{\partial \beta}\right)_0 \cdot \left[\left(\frac{\partial \boldsymbol{A}}{\partial \gamma}\right)_0 \left(\frac{\partial \boldsymbol{A}}{\partial x}\right)_0\right]$$

$$= \left[\left(\frac{\partial \boldsymbol{A}}{\partial \beta}\right)_0 \cdot \left(\frac{\partial \boldsymbol{A}}{\partial \gamma}\right)_0\right] \cdot \left(\frac{\partial \boldsymbol{A}}{\partial x}\right)_0 = x^2 + \gamma^2 \left(\frac{\partial \xi_{n-1}}{\partial \gamma}\right)^2 + \gamma^2 \left(\frac{\partial \xi_{n-2}}{\partial \gamma}\right)^2 .$$

Since γ is positive, it is evident that the stability region should lie on the right side of the surface of critical stability.

Thus, if the characteristic vector of the physical system has its end-point within the stability region, the system is stable, but if the characteristic vector has its end-point on the critical surface or outside of the stability region, then the system is unstable.

When the three-dimensional stability region of the vector $(\xi_{n-2}, \xi_{n-1}, \xi_n)$ is cut by a plane, the two-dimensional stability region bounded by a line of critical stability is obtained, and the stability region lies on the right side of this line in reference to γ increasing, but never lies on the left side (Fig. 7).

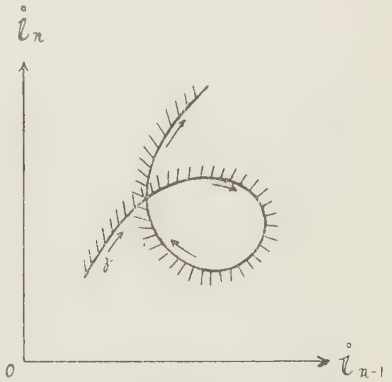

Fig. 7

Some examples of the section of the hypersurface of critical stability of the n-dimensional vector space by a plane parallel to the n-th and the $(n-1)$-th axes are shown in the following diagrams.

i) When $n = 3$, from (22) the surface of critical stability is given by:

$$\left.\begin{aligned} \xi_2 &= \gamma \xi_0 = \gamma , \\ \xi_3 &= \gamma \xi_1 , \end{aligned}\right\}$$

which are transformed to

$$\xi_2' = \xi_3' = \gamma ,$$

where

$$\left.\begin{aligned} \xi_2' &= \xi_2/\xi_0 , \\ \xi_3' &= \xi_3/\xi_1 . \end{aligned}\right\}$$

Thus the surface (line) of critical stability is shown on the (ξ_2', ξ_3')-plane as in Fig. 8.

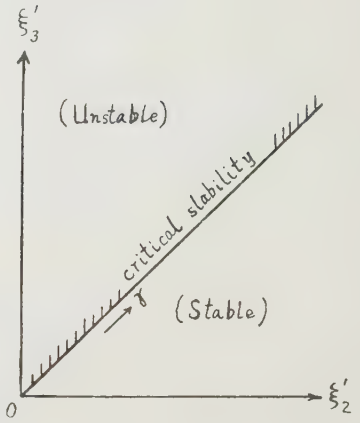

Fig. 8.

ii) When $n = 4$, we have likewise:

$$\left.\begin{aligned} \xi_3 &= \gamma\xi_1 , \\ \xi_4 &= \gamma\xi_2 - \gamma^2\xi_0 = \gamma\xi_2 - \gamma^2 , \end{aligned}\right\}$$

which are transformed to

$$\left.\begin{aligned} \xi_3' &= \gamma , \\ \xi_4' &= \gamma\xi_2' - \gamma^2 = \xi_3'(\xi_2' - \xi_3') , \end{aligned}\right\}$$

where

$$\xi_2' = \xi_2/\xi_0 , \quad \xi_3' = \xi_3/\xi_1 \quad \text{and} \quad \xi_4' = \xi_4/\xi_0 ,$$

and further to

$$\left.\begin{aligned} \xi_3'' &= \gamma' , \\ \xi_4'' &= \xi_3''(1 - \xi_3'') , \end{aligned}\right\}$$

where $\gamma' = \gamma/\xi_2'$, $\xi_3'' = \xi_3'/\xi_2'$ and $\xi_4'' = \xi_4'/(\xi_2')^2$.

The surface (line) of critical stability is shown in Fig. 9.

iii) When $n = 5$, we have:

$$\left.\begin{aligned} \xi_4 &= \gamma\xi_2 - \gamma^2\xi_0 , \\ \xi_5 &= \gamma\xi_3 - \gamma^2\xi_1 , \end{aligned}\right\}$$

which are transformed to

$$\left.\begin{aligned} \xi_4' &= \gamma\xi_2' - \gamma^2 , \\ \xi_5' &= \gamma\xi_3' - \gamma^2 , \end{aligned}\right\}$$

where

$$\left.\begin{aligned} \xi_{2\nu}' &= \xi_{2\nu}/\xi_0 , \\ \xi_{2\nu+1}' &= \xi_{2\nu+1}/\xi_1 , \end{aligned}\right\}$$

and further to

$$\left.\begin{aligned} \xi_4'' &= \gamma' - \gamma'^2 , \\ \xi_5'' &= \gamma'\xi_3'' - \gamma'^2 , \end{aligned}\right\}$$

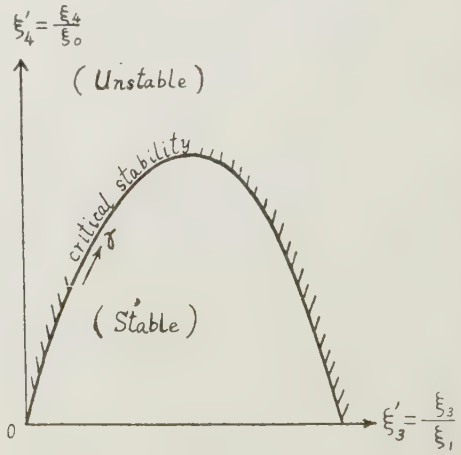

Fig. 9.

where $\gamma' = \gamma/\xi_2'$, $\xi_{2\nu}'' = \xi_{2\nu}'/(\xi_2')^\nu$ and $\xi_{2\nu+1}'' = \xi_{2\nu+1}'/(\xi_2')^\nu$.

The surface (line) of critical stability is shown in Fig. 10.

These sections of the surface of critical stability are useful not only for stability discrimination but also for constructing the surface of critical stability of higher dimensions.

Another practical form of criterion which is also convenient is the section of the hypersurface of critical stability by a plane parallel to the n-th and $(n-2)$-th axes. This time the section consists of some straight lines.

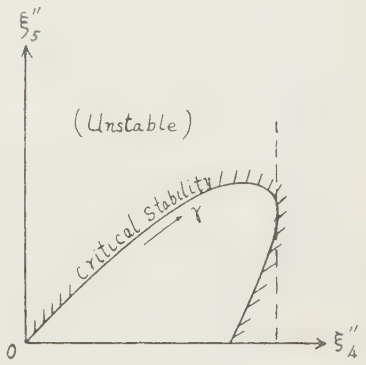

Fig. 10.

If in the pair of equations of the hypersurface of critical stability (21) which contain γ as a parameter, we suppose that $\xi_{n-1}, \xi_{n-3}, \xi_{n-4}, \xi_{n-5}, \cdots\cdots$, excepting ξ_n and ξ_{n-2}, are fixed at given constants, from the first equation of (21), the values of γ are obtained as roots, and these values of γ will determine the straight lines in the (ξ_n, ξ_{n-2})-plane by the second equation of (21).

When the physical system is stable, the first equation of (21) has real roots only. The reason is as follows. If the degree of this equation with respect to γ is m, and $\xi_{n-3}, \xi_{n-5}, \cdots\cdots$ are fixed and ξ_{n-1} is considered to be variable and fixed later, as seen from Fig. 11, the ξ_{n-1} of the stable vector lies between the largest minimum value and the smallest maximum value of the expression of the right-hand side of the equation. Therefore, the straight line $\xi_{n-1} =$ constant passing through (ξ_{n-1}, ξ_n) stability region intersects the line of critical stability at m points which correspond to m real roots. So if the equation has any non-real root, the physical system cannot have any stability region.

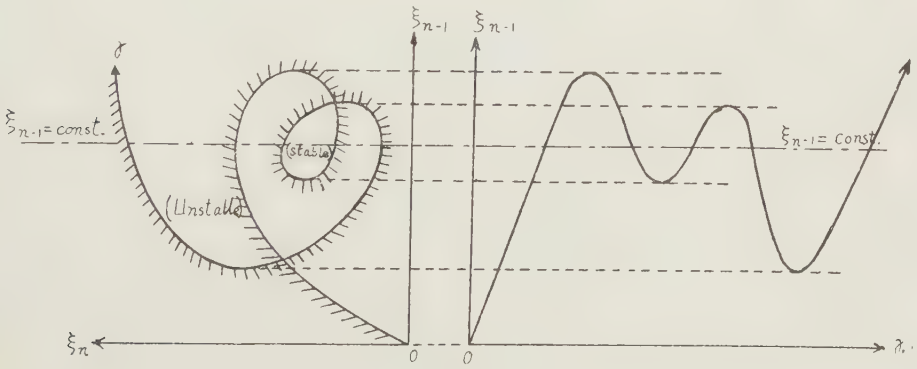

Fig. 11.

When the roots of one equation of (21) are all real, the straight lines determined by the other equation of (21), and those roots, will give the stability region as follows.

If all the real roots of the first equation of (21) are $\gamma_1, \gamma_2, \gamma_3, \cdots\cdots \gamma_m$, such that

$$\gamma_1 < \gamma_2 < \gamma_3 < \cdots < \gamma_m ,$$

the stability region is on the right side of each straight line corresponding to $\gamma_{2\nu-1}$, $(\nu = 1, 2, \cdots)$ and on the left side of each straight line corresponding to $\gamma_{2\nu}$, but never exists on the opposite sides, as shown in Fig. 12, in which the shaded sides of the γ–straight-lines are instability regions, and all the segments of γ–straight lines which bound the stability region are the stability criterion.

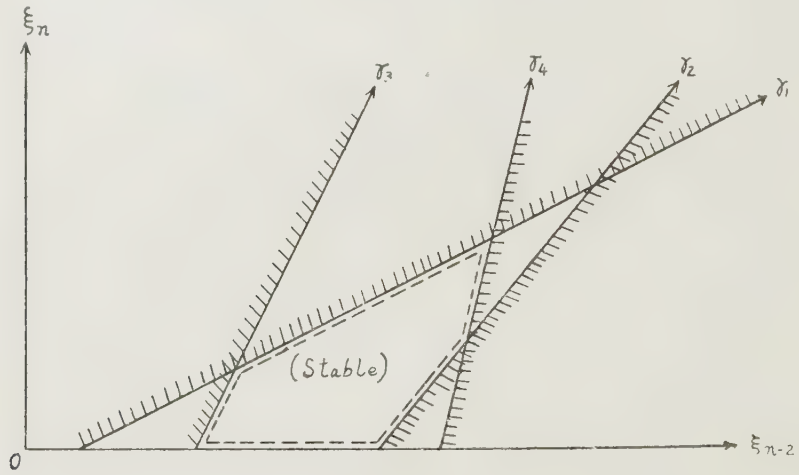

Fig. 12.

8. Relations with other stability criteria

1) Relation with Nyquist's criterion

If the closed-loop of the automatic control system is disconnected at the detector terminals, the input quantity $f(t)$ and the output quantity $y(t)$ of this open loop are related as follows:

$$(p^n + a_1 p^{n-1} + a_2 p^{n-2} + \cdots\cdots + a_n) y(t) = f(t) . \tag{29}$$

When this open loop is connected again and formed into a closed loop control system, the control equation becomes:

$$(p^n + a_1 p^{n-1} + a_2 p^{n-2} + \cdots\cdots + a_n) y(t) = -y(t) ,$$

and from this the characteristic equation is derived:

$$p^n + a_1 p^{n-1} + a^2 p^{n-2} + \cdots\cdots + a_n + 1 = 0 .$$

Thus, the characteristic vector of the closed loop becomes:

$$\begin{vmatrix} \xi_1 \\ \xi_2 \\ \xi_3 \\ \vdots \\ \xi_{n-1} \\ \xi_n \end{vmatrix} = \begin{vmatrix} a_1 \\ a_2 \\ a_3 \\ \vdots \\ a_{n-1} \\ a_n+1 \end{vmatrix} .$$

Therefore, the equation of the section of the hypersurface of critical stability by (ξ_{n-1}, ξ_n)-plane is given from (21) by

$$\left.\begin{aligned} \xi_n = x &= \gamma a_{n-2} - \gamma^2 a_{n-4} + \gamma^3 a_{n-6} - \cdots\cdots , \\ \xi_{n-1} = y &= \gamma a_{n-3} - \gamma^2 a_{n-5} + \gamma^3 a_{n-7} - \cdots\cdots . \end{aligned}\right\} \tag{30}$$

It should be noticed that the selection of x and y here differs from that in § 7, and so the stability region exists on the left side of the line of critical stability while in § 7 the stability region existed on the right side.

When a sinusoidal input $f(t) = A \sin \omega t$ is impressed at the detector terminals of the open-loop control system, the output will also be a sinusoidal quantity $y(t) = B \sin(\omega t - \varphi)$ in the steady state. Accordingly, if we put $f(t) = Ae^{j\omega t}$ and $y(t) = Be^{j(\omega t - \varphi)}$ in (29), we obtain

$$a_0(j\omega)^n + a_1(j\omega)^{n-1} + \cdots + a_{n-2}(j\omega)^2 + a_{n-1}(j\omega) + a_n = \frac{A}{B} e^{j\varphi} ,$$

or

$$\left.\begin{aligned} a_n - \omega^2 a_{n-2} + \omega^4 a_{n-4} - \omega^6 a_{n-6} + \cdots &= \frac{A}{B} \cos\varphi , \\ \omega a_{n-1} - \omega^3 a_{n-3} + \omega^5 a_{n-5} - \omega^7 a_{n-7} + \cdots &= \frac{A}{B} \sin\varphi , \end{aligned}\right\} \tag{31}$$

Putting $\gamma = \omega^2$ in (31), and comparing (31) with (30), we obtain

$$\left.\begin{aligned} a_n - x &= \frac{A}{B} \cos\varphi , \\ \omega a_{n-1} - y &= \frac{A}{B} \sin\varphi , \end{aligned}\right\} \tag{32}$$

or

$$\begin{bmatrix} a_n \\ a_{n-1} \end{bmatrix} - \begin{bmatrix} x \\ y \end{bmatrix} = \frac{A}{B} \begin{bmatrix} 1 & 0 \\ 0 & 1/\omega \end{bmatrix} \cdot \begin{bmatrix} \cos\varphi \\ \sin\varphi \end{bmatrix} . \tag{32'}$$

In the method of Nyquist and that of Leonhard, one must impress the input signal $Ae^{j\omega t}$ on the open-loop control system, and seek for the ratio of the output $Be^{j(\omega t - \varphi)}$ to the input as a function of ω:

$$\frac{Be^{j(\omega t - \varphi)}}{Ae^{j\omega t}} = \frac{B}{A} e^{-j\varphi} = \frac{B}{A} (\cos\varphi - j \sin\varphi) ,$$

or

$$\frac{B}{A}\begin{bmatrix}\cos\varphi\\ -\sin\varphi\end{bmatrix}.$$

The vector which represents the ratio is called Nyquist vector, and the locus of the end-point of Nyquist vector is called Nyquist locus.

Then, in Nyquist's method the stability of the system is determined by judging on which side of the locus the point $(-1, 0)$ is situated.

Denoting the Nyquist's vector with $[x_N, y_N]$, we obtain:

$$\begin{bmatrix}x_N\\ y_N\end{bmatrix}=\frac{B}{A}\begin{bmatrix}\cos\varphi\\ -\sin\varphi\end{bmatrix}=\frac{B}{A}\begin{bmatrix}1 & 0\\ 0 & -1\end{bmatrix}\begin{bmatrix}\cos\varphi\\ \sin\varphi\end{bmatrix},$$

or

$$\begin{bmatrix}\cos\varphi\\ \sin\varphi\end{bmatrix}=\frac{A}{B}\begin{bmatrix}1 & 0\\ 0 & -1\end{bmatrix}\begin{bmatrix}x_N\\ y_N\end{bmatrix}.$$

Then, from (32), the following equation is derived:

$$\begin{bmatrix}a_n\\ a_{n-1}\end{bmatrix}-\begin{bmatrix}x\\ y\end{bmatrix}=\left(\frac{A}{B}\right)^2\begin{bmatrix}1 & 0\\ 0 & 1/\omega\end{bmatrix}\cdot\begin{bmatrix}1 & 0\\ 0 & -1\end{bmatrix}\cdot\begin{bmatrix}x_N\\ y_N\end{bmatrix}. \tag{33}$$

On the other hand, in the case of the closed-loop control system, the section of the characteristic vector by the (ξ_n, ξ_{n-1})-plane is

$$\begin{bmatrix}x_0\\ y_0\end{bmatrix}=\begin{bmatrix}a_{n+1}\\ a_n\end{bmatrix}=\begin{bmatrix}a_n\\ a_{n-1}\end{bmatrix}+\begin{bmatrix}1\\ 0\end{bmatrix},$$

when we transfer the origin of the coordinates to (a_n, a_{n-1}), the characteristic vector of the closed-loop system is transformed into a fixed vector as follows:

$$\begin{bmatrix}x_0'\\ y_0'\end{bmatrix}=\begin{bmatrix}x_0\\ y_0\end{bmatrix}-\begin{bmatrix}a_n\\ a_{n-1}\end{bmatrix}=\begin{bmatrix}1\\ 0\end{bmatrix}. \tag{34}$$

And the section of the author's vector of critical stability is also transformed to:

$$\begin{bmatrix}x'\\ y'\end{bmatrix}=\begin{bmatrix}x\\ y\end{bmatrix}-\begin{bmatrix}a_n\\ a_{n-1}\end{bmatrix}. \tag{35}$$

Comparing (35) with (33), we obtain the following relation:

$$\begin{bmatrix}x'\\ y'\end{bmatrix}=-\left(\frac{A}{B}\right)^2\begin{bmatrix}1 & 0\\ 0 & 1/\omega\end{bmatrix}\cdot\begin{bmatrix}1 & 0\\ 0 & -1\end{bmatrix}\cdot\begin{bmatrix}x_N\\ y_N\end{bmatrix}. \tag{36}$$

Accordingly, if the end-point of the characteristic vector (34), i. e. the characteristic point (1, 0), is situated within the stability region, the system is stable. And the vector of critical stability (35) is obtained by the transformation (36) from the Nyquist vector. It is shown in Fig. 13, that the stability region exists on the left side of the Nyquist locus in reference to ω increasing.

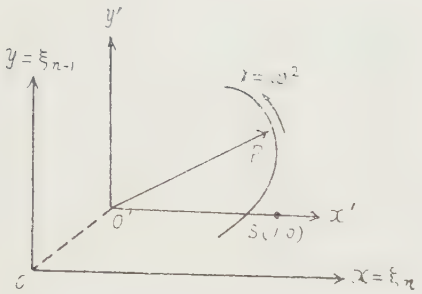

Fig. 13.

$\overrightarrow{OO'} = \begin{bmatrix} a_n \\ a_{n-1} \end{bmatrix}$

$\overrightarrow{O'S} = \begin{bmatrix} 1 \\ 0 \end{bmatrix}$: characteristic vector of the closed-loop system

$\overrightarrow{OP} = \begin{bmatrix} x \\ y \end{bmatrix}$: vector of critical stability (in old coordinates)

$\overrightarrow{O'P} = \begin{bmatrix} x' \\ y' \end{bmatrix}$: vector of critical stability (in new coordinates)

$\overrightarrow{PO'}$: Nyquist vector (transformed)

Fig. 13 shows a case of an unstable system whose characteristic point $S(1, 0)$ is situated on the right side of the line of critical stability.

Taking the origin of coordinates at the characteristic point (x_0, y_0) of the closed-loop physical system, the vector of critical stability becomes

$$\begin{bmatrix} x'' \\ y'' \end{bmatrix} \equiv \begin{bmatrix} x \\ y \end{bmatrix} - \begin{bmatrix} x_0 \\ y_0 \end{bmatrix},$$

and we obtain, from 33 ,

$$\begin{bmatrix} x'' \\ y'' \end{bmatrix} + \left(\frac{A}{B}\right)^2 \begin{bmatrix} 1 & 0 \\ 0 & 1/\omega \end{bmatrix} \cdot \begin{bmatrix} 1 & 0 \\ 0 & -1 \end{bmatrix} \cdot \begin{bmatrix} x_N \\ v_N \end{bmatrix} = \begin{bmatrix} -1 \\ 0 \end{bmatrix}. \tag{37}$$

This shows that the resultant of the author's vector of critical stability and the Nyquist vector (transformed) is a fixed vector $\begin{bmatrix} -1 \\ 0 \end{bmatrix}$, as is seen in Fig. 14.

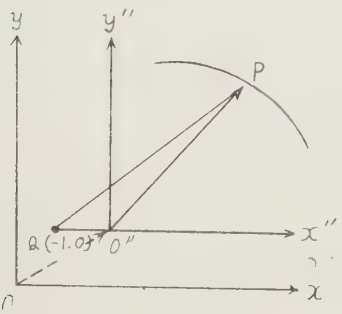

Fig. 14.

$\overrightarrow{OO''} = \begin{bmatrix} x_0 \\ y_0 \end{bmatrix}$: characteristic vector of the closed-loop system

$\overrightarrow{O''P} = \begin{bmatrix} x'' \\ y'' \end{bmatrix}$: vector of critical stability

$\overrightarrow{PQ}$: Nyquist vector (transformed)

From the above mentioned, it is clear that the author's vector of critical stability, when it is transformed by (35), coincides with Nyquist vector, operated as shown in (36). In other words, Nyquist locus and the author's line of critical stability are only different expressions of the same contents.

And, in Nyquist's method, it is necessary to consider different Nyquist loci according to different physical systems, because the group a_n, a_{n-1}, ... take different

values, while in the author's method, each line of critical stability is considered as a section of the hypersurface of critical stability independent of the group a_n, $a_{n-1}, \cdots$ of the system. So, the author's method may be more general and more universal, as it makes clear the relation between the physical constants and the critical stability.

ii) Relation with Hurwitz's criterion

If the characteristic equation of the feed-back physical system is

$$a_0 p^n + a_1 p^{n-1} + a_2 p^{n-2} + \cdots + a_{n-1} p + a_n = 0 , \tag{38}$$

Hurwitz's stability criterion is that the conditions for stability are

$$a_\nu > 0, \ (\nu = 0, 1, 2, \ldots , n)$$

$$\begin{vmatrix} a_1 & a_0 & 0 & 0 & \cdots \\ a_3 & a_2 & a_1 & a_0 & \cdots \\ a_5 & a_4 & a_3 & a_2 & \cdots \\ a_7 & a_6 & a_5 & a_4 & \cdots \\ \cdots & \cdots & \cdots & \cdots & \cdots \\ \cdots & \cdots & \cdots & \cdots & \cdots \\ \cdots & \cdots & \cdots & \cdots & \cdots \end{vmatrix} > 0 , \tag{39}$$

its principal minor-determinants all being positive.

We consider the relation between Hurwitz's stability criterion and that of the author.

The hypersurface of critical stability of the physical system, whose characteristic equation is given by (38), is determined from (21) by the following pair of equations with a parameter γ:

For $n = 2m$,

$$\left.\begin{aligned} \xi_1 \gamma^{m-1} - \xi_3 \gamma^{m-2} + \xi_5 \gamma^{m-3} - \cdots + (-1)^{m-1} \xi_{m-1} = 0 , \\ \xi_0 \gamma^m - \xi_2 \gamma^{m-1} + \xi_4 \gamma^{m-2} - \cdots + (-1)^m \xi_m = 0 , \end{aligned}\right\}$$

and for $n = 2m+1$,

$$\left.\begin{aligned} \xi_1 \gamma^m - \xi_2 \gamma^{m-1} + \xi_5 \gamma^{m-2} - \cdots + (-1)^m \xi_m = 0 , \\ \xi_0 \gamma^m - \xi_2 \gamma^{m-1} + \xi_4 \gamma^{m-2} - + (-1)^m \xi_{m-1} = 0 . \end{aligned}\right\} \tag{40}$$

Since the process is common to both cases, it is sufficient to consider only the case when $n = 2m+1$.

Each equation of (40) expresses a hyperplane in the n-dimensional space. The pair of equations (40) determine a hyper straight line which moves with the varying parameter γ, and generates a ruled hypersurface, which is the hypersurface of critical stability. This hypersurface divides the space into the stability and the instability regions.

Multiplying (40) n times successively by $-\gamma^{-1}$ we obtain the following group of $(2m+2)$ equations:

$$
\left.\begin{aligned}
&\xi_1\gamma^n - \xi_3\gamma^{n-1} + \xi_5\gamma^{n-2} - \cdots + (-1)^n\xi_n = 0\,,\\
&\xi_0\gamma^n - \xi_2\gamma^{n-1} + \xi_4\gamma^{n-2} - \cdots + (-1)^n\xi_{n-1} = 0\,,
\end{aligned}\right\}
$$

$$
\left.\begin{aligned}
&-\xi_1\gamma^{n-1} + \xi_3\gamma^{n-2} - \xi_5\gamma^{n-3} + \cdots + (-1)^{n+1}\xi_n\gamma^{-1} = 0\,,\\
&-\xi_0\gamma^{n-1} + \xi_2\gamma^{n-2} - \xi_4\gamma^{n-3} + \cdots + (-1)^{n+1}\xi_{n-1}\gamma^{-1} = 0\,,
\end{aligned}\right\}
$$

$$
\left.\begin{aligned}
&\xi_1\gamma^{n-2} - \xi_3\gamma^{n-3} + \xi_5\gamma^{n-4} - \cdots + (-1)^{n+2}\xi_n\gamma^{-2} = 0\,,\\
&\xi_0\gamma^{n-2} - \xi_2\gamma^{n-3} + \xi_4\gamma^{n-4} - \cdots + (-1)^{n+2}\xi_{n-1}\gamma^{-2} = 0\,,
\end{aligned}\right\} \qquad (41)
$$

$$
\cdots\cdots\cdots\cdots\cdots\cdots
$$

$$
\cdots\cdots\cdots\cdots\cdots\cdots
$$

$$
\left.\begin{aligned}
&(-1)^n\xi_1 + (-1)^{n+1}\xi_3\gamma^{-1} + (-1)^{n+2}\xi_5\gamma^{-2} + \cdots + (-1)^{2n}\xi_n\gamma^{-n} = 0\,,\\
&(-1)^n\xi_0 + (-1)^{n+1}\xi_2\gamma^{-1} + (-1)^{n+2}\xi_4\gamma^{-2} + \cdots + (-1)^{2n}\xi_{n-1}\gamma^{-n} = 0\,.
\end{aligned}\right\}
$$

Transforming the variables in (41) by

$$
x_\nu = (-1)^{\nu-1}\gamma^{n-\nu+1},\ (\nu = 1, 2, 3, \ldots, 2m+1)\,,
$$

we get

$$
\begin{aligned}
&\xi_1x_1 + \xi_3x_2 + \xi_5x_3 + \cdots\cdots\cdots + \xi_nx_{m+1} &&= 0\,,\\
&\xi_0x_1 + \xi_2x_2 + \xi_4x_3 + \cdots\cdots\cdots + \xi_{n-1}x_{m+1} &&= 0\,,\\
&\xi_1x_2 + \xi_3x_3 + \xi_5x_4 + \cdots\cdots\cdots + \xi_{n-2}x_{m+1} + \xi_nx_{m+2} &&= 0\,,\\
&\xi_0x_2 + \xi_2x_3 + \xi_4x_4 + \cdots\cdots\cdots + \xi_{n-3}x_{m+1} + \xi_{n-1}x_{m+2} &&= 0\,,\\
&\xi_1x_3 + \xi_3x_4 + \xi_5x_5 + \cdots + \xi_{n-4}x_{m+1} + \xi_{n-2}x_{m+2} + \xi_nx_{m+3} &&= 0\,,\\
&\xi_0x_3 + \xi_2x_4 + \xi_4x_5 + \cdots + \xi_{n-5}x_{m+1} + \xi_{n-3}x_{m+2} + \xi_{n-1}x_{m+3} &&= 0\,,\\
&\cdots\cdots\cdots\cdots\cdots\cdots\cdots\cdots &&\\
&\cdots\cdots\cdots\cdots\cdots\cdots\cdots\cdots &&\\
&\xi_1x_{m+1} + \xi_3x_{m+2} + \cdots + \xi_nx_{2m+1} &&= 0\,,\\
&\xi_0x_{m+1} + \xi_2x_{m+2} + \cdots + \xi_{n+1}x_{2m+1} &&= 0\,.
\end{aligned} \qquad (42)
$$

These equations excepting the last one are expressed in the following matrix form:

$$
\begin{pmatrix}
\xi_1 & \xi_3 & \xi_5 & \xi_7 & \xi_9 & \cdots & \xi_n & 0 & 0 & \cdots & 0\\
\xi_0 & \xi_2 & \xi_4 & \xi_6 & \xi_8 & \cdots & \xi_{n-1} & 0 & 0 & \cdots & 0\\
0 & \xi_1 & \xi_3 & \xi_5 & \xi_7 & \cdots & \xi_{n-2} & \xi_n & 0 & \cdots & 0\\
0 & \xi_0 & \xi_2 & \xi_4 & \xi_6 & \cdots & \xi_{n-3} & \xi_{n-1} & 0 & \cdots & 0\\
0 & 0 & \xi_1 & \xi_3 & \xi_5 & \cdots & \xi_{n-4} & \xi_{n-2} & \xi_n & \cdots & 0\\
0 & 0 & \xi_0 & \xi_2 & \xi_4 & \cdots & \xi_{n-5} & \xi_{n-3} & \xi_{n-1} & \cdots & 0\\
 & & \cdots\cdots & & & & & & & & \\
 & & \cdots\cdots & & & & & & & & \\
 & & \cdots\cdots & & & & & & & & \\
0 & 0 & 0 & 0 & 0 & \cdots & \xi_1 & \xi_3 & \xi_5 & \cdots & \xi_n
\end{pmatrix}
\begin{pmatrix} x_1\\ x_2\\ x_3\\ x_4\\ x_5\\ x_6\\ \cdots\\ \cdots\\ \cdots\\ x_n \end{pmatrix}
=
\begin{pmatrix} 0\\ 0\\ 0\\ 0\\ 0\\ 0\\ \vdots\\ \vdots\\ \vdots\\ 0 \end{pmatrix}. \qquad (42')
$$

In order that the relation (42) or (42′) holds independent of any positive value of γ, the following equation must be satisfied which is obtained by eliminating x_ν, $(\nu = 1, 2, \cdots n)$ from the first $n = 2+1$ equations of (42′):

$$\Delta_n = \begin{vmatrix} \xi_1 & \xi_3 & \xi_5 & \xi_7 \cdots \xi_n & 0 & 0 \cdots 0 \\ \xi_0 & \xi_2 & \xi_4 & \xi_6 \cdots \xi_{n-1} & 0 & 0 \cdots 0 \\ 0 & \xi_1 & \xi_3 & \xi_5 \cdots \xi_{n-2} & \xi_n & 0 \cdots 0 \\ 0 & \xi_0 & \xi_2 & \xi_4 \cdots \xi_{n-3} & \xi_{n-1} & 0 \cdots 0 \\ & & & \cdots\cdots\cdots & & \\ & & & \cdots\cdots\cdots & & \\ & & & \cdots\cdots\cdots & & \\ 0 & 0 & 0 & 0 \cdots \xi_1 & \xi_3 & \xi_5 \cdots \xi_n \end{vmatrix} = 0 . \tag{43}$$

This is the equation for the hypersurface of critical stability which can also be derived by eliminating γ from (40), and this equation is the same as Hurwitz's stability criterion which states that the system is stable when

$$\Delta_\nu > 0 , \qquad (\nu = 1, 2, \cdots , n)$$

and unstable otherwise. From the above it is evident that Hurwitz's stability criterion is closely related with the author's criterion.

But, while Hurwitz's stability criterion scarcely makes one catch any physical meaning, the author's conception of hypersurface of critical stability can be grasped geometrically and serves for constructing successively the stable regions of higher dimensions.

9. Conclusion

In this paper, the author has made matrix representation of the feed-back physical system such as an automatic control system and others.

The matrix representation makes one easily grasp the relations among elements of the system and intuitively understand the behaviour of the system. From this representation the characteristic equation of the system and the characteristic vector are derived and with this vector one can discuss the stability geometrically.

From the roots of the characteristic equation, one can represent stability regions and hypersurfaces of critical stability in the Euclidian space of the characteristic vector, and moreover this form of stability criteria serves to let one know how the stability of the system varies with the increasing dimensions of the system.

Generally the hypersurfaces of critical stability form stability criteria, but practically convenient criteria are given by the section of the hypersurfaces of critical stability by a two-dimensional plane. Especially in the diagram plotting the section by the plane which is parallel to the last two coordinate axes, the stability region exists on the definite side of the line of critical stability but not on the opposite side, and this line is useful for seeking successively for the lines of critical stability of for systems of higher dimensions.

Further the section of the hypersurface of critical stability by the plane which is parallel to the last axis and the third axis from the last, gives the line of critical stability composed of only straight line segments and very convenient to judge the stability.

The author has also discussed the relations between the author's stability criterion and Nyquist's and Hurwitz's stability criteria.

Thus, the author hopes that the present method will offer convenient and effective stability criteria for the feed-back physical system.

In conclusion, the author should like to express his sincere thanks to Prof. I. Takahashi for his helpful advices and discussions about this work.

REFERENCES

1. A. HURWITZ: Über die Bedingungen, unter welchen eine Gleichung nur Wurzeln mit negativen reellen Theilen besitzt., *Math. Ann.* **44** (1895), 273.
   E. J. ROUTH: *Advanced Rigid Dynamics.* (1905).
2. H. NYQUIST: Regeneration theory, *Bell System Techn. Jour.* (1932), 126–147.
   A. VAZSONYI: A generalization of Nyquist's stability criteria, *J. Appl. Phys.* **20** (1949), 864–867.
3. K. KÜPFMÜLLER: Über die Dynamik der selbsttätigen Verstärkungaregler, E. N. T., **5** (1928), 459.
   A. LEONHARD: *Selbsttätige Regelung in der Elecktrotechnik,* (1940, Springer).
   T. SAMUKAWA: *Theory and Practice of Automatic Control,* Vol. 1,2. (1952), Nihon Kikai Gakki.
   JAMES, NICHOLS, and PHILLIPS: *Theory of Servomechanisms,* M. I. T. Radiation Laboratory Series, **25** (1947, McGraw-Hill).
   G. S. BROWN and D. P. CAMPBELL: *Principles of Servomechanisms,* (1948, John Wiley & Sons).

MEMOIRS OF THE COLLEGE OF SCIENCE, University of Kyoto, Series A,
Vol. XXVII, No. 2, Article 6, 1954

VECTORIAL STABILITY CRITERIA OF THE FEED-BACK PHYSICAL SYSTEM
PART II

BY

Kentaro TASHIRO

(*Received October 15, 1952*)

1. Introduction

The behaviour of the feed-back physical system is determined by its characteristic equation. In the preceding paper (1), the author has expressed the system with the characteristic vector which is composed of the coefficients of the characteristic equation and shown that the stability region $[\xi_\mu^n]$, $(\mu = 0, 1, 2, \ldots\ldots, n)$ of the n-dimensional system is related with the stability region $[\zeta_\nu^{n-2}]$, $(\nu = 0, 1, 2, \ldots\ldots, n-2)$ of the $(n-2)$-dimensional vector, as follows:

$$\begin{pmatrix} \xi_0 \\ \xi_1 \\ \xi_2 \\ \vdots \\ \xi_{n-2} \\ \xi_{n-1} \\ \xi_n \end{pmatrix} = \begin{pmatrix} 1 & & & & & \\ \beta & 1 & & & & \\ \gamma & \beta & 1 & & & \\ & \ddots & \ddots & \ddots & & \\ & & \gamma & \beta & 1 & \\ & & & \gamma & \beta & 1 \\ & & & & \gamma & \beta & 1 \end{pmatrix} \cdot \begin{pmatrix} \xi_0 \\ \xi_1 \\ \xi_2 \\ \vdots \\ \xi_{n-2} \\ 0 \\ 0 \end{pmatrix},$$

where $$\beta > 0, \quad \gamma > 0.$$

And it has also been shown that the stability criteria are introduced by putting $\beta = 0$ in the stable vectors, but no detailed descriptions about the construction of the stability criteria and the stability regions have been presented there.

In this paper, the geometrical properties and the constructions of the stability criteria and the stability regions are discussed. Further, the stabilizations by multiple feed-back are discussed and the theoretical results are ascertained by experiments.

2. $[\xi_{n-1}, \xi_n]$-stability criterion

From (21) of §6 in the preceding paper (1) (we shall denote it with (I. 6. 21) and use such notations in the following), the hypersurface of critical stability of an m-

dimensional vector is given by the following equations:

$$\left.\begin{aligned}\xi_{n-1} &= \gamma\xi_{n-3} - \gamma^2\xi_{n-5} + \gamma^3\xi_{n-7} - \cdots\cdots,\\ \xi_n &= \gamma\xi_{n-2} - \gamma^2\xi_{n-4} + \gamma^3\xi_{n-6} - \cdots\cdots.\end{aligned}\right\} \tag{1}$$

By fixing $\xi_{n-2}, \xi_{n-3}, \ldots, \xi_1, \xi_0$ at constant values in (1), the line of critical stability, i.e., $[\xi_{n-1}, \xi_n]$-curve of stability criterion is obtained.

This curve can be drawn both from $[\zeta_{n-3}, \zeta_{n-2}]$-curve of stability criterion of the $(n-2)$-dimensional vector and from $[\zeta_{n-2}, \zeta_{n-1}]$-curve of stability criterion of the $(n-1)$-dimensional vector.

i) Just as (1) has been derived, the hypersurface of critical stability of the $(n-2)$-dimensional vector is derived:

$$\left.\begin{aligned}\zeta_{n-3} &= \gamma\zeta_{n-5} - \gamma^2\zeta_{n-7} + \gamma^3\xi_{n-9} - \cdots\cdots,\\ \zeta_{n-2} &= \gamma\zeta_{n-4} - \gamma^2\zeta_{n-6} + \gamma^3\zeta_{n-8} - \cdots\cdots.\end{aligned}\right\} \tag{2}$$

By fixing $\zeta_{n-4}, \zeta_{n-5}, \ldots, \zeta_0$ at constant values

$$\zeta_{n-4} = \xi_{n-4}, \quad \zeta_{n-5} = \xi_{n-5}, \quad \ldots, \quad \zeta_0 = \xi_0 \tag{3}$$

in (2), $[\zeta_{n-3}, \zeta_{n-2}]$-curve of stability criterion is obtained, and from (1), (2) and (3), we derive

$$\left.\begin{aligned}\xi_{n-1} &= \gamma(\xi_{n-3} - \zeta_{n-3}),\\ \xi_n &= \gamma(\xi_{n-2} - \zeta_{n-2}).\end{aligned}\right\} \tag{4}$$

Since, in (4), (ξ_{n-3}, ξ_{n-2}) is a given point of the physical system and $(\zeta_{n-3}, \zeta_{n-2})$ is a varying point with γ on the curve of stability criterion of the $(n-2)$-dimensional vector, $[\xi_{n-1}, \xi_n]$-curve of stability criterion of the n-dimensional vector is simply obtained vectorially from the $[\zeta_{n-3}, \zeta_{n-2}]$-curve of stability criterion of the $(n-2)$-dimensional vector by use of (4) as shown in Fig. 1, in which

$\overrightarrow{OP} = [\zeta_{n-3}, \zeta_{n-2}]$: section of the $(n-2)$-dimensional vector of critical stability (variable),

$\overrightarrow{OQ} = [\xi_{n-3}, \xi_{n-2}]$: section of the fixed n-dimensional vector,

$\overrightarrow{QR} = [\xi_{n-1}, \xi_n] = \gamma \cdot \overrightarrow{PQ}$: section of the m-dimensional vector of critical stability (variable with PQ).

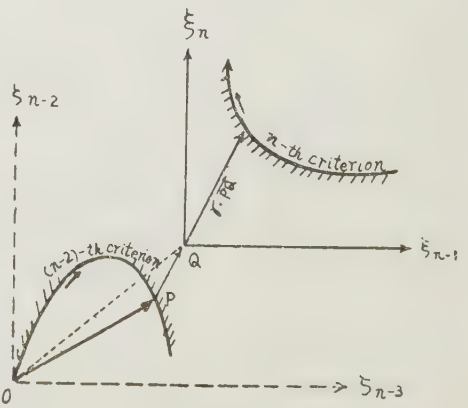

Fig. 1.

ii) The equation of the hypersurface of critical stability of the $(n-1)$-dimensional vector is given by

$$\left.\begin{aligned}\zeta_{n-2} &= \gamma\zeta_{n-4} - \gamma^2\zeta_{n-6} + \cdots\cdots,\\ \zeta_{n-1} &= \gamma\zeta_{n-3} - \gamma^2\zeta_{n-5} + \cdots\cdots.\end{aligned}\right\} \tag{5}$$

Fixing $\zeta_{n-3}, \zeta_{n-4}, \cdots, \zeta_0$ at constant values

$$\zeta_{n-3} = \xi_{n-3},\ \zeta_{n-4} = \xi_{n-4},\ \cdots,\ \zeta_0 = \xi_0$$

in (5) and combining with (1), we get

$$\left.\begin{aligned}\xi_{n-1} &= \zeta_{n-1},\\ \xi_n &= \gamma(\xi_{n-2} - \zeta_{n-2}),\end{aligned}\right\} \tag{6}$$

where $(\zeta_{n-2}, \zeta_{n-2})$ is a variable point on the line of critical stability of the $(n-1)$-dimensional vector, and ξ_{n-2} is a given component of the n-dimensional vector.

By (6), the $[\xi_{n-1}, \xi_n]$-curve of critical stability of the n-dimensional vector can be graphically obtained as shown in Fig. 2, in which

P: moving point on the curve of stability criterion of the $(n-1)$-dimensional vector,

S: fixed point $(\xi_{n-2}, 0)$,

$\overrightarrow{OX} = \overrightarrow{SQ} = \xi_{n-1} = \zeta_{n-1}$,

$\overrightarrow{XR} = \gamma\cdot\overrightarrow{QP}$: $\xi_n = \gamma(\xi_{n-2} - \zeta_{n-2})$,

and the locus of the point R is the $[\xi_{n-1}, \xi_n]$-curve of critical stability of the n-dimensional vector.

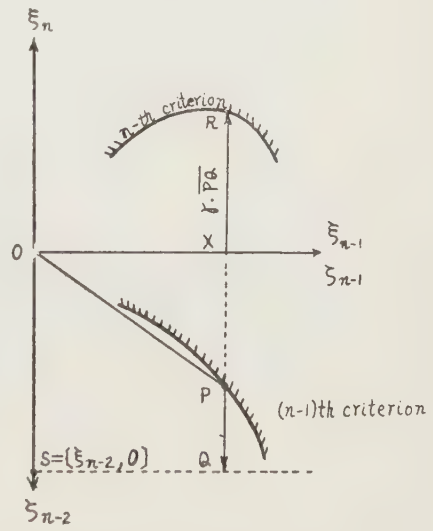

Fig. 2.

iii) As stated above, each line of critical stability of higher dimensions can be successively derived from either of the lines of critical stability of the 2- and 3-dimensional vectors shown in Fig. 3.

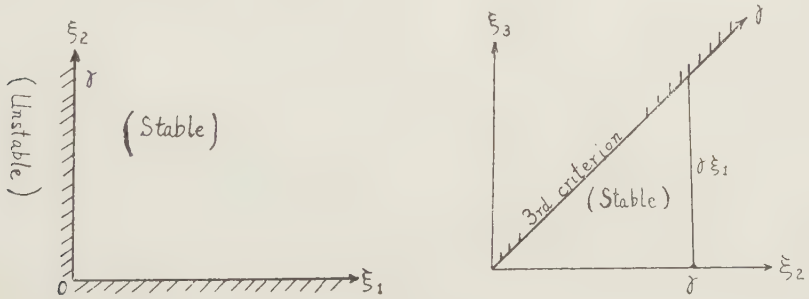

Fig. 3.

As stated in the preceding paper, the stability region can exist only on the right side of the curve of stability criterion thus obtained. In Fig. 4 are shown the curves of stability criterion of vectors of different dimensions which are obtained successively as well as the stability regions.

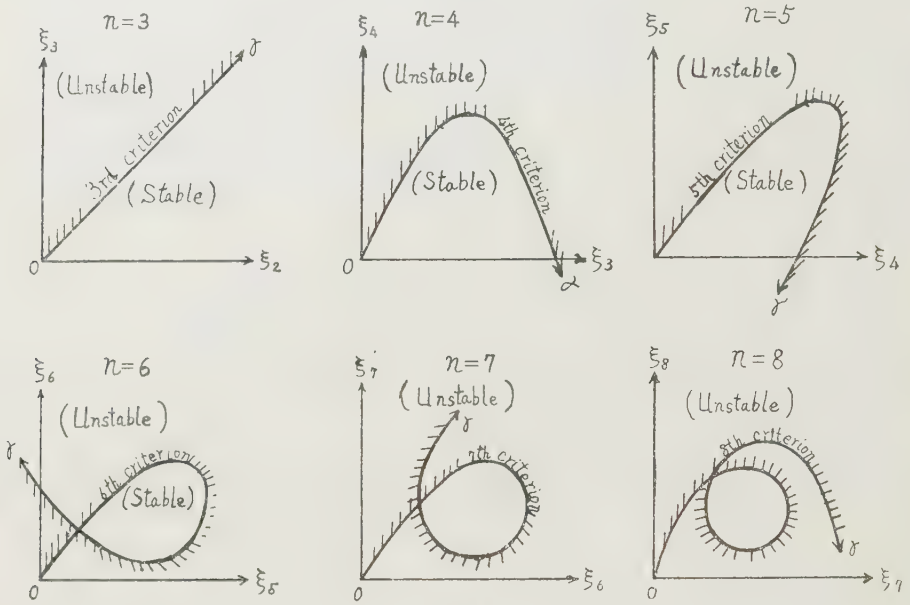

Fig. 4.

3. $[\xi_1, \xi_0]$-stability criterion

By (I. 5. 14′), the n-dimensional stable vector $[\xi]$ is derived from the $(n-2)$-dimensional vector $[\zeta]$ as follows:

$$\begin{pmatrix} \xi_0 \\ \xi_1 \\ \xi_2 \\ \vdots \\ \xi_{n-2} \\ \xi_{n-1} \\ \xi_n \end{pmatrix} = \begin{pmatrix} 1 & & & & \\ \beta & 1 & & & \\ \gamma & \beta & 1 & & \\ & \gamma & \beta & \ddots & \\ & & \gamma & \ddots & 1 \\ & & & \ddots & \beta \\ & & & & \gamma \end{pmatrix} \cdot \begin{pmatrix} \zeta_0 \\ \zeta_1 \\ \zeta_2 \\ \vdots \\ \zeta_{n-2} \end{pmatrix} \tag{7}$$

By putting $\xi_\nu' = \xi_\nu/\xi_n$, $\zeta_\nu' = \zeta_\nu/\zeta_{n-2}$, (7) becomes

$$\begin{pmatrix} \xi_0' \\ \xi_1' \\ \xi_2' \\ \vdots \\ \xi_{n-1}' \\ \xi_n' \end{pmatrix} = \begin{pmatrix} \gamma' & & & & \\ \beta' & \gamma' & & & \\ 1 & \beta' & \ddots & & \\ & 1 & \ddots & \gamma' & \\ & & \ddots & \beta' & \\ & & & 1 & \end{pmatrix} \cdot \begin{pmatrix} \zeta_0' \\ \zeta_1' \\ \zeta_2' \\ \vdots \\ \zeta_{n-1}' \end{pmatrix}, \tag{8}$$

where $\gamma' = 1/\gamma$, $\beta' = \beta/\gamma$, or

$$\begin{pmatrix} \xi_n' \\ \xi_{n-1}' \\ \xi_{n-3}' \\ \vdots \\ \xi_1' \\ \xi_0' \end{pmatrix} = \begin{pmatrix} 1 & & & & \\ \beta' & 1 & & & \\ \gamma' & \beta' & \ddots & & \\ & \gamma' & \ddots & 1 & \\ & & \ddots & \beta' & \\ & & & \gamma' & \end{pmatrix} \cdot \begin{pmatrix} \zeta_{n-2}' \\ \zeta_{n-3}' \\ \zeta_{n-4}' \\ \vdots \\ \zeta_1' \\ \zeta_0' \end{pmatrix}. \tag{9}$$

Consequently, the n-dimensional vector $[\xi']$ of critical stability is derived from the $(n-2)$-dimensional vector $[\zeta']$ by the following equations:

$$\left.\begin{aligned} [\xi_{2\nu}'] &= [C_{\gamma'}] \cdot [\zeta_{2\nu}'], \\ [\xi_{2\nu+1}'] &= [C_{\gamma'}] \cdot [\zeta_{2\nu+1}'], \end{aligned}\right\} \tag{10}$$

where $\nu = 0, 1, 2, 3, \ldots,$ and

$$[C_{\gamma'}] = \begin{pmatrix} 1 & & & & \\ \gamma' & 1 & & & \\ & \gamma' & \ddots & & \\ & & \ddots & 1 & \\ & & & \gamma' & \end{pmatrix}.$$

This is the case of n being odd, but the case of even n can be treated in a quite similar manner.

Therefore, if we take $\xi_\mu = \xi_{n-\mu}'$, $(\mu = 0, 1, 2, \ldots, n-2)$, the line of critical stability of ξ'-vector on the (ξ_1', ξ_0')-plane is quite alike that of ξ-vector on the (ξ_{n-1}, ξ_n)-plane, but the directions of increasing γ in these two lines are reverse to each other as shown in Fig. 5.

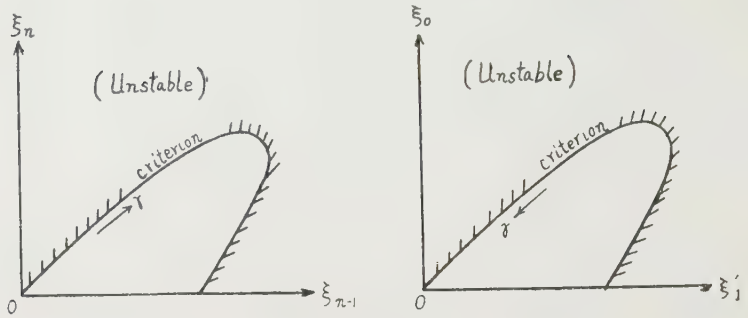

Fig. 5.

4. $[\xi_r, \xi_{r+1}]$–stability criterion

We assume that the components of the n–dimensional characteristic vector $[\xi]$ are fixed at constants, excepting ξ_r and ξ_{r+1}, and resolve this vector into the following two vectors, of which one is $(r+1)$–dimensional and the other, $(n-r)$–dimensional:

$$[\xi_0, \xi_1, \xi_2, \cdots, \xi_{r-1}, \xi_r', \xi_{r+1}'], \qquad [\mathrm{A}']$$

$$[\xi_r'', \xi_{r+1}'', \xi_{r+2}, \cdots, \xi_{n-2}, \xi_{n-1}, \xi_n], \qquad [\mathrm{A}'']$$

where ξ_r', ξ_{r+1}', ξ_r'' and ξ_{r+1}'' are variables.

The stability region of the n–dimensional characteristic vector is given from the $(n-2)$–dimensional stable vector $[\zeta]$, taking $\beta > 0$ and $\gamma > 0$ as parameters, by (I. 5. 14′) as follows:

$$\begin{pmatrix} \xi_0 \\ \xi_1 \\ \xi_2 \\ \vdots \\ \xi_{r-1} \\ \xi_r \\ \xi_{r+1} \\ \xi_{r+2} \\ \vdots \\ \xi_{n-1} \\ \xi_n \end{pmatrix} = \begin{pmatrix} 1 & & & & & & & \\ \beta & 1 & & & & & & \\ \gamma & \beta & \ddots & & & & & \\ & \gamma & \ddots & \ddots & & & & \\ & & \ddots & \ddots & 1 & & & \\ & & & \ddots & \beta & 1 & & \\ & & & & \gamma & \beta & & \\ & & & & & \gamma & \ddots & \\ & & & & & & \ddots & 1 \\ & & & & & & & \beta \\ & & & & & & & \gamma \end{pmatrix} \cdot \begin{pmatrix} \zeta_0 \\ \zeta_1 \\ \zeta_2 \\ \vdots \\ \zeta_{r-1} \\ \zeta_r \\ \zeta_{r+1} \\ \xi_{r+2} \\ \vdots \\ \zeta_{n-2} \end{pmatrix}.$$

On the other hand, the stable vectors of [A′] and [A″] are given by

$$\begin{pmatrix} \xi_0 \\ \xi_1 \\ \xi_2 \\ \vdots \\ \xi_r' \\ \xi_{r+1}' \end{pmatrix} = \begin{pmatrix} 1 & & & & \\ \beta & 1 & & & \\ \gamma & \beta & \ddots & & \\ & \gamma & \ddots & 1 & \\ & & \ddots & \beta & \\ & & & \gamma & \end{pmatrix} \cdot \begin{pmatrix} \zeta_0 \\ \zeta_1 \\ \zeta_2 \\ \vdots \\ \zeta_{r-2} \\ \zeta_{r-1} \end{pmatrix}, \tag{11 a}$$

and

$$\begin{pmatrix} \xi_r'' \\ \xi_{r+1}'' \\ \xi_{r+1} \\ \vdots \\ \xi_{n-1} \\ \xi_n \end{pmatrix} = \begin{pmatrix} 1 & & & & \\ \beta & 1 & & & \\ \gamma & \beta & \ddots & & \\ & \gamma & \ddots & 1 & \\ & & \ddots & \beta & \\ & & & \gamma & \end{pmatrix} \cdot \begin{pmatrix} \zeta_r \\ \zeta_{r+1} \\ \zeta_{r+2} \\ \vdots \\ \zeta_{n-3} \\ \zeta_{n-2} \end{pmatrix}. \tag{11 b}$$

From the relation:

$$\begin{pmatrix} \xi_r \\ \xi_{r+1} \end{pmatrix} = \begin{pmatrix} \xi_r' \\ \xi_{r+1}' \end{pmatrix} + \begin{pmatrix} \xi_r'' \\ \xi_{r+1}'' \end{pmatrix}, \tag{11c}$$

if $[\xi']$ and $[\xi'']$ are stable, $[\xi]$ is stable.

Consequently, by adding two stable vectors $[\xi']$ and $[\xi'']$ with reference to the same values of β and γ on the (ξ_r, ξ_{r+1})-plane, the stability region of $[\xi]$ and the stability criterion is obtained as shown in Fig. 6.

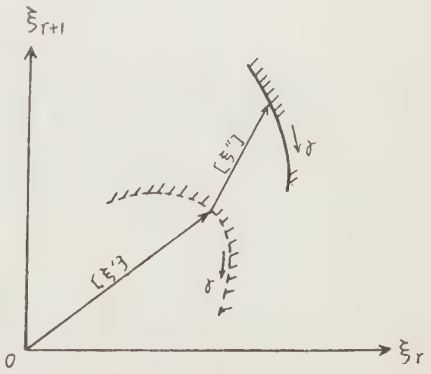

Fig. 6.

5. $[\xi_{n-2}, \xi_{n-1}, \xi_n]$-stability criterion

We put $\beta = 0$ in (7), and resolving it into the following two equations:

$$\begin{pmatrix} \xi_0 \\ \xi_1 \\ \xi_2 \\ \vdots \\ \xi_{n-3} \end{pmatrix} = \begin{pmatrix} 1 & & & & \\ 0 & 1 & & & \\ \gamma & 0 & \ddots & & \\ & \gamma & \ddots & 1 & \\ & & \ddots & 0 & \\ & & & \gamma & \end{pmatrix} \cdot \begin{pmatrix} \zeta_0 \\ \zeta_1 \\ \zeta_2 \\ \vdots \\ \zeta_{n-3} \end{pmatrix}, \tag{12 a}$$

and

$$\begin{pmatrix} \xi_{n-2} \\ \xi_{n-1} \\ \xi_n \end{pmatrix} = \begin{pmatrix} \gamma & 0 & 1 \\ 0 & \gamma & 0 \\ 0 & 0 & \gamma \end{pmatrix} \cdot \begin{pmatrix} \zeta_{n-4} \\ \zeta_{n-3} \\ \zeta_{n-2} \end{pmatrix}. \tag{12b}$$

Then (12b) gives the surface of critical stability when ξ_ν, $(\nu = 0, 1, 2, 3, \ldots, n-3)$, are fixed at constant values. When ξ_ν, $(\nu = 0, 1, 2, 3, \ldots, n-3)$, are fixed at constant values, ζ_ν $(\nu = 0, 1, 2, 3, \ldots, n-3)$, are obtained as functions of γ only from (12a), and the vector of critical stability (12b) has its components ξ_{n-2}, ξ_n as functions of γ and ζ_{n-2}, and component ξ_{n-1} as a function of γ only.

Accordingly, the vector of critical stability (12b) lies on the plane parallel to ξ_{n-2}- and ξ_n-axes, having the gradient of $\tan^{-1}\gamma$ against ξ_{n-2}-axis, and as ξ_{n-1} depends only on the frequency, the oscillating frequency of the system will be determined by ξ_{n-1}.

If we assume $\zeta_{n-2} = 0$, equation (12b) becomes:

$$\begin{pmatrix} \xi_{n-2} \\ \xi_{n-1} \end{pmatrix} = \begin{pmatrix} \gamma & 0 \\ 0 & \gamma \end{pmatrix} \cdot \begin{pmatrix} \zeta_{n-4} \\ \zeta_{n-3} \end{pmatrix}, \tag{13}$$

which is the $[\xi_{n-2}, \xi_{n-1}]$-stability criterion of the $(n-1)$-dimensional vector.

6. $[\xi_r, \xi_{r+2}]$- and $[\xi_{n-2}, \xi_n]$- stability criteria

As (I. 6. 19) in §6 of Part I, the vector of critical stability is resolved into two vectors, of which one is a vector which has all zero components in reference to the odd-number-axes, and the other is a vector which has all zero components referring to the even-number-axes.

Eliminating $\zeta_{2\nu}$ and $\zeta_{2\nu+1}$ from the two equations of (I. 6. 19) respectively, we obtain

$$\left.\begin{aligned} \sum_\nu (-1)^\nu \gamma^\nu \xi_{n-(2\nu+1)} = 0\,, \\ \sum_\nu (-1)^\nu \gamma^\nu \xi_{n-2\nu} = 0\,. \end{aligned}\right\} \tag{14}$$

Now, if we fix all the components excepting ξ_r and ξ_{r+2} which are obtained only in one of (14), for instance the latter, the values of γ will be determined from the other equation (in this case the former) of (14), which does not contain ξ_r and ξ_{r+2}. For each determined value of γ, the latter equation of (14) represents a straight line on (ξ_r, ξ_{r+2})-plane, and the set of these straight lines determine the stability criterion as shown in Fig. 7.

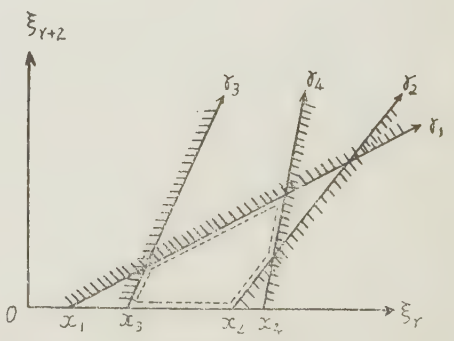

Fig. 7.

The latter equation of (14) is expressed for one determined value γ_λ, as follows:

$$\xi_{r+2} = \gamma_\lambda(\xi_r - x_\lambda),$$

where

$$x_\lambda = \gamma_\lambda \left\{ \sum_{\mu=1}^{\rho} (-\gamma_\lambda)^{\mu-1} \xi_{r-2\mu} + \sum_{\nu=2}^{n-\rho} (-\gamma_\lambda)^{-\nu-1} \xi_{r+2\nu} \right\},$$

with $\begin{cases} \rho = r/2 & \text{for even } r, \\ \rho = (r-1)/2 & \text{for odd } r, \end{cases}$ $\begin{cases} \lambda = 1, 2, \ldots, n/2 & \text{for even } n, \\ \lambda = 1, 2, \ldots, (n-1)/2 & \text{for odd } n. \end{cases}$

Putting especially $r = n-2$, we obtain $[\xi_{n-2}, \xi_n]$-stability criterion as follows:

$$\xi_n = \gamma_\lambda(\xi_{n-2} - x_\lambda),$$

where

$$x_\lambda = \sum_{\mu=1}^{\rho} (-1)^{\mu+1} \gamma_\lambda^{\mu} \xi_{n-2(\mu+1)},$$

with $\lambda = 1, 2, \ldots, \rho+1$

and $\begin{cases} \rho = (n-2)/2 & \text{for even } n, \\ \rho = (n-3)/2 & \text{for odd } n. \end{cases}$

7. Composition of stability criteria

Let $[\xi_\nu']$, $(\nu = 0, 1, 2, 3, \ldots, n)$, denote an n-dimensional stable vector and $[\xi_\mu'']$, $(\mu = 0, 1, 2, \ldots, m)$, an m-dimensional stable vector. When all components of these vectors excepting ξ_{n-1}', ξ_n', ξ_0'' and ξ_1'' are fixed at constant values, $[\xi_{n-1}, \xi_n]$-stability region of the $(n+m-1)$-dimensional characteristic vector $[\xi_\nu]$, $(\nu = 0, 1, 2, 3, \ldots, n+m-1)$, is obtained as follows.

By the methods in §2 and §3, the $[\xi_{n-1}', \xi_n']$-stability region of the $[\xi_\nu']$-vector and $[\xi_0'', \xi_0'']$-stability region of the $[\xi_\mu'']$-vector are readily obtained, and corresponding stable vectors are expressed as (15 a, b) and (16 a, b) respectively:

$$\begin{pmatrix} \xi_0' \\ \xi_1' \\ \xi_2' \\ \vdots \\ \xi_{n-3}' \\ \xi_{n-2}' \end{pmatrix} = \begin{pmatrix} 1 & & & & & \\ \beta & 1 & & & & \\ \gamma & \beta & 1 & & & \\ & \gamma & \beta & \ddots & & \\ & & \gamma & \ddots & \ddots & \\ & & & \ddots & \ddots & 1 \end{pmatrix} \cdot \begin{pmatrix} \zeta_0' \\ \zeta_1' \\ \zeta_2' \\ \vdots \\ \zeta_{n-3}' \\ \zeta_{n-2}' \end{pmatrix}, \tag{15 a}$$

$$\begin{pmatrix} \xi_{n-1}' \\ \xi_n' \end{pmatrix} = \begin{pmatrix} \gamma & \beta \\ 0 & \gamma \end{pmatrix} \cdot \begin{pmatrix} \zeta_{n-3}' \\ \zeta_{n-2}' \end{pmatrix}, \tag{15 b}$$

$$\begin{pmatrix} \xi_0'' \\ \xi_1'' \end{pmatrix} = \begin{pmatrix} \gamma'' & 0 \\ \beta'' & \gamma'' \end{pmatrix} \cdot \begin{pmatrix} \zeta_0'' \\ \zeta_1'' \end{pmatrix}, \tag{16 a}$$

$$\begin{pmatrix} \xi_2'' \\ \xi_3'' \\ \xi_4'' \\ \vdots \\ \xi_{m-1}'' \\ \xi_m'' \end{pmatrix} = \begin{pmatrix} 1 & \beta'' & \gamma'' & & & & \\ & 1 & \beta'' & \ddots & & & \\ & & 1 & \ddots & \ddots & & \\ & & & \ddots & \ddots & \gamma'' & \\ & & & & \ddots & \beta'' & \gamma'' \\ & & & & & 1 & \beta'' \\ & & & & & & 1 \end{pmatrix} \cdot \begin{pmatrix} \zeta_0'' \\ \zeta_1'' \\ \zeta_2'' \\ \vdots \\ \zeta_{n-1}'' \\ \zeta_{m-1}'' \end{pmatrix}. \tag{16 b}$$

From (15 a, b) and (16 a, b), the $(n+m-1)$-dimensional stable vector $[\xi_\sigma]$, $(\sigma = 0, 1, 2, \ldots, n+m-1)$, is obtained as follows:

$$\begin{aligned} \xi_\sigma &= \xi_\sigma' && (\sigma = 0, 1, 2, \ldots, n-2), \\ \xi_{n-1} &= \xi_{n-1}' + \xi_0'', \\ \xi_n &= \xi_n' + \xi_1'', \\ \xi_\sigma &= \xi_{\sigma-n+1}'' && (\sigma = n-1, n-2, n-3, \ldots, n+m-1). \end{aligned}$$

When the components $\xi_\sigma (\sigma = 0, 1, 2, \ldots, n+m-1)$ in the above equations are fixed at constant values, the stability region of the $(m+n-1)$-dimensional characteristic vector is given by

$$\begin{pmatrix} \xi_{n-1} \\ \xi_n \end{pmatrix} = \begin{pmatrix} \xi_{n-1}' \\ \xi_n' \end{pmatrix} + \begin{pmatrix} \xi_0'' \\ \xi_1'' \end{pmatrix} = \begin{pmatrix} \gamma & \beta & \gamma'' & 0 \\ 0 & \gamma & \beta'' & \gamma'' \end{pmatrix} \begin{pmatrix} \zeta_{n-3}' \\ \zeta_{n-2}' \\ \zeta_{n-1}'' \\ \zeta_n'' \end{pmatrix}$$

$$= \begin{pmatrix} \gamma & \beta & 1 & 0 \\ 0 & \gamma & \beta & 1 \end{pmatrix} \cdot \begin{pmatrix} \zeta_{n-3} \\ \zeta_{n-2} \\ \zeta_{n-1} \\ \zeta_n \end{pmatrix},$$

where

$$\begin{aligned} &\zeta_{n-3} = \zeta_{n-3}', \quad \zeta_{n-1} = \zeta_0''/\gamma, \quad \beta'' = \beta/\gamma, \\ &\zeta_{n-2} = \zeta_{n-2}', \quad \zeta_n = \zeta_1''/\gamma, \quad \gamma'' = 1/\gamma. \end{aligned}$$

Putting $\beta = 0$ in these equations, the stability criterion of the $(m+n-1)$-dimensional characteristic vector will be obtained.

For example, we shall show the composition of the stability criterion of the 5-dimensional vector from the two stability criteria of 3-dimensional vectors $[\xi']$ and $[\xi'']$.

If

$$\left.\begin{aligned}\xi_1' &= \zeta_1' = \xi_1\\ \xi_1' &= \zeta_1' = \xi_1\end{aligned}\right\} : \left\{\begin{aligned}&\text{fixed components of the 5-dimensional}\\ &\text{vector } [\xi],\end{aligned}\right.$$

$$\left.\begin{aligned}\xi_2' &= \gamma\zeta_1'\\ \xi_3' &= \gamma\zeta_1'\end{aligned}\right\} : \left\{\begin{aligned}&[\xi_2', \xi_3']\text{-stability criterion of the 3-}\\ &\text{dimensional vector } [\xi'],\end{aligned}\right.$$

$$\left.\begin{aligned}\xi_0'' &= \zeta_0''/\gamma\\ \xi_1'' &= \zeta_1''/\gamma\end{aligned}\right\} : \left\{\begin{aligned}&[\xi_0'', \xi_1'']\text{-stability criterion of the 3-}\\ &\text{dimensional vector } [\xi''],\end{aligned}\right.$$

$$\left.\begin{aligned}\xi_2'' &= \zeta_2'' = \xi_4\\ \xi_3'' &= \zeta_1'' = \xi_5\end{aligned}\right\} : \left\{\begin{aligned}&\text{fixed components of the 5-dimensional}\\ &\text{vector } [\xi],\end{aligned}\right.$$

the $[\xi_2, \xi_3]$-stability criterion of the 5-dimensional characteristic vector can be obtained by the following equations, as shown graphically in Fig. 8,

$$\xi_2 = \xi_2' + \xi_0'' = \gamma\zeta_0' + \zeta_0''/\gamma,$$
$$\xi_3 = \xi_3' + \xi_1'' = \gamma\zeta_1' + \zeta_1''/\gamma,$$

where all the components of the 5-dimensional characteristic vector $[\xi]$ excepting ξ_2 and ξ_3, are fixed at constant values.

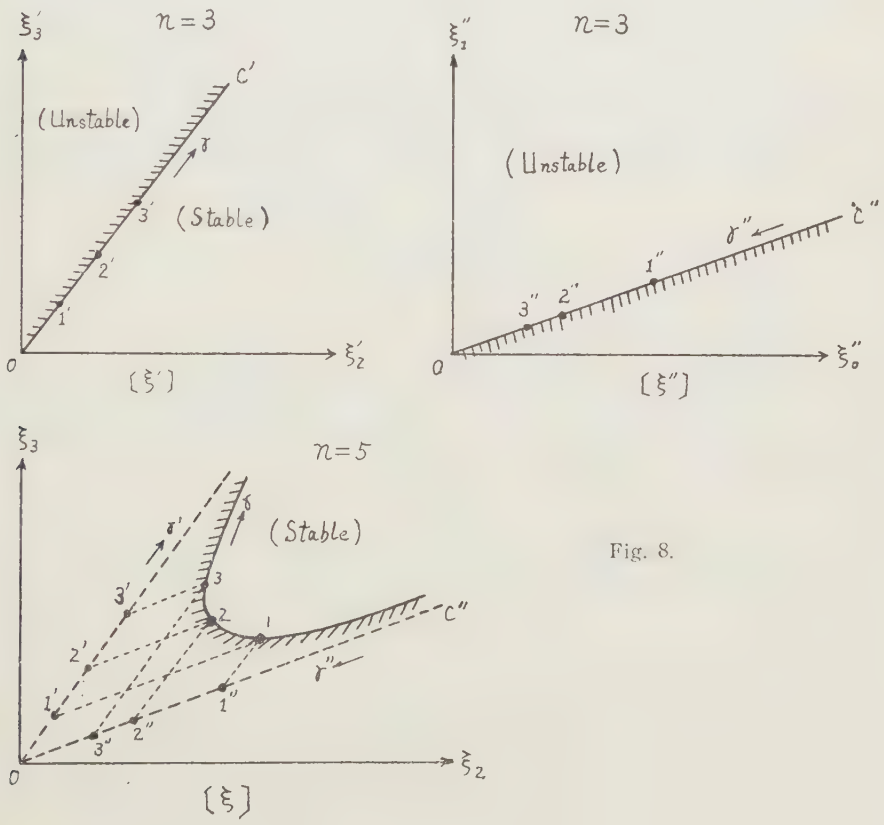

Fig. 8.

8. γ-scale on the line of critical stability

In order to construct the stability criterion of higher dimensions from those of lower dimensions, it is necessary to scale the value of γ as a function of frequency on the line of critical stability. In the following, some properties of γ-scale is described.

As stated in § 7 of the preceding paper, in order that the feed-back physical system may be stable, it is necessary that both equations of the hypersurface of critical stability have all real roots of γ.

At one point of γ-scale, the characteristic equation has the factor $(p^2+\gamma)$, and has the roots $\pm j\sqrt{\gamma}$. Consequently, the oscillating frequency of the system is given by:

$$\omega = \sqrt{\gamma}\,.$$

The $[\xi_0, \xi_1]$-line of critical stability has the scale of $\gamma' = 1/\gamma$ instead of γ, and in this case, the oscillating frequency is given by

$$\omega = 1/\sqrt{\gamma'}\,.$$

In the case of the normalized characteristic vector, $\xi_\nu' = \xi_\nu/(\xi_1)^\nu$, $(\nu = 1, 2, \ldots, n)$, the characteristic equation has the factor $\{(\xi_1 p)^2+\gamma\}$. So the oscillating frequency is given by

$$\omega = \sqrt{\gamma}/\xi_1\,.$$

9. Stabilization by multiple feed-back

The additional feed-back is often used for stabilizing the feed-back physical system as shown in Fig. 9, in which the output signal of Z_s is fed back to the input of Z_r through the feed-back element Z_{rs}.

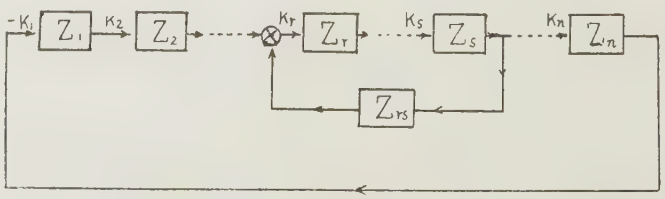

Fig. 9.

The characteristic matrix of this system is given as follows:

$$[Z] = \begin{vmatrix} Z_1 & & & & K_1 \\ -K_2 & Z_2 & & & \\ & \ddots & \ddots & & \\ & & -K_r & Z_n & Z_{rs} \\ & & & \ddots & \ddots \\ & & & -K_s & Z_s \\ & & & & \ddots & \ddots \\ & & & & -K_n & Z_n \end{vmatrix}. \tag{17}$$

By expanding the determinant of (17) with respect to the r–th row, the characteristic equation of the system is expressed in the following form :

$$|[Z]| = |[Z]_0| + |[Z]_I| = 0,$$

where $[Z]_0$: the characteristic matrix of the system without any additional feed-back,

$[Z]_I$: the feed-back matrix which is produced by substituting Z_{rs} for the (r, s)–element and making zero all other elements of the r–th row in $[Z]_I$, so that $|[Z]_I|$ is the co-factor of Z_{rs} of $|[Z]|$ multiplied by Z_{rs}, namely :

$$[Z]_0 = \begin{vmatrix} Z_1 & & & & K_1 \\ -K_2 & Z_2 & & & \\ & \ddots & \ddots & & \\ & & -K_r & Z_r & \\ & & & \ddots & \ddots \\ & & & -K_s & Z_s \\ & & & & \ddots & \ddots \\ & & & & -K_n & Z_n \end{vmatrix},$$

and

$$[Z]_I = \begin{vmatrix} Z_1 & & & & K_1 \\ -K_2 & Z_2 & & & \\ & \ddots & \ddots & & \\ & & 0 & 0 & Z_{rs} \\ & & & \ddots & \ddots \\ & & & -K_s & Z_s \\ & & & & \ddots & \ddots \\ & & & & -K_n & Z_n \end{vmatrix}.$$

Accordingly, the change in the characteristic equation by the additional feed-back is

$$|[Z]_{\mathrm{I}}| = (-1)^{r+s} Z_{rs} \begin{vmatrix} Z_1 & & & & & & K_1 \\ -K_2 & Z_2 & & & & & \\ & \ddots & \ddots & & & & \\ & & -K_{r-1} & Z_{r-1} & & & \\ & & & -K_{r+1} & Z_{r+1} & & \\ & & & & \ddots & \ddots & \\ & & & & & -K_{s-1} & Z_{s-1} \\ & & & & & & -K_s \\ & & & & & & Z_{s+1} \\ & & & & & & -K_{s+2} \quad Z_{s+2} \\ & & & & & & \ddots \quad \ddots \\ & & & & & & -K_n \quad Z_n \end{vmatrix}$$

$$= (-1)^{r+s} Z_{rs} Z_1 Z_2 \cdots\cdots Z_{r-1} (-1)^{s-r} K_{r+1} K_{r+2} \cdots\cdots K_s Z_{s+1} Z_{s+2} \cdots\cdots Z_n$$

$$= (K_{r+1} K_{r+2} \cdots\cdots K_s)\ (Z_1 Z_2 \cdots\cdots Z_{r-1} Z_{s+1} \cdots\cdots Z_n) Z_{rs} . \qquad (18)$$

Thus, the change of the characteristic vector due to the additional feed-back depends on all other elements and connection coefficients of the system excepting Z_r, Z_{r+1}, ..., Z_s, K_1, K_2, ..., K_r and K_{s+1}, ..., K_n. This change is called the feed-back vector and is easily obtained from $|[Z]_{\mathrm{I}}|$.

The stabilization by an additional feed-back is actually performed by feeding back the time rate of change of the manipulator output to the detector input, as shown in Fig. 10.

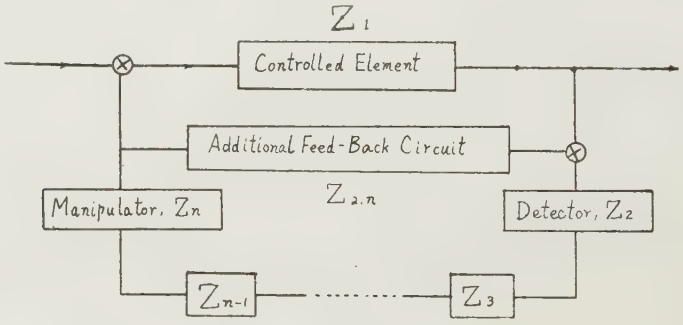

Fig. 10.

The feed-back matrix of the system as shown in Fig. 10, is given by

$$[Z]_{\mathrm{I}} = \begin{matrix} Z & & & & 0 \\ 0 & 0 & & & Z_{2,n} \\ & -K_3 & Z_3 & & \\ & & \ddots & \ddots & \\ & & & -K_{n-1} & Z_{n-1} \\ & & & & -K_n \quad Z_n \end{matrix} ,$$

and since $Z_{2,n} = xp = xd/dt$, the determinant of this matrix becomes:

$$|[Z_1]| = K_3K_4 \cdots\cdots K_n x p Z_1 ,$$

where x is a proportional constant called the feed-back coefficient. In the case of $Z_1 = L_1p + R_1$, it becomes:

$$|[Z]_1| = Kx(L_1p^2 + R_1p) ,$$

where $K = K_3K_4 \cdots\cdots K_n$.

Thus, the feed-back vector is obtained as follows:

$$\left.\begin{aligned} \xi_\nu &= 0, \quad (\nu = 0, 1, 2, \ldots, n-3, n) \\ \begin{pmatrix} \xi_{n-2} \\ \xi_{n-1} \end{pmatrix}_1 &= Kx \begin{pmatrix} L_1 \\ R_1 \end{pmatrix} . \end{aligned}\right\}$$

Therefore, the characteristic vector is changed in two components only, by the additional feed-back element connected, that is:

$$\begin{pmatrix} \xi_{n-2} \\ \xi_{n-1} \end{pmatrix} = \begin{pmatrix} \xi_{n-2} \\ \xi_{n-1} \end{pmatrix}_0 + Kx \begin{pmatrix} L_1 \\ R_1 \end{pmatrix} .$$

Thus, the magnitude of the feed-back vector is proportional to this feed-back coefficient x, and its direction is determined by the time constant $T = L_1/R_1$ of the element $Z_1 = L_1p + R_1$, independent of x, as shown in Fig. 11, in which

$\overrightarrow{OP} = [\xi_\nu]_0$: characteristic vector without any additional feed-back,

$\overrightarrow{PQ} = [\xi_\nu]_1$: feed-back vector,

$\tan\theta = 1/T_1$,

$T_1 = L_1/R_1$: time constant of the controlled element.

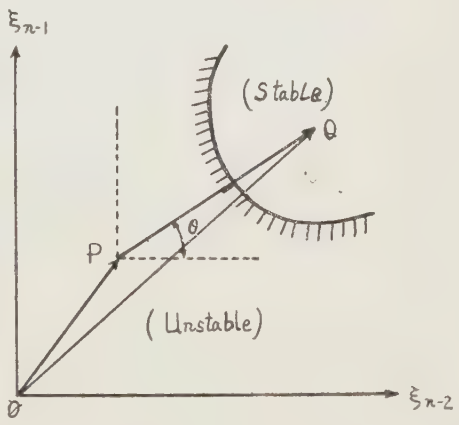

Fig. 11.

As will be seen from Fig. 11, the characteristic vector $\overrightarrow{OP}$ of the control system which is unstable without an additional feed-back, can be changed to the stable vector $\overrightarrow{OQ}$ by adjusting the feed-back coefficient x.

10. Improvement of characteristics by an additional feed-forward

The additional feed-forward which is performed such that through the element Z_{sr}, the output signal of Z_r is fed to the input of Z_s as shown in Fig. 12, has

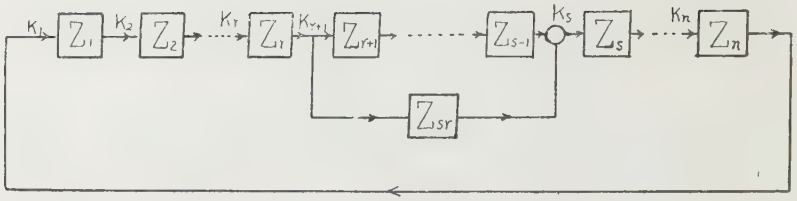

Fig. 12.

similar effects to the additional feed-back and is used to improve the stability and the response of the control system.

The characteristic matrix of this system is given by

$$[\boldsymbol{Z}] = \begin{pmatrix} Z_1 & & & & & & K_1 \\ -K_2 & Z_2 & & & & & \\ & \ddots & \ddots & & & & \\ & & K_r & Z_r & & & \\ & & \ddots & \ddots & \ddots & & \\ & & Z_{sr} & -K_s & Z_s & & \\ & & & \ddots & \ddots & \ddots & \\ & & & & -K_{n-1} & Z_{n-1} & \\ & & & & & -K_n & Z_n \end{pmatrix}.$$

So, the characteristic equation becomes:

$$|[\boldsymbol{Z}]| = |[\boldsymbol{Z}]_0| + |[\boldsymbol{Z}]_{II}| = 0\,,$$

where $[\boldsymbol{Z}]_0$ is the characteristic matrix of the system without any feed-forward, and $[\boldsymbol{Z}]_{II}$ is the feed-forward matrix, which is produced by substituting Z_{sr} for the (s, r) element, and making zero all other elements of the s-th row in $[\boldsymbol{Z}]_0$.

Thus, we have:

$$|[\boldsymbol{Z}]_{II}| = (-1)^{r+s} Z_{s,r} \begin{vmatrix} Z_1 & & & & & & & K_1 \\ -K_2 & Z_2 & & & & & & \\ & \ddots & \ddots & & & & & \\ & & -K_{r-1} & Z_{r-1} & & & & \\ & & & -K_r & & & & \\ & & & & Z_{r+1} & & & \\ & & & & -K_{r+2} & Z_{r+2} & & \\ & & & & & \ddots & \ddots & \\ & & & & & & -K_{s-1} & Z_{s-1} \\ & & & & & & & -K_{s+1} & Z_{s+1} \\ & & & & & & & & \ddots & \ddots \\ & & & & & & & & & -K_n & Z_n \end{vmatrix}$$

$$= K' Z_{s,r} (Z_{r+1} Z_{r+2} \cdots\cdots Z_{s-1})\,,$$

where $K' = K_1K_2\cdots\cdots K_rK_{s-1}\cdots\cdots K_n$.

Hence, the change of the characteristic vector due to an additional feed-forward depends upon Z_{r+1}, Z_{r+2}, ..., Z_{s-1}, $Z_{s,r}$ and K_1, K_2, ..., K_r, K_{s+1}, ..., K_n. This change is called the "feed-forward vector".

If the time rate of change of the output of Z_{r-1} is fed forward to the input of Z_{r+1}, as it is often used, the feed-forward vector is given by:

$$\begin{pmatrix} \xi_{n-2} \\ \xi_{n-1} \end{pmatrix} = K'x \begin{pmatrix} L_r \\ R_r \end{pmatrix},$$

where $Z_r \equiv L_r p + R_r$.

Thus, quite similarly to the case of the additional feed-back, the stabilization of the system is performed and the magnitude of the feed-forward vector varies with the feed-forward coefficient x, and the direction is determined by the time constant $T_r = L_r/R_r$ of the element Z_r, as shown in Fig. 13, in which

$\overrightarrow{OP}$: characteristic vector without any additional feed-forward,

$\overrightarrow{PQ}$: feed-forward vector, and $\tan\theta = 1/T_r$.

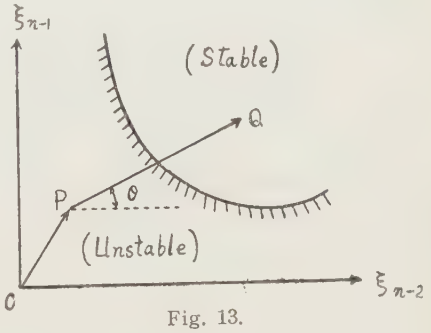

Fig. 13.

11. Experimental confirmation

i) Experimental apparatus

In order to confirm experimentally the author's stability criteria of the feed-back physical system, the stabilizing experiments of the speed control of a D.C. shunt motor by means of an additional feed-back (antihunting device) have been carried out.

The experimental apparatus consists of Ward-Leonard system with feed-back elements, whose connection diagram and elements are given in Fig. 14, and Table I, respectively.

The speed of the D.C. shunt motor in Ward-Leonard system, that is, the controlled variable, should be kept constant by means of the feed-back, whose mechanism is as follows. First, the motor speed is detected by a tachometer generator as a speed voltage, which passing through a filter is compared with the set value of the speed voltage and difference voltage, after amplified 1400 times as large, is converted into a shift angle of phase by a phase shifter, and deformed into a peak voltage through the peak-generating device, and this phase shift of peak voltage, impressed on the grids of two thyratrons, controls their ignition angles, and their output current excites the

Table I

Department	Symbol	Element	Rating
Controlled system	PM	3 phase induction motor for prime mover	3 HP, 1430rpm, 110V
	G	Ward-Leonard D.C. generator	2kW, 1500rpm, 110V
	M	Controlled D.C. shunt motor	1kW, 1500rpm, 105V
	LG	D. C. generator for load	1kW, 1500rpm, 105V
	Ra	Total resistance of armature circuit of Leonard {motor / generator}	
	R_L	Resistance load (lamp bank)	
Detecting device	T	Tachometer generator	1000 rpm, 6V, 3 mA
	r_T	Armature resistance of tachometer generator	100 Ω
	R_V	Internal resistance of voltmeter	2 kΩ
	r_1	Resistance of choking coil	1.5 kΩ
	L_1	Inductance of choking coil	30 H
	C_1	Condenser	3.5 μF
	R_1	Resistance	30 kΩ
Amplifier	V_1	First step amplifier tube UZ-6C6	μ=1500, r_p=1.5MΩ
	V_6	Glow tube for stabilizing voltage	VRA 135V/60mA
	V_7	Glow tube for stabilizing voltage	VRA 65V/80mA
	R_2	Resistance load of the 1st step amplifier tube	100kΩ
	C_2	Condenser	2.46μF
	V_2	Second step amplifier tube UY-76	μ=13.8, r_p=9.5kΩ
	V_8	Glow tube for stabilizing voltage	VRA 150V/30mA
	R_3	Resistance load of the 2nd step amp. tube	30kΩ
Phase shifter	V_3	Vacuum tube for variable resistance of phase shifter	UX-2A3
	C_3	Condenser (phase shifting circuit)	0.76μF
	R_4	Resistance for phase-adjusting	3.6 kΩ
Peak generating device	V_4	Vacuum tube for peak generator	UZ-42
	R_3	Resistance load of peak generating tubes	
Manipuator	Th	Grid glow mercury tube TX-920	200V, 2.5A peak load 15A

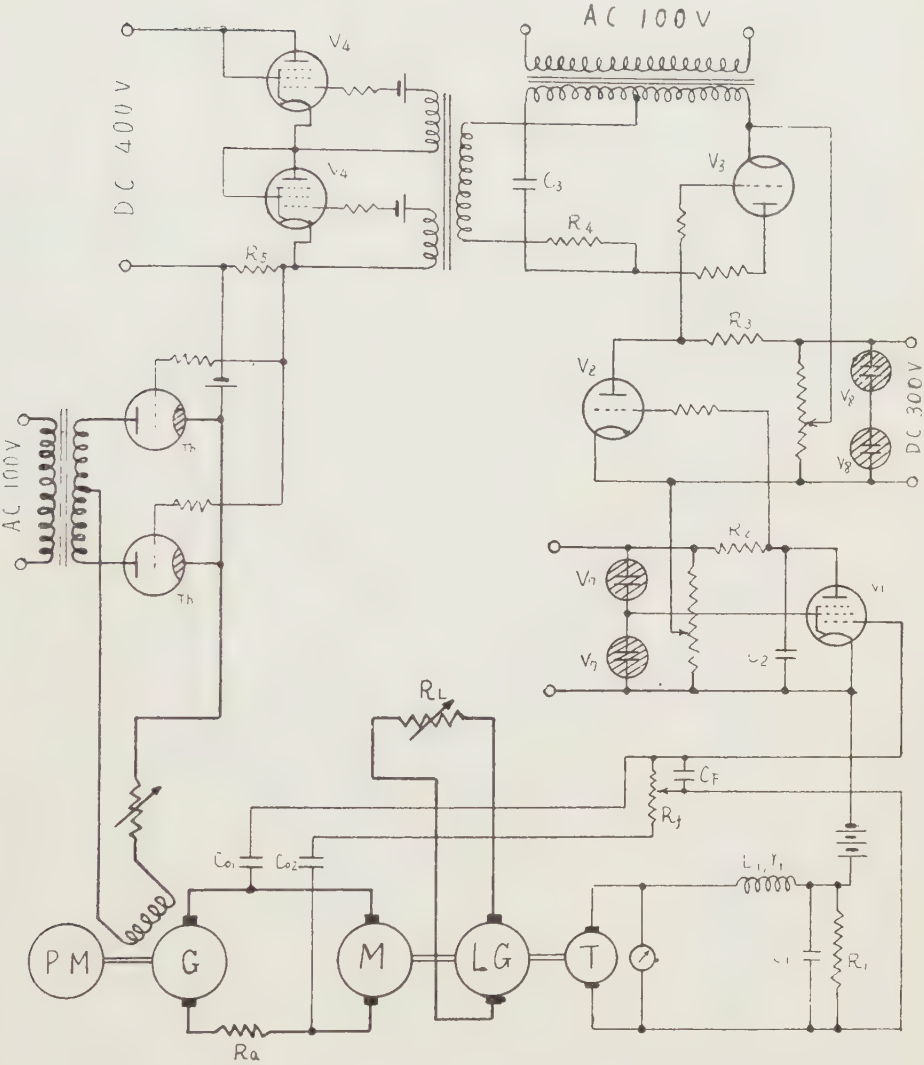

Fig. 14. Diagram of the automatic speed control in Ward-Leonard system

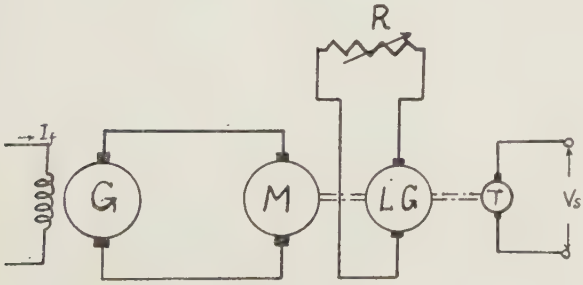

G: Leonard generator
M: Controlled motor
LG: Load-generator
T: Tachometer generator

Fig. 15.

field of the Ward-Leonard generator so that the motor speed is kept constant.

Since the deviation of the motor speed is very small, the system may be assumed to be linear, and on this assumption the calculation has been performed.

ii) Characteristic impedance of each element

a) Controlled system

The controlled system consists of a set of Ward-Leonard system with loads and a tachometer generator as shown in Fig. 15, and the input signal is the deviation in the field current of Leonard-generator ΔI_f, while the output signal is the deviation in the generated voltage of tachometer ΔV_s.

If the deviation of field current ΔI_f is small, it may be assumed to be proportional to the change of generated voltage ΔE_g of the generator G, that is,

$$\Delta E_g = K_f \Delta I_f . \qquad \text{(see Fig. 16)}$$

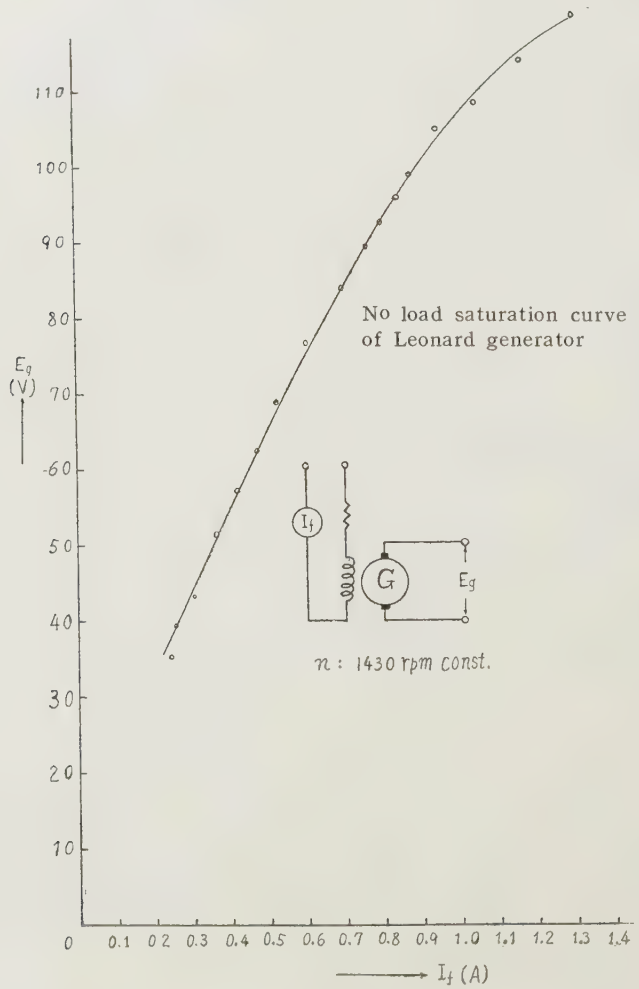

Fig. 16.

The deviation of motor speed $\Delta\dot{\theta}$, which is induced from the voltage deviation ΔE_g, is given by the following equation:

$$J\frac{d\Delta\dot{\theta}}{dt}+\left(f+\frac{K_1^2}{R_a}+\frac{K_2^2}{R_L}\right)\Delta\dot{\theta}=\frac{K_1}{R_a}\Delta E_g,$$

where K_1, K_2 are torque coefficient and induced emf coefficient of motor and generator, because the motor and the generator are of the same structure.

As the speed of motor $\dot{\theta}$ is proportional to the induced emf V_s of the tachometer generator T, that is, $\dot{\theta}=K_T V_S$, hence, if the input signal is the field current diviation ΔI_f of Leonard-generator and the output signal is the deviation of speed emf ΔV_S, the performance equation of controlled system is

$$J'\frac{d\Delta V_F}{dt}+f'\Delta V_S=\Delta I_f,$$

where

$$\begin{cases} J'=\dfrac{K_T}{K_f}\cdot\dfrac{R_a}{K_1}J, \\ f'=\dfrac{K_T}{K_f}\cdot\dfrac{R_a}{K_1}\left(f+\dfrac{K_1^2}{R_a}+\dfrac{K_2^2}{R_L}\right), \end{cases}$$

with
$\begin{cases} J: \text{ moment of inertia of motor with loads,} \\ f: \text{ friction coefficient of motor with loads.} \end{cases}$

Thus, the impedance of controlled system is given by

$$Z_1=J'p+f'.$$

The measured values of J' and f' are as follows (see Fig. 17).

Loads	Time constant	J'	f'
no load	0.258	0.0445	0.172
1 load	0.228	0.0438	0.192
2 loads	0.203	0.0440	0.217

b) Detector with filter

The detecting device is a tachometer generator with filter, which converts the speed signal into the voltage signal. However, as the performance equation of detector, that is $\dot{\theta}=K_T V_S$, has been contained in the performance equation of controlled system, it is sufficient here to consider the performance of the filter only. The filter is illustrated in Fig. 18, in which

r_T: armature resistance of tachometer generator (100 Ω),

R_V: internal resistance of voltmeter (2KΩ),

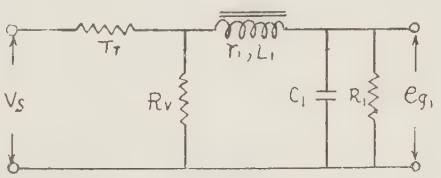

Fig. 18.

I_f~V_s Characteristic Curve
Speed of generator; 1430 rpm

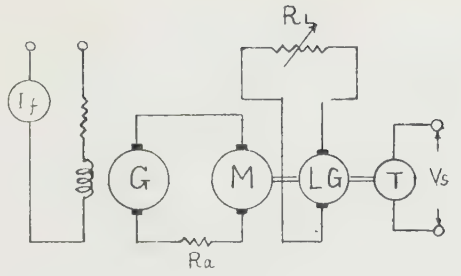

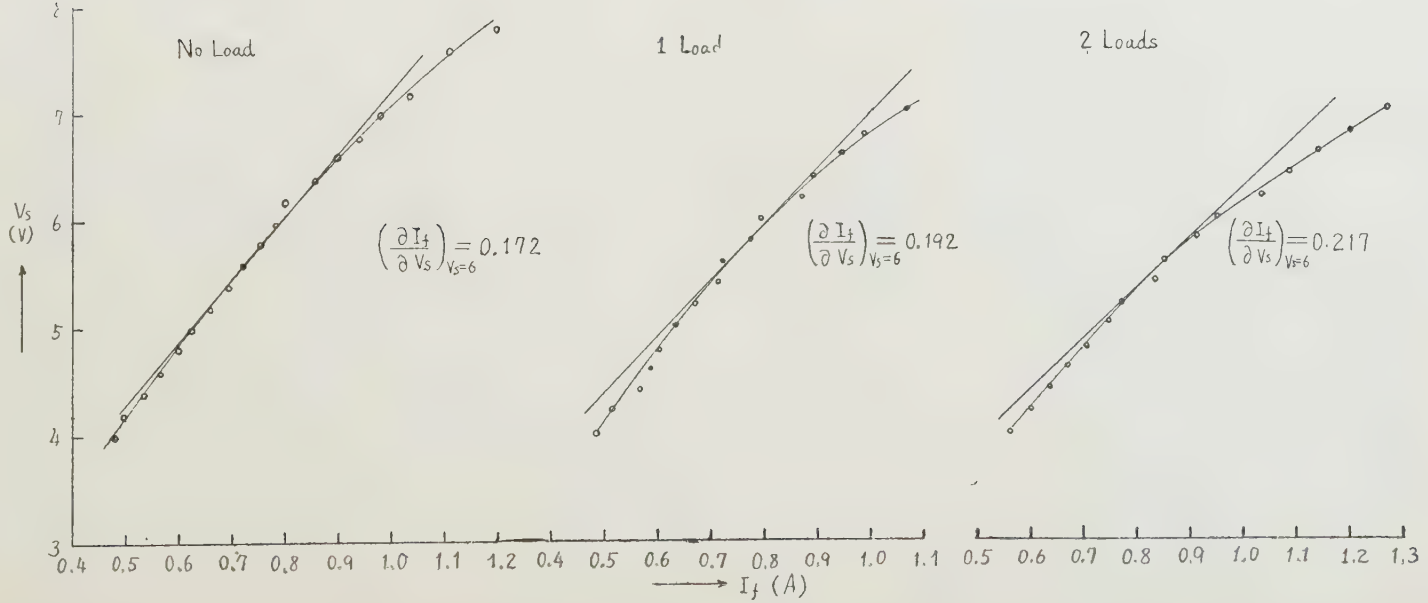

Fig. 17.

r_1, L_1: resistance and inductance of choking coil (1.5 KΩ, 30 H),

C_1 : condenser (3.5 μF),

R_1 : resistance (30 KΩ).

The performance equation of this filter is

$$k_1 V_S = L_1 C_1 \frac{d^2 e_{g1}}{dt^2} + \left(\frac{L_1}{R_1} + C_1 r_1\right) \frac{de_{g1}}{dt} + \left(\frac{r_1}{R_1} + 1\right) e_{g1},$$

where $$k_1 = R_V/(r_T + R_V) = 2/(2+0.1) = 0.95.$$

Hence, the performance relation between the input signal ΔV_S and the output signal Δe_{g1} of detector is expressed as follows:

$$k_1 \Delta V_S = \left\{L_1 C_1 p^2 + \left(\frac{L_1}{R_1} + C_1 r_1\right) p + \left(\frac{r_1}{R_1} + 1\right)\right\} \Delta e_{g1},$$

or

$$0.95\, \Delta V_S = (1.05 \times 10^{-4} p^2 + 6.25 \times 10^{-3} p + 1.05)\, \Delta e_{g1}.$$

c) Amplifier

Fig. 19 shows the actual circuit of the two stage amplifier.

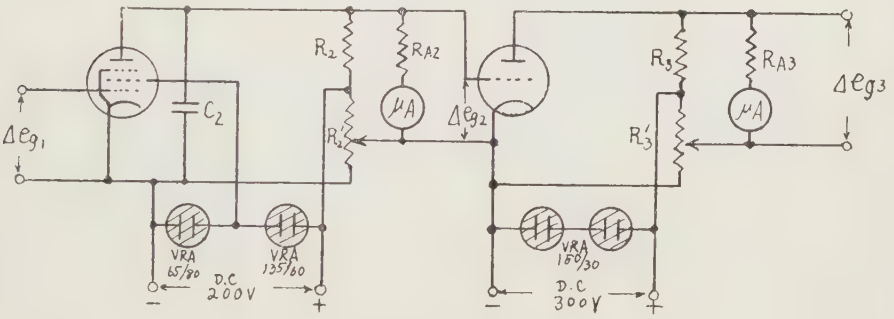

R_2: load resistance of UZ-6C6 (100 KΩ),
R_3: load resistance of UY-76 (30 KΩ),
R_2': variable resistance (500 KΩ),
R_3': variable resistance (350 KΩ),
R_{A2}: resistance (500 KΩ),
R_{A3}: resistance (250 KΩ),
C_2: condenser (2.45 μF),
Δe_{g1}: deviation of input signal voltage in the 1st stage,
Δe_{g2}: deviation of input signal voltage in the 2nd stage,
Δe_{g3}: deviation of output signal voltage in the amplifier,
μ: amplification constant of UZ-6C6,
r_{p2}: internal resistance of UZ-6C6,
R_2'': resultant resistance of parallel connection of R_2 and the anode part of R_2'.

Fig. 19.

The actual circuit of the first stage of the amplifier is equivalent to the simple circuit as shown in Fig. 20, for small deviation of input signal voltage. Thus, we have

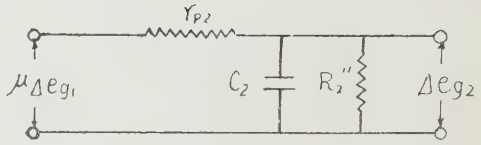

Fig. 20.

$$-\mu \Delta e_{g1} = \left\{ C_2 r_{p2} p + \left(1 + \frac{r_{p2}}{R_2''} \right) \right\} \Delta e_{g2} ,$$

or

$$-1260\, \Delta e_{g1} = (3.7p + 18.7)\, \Delta e_{g2} . \qquad \text{(see Fig. 21)}$$

The performance of the second stage is expressed by

$$K_3' \Delta e_{g2} = \Delta e_{g3} . \qquad \text{(see Fig. 22)}$$

As $K_3' = -11$ is obtained by experiment, the performance equation of the whole set of amplifier is obtained as follows:

$$-\mu \Delta e_{g1} = \left[C_2 r_{p2} p + \left(1 + \frac{r_{p2}}{R_2''} \right) \right] \frac{1}{K_3'} \Delta e_{g3} .$$

d) Manipulator with phase shifter

The manipulator consists of three parts, i. e., phase shifter, impulse generator and thyratron circuit. The input signal, that is, the output voltage deviation of amplifier, is converted into the shift angle of phase by phase shifter, and is deformed by impulse generator into the phase shift of peak voltage, which is impressed on the grids of thyratrons, and the output current of the thyratrons controls the field of Leonard-generator, as shown in Fig. 23.

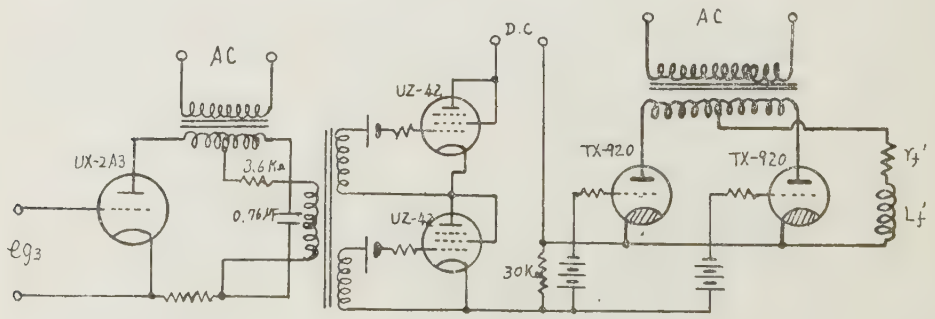

(Phase shifter) (Impulse generator) (Thyratron circuit)

Fig. 23.

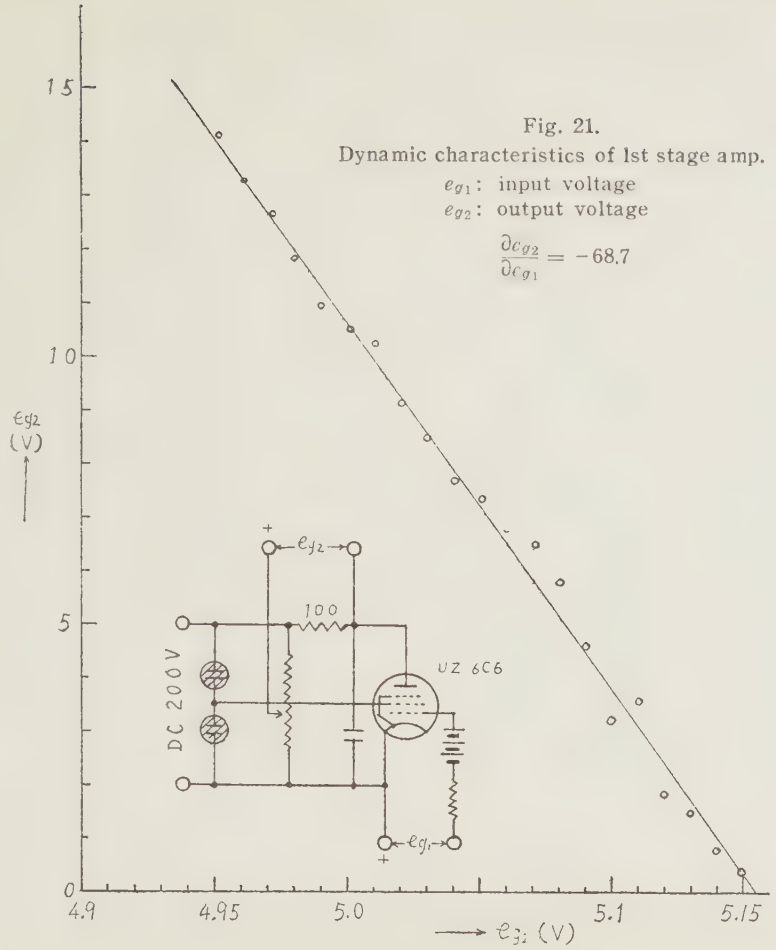

Fig. 21.
Dynamic characteristics of 1st stage amp.
e_{g1}: input voltage
e_{g2}: output voltage

$$\frac{\partial e_{g2}}{\partial e_{g1}} = -68.7$$

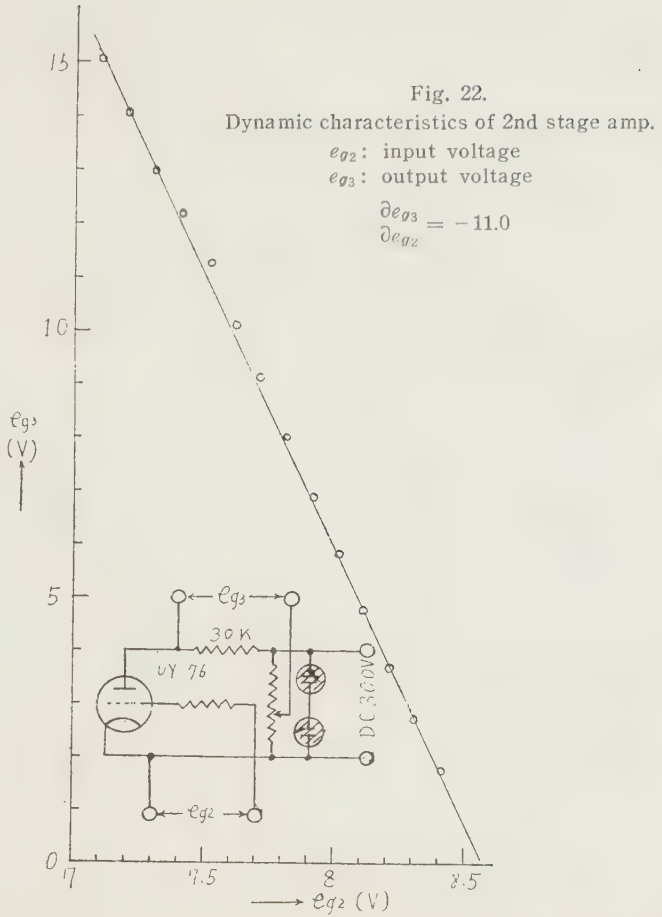

Fig. 22.
Dynamic characteristics of 2nd stage amp.
e_{g2}: input voltage
e_{g3}: output voltage

$$\frac{\partial e_{g3}}{\partial e_{g2}} = -11.0$$

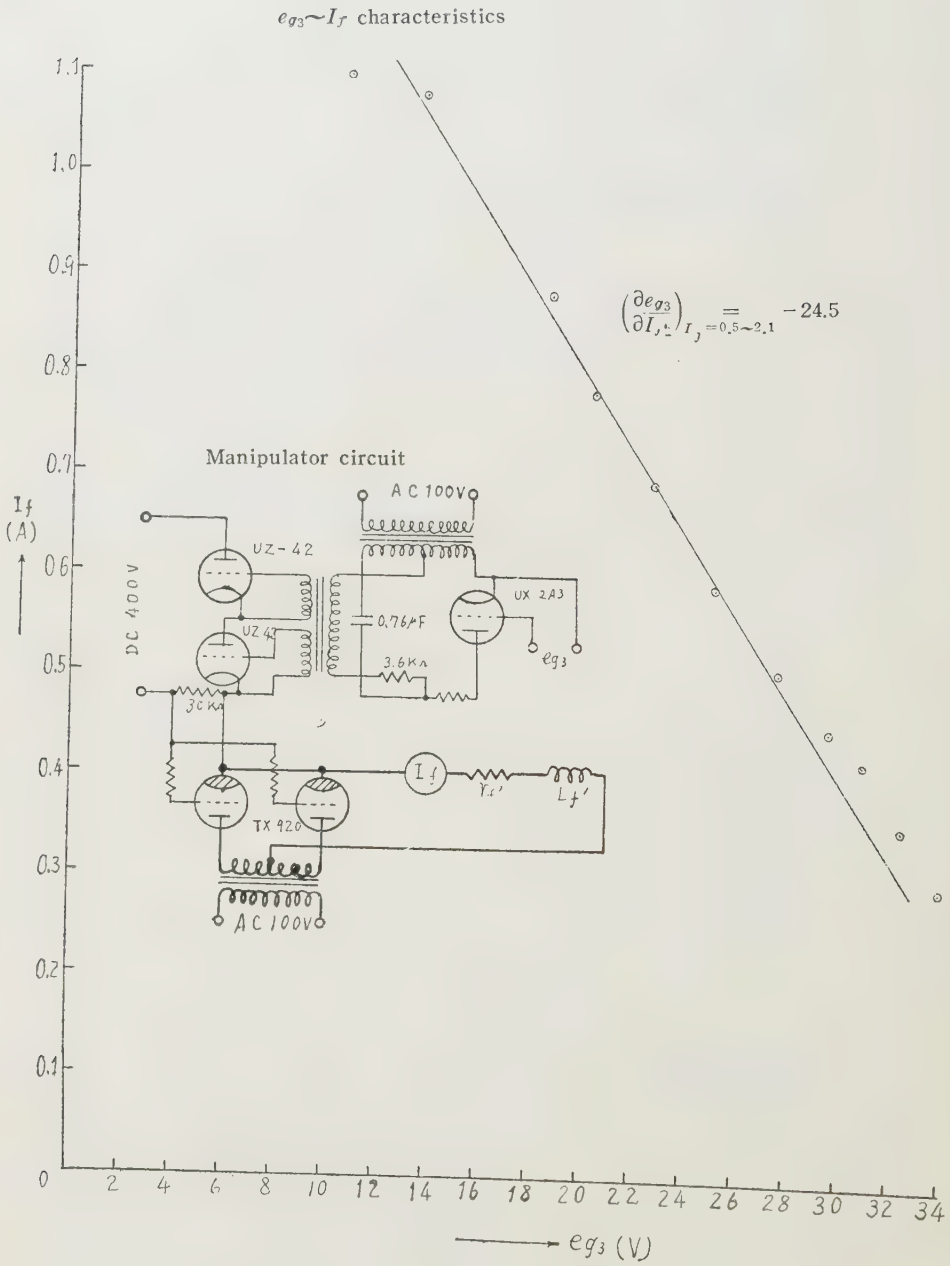
e_{g_3}~I_f characteristics
$\left(\frac{\partial e_{g_3}}{\partial I_f}\right)_{I_f=0.5\sim2.1} = -24.5$
Manipulator circuit
AC 100V
UZ-42
UZ 42
DC 400V
UX 2A3
0.76μF
3.6KΩ
30KΩ
e_{g_3}
I_f
r_f'
L_f'
TX 920
AC 100V
I_f (A)
1.1
1.0
0.9
0.8
0.7
0.6
0.5
0.4
0.3
0.2
0.1
0
2 4 6 8 10 12 14 16 18 20 22 24 26 28 30 32 34
e_{g_3} (V)

Fig. 24.

The performance characteristics of manipulator have been obtained as follows by oscillographical measurements. The time constants of phase shifter and impulse generator are estimated to be negligibly small both by measurements and by calculation (ca. 0.8/1000 sec) from the internal resistance of UX-2A3 (0.8 KΩ) and the capacity of condenser $C_3(1\,\mu\text{F})$. Thus, the time constant of the whole set depends only upon that of the field winding of Leonard-generator, and is obtained experimentally. Then, the values of constants r_f' and L_f' are calculated from $e_{g3}\sim I_f$ characteristics at operating conditions and the measured time constant $T=0.155$ sec of the field winding as follows:

$$r_f' = \left(\frac{\partial e_{g3}}{\partial I_f}\right)_{1\cdot0>I_f>0\cdot5} = 24.5, \quad L_f' = 24.5\times0.155 = 3.8\,.$$

Accordingly, the performance equation of the whole set of manipulator is given by

$$-\Delta e_{g3} = K_3\Delta e_{g2} = (L_f'p+r_f')\,\Delta I_f\,, \qquad \text{(see Fig. 24)}$$

and $$K_3 = -K_3' = 11\,.$$

Thus, $$Z \equiv L_f'p+r_f' = 3.8\,p+24.5\,.$$

iii) Characteristic vector

The block diagram of this automatic control system is obtained from the above-mentioned impedances of all elements as follows:

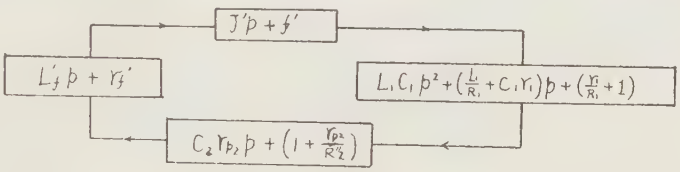

Fig. 25.

Hence, the characteristic matrix of this control system is

$$[Z] = \begin{pmatrix} J'p+f' & & 1 \\ -K_1 & L_1C_1p^2+\left(\dfrac{L_1}{R_1}+C_1r_1\right)p+\left(\dfrac{r_1}{R_1}+1\right) & \\ & -K_2 & C_2r_{p_2}p+\left(1+\dfrac{r_{p^2}}{R_2''}\right) \\ & & -K_3 \qquad L_f'p+r_f' \end{pmatrix}.$$

It gives the characteristic equation of the system as:

$$|[Z]| = 0\,,$$

or

$$\left(J'p+f'\right)\left\{L_1C_1p^2+\left(\frac{L_1}{R_1}+C_1r_1\right)p+\left(\frac{r_1}{R_1}+1\right)\right\}\left\{C_2r_{p_2}p+\left(1+\frac{r_{p_2}}{R_2}\right)\right\}\left(L_f'p+r_f'\right)+K_1K_2K_3=0.$$

Arranging the equation in descending powers of p, we get

$$a_0 p^5 + a_1 p^4 + a_2 p^3 + a_3 p^2 + a_4 p + a_5 = 0 .$$

If the characteristic vector $[a\mu/a_0]$, $(\mu=1, 2, 3, 4, 5)$ is transformed by

$$\left.\begin{aligned} \xi_{2\nu} &= \frac{a_{2\nu}}{a_0} \Big/ \left(\frac{a_2}{a_0}\right)^{\nu}, \\ \xi_{2\nu+1} &= \frac{a_{2\nu+1}}{a_1} \Big/ \left(\frac{a_2}{a_0}\right)^{\nu}, \end{aligned}\right\} \qquad (\nu = 0, 1, 2)$$

the following components of the normalized characteristic vector are obtained:

$$\xi_0 = 1, \quad \xi_1 = 1, \quad \xi_2 = 1,$$
$$\xi_3 = \frac{a_3}{a_1} \Big/ \left(\frac{a_2}{a_0}\right), \quad \xi_4 = \frac{a_4}{a_0} \Big/ \left(\frac{a_2}{a_0}\right)^2, \quad \xi_5 = \frac{a_5}{a_1} \Big/ \left(\frac{a_2}{a_0}\right)^2 .$$

Putting numerical values of physical constants at different states of load, we obtain:

a) *No load*:

The characteristic equation is given by

$$6.24\times10^{-5}\, p^5 + 4.933\times10^{-3}\, p^4 + 7.09\times10^{-1}\, p^3 + 10.38\, p^2 + 51.0\, p + 13483 = 0,$$

and the characteristic vector has the components:

$$\left.\begin{aligned} \xi_3 &= \frac{10.38 \times 6.54}{4.933 \times 7.09} \times 10^{-1} = 0.203 , \\ \xi_4 &= \frac{51.9 \times 6.54}{7.09 \times 7.09} \times 10^{-3} = 0.00663 , \\ \xi_5 &= \frac{13483 \times 6.54^2}{4.933 \times 7.09^2} \times 10^{-5} = 0.0232 . \end{aligned}\right\}$$

b) *One load*:

The characteristic equation is

$$6.44\times10^{-5}\, p^5 + 4.9\times10^{-3}\, p^4 + 7.11\times10^{-1}\, p^3 + 10.58\, p^2 + 54.05\, p + 13492 = 0 ,$$

and the characteristic vector has the components:

$$\left.\begin{aligned} \xi_3 &= \frac{10.58 \times 6.44}{4.90 \times 7.11} 10^{-1} = 0.1955 , \\ \xi_4 &= \frac{54.05 \times 6.44}{7.11^2} 10^{-3} = 0.00683 , \\ \xi_5 &= \frac{13492 \times 6.44^2}{4.90 \times 7.11^2} 10^{2-} = 0.0223 . \end{aligned}\right\}$$

c) *Two loads*:

The characteristic equation is

$$6.48\times10^{-5}\,p^5+4.95\times10^{-3}\,p^4+7.17\times10^{-1}\,p^3+11.0\,p^2+58.6\,p+13504=0,$$

and the characteristic vector has the components:

$$\xi_3=\frac{11.0\ \times\ 6.48}{4.95\ \times\ 7.17}\times10^{-1}=0.2005\,,$$

$$\xi_4=\frac{58.6\ \times\ 6.48}{7.17^2}\times10^{-3}=0.0074\,,$$

$$\xi_5=\frac{13504\times6.48^2}{4.95\times7.17^2}\times10^{-5}=0.0225\,.$$

From the above-mentioned calculations, we get the following table of the characteristic vector components:

States of load	ξ_3	ξ_4	ξ_5	Stability
no load	0.2030	0.00663	0.0232	unstable
1 load	0.1955	0.00683	0.0223	unstable
2 loads	0.2005	0.00740	0.0225	unstable

Thus, the automatic control system in each of the above-mentioned cases a), b) and c) has been concluded to be unstable as shown with the point P in Fig. 29, and this instability has also been shown in the experiments in which the remarkable hunting has appeared.

iv) Feed-back to detector

In order to stabilize the unstable system, the additional feed-back circuit has been inserted between the output of manipulator Z_4 and the input of detector Z_2. The additional feed-back circuit $Y_{f.b.}$ is shown in Fig. 26.

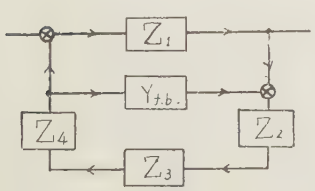

Fig. 26.

$Z_1=J'p+f'$: controlled element (Leonard-motor),

$Z_2=L_1C_1p^2+\left(\frac{L_1}{R_1}+C_1r_1\right)p+\left(\frac{r_1}{R_1}+1\right)$: detector with filter,

$Z_3=C_2r_{p2}p+\left(\frac{r_{p2}}{R_2''}+1\right)$: amplifier,

$Z_4=L_f'p+r_f'$: manipulator,

$Y_{f.b.}=xp$: feed-back element,

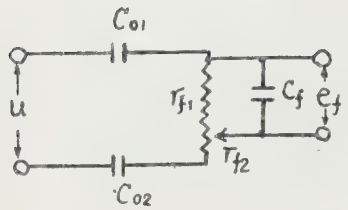

Fig. 27.

u = input voltage,
e_f = output voltage,
$C_{01} = 2.11\,\mu$F,
$C_{02} = 7.0\,\mu$F,
$C_f = 2.46\,\mu$F,
r_{f1}, r_{f2} = variable resistances ($r_{f1}+r_{f2} = 2000\,\Omega$),
$C_0 = C_{01}C_{02}/(C_{01}+C_{02}) = 1.62\,\mu$F.

With R_g = armature resistance of Leonard-generator and R_m = armature resistance of Leonard-motor (controlled motor), we obtain:

$$Y_{f.b.} = C_0 r_{f1} K_f \frac{R_m}{R_g + R_m} p = xp = 0.0562\, r_{f1} p\,,$$

and

$$|[\boldsymbol{Z}]| = \begin{vmatrix} Z_1 & & & 1 \\ -K_1 & Z_2 & & Y_{f.b.} \\ & -K_2 & Z_3 & \\ & & -K_3 & Z_4 \end{vmatrix} = |[\boldsymbol{Z}]_0| + Y_{f.b.}|[\boldsymbol{Z}]_{\mathrm{I}}| = 0\,,$$

where $[\boldsymbol{Z}]_0$: characteristic matrix without any additional feed-back,

$$|[\boldsymbol{Z}]_{\mathrm{I}}| = \begin{vmatrix} Z_1 & & \\ -K_2 & Z_3 & \\ & -K_3 & \end{vmatrix} = K_2K_3Z_1 = K_2K_3(J'p+f')\,.$$

Hence, the feed-back vector is given by

$$\begin{pmatrix} \xi_3 \\ \xi_4 \end{pmatrix}_{\mathrm{I}} = K_2K_3x \begin{pmatrix} J' \\ f' \end{pmatrix} = 0.0562\, K_2K_3 r_{f1} \begin{pmatrix} J' \\ f' \end{pmatrix}.$$

Then, the characteristic vector of the system, with the additional feed-back element $Y_{f.b.}$ ($r_{f1} = 1.0\,\mathrm{K}\Omega$), has the components:

Load	ξ_0	ξ_1	ξ_2	ξ_3	ξ_4	ξ_5
no load	6.54×10^{-5}	4.933×10^{-3}	7.09×10^{-1}	45.48	187.0	13483
1 load	6.44×10^{-5}	4.90×10^{-3}	7.11×10^{-1}	45.05	205.5	13492
2 loads	6.48×10^{-5}	4.95×10^{-3}	7.17×10^{-1}	45.80	229.6	13504

and is normalized as follows:

Load	ξ_0''	ξ_1''	ξ_2''	ξ_3''	ξ_4''	ξ_5''	Stability
no load	1	1	1	0.890	0.0244	0.0232	unstable
1 load	1	1	1	0.836	0.0257	0.0223	unstable
2 loads	1	1	1	0.835	0.0290	0.0225	stable

The above-calculated vector-components are illustrated in Fig. 29, and the experiments have quite agreed with these theoretical calculations, showing that the system is completely stabilized only in the case of two loads. And the measured values of resistance r_{f1} for the system being in critical stability are quite consistent with the author's theoretical calculations, as follows.

Load	Theoretical values	Measured values
no load	1.04 KΩ	1.12 KΩ
1 load	1.01 KΩ	1.10 KΩ
2 loads	0.96 KΩ	0.94 KΩ

v) Feed-back to amplifier

When the additional feed-back circuit $Y_{f\cdot b}$, which is shown in Fig. 28, is inserted between the output of manipulator and the input of amplifier, in order to stabilize the hunting system, the block diagram of the whole system is given as follows:

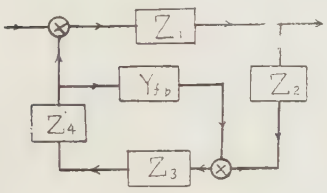

Fig. 28.

$Z_1 = J'p+f'$: controlled element (Leonard-motor),

$Z_2 = L_1C_1p^2+\left(\frac{L_1}{R_1}+C_1r_1\right)p+\left(\frac{r_1}{R_1}+1\right)$: detector with filter,

$Z_3 = C_2r_{p^2}p+\left(\frac{r_{p^2}}{R_2''}+1\right)$: amplifier,

$Z_4 = L_f'p+r_f'$: manipulator,

$Z_{f\cdot b} = xp$: feed-back element.

The characteristic equation is

$$\begin{vmatrix} J'p+f' & & & 1 \\ -K_1 & L_1C_1p_2+\left(\frac{L_1}{R_1}+C_1r_1\right)p+\left(\frac{r_1}{R_1}+1\right) & & \\ & -K_2 & C_2r_{p^2}p+\left(\frac{r_{p^2}}{R_2''}+1\right) & Y_{f\cdot b} \\ & & -K_3 & L_f'p+r_f' \end{vmatrix} = 0 .$$

This is expanded as follows:

$$|[Z]_0| + Y_{f\cdot b}\cdot|[Z]_1| = 0 ,$$

where $[Z]_0$: characteristic matrix without any additional feed-back,

$$|[Z]_1| = -\begin{vmatrix} Z_1 & & \\ -K_1 & Z_2 & \\ & -K_3 & \end{vmatrix} = K_3Z_1Z_2 = K_3(J'p+f')\left\{L_1C_1p^2+\left(\frac{L_1}{R_1}+C_1r_1\right)p+\left(\frac{r_1}{R_1}+1\right)\right\}$$

$$= J'L_1C_1K_3p^3+K_3\left\{J'\left(\frac{L_1}{R_1}+C_1r_1\right)+f'L_1C_1\right\}p^2$$

$$+K_3\left\{J'\left(\frac{r_1}{R_1}+1\right)+f'\left(\frac{L_1}{R_1}+C_1r_1\right)\right\}p+K_3f'\left(1+\frac{r_1}{R_1}\right).$$

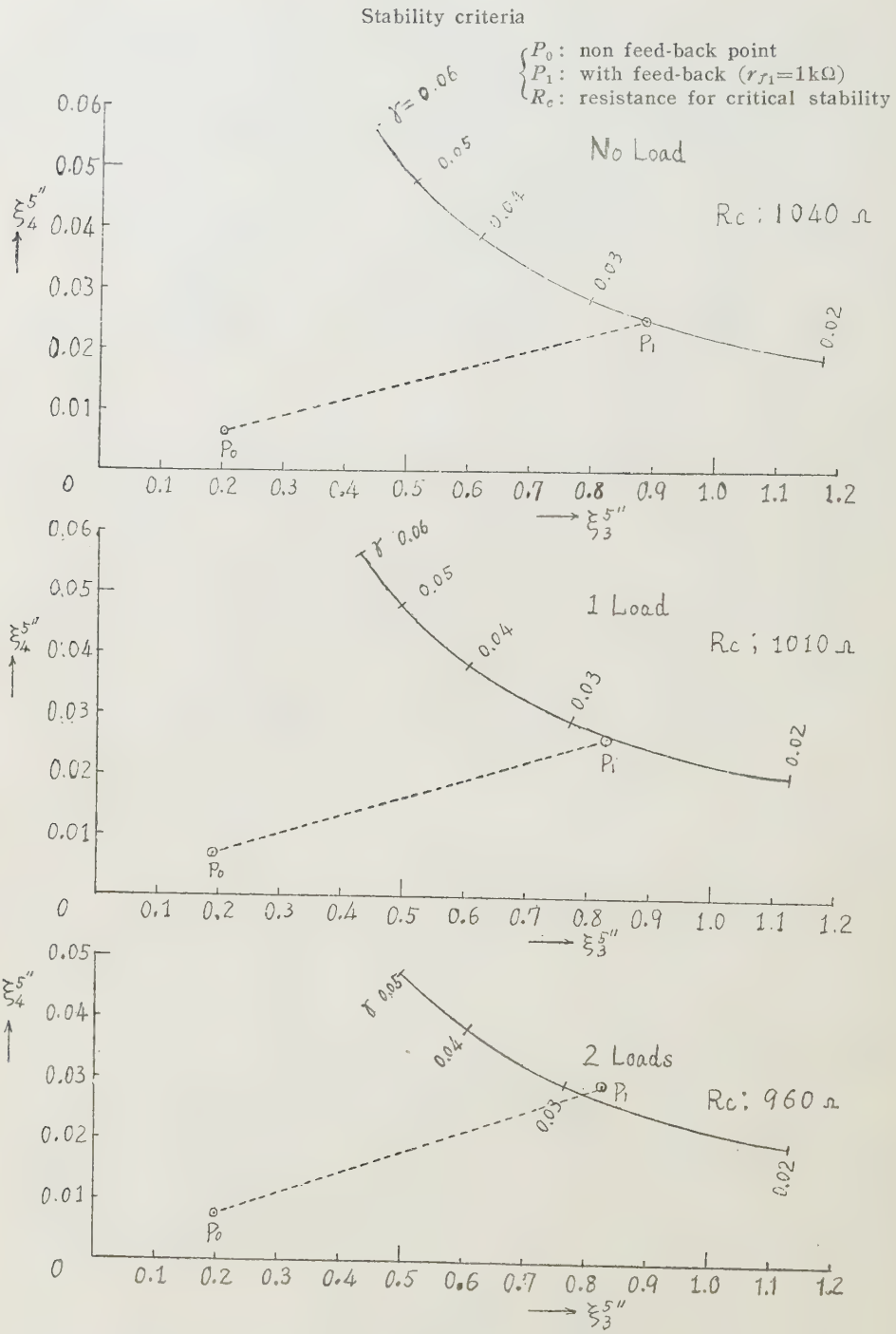
Stability criteria
P_0 : non feed-back point
P_1 : with feed-back (r_{f1}=1kΩ)
R_c : resistance for critical stability
No Load
Rc : 1040 Ω
1 Load
Rc ; 1010 Ω
2 Loads
Rc: 960 Ω
γ=0.06
0.05
0.04
0.03
0.02
P_0
P_1
$\xi_4^{5''}$
$\xi_3^{5''}$

Fig. 29.

The feed-back vector or stablizing vector is

$$\begin{Bmatrix}\xi_1\\ \xi_2\\ \xi_3\\ \xi_4\end{Bmatrix} = K_3 x \begin{Bmatrix} J'L_1C_1 \\ J'\left(\frac{L_1}{R_1}+C_1r_1\right)+f'L_1C_1 \\ J'\left(\frac{r_1}{R_1}+1\right)+f'\left(\frac{L_1}{R_1}+C_1r_1\right) \\ f'(r_1/R_1+1)\end{Bmatrix} = r_{f1}\begin{Bmatrix} J'\times 8.3\times 10^{-2} \\ J'\times 4.95+f'\times 8.3\times 10^{-3} \\ J'\times 830+f'\times 4.95 \\ f'\times 830\end{Bmatrix},$$

and it has the following numerical components for $r_{f1}=1.0\,\mathrm{K}\Omega$.

Load	ξ_1	ξ_2	ξ_3	ξ_4
no load	3.7×10^{-4}	0.230	37.85	143.0
1 load	3.66×10^{-4}	0.234	37.55	159.0
2 loads	3.64×10^{-4}	0.236	37.48	180.0

So the characteristic vector, with additional feed-back, has the components:

Load	ξ_0	ξ_1	ξ_2	ξ_3	ξ_4	ξ_5
no load	6.54×10^{-5}	5.303×10^{-3}	0.939	48.23	194.0	13483
1 load	6.44×10^{-5}	5.266×10^{-3}	0.945	48.13	213.0	13492
2 loads	6.48×10^{-5}	5.314×10^{-3}	0.953	48.48	238.6	13504

and by normalization, these become:

Load	ξ_0''	ξ_1''	ξ_2''	ξ_3''	ξ_4''	ξ_5''
no load	1	1	1	0.603	0.0144	0.0122
1 load	1	1	1	0.626	0.0154	0.0119
2 loads	1	1	1	0.621	0.0170	0.0118

Next, the feed-back vector for $r_{f1}=1.5\,\mathrm{K}\Omega$ has the following components:

Load	ξ_1	ξ_2	ξ_3	ξ_4
no load	0.555×10^{-3}	0.345	56.78	214.5
1 load	0.549×10^{-3}	0.351	56.33	238.5
2 loads	0.546×10^{-3}	0.354	56.22	270.0

So the characteristic vector with additional feed-back is given by the following components:

Load	ξ_0	ξ_1	ξ_2	ξ_3	ξ_4	ξ_5
no load	6.54×10^{-5}	5.488×10^{-3}	1.054	67.16	265.5	13492
1 load	6.44×10^{-5}	5.449×10^{-3}	1.062	66.885	292.5	13492
2 loads	6.48×10^{-5}	5.496×10^{-3}	1.017	67.22	328.6	13504

By normalization, these components become:

Load	ξ_0''	ξ_1''	ξ_2''	ξ_3''	ξ_4''	ξ_5''
no load	1	1	1	0.762	0.0157	0.00945
1 load	1	1	1	0.740	0.0167	0.00905
2 loads	1	1	1	0738	0.0185	0.00897

By the author's stability criterion, the characteristic vectors for all cases without any additional feed-back and for a case with the additional feed-back of $r_{f1} = 1.0\,\mathrm{K}\Omega$, whose components have been calculated above, are theoretically concluded to be unstable, while the characteristic vectors for cases with the additional feed-back of $r_{f1} = 1.5\,\mathrm{K}\Omega$ are all theoretically concluded to be stable (see Fig. 30). The experiments have quite agreed with the author's theoretical conclusions.

vi) Period of hunting

For example, we repeat here the case of no load and feed-back to amplifier. The characteristic vector in the state of critical stability has the components:

Load	ξ_0	ξ_1	ξ_2	ξ_3	ξ_4	ξ_5
no load	6.54×10^{-5}	5.488×10^{-3}	1.054	67.16	265.5	13492

which are normalized as follows:

Load	ξ_0''	ξ_1''	ξ_2''	ξ_3''	ξ_4''	ξ_5''
no load	1	1	1	0.762	0.0157	0.00945

This normalized characteristic vector is represented by a point, scaled $\gamma'' = 0.016$ on the normalized line of critical stability of the 5-dimensional vector in Fig. 30.

Accordingly, the hunting frequency of this unstable system is given as follows:

$$f = \frac{\omega}{2\pi} = \frac{\sqrt{\gamma}}{2\pi} = \frac{1}{2\pi}\sqrt{\gamma''\left(\frac{\xi_2}{\xi_0}\right)} = \frac{1}{2\pi}\sqrt{0.016\times\frac{1.054}{6.54\times10^{-5}}} = 0.58 \ \text{(1/sec)},$$

or

$$T = 1/f = 0.387 \ \text{(sec)}.$$

This theoretical value of hunting frequency may be considered to be quite consistent with the measured value 2.8 (cycles per second), or $T = 0.357$ (seconds), if we take into account the non-linearity of elements and the experimental errors.

vii) Straight-line stability criterion

So far we have considered the section of the 5-dimensional vector by (ξ_4, ξ_5)-plane. As described in § 7 of the preceding paper, if (ξ_3, ξ_5)-plane is considered

Stability criteria

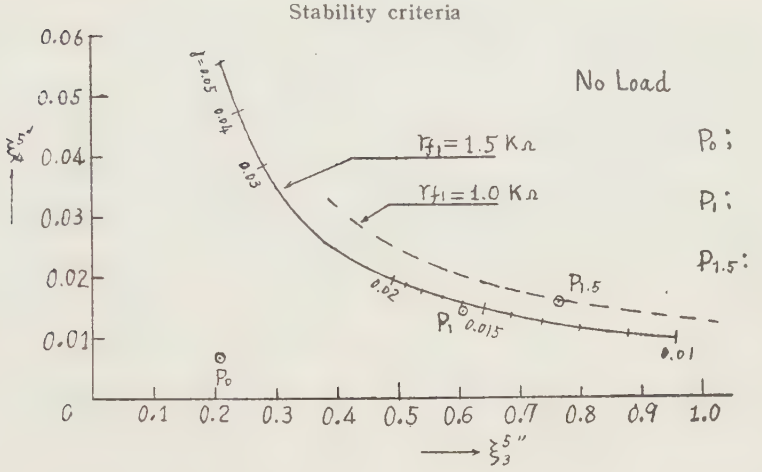

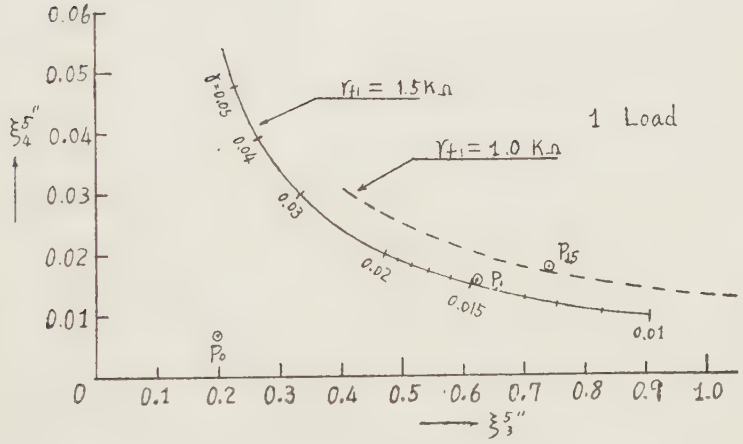

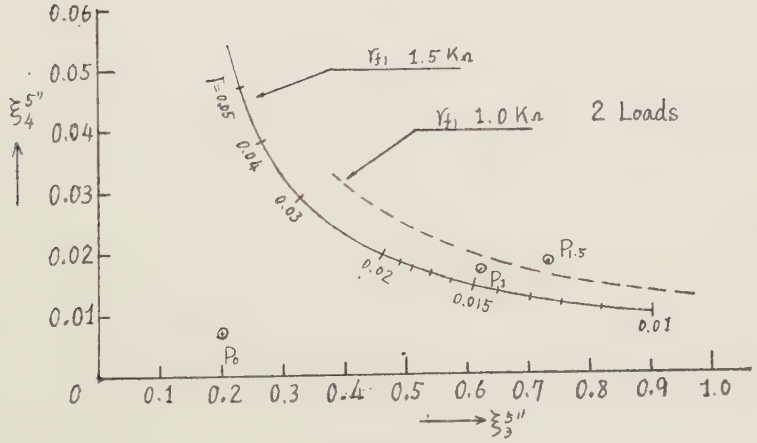

Fig. 30.

instead of (ξ_4, ξ_5)-plane, we obtain a very simple stability criterion which consists of some straight lines.

For example, in the case of feed-back to detector, the normalized characteristic vector has the components:

States of load	ξ_0''	ξ_1''	ξ_2''	ξ_3''	ξ_4''	ξ_5''
no load	1	1	1	0.890	0.0244	0.232
1 load	1	1	1	0.836	0.0257	0.223
2 loads	1	1	1	0.835	0.0290	0.225

Now, cutting the hypersurface of critical stability of the 5-dimensional vector,

$$\left.\begin{aligned} \xi_4'' &= \gamma''(1-\gamma'') \,, \\ \xi_5'' &= \gamma''(\xi_3''-\gamma'') \,, \end{aligned}\right\}$$

with a plane $\xi_4'' =$ constant (any value of ξ_4'' in the above table), we obtain (ξ_3'', ξ_5'')-stability criterion which consists of two straight lines as:

$$\xi_5'' = \gamma_1''(\xi_3''-\gamma_1'') \,, \qquad (\gamma_1\text{-line})$$

$$\xi_5'' = \gamma_2''(\xi_3''-\gamma_2'') \,, \qquad (\gamma_2\text{-line})$$

where γ_1'' and γ_2'' are the roots of the equation:

$$\xi_4'' = \gamma''(1-\gamma'')$$

for given value of ξ_4''-component, as shown in the following table:

State of load	ξ_4''	γ_1''	γ_2''
no load	0.0244	0.024	0.976
1 load	0.0257	0.027	0.973
2 loads	0.0290	0.030	0.970

The stability criteria by these straight lines are illustrated in Fig. 32, and the results are completely in accordance with those of (ξ_4'', ξ_5'')-stability criterion.

12. Conclusion

In this paper, the stability of the feed-back physical system, the relations between the stability regions of the n-dimensional characteristic vector and those of the $(n-1)$-dimensional vector and also the relations between those of the n-dimensional vector and the $(n-2)$-dimensional vector have first been discussed in detail, and the methods of constructing the stability criteria of higher dimensions from

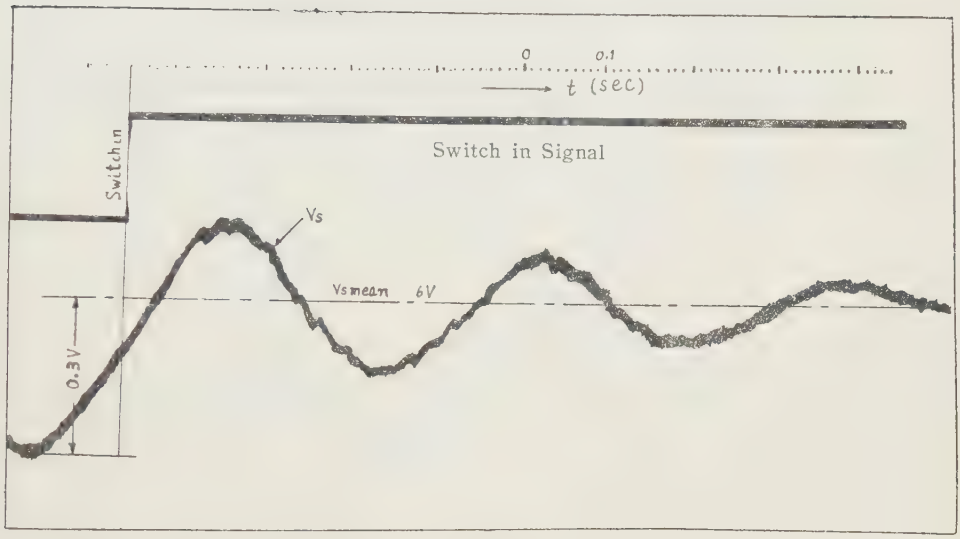

Fig. 31 a. Transient performance with anti-hunting feed-back to amplifier (r_{f1}=1.5 KΩ). No load.

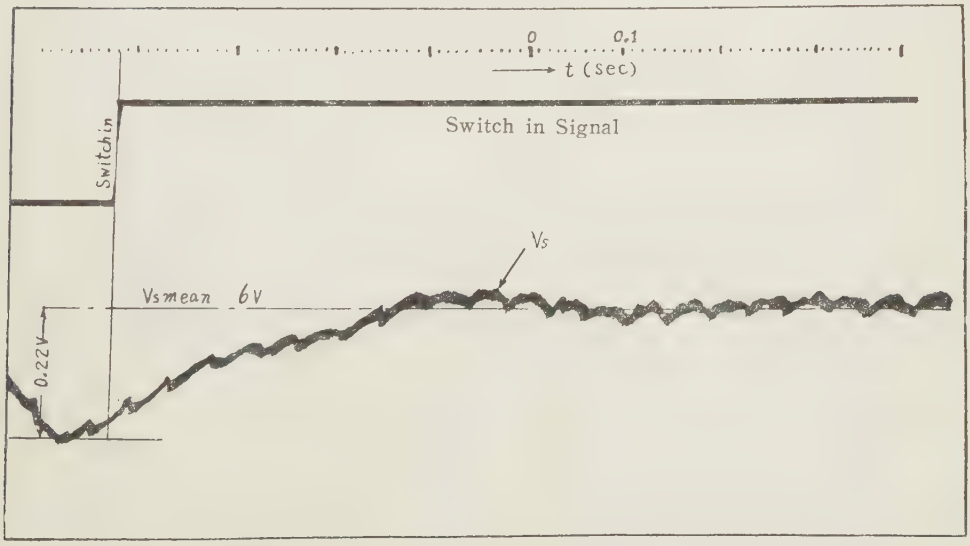

Fig. 31 b. Transient performance with anti-hunting feed-back to amplifier (r_{f1}=2 KΩ). 1 load.

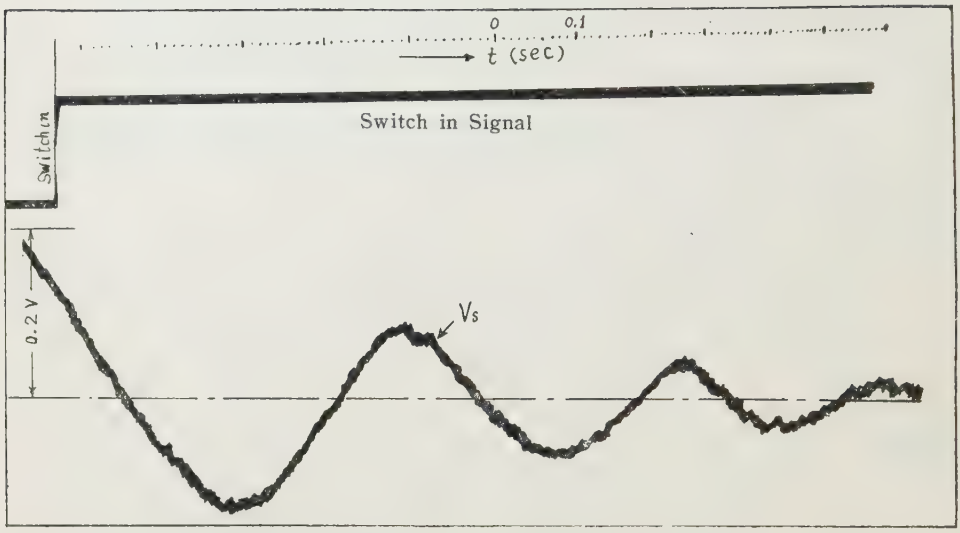

Fig. 31 c. Transient performance with anti-hunting feed-back to amplifier (r_{f_1}=1.5 KΩ). 2 loads.

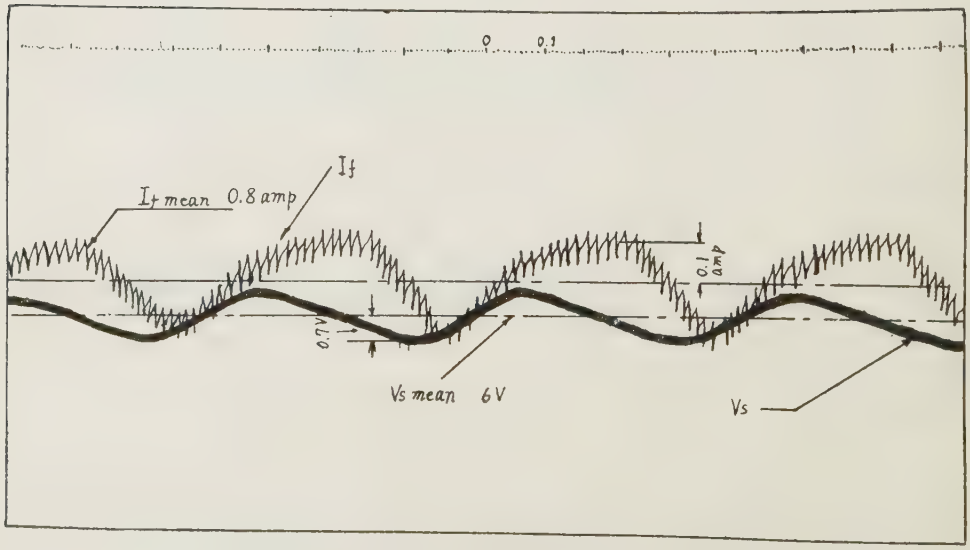

Fig. 31 d. Stationary hunting without feed-back.

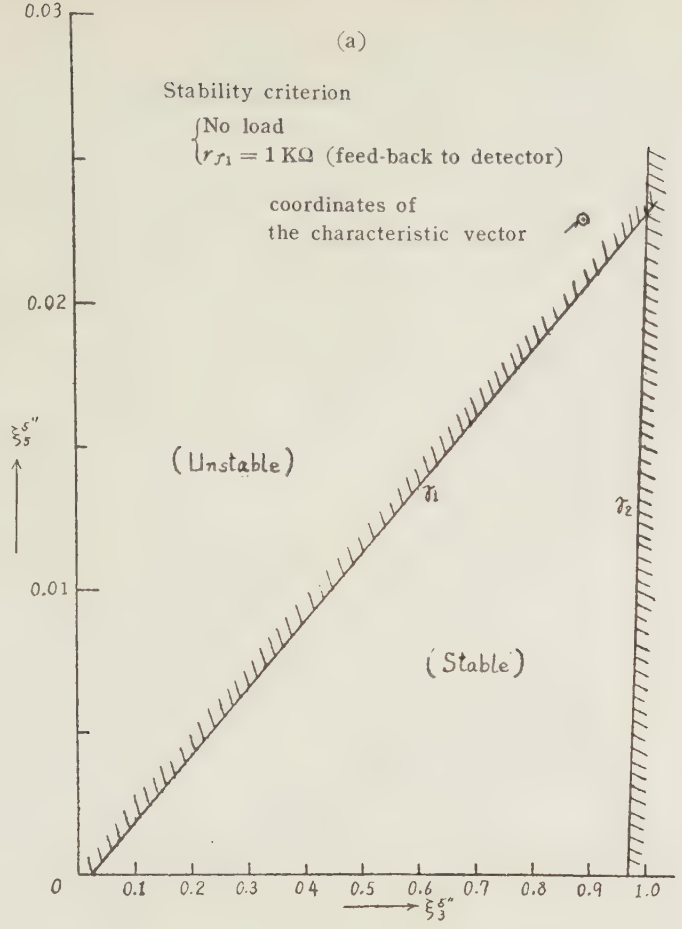
(a)
Stability criterion
No load
$r_{f1} = 1\,K\Omega$ (feed-back to detector)
coordinates of
the characteristic vector
(Unstable)
(Stable)
γ_1
γ_2
0.03
0.02
0.01
0
0.1 0.2 0.3 0.4 0.5 0.6 0.7 0.8 0.9 1.0
$\xi_3^{5''}$
$\xi_5^{5''}$

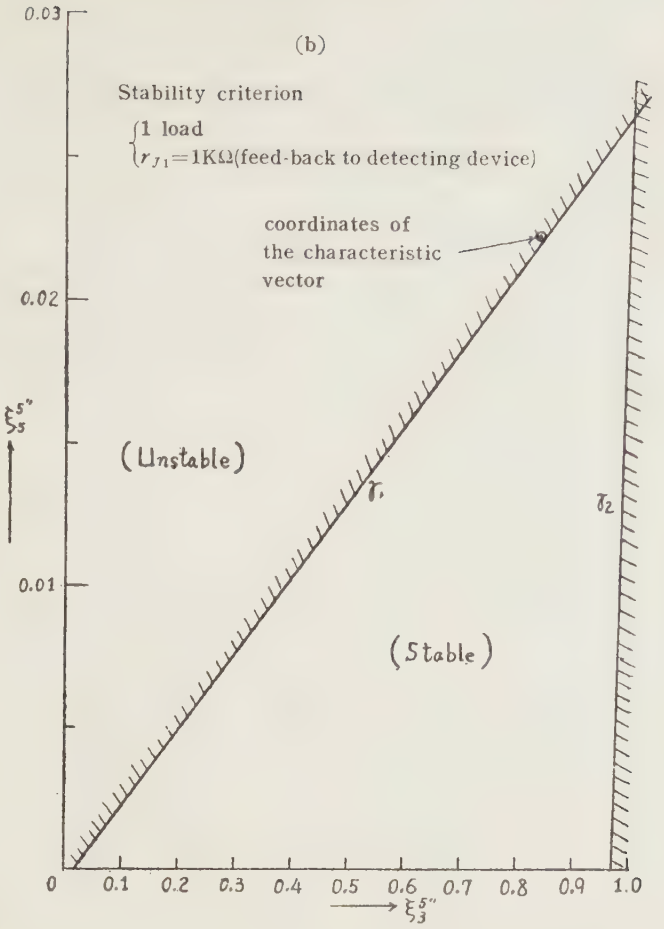
(b)
Stability criterion
1 load
r_{f1}=1KΩ(feed-back to detecting device)
coordinates of
the characteristic
vector
(Unstable)
(Stable)
γ_1
γ_2
0.03
0.02
0.01
0
0.1 0.2 0.3 0.4 0.5 0.6 0.7 0.8 0.9 1.0
$\xi_3^{5''}$
$\xi_5^{5''}$

Fig. 32.

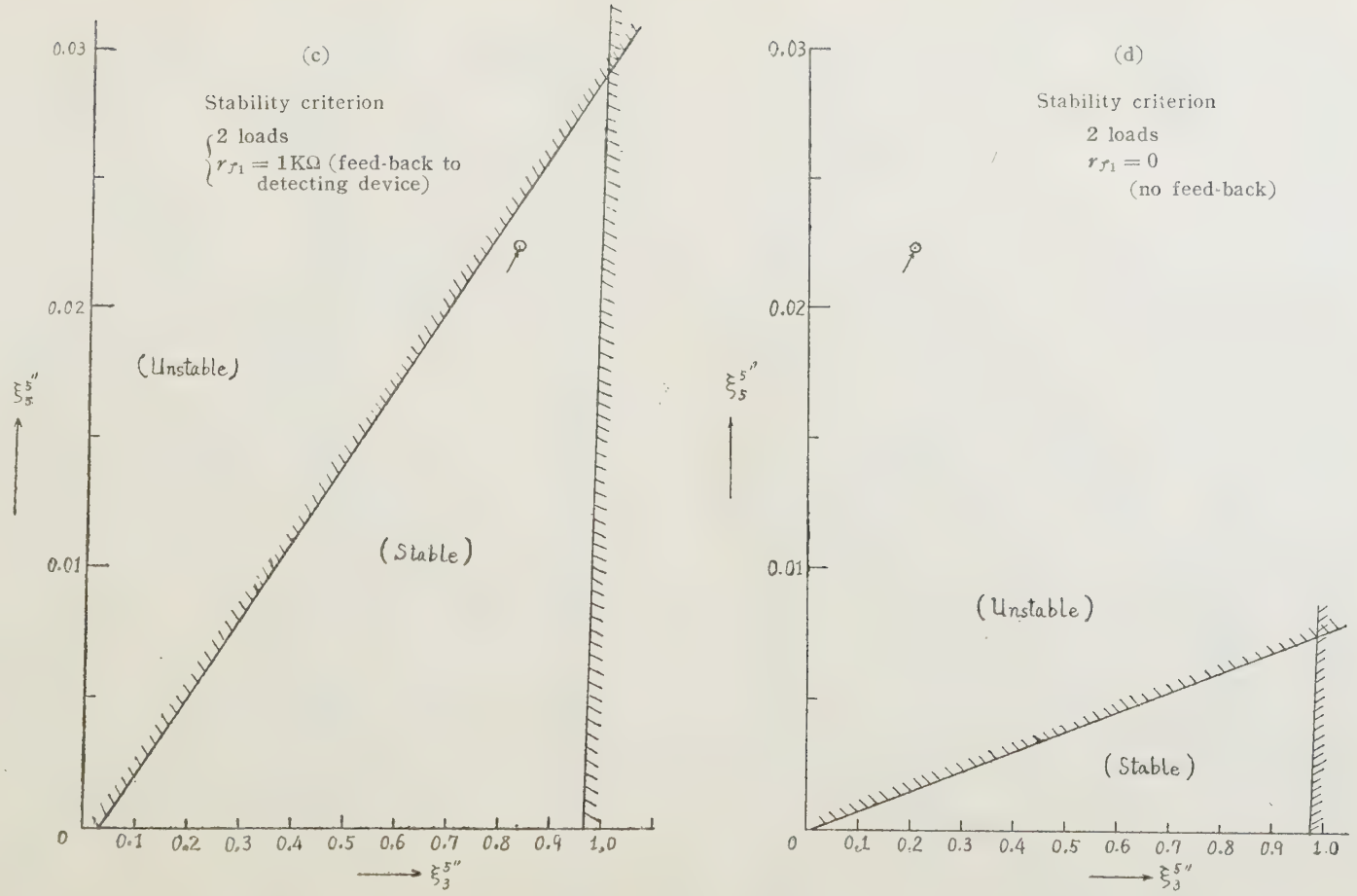
(c)
Stability criterion
2 loads
$r_{f_1} = 1\text{K}\Omega$ (feed-back to detecting device)
(Unstable)
(Stable)
0.03
0.02
0.01
0
0.1 0.2 0.3 0.4 0.5 0.6 0.7 0.8 0.9 1.0
$\xi_5^{5''}$
$\xi_3^{5''}$
(d)
Stability criterion
2 loads
$r_{f_1} = 0$
(no feed-back)
(Unstable)
(Stable)
0.03
0.02
0.01
0
0.1 0.2 0.3 0.4 0.5 0.6 0.7 0.8 0.9 1.0
$\xi_5^{5''}$
$\xi_3^{5''}$

Fig. 32.

those of lower dimensions have been described. Accordingly, from the simple stability criteria of the 2- or 3-dimensional vectors, the stability criteria of the 4- and 5- and higher dimensional vectors are readily obtained successively.

The stability criteria on any (ξ_r, ξ_{r+1})-plane, besides those on (ξ_{n-1}, ξ_n)-plane, have also been discussed. Moreover, the stability criteria on (ξ_{n-2}, ξ_n)-plane, which consists of some straight lines, have been shown to be very simple and convenient.

It has been shown in § 7 that the stability criteria of higher dimensional vectors are drawn by adding two criteria of lower dimensional vectors. This method makes also the stability criteria very simple and convenient.

We have also shown that from the γ-scale on the line of critical stability, the hunting frequency in the case of automatic control system as well as the oscillating frequency in the case of oscillator is calculated.

It has also been discussed how simply the additional feed-back and the additional feed-forward, which are commonly used for stabilizing the automatic control system, can be treated by the author's vectorial considerations.

Lastly, the experiments on the stabilization of the speed control system have shown the complete accordance with the theoretical results and thus the confirmation of the author's methods has been achieved.

In conclusion the author should like to express his sincere thanks to Prof. I. Takahashi for his helpfull advices and discussions about this paper, and to Prof. Y. Omoto who has kindly afforded facility to this work.

REFERENCE

1. K. TASHIRO, Vectorial stability criteria of the feed-back physical system. Part I. *Memoirs Coll. Sci., Univ. of Kyoto*, Series A, **27** (1954), 157.

CONTENTS

The Vertical Distributions of the Temperature and Density in the Lower Ionosphere

By *Yuji Inoue* 67

On the Megnetic Anomalies and their Secular Variations around Maeyama on Simabara Peninsula

By *Wasiro Yoda* 101

Seismometric Investigation of the Earth's Interior. Part I. On the Structure of the Earth's Upper Layer

By *Yoshimichi Kishimoto* 125

An Expansion Formula for the Lift on a Circular-arc Aerofoil in a Stream bounded by a Plane Wall

By *S. Tomotika* AND *H. Fujikawa* 145

Vectorial Stability Criteria of the Feed-back Physicai System. Part I.

By *Kentaro Tashiro* 157

Vectorial Stability Criteria of the Feed-back Physical System. Part II.

By *Kentaro Tashiro* 185

Printed by NIPPON INSATU SHUPPAN

Fukushima, Osaka